



HAL
open science

Impact of packing and porosity filler use in G/S and G/L/S packed bed millireactors : experimental and numerical studies

Vittorio Petrazzuoli

► **To cite this version:**

Vittorio Petrazzuoli. Impact of packing and porosity filler use in G/S and G/L/S packed bed millireactors : experimental and numerical studies. Catalysis. Université de Lyon, 2020. English. NNT : 2020LYSE1273 . tel-03593407

HAL Id: tel-03593407

<https://theses.hal.science/tel-03593407>

Submitted on 2 Mar 2022

HAL is a multi-disciplinary open access archive for the deposit and dissemination of scientific research documents, whether they are published or not. The documents may come from teaching and research institutions in France or abroad, or from public or private research centers.

L'archive ouverte pluridisciplinaire **HAL**, est destinée au dépôt et à la diffusion de documents scientifiques de niveau recherche, publiés ou non, émanant des établissements d'enseignement et de recherche français ou étrangers, des laboratoires publics ou privés.

N°d'ordre NNT : 2020LYSE1273



THESE de DOCTORAT DE L'UNIVERSITE DE LYON

opérée au sein de

l'Université Claude Bernard Lyon 1

**École Doctorale N° 206
(École Doctorale de Chimie)**

Spécialité de doctorat : Chimie

Soutenue publiquement le 02/12/2020, par :

Vittorio Petrazzuoli

Titre de la thèse :

**Impact of packing and porosity filler use in G/S
and G/L/S packed bed millireactors: experimental
and numerical studies**

Devant le jury composé de :

Boccardo, Gianluca	Professeur Associé, Politecnico di Torino	Rapporteur
Toye, Dominique	Professeure, Université de Liège	Rapporteuse
Boudiguel, Hugues	Professeur, Institut Polytechnique de Grenoble	Examineur
Schuurman, Yves	Directeur de recherche CNRS, UCBL Lyon 1	Directeur de thèse
Tayakout-Fayolle, Melaz	Professeure, UCBL Lyon 1	Examinatrice
Mekki-Berrada, Adrien	Ingénieur de recherche, IFPEN	Invité
Rolland, Matthieu	Ingénieur de recherche, IFPEN	Invité

Index

Index.....	2
Summary	7
Résumé long.....	9
Nomenclature	13
1 Introduction	20
1.1 The catalyst's development cycle.....	20
1.2 Testing reactors in heterogeneous catalysis.....	22
1.3 Testing reactors: towards miniaturization and parallelization.....	22
1.3.1 Miniaturization	22
1.3.2 Parallelization.....	25
1.4 Thesis context.....	26
2 Physics and modeling of packed beds	28
2.1 The particles disposition in packed bed reactors and millireactors	28
2.1.1 The importance of a reproducible packing	32
2.2 Packed beds modeling	33
2.2.1 Deviation from the ideal plug flow: the axial dispersion model	34
2.2.2 External mass transfer limitations	36
2.2.2.1 Film theory applicability for packed bed millireactors	38
3 Literature review on packed beds.....	40
3.1 Introduction	40
3.2 Flow in packed bed reactors and millireactors	41
3.2.1 Single-phase flows.....	41
3.2.2 Gas-liquid co-current downflow.....	41
3.3 The measurement of dispersion and liquid holdup.....	45
3.3.1 Dispersion measurement techniques	45
3.3.2 Liquid holdup measurement techniques	47
3.4 Dispersion in packed beds.....	48
3.4.1 Effect of the fluid velocity.....	48

3.4.2	Effect of the reactor/particle diameter ratio.....	54
3.5	Liquid holdup	56
3.5.1	Effect of the fluid velocities	56
3.6	Addition of inert powder	58
3.6.1	Effect on the dispersion	59
3.6.2	Effect on the liquid holdup	60
3.6.3	Effect on the reactive performances of packed bed millireactors.....	61
3.7	Literature summary	66
4	Computation Fluid Dynamics in packed beds.....	69
4.1	The packed bed generation.....	69
4.2	Mean age theory and Pe number calculation.....	71
4.3	Literature on DNS in packed beds.....	73
4.4	Synthesis on CFD.....	74
5	Thesis strategy	75
6	Gas-solid case.....	77
6.1	High Throughput Experimentation (HTE) unit presentation	78
6.2	Hydrodynamic and reactive experimental tests.....	82
6.2.1	Introduction	84
6.2.2	Materials and methods.....	88
6.2.2.1	RTD measurements	89
6.2.2.2	Reactive tests: unit description and experimental conditions.....	94
6.2.3	Results and discussion: RTD experiments	96
6.2.3.1	Plug flow behavior	96
6.2.3.2	Effect of the bed length	98
6.2.3.3	Effect of reactor/particle diameter ratio.....	99
6.2.3.4	Effect of superficial gas velocity	102
6.2.3.5	Effect of inert powder addition as porosity filler	103
6.2.3.6	Criterion for axial dispersion limitations.....	106
6.2.4	Results and discussion: reactive tests	108
6.2.4.1	Check of thermal transfer and axial dispersion limitations	109
6.2.4.2	Porosity filler effect on the conversion: <i>n</i> -heptane reforming reaction.....	110
6.2.4.3	Porosity filler effect on the conversion: methylcyclohexane dehydrogenation reaction...	116
6.2.5	Conclusions	118

6.3	CFD simulations in absence of porosity fillers	120
6.3.1	Introduction	121
6.3.1.1	Fixed bed downscaling	121
6.3.1.2	Plug flow behavior	123
6.3.1.3	Pe number evaluation using CFD	126
6.3.2	Aim of the work	127
6.3.3	Materials and methods	128
6.3.3.1	Detailed simulation Workflow	128
6.3.3.2	Mesh convergence	129
6.3.3.3	Workflow Validation	132
6.3.4	Results	135
6.3.4.1	Pe number in narrow reactors	135
6.3.4.2	Repeatability of the Pe number profiles in narrow reactors	147
6.3.5	Conclusions and perspectives	151
6.4	CFD simulations exploring the effect of porosity fillers	153
6.4.1	Case description	153
6.4.2	Pe number with and without porosity filler	154
6.4.2.1	Mesh convergence	154
6.4.2.2	Different flow patterns	155
6.4.2.3	Pe number profiles along the bed	157
6.4.3	Mass transfer	161
6.4.3.1	Porosity filler effect on mass transfer	163
6.4.4	Conclusion on CFD with porosity filler	172
7	Gas-liquid-solid case	173
7.1	Hydrodynamic experiments	173
7.1.1	Strategy and scope of the tests	173
7.1.2	Experimental bench description	174
7.1.3	Experimental protocol	178
7.1.4	Data interpretation: from the concentrations to Pe number	179
7.1.5	Differing inlet and outlet curves integrals	181
7.1.6	Repeating the pulses	188
7.1.7	Results: The flow regimes observation	189
7.1.8	Results on liquid holdup and plug flow behavior	191

7.1.8.1	Comparison with literature	191
7.1.8.2	An effect of the start-up procedure.....	194
7.1.8.3	Hydrodynamics in absence of porosity filler.....	196
7.1.8.4	Hydrodynamics with porosity filler.....	206
7.1.9	Conclusions on the hydrodynamic experiments.....	209
7.2	Reactive tests.....	212
7.2.1	Materials and unit constraints.....	212
7.2.1.1	The catalyst.....	212
7.2.1.2	The reactors and loadings.....	213
7.2.1.3	The liquid feedstock	214
7.2.1.4	Operating conditions and unit constraints	214
7.2.1.5	$D_r=2$ mm reactors isothermicity	215
7.2.2	Results	216
7.2.2.1	The experimental plan	217
7.2.2.2	Expected hydrodynamic conditions.....	217
7.2.2.3	Catalyst deactivation	219
7.2.2.4	Apparent activation energy estimations	220
7.2.2.5	Hydrogen partial pressure effect	222
7.2.2.6	Porosity filler effect.....	224
7.2.3	Conclusions on the reactive tests.....	244
8	General conclusions and perspectives.....	247
8.1	Synthesis of the work	247
8.1.1	Gas-solid case.....	247
8.1.2	Gas-liquid-solid case	248
8.1.3	Summary and recommendations when using packed bed millireactors.....	250
8.2	Perspectives.....	252
8.2.1	Mass transfer coefficient calculations	252
8.2.2	The hydrodynamic descriptors	252
8.2.3	G/L/S RTD tracer optimization.....	253
8.2.4	CFD in presence of porosity fillers	254
8.2.5	Polydisperse and « special » packings.....	254
Annex A:	Vaporization problems in the HTE reactors	256
Annex B:	Deviations from the axial dispersion model in presence of porosity fillers.....	258

Annex C: The Sc number effect (CFD simulations) 260
Annex D: Second practical case of choosing the right combination of reactor and particle diameter (CFD simulations) 262
References 264

Summary

Packed bed millireactors, packed beds with reactor diameters of millimeters, are increasingly used for the screening phase of the catalyst development cycle. The possibility to use these reactors for catalysts performance prediction studies (i.e. kinetic studies) is quite attractive, but it requires a better knowledge of the flow characteristics in these reactors.

This work focuses on the study of hydrodynamics and mass transfer of packed bed millireactors operated on gas-solid and gas-liquid-solid co-current downflow conditions and packed with millimetric particles.

For the gas-solid case, residence time distributions (RTD) experiments have been performed to characterize the hydrodynamics of these reactors. The axial dispersion model has been used to evaluate the amount of dispersion. Then, CFD simulations with OpenFOAM[®] have been performed to obtain local information on the evolution of the flow in packed bed millireactors, including accurate prediction of Pe numbers using steady-state simulations. Last, gas-solid reactive experiments on *n*-heptane reforming and methylcyclohexane dehydrogenation have been performed to study the mass transfer properties of these reactors, and in particular the effect of porosity fillers (size and shape).

For the gas-liquid-solid case, residence time distribution (RTD) experiments and flow observations have been performed to characterize the liquid hydrodynamics in these reactors. Then gas-liquid-solid reactive tests on α -methylstyrene hydrogenation have been performed to explore the effect of porosity fillers on the conversion.

The major findings are that the value of reactor/particle diameter ratio is crucial and determines the flow characteristics of packed bed millireactors in single-phase flow, and that the use of porosity

fillers improves hydrodynamics and mass transfer. CFD simulations have proven to be accurate and faster than experiments to predict Pe numbers. The results from the gas-liquid-solid part show that the flow regime is often pulsed and the amount of dispersion often not negligible, but this can be corrected using porosity fillers.

Résumé long

Les réacteurs milli lits fixes, lits fixes avec des diamètres de quelques millimètres, sont de plus en plus utilisés pour la phase de “screening” du cycle de développement des catalyseurs. Utiliser ces réacteurs pour des études de prédiction des performances des catalyseurs (pour exemple des études cinétiques) est très attrayante, mais nécessite une meilleure connaissance des caractéristiques d'écoulement dans les réacteurs.

Ce travail porte sur l'étude de l'hydrodynamique et du transfert de matière des milli lits fixes fonctionnant en écoulement gaz-solide et gaz-liquide-solide co-courant.

Pour le cas gaz-solide, des expériences de distribution de temps de séjour (DTS) ont été réalisées afin de caractériser l'hydrodynamique des milli-réacteurs. Le modèle piston - dispersion axiale a été utilisé pour en déduire la dispersion. Le comportement de ces réacteurs a été trouvé similaire à celui des réacteurs de laboratoire plus grands, à l'exception de géométries spécifiques dans lesquelles les contraintes géométriques conduisent à un empilement avec des grands passages préférentiels. Dans ces cas, les performances des réacteurs sont médiocres et il convient les éviter. À part ces exceptions, des valeurs suffisantes du nombre de Péclet (Pe) en absence de remplisseurs de porosité ont été trouvées pour des géométries courtes (4-10 cm), ce qui signifie que les effets de dispersion peuvent être négligés pour la plupart des réactions. Les poudres de remplissage ont des effets bénéfiques dans tous les réacteurs testés du point de vue hydrodynamique.

Des simulations CFD stationnaires avec OpenFOAM® ont été réalisées afin d'obtenir des informations locales sur l'évolution du flux dans les réacteurs, y compris la prédiction du nombre de Péclet. Les simulations CFD se sont avérées précises et plus rapides que les expériences pour prédire le nombre de Péclet. Ils ont permis d'explorer en détail l'évolution du nombre de Pe en

fonction de différents paramètres comme le ratio entre le diamètre du réacteur et celui des particules, vitesse superficielle du fluide et diffusivité moléculaire. Nous recommandons de rester vigilants en ce qui concerne les réacteurs filaires avec un ratio des diamètres réacteur/particule inférieur à 1.3 pour lesquels les simulations CFD surestiment souvent les nombres de Pe et Bo, même si aucune raison n'a été trouvée pour mettre en cause les simulations.

Des tests réactifs ont été conduits sur une unité d'Expérimentation à Haut Débit (EHD). Les remplisseurs de porosité ont été trouvés bénéfiques dans tous les chargements testés. Même pour des réacteurs à faible dispersion, l'ajout des remplisseurs de porosité a permis de gagner de 1 à 6-7 points de conversion selon les cas (une augmentation en tout cas inférieure à 10%). Nous attribuons ce gain à un meilleur transfert de matière gaz-solide en raison de vitesses interstitielles plus élevées. Des tests répétés ont montré une contribution bénéfique plus élevée (mais très faiblement) des remplisseurs de porosité sphériques (ZirBlast[®]) par rapport à ceux de forme irrégulière (SiC). Nous évaluons la répétabilité de l'unité EHD utilisée à $\sim \pm 1$ point de conversion dans des applications réactives gaz-solide, ce qui fixe une limite sur le type de réaction qui peut être étudié en utilisant des unités EHD.

Pour le cas gaz-liquide-solide, des expériences de distribution de temps de séjour (DTS) et des observations d'écoulement ont été réalisées afin de caractériser l'hydrodynamique de la phase liquide dans ces réacteurs. Deux principaux régimes d'écoulement ont été observés : un écoulement stable gouverné par les forces capillaires et un écoulement irrégulier gouverné par la gravité. Ces régimes d'écoulement sont différents de ceux observés dans les lit fixes traditionnels ("trickle flow" et écoulement pulsé). La transition entre ces deux écoulements est bien prédite à l'aide du nombre d'Irrigation, et elle est notamment gouvernée par la vitesse de la phase liquide et la taille des particules. Quand l'écoulement est instable dans les réacteurs remplis que des particules de

catalyseur, l'utilisation des remplisseurs de porosité permet de stabiliser l'écoulement à l'intérieur des lits. De très petites valeurs du nombre de Pe (<10) ont été trouvées pour des géométries courtes (4-10 cm) en absence de remplisseurs de porosité, de sorte que les effets de dispersion sont très importants et l'utilisation des remplisseurs de porosité nécessaire pour conduire à des valeurs du nombre de Pe plus élevées.

Ensuite, des expériences réactives gaz-liquide-solide sur l'hydrogénation du α -méthylstyrène ont été réalisées (sur la même unité utilisée dans les expériences réactives gaz-solide) afin d'explorer l'effet des remplisseurs de porosité sur la conversion. Les tests réactifs sans remplissage de porosité montrent une très grande sensibilité à la disposition des particules à l'intérieur du lit. Lorsque l'on remplit un réacteur plusieurs fois avec les mêmes particules, la disposition finale n'est jamais exactement la même. Dans nos résultats expérimentaux, nous avons observé de très grandes différences de conversion entre les réacteurs remplis avec la même masse de catalyseur mais avec les particules disposées différemment. Nous pensons que une partie du liquide coule en paroi du réacteurs sans rencontrer le catalyseurs, et que cette quantité dépend de la disposition des particules dans le réacteur. L'utilisation de petites quantités de catalyseur rend cet aspect encore plus critique car les éventuels défauts de remplissage ne sont pas lissés sur la longueur du lit. L'effet est réduit, mais toujours présent, lorsque l'on utilise des remplisseurs de porosité ou lorsque les empilements sont géométriquement contraints et donc reproductibles : c'est le cas des réacteurs filaires avec un ratio des diamètres réacteur/particule inférieur à ~ 1.5 , ou lorsque les lits sont grands par rapport à la taille des particules et donc plus uniformes.

Les remplisseurs de porosité se sont avérés bénéfiques dans tous les réacteurs testés, tant du point de vue hydrodynamique que "réactif". Ils conduisent à un régime d'écoulement contrôlé par la force de gravité à un régime contrôle par les forces capillaires, ce qui assure un meilleur mouillage du

catalyseur. D'autres raisons pour les gains de performance sont la réduction de la dispersion (nombre de Pe plus élevé) et une distribution plus uniforme des phases fluides sur la section du réacteur (empêchant notamment les passages de liquide en paroi). Les remplisseurs de porosité de forme irrégulière se sont avérés plus avantageux que ceux sphériques. La raison est que les remplisseurs de porosité de forme sphérique peuvent créer localement des zones très denses dans lesquelles le liquide est susceptible de stagner et qui ne sont pas accessibles à la phase gazeuse. Certains grains de catalyseur peuvent ainsi être protégés du liquide ou du gaz.

Nomenclature

Roman letters

A:	Surface exchange area [m^2]
a:	Age of the molecules [s]
a_c :	Specific interfacial area between two phases [m^2/m^3]
a_s :	Specific area of the bed [m^2/m^3]
C or c:	Concentration [mol/m^3]
D_{ax} :	Axial dispersion coefficient [m^2/s]
D_{cyl} :	Cylinders diameter [mm]
D_m :	Molecular diffusivity [m^2/s]
d_p :	Particle diameter [mm]
D_r or ID:	Reactor internal diameter [mm]
dz:	Spatial discretization interval [m]
E_a :	Activation energy [J/mol]
$E(t)$:	Normalized response to a Dirac function [s^{-1}]
F:	Molar flow rate [mol/m^3]
F_{ij} :	Molar flux between two phases i and j [$\text{mol}/(\text{m}^2 \cdot \text{s})$]
$F(t)$:	Normalized response to a Heaviside function
g:	Gravitational acceleration [m/s^2]
GHSV:	Gas hourly space velocity [$\text{m}^3_{\text{gas}}/(\text{m}^3_{\text{cat}} \cdot \text{h})$]

$H(t-t_0)$:	Heaviside function
HSV:	Generic hourly space velocity [$\text{m}^3/(\text{m}^3_{\text{cat}} \cdot \text{h})$]
k :	Kinetic constant [depending on the reaction order]
k_{ij} :	Mass transfer coefficient between two phases i and j [m/s]
L :	Bed length [m]
L_{cyl} :	Cylinders length [mm]
LHSV:	Liquid hourly space velocity [$\text{m}^3_{\text{liq}}/(\text{m}^3_{\text{cat}} \cdot \text{h})$]
m :	Mean
m_{cat} :	Catalyst mass [mg]
M_l :	Liquid mass flow on reactor section [$\text{kg}/(\text{m}^2 \cdot \text{s})$]
M_n :	Moment of order n of the $E(t)$ curve [s^n]
n_r :	Reaction order
n :	$E(t)$ moments order
N :	Number of realizations
N_{beads} :	Beads number
P :	Pressure [bar]
Q :	Volumetric flow rate [m^3/s]
R :	Gas constant [$8.314 \text{ J}/(\text{K} \cdot \text{mol})$]
r :	Radial coordinate [m]
R_v :	Volumetric reaction rate [$\text{mol}/\text{m}^3_{\text{catalyst}} \cdot \text{s}$]

s:	Standard deviation
S:	Particles surface [m ²]
t:	Time [s]
\bar{t} :	Mean fluid residence time [s]
T:	Temperature [K]
t _s :	Medium residence time [s]
U95%:	Relative 95% confidence level uncertainty
u:	Superficial velocity [m/s]
u _i : $\frac{u}{\varepsilon}$	Interstitial velocity [m/s]
v:	Velocity vector [m/s]
V _{cat} :	Volume of the catalyst [mL]
V _e :	Empty volume of the reactor [mL]
V _l :	Volume occupied by the liquid [mL]
V _r :	Volume of the reactor [mL]
V _s :	Volume occupied by the solid [mL]
W:	Mass flow [kg/s]
WHSV:	Reactant hourly velocity per catalyst mass unit [g _{reactant} /(h·g _{cat})≈h ⁻¹]
X:	Reactive conversion
y:	Molar fraction
z:	Axial coordinate [m]

Greek letters

α_w :	Wall heat transfer coefficient [W/(m ² ·K)]
δ : $\frac{D_r}{d_p}$	Reactor/particle diameter ratio (spheres case)
δ' : $\frac{D_r}{D_{cyl}}$	Reactor/particle diameter ratio (cylinders case)
ΔH_0 :	Standard reaction enthalpy [J/mol]
ΔP :	Pressure drop [bar]
ΔPe :	Difference in Pe number between two reactor plans
ΔT_{rad} :	Difference of temperature in the radial direction [K]
ΔX :	Difference in reactive conversion between two packing types
$\Delta(t-t_0)$:	Dirac function
ε : $\frac{V_e}{V_r}$	Void fraction of the reactor
ε_l : $\frac{V_l}{V_r}$	Liquid holdup
λ :	Thermal conductivity [W/(m·K)]
μ :	Fluid viscosity [Pa·s]
ρ :	Fluid density [kg/m ³]
σ :	Variance
τ :	Tortuosity factor
ϕ :	Sphericity of the particle

Φ_g :	Gas volume flow rate [mL/min]
Φ_l :	Liquid volume flow rate [mL/min]
Ψ :	$\frac{L_{cyl}}{D_r}$ Cylinders length/reactor diameter ratio

Dimensionless numbers

Bo:	$\frac{u_i * d_p}{D_{ax}}$ Bodenstein number
Ca:	$\frac{\mu_l * u_l}{\sigma}$ Capillary number
Ga:	$\frac{\rho^2 * g * d_p^3}{\mu^2}$ Galileo number
I:	$\frac{\mu_l * u_l}{(\rho_l - \rho_g) * g * d_p^2}$ Irrigation number
Pe:	$\frac{u_i * L}{D_{ax}}$ Reactor Peclet number
Pe _m :	$\frac{u_i * d_p}{D_m}$ Molecular Peclet number
Re:	$\frac{\rho * u_i * d_p}{\mu}$ Reynolds number
Sc:	$\frac{\mu}{\rho * D_m}$ Schmidt number
Sh:	$\frac{k_{ij} * d_p}{D_m}$ Sherwood number

Subscripts

G or g:	related to the gas phase
L or l:	related to the liquid phase
S or s:	related to the solid phase

exp: obtained through experiments

mod: obtained through models

Acronyms

AMS: α -methylstyrene

bpd: Blocks per diameter

CFD: Computational Fluid Dynamics

CSTR: Continuously Stirred Tank Reactor

DEM: Discrete Element Method

DNS: Direct Numerical Simulation

G/S: Gas-Solid

G/L/S: Gas-Liquid-Solid

GC: Gas chromatograph

HDS: Hydrodesulphurization

HTE: High Throughput Experimentation

iC16: iso-hexadecane (2,2,4,4,6,8,8-heptamethylnonane)

MCH: Methylcyclohexane

MS: Mass Spectrometry or Spectrometer

nC7: *n*-heptane

RSE: Relative Square Error

RMSE: Root Mean Square Error

RTD:	Residence Time Distribution
SiC:	Silicon Carbide
SPSR:	Single Pellet String Reactor
ZB or Z:	ZirBlast [®]

1 Introduction

1.1 The catalyst's development cycle

More than 80% of the commercial chemical processes (pharmaceuticals, petrochemicals, etc.) are catalytic processes, and most of them make use of solid catalysts particles. These particles have millimetric size and they can have different shapes (spheres, cylinders, trilobes...). Catalysts allow an efficient pathway to the desired products by reducing the energetic cost (pressure and/or temperature) to achieve a desired yield and by selectively orientating the reactions. Despite many decades of work, it is still impossible to design the ideal catalyst for a specific reaction: experiments are required for the development of processes.

The scheme in Figure 1 summarizes the course of catalyst development [1].

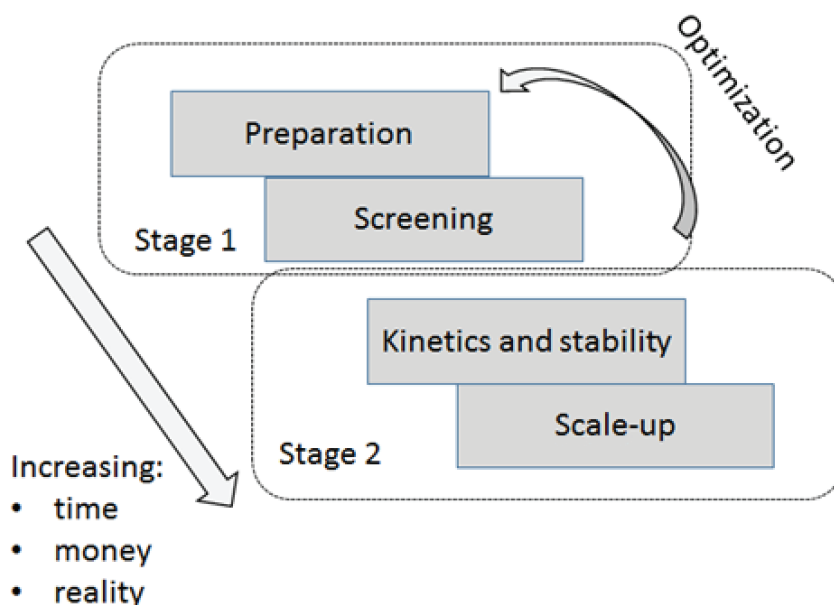


Figure 1. Development cycle of a catalyst, after [1]

The development cycle of a catalyst begins with a broad screening of many samples (the discovery phase, stage 1), followed by a detailed investigation of the best candidates (stage 2) aiming at a design of the industrial plant and at guaranteeing performances. Contrarily to the academic work that focuses on intrinsic kinetics and that prefers to test powder catalysts to avoid internal mass transfer limitations, industrial catalyst development is often based on the final catalyst size (~mm) to reduce development delays and risks when extrapolating from powder to catalyst pellets. The product to characterize is the catalyst that will be used in the industrial process that is the millimetric catalyst. As impregnation may depend on catalyst size, especially if the impregnation solutions are very viscous, all catalysts are prepared with millimetric size pellets. Testing powders thus requires an additional step of crushing which may introduce some variability (i.e. small changes in the powder size distribution, pollution of metallic parts, etc.). Then, powder catalysts will mostly perform differently in terms of conversion and selectivity so that a model coupling kinetic and mass transfer is necessary to predict the millimetric size catalyst performances [2]. Even if this may appear “simple”, it is not so straightforward for complex reaction networks with thousands of molecules and when the size of molecules is in the lower end of the pore size distribution, meaning interaction with the solid surface during transport. Due to this high complexity, grain size kinetic modeling is in practice only performed on low complexity matrixes. As any modeling work, the model will not be perfect and will introduce uncertainties in the predictions. Due to the high stakes, both in catalyst cost and performance guarantees, the model will need to be validated on millimetric size catalysts before being used to design a unit. Experimental tests on pellets are thus mandatory and it is much more efficient to perform only millimetric catalyst testing than millimetric and powder catalysts testing.

Catalyst testing aims at collecting sufficient information while operating within safety standards and trying to lower the costs and to increase the productivity. During the screening stage, simplified analysis allows different candidates to be ranked on a limited number of criteria. This stage has benefited significantly from advances in robotics and fabrication techniques [3], in a trend known as High Throughput Experimentation (HTE).

1.2 Testing reactors in heterogeneous catalysis

Two types of reactors are generally used to perform tests on solid catalysts: stirred reactors and packed beds. Stirred reactors consist of a vessel, controlled in pressure and temperature, which contains the reactive species, the catalyst particles, and a stirrer. The catalyst may be contained in a basket or dispersed in a liquid phase. These reactors can be operated in different ways:

- Closed to the reagent species (batch);
- Opened to the reagent species (Continuously Stirred Tank Reactor, CSTR);
- Closed with possibility to feed one of the reagents (semi-batch).

Packed bed reactors are instead always operated continuously (always opened to the reagent species). They generally consist in cylindrical tubes, filled with the catalyst particles, in which the fluids are injected. In this work, we will focus on packed bed reactors.

1.3 Testing reactors: towards miniaturization and parallelization

1.3.1 Miniaturization

A general trend in industry has been the reduction in size of the catalyst testing reactors (Figure 2) while the catalyst size remains the same. The advantages of the reduction in size are all related to

the reduction of the development costs and delays. This means: less catalyst used [1], less amount of chemicals required and consequently less amount of waste materials produced [4, 5], easier temperature control [5] as there are smaller temperature gradients inside the reactor, more reactors per unit area and per man-hour and reduced safety risks compared to the operation of larger reactors [6]. Depending on the design, small reactors may also require less time to reach tightness and thus shorten the overall test length.

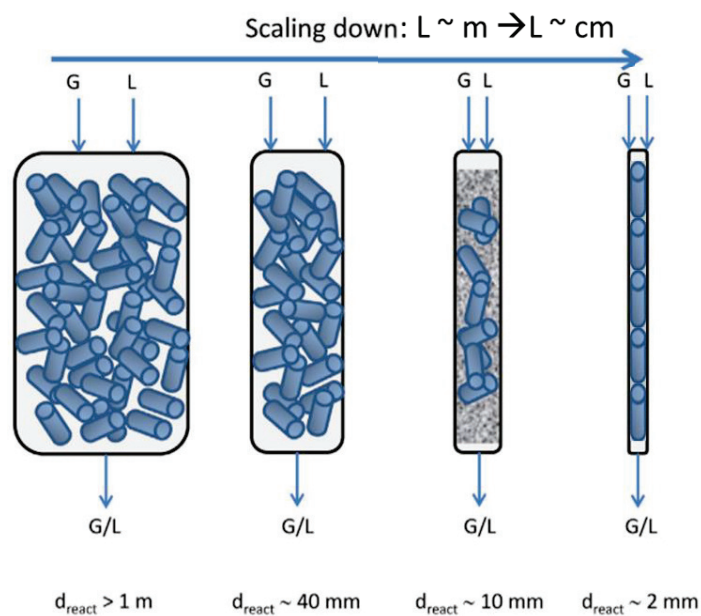


Figure 2. Representation of reactors at different scales, after [7]

For the screening tests, the important information is the ranking and some indication of the performance gains. It is admissible that the information is dependent on the reactor size. On the opposite, for scaling-up tests, the information ought to be independent of the reactor used. The reason is more practical than scientific as, in theory, the reactor characterizations and models can explain the differences. In practice the reactor models are not perfect, and their use introduces

uncertainties in the kinetic model optimization, uncertainties that will propagate in the final industrial design. In practice, it is therefore preferable if the information can be used without any reactor model. This means that either on every scale the process is running in chemical regime or that the mass and heat transfer limitations are identical at every scale.

Downscaling is performed while keeping gas and liquid space (GHSV and LHSV) hourly velocities constant. The gas/liquid superficial velocities [m/h] can be expressed as:

$$\mathbf{u} = \mathbf{G \textit{ or } LHSV} * \mathbf{L} \quad \text{Equation 1}$$

in which: u is the gas or liquid superficial velocity [m/h], G or $LHSV$ is the gas or liquid hourly space velocity [h^{-1}] and L is the length of the bed [m]. Considering that also bed lengths are reduced in the downscaling, the downscaling leads to a reduction of the gas and liquid superficial velocities. Low gas and liquid velocities result in a change in the flow patterns: friction and inertia are reduced while gravity and capillary forces remain the same. In small reactors, phase distribution, wetting, and axial dispersion are different as much as the mass transfer resistance. Remedies for these problems have been in the 70's to operate in the bubble regime (upflow reactors) while industrial reactors are mostly operated in trickle bed regimes (downflow). More recently, with even smaller reactors, the remedies have been to use inert powders, finer than the catalyst particles, to dilute the catalytic bed. Capillary and viscous forces are then greatly enhanced leading to lower liquid axial dispersion and near total wetting of the catalyst [8, 9].

The risks in operating reactors in the order of millimeters of diameter, other than the lower superficial velocities, are: very small amount of catalyst mass to be measured, potential packing issues (local reactor porosities, grain size differences and orientation), mass flow control and lower effluents amounts which may be limiting for the analysis. In fact, considering that the size of the

catalyst particles has not changed while the one of the reactors is strongly reduced, these reactors are operated in conditions usually excluded by the concept criteria of the past years.

1.3.2 Parallelization

The size reduction of the testing reactors has another interesting advantage: an easier implementation of parallel reactor systems (example in Figure 3) that allows for evaluating more catalyst options at the same time [6] and replication/determination of the statistical significance of the results. Since the early days of industrial catalyst developments, test rigs have been used in parallel for testing new catalysts. In those cases, all process functions were duplicated, and the investment was proportional to the number of reactors. Recent HTE systems offer ten or more reactors in parallel for the cost of a single unit. The reactors share most of the essential functions like analyzers, mass flow controllers, utilities, furnaces, feedstock, and backpressure controllers. Sharing reduces the investment cost but also the possible experimental space. This sharing is quite interesting for screening tools where feedstock, flow rates, pressure and temperature can be identical for all reactors.

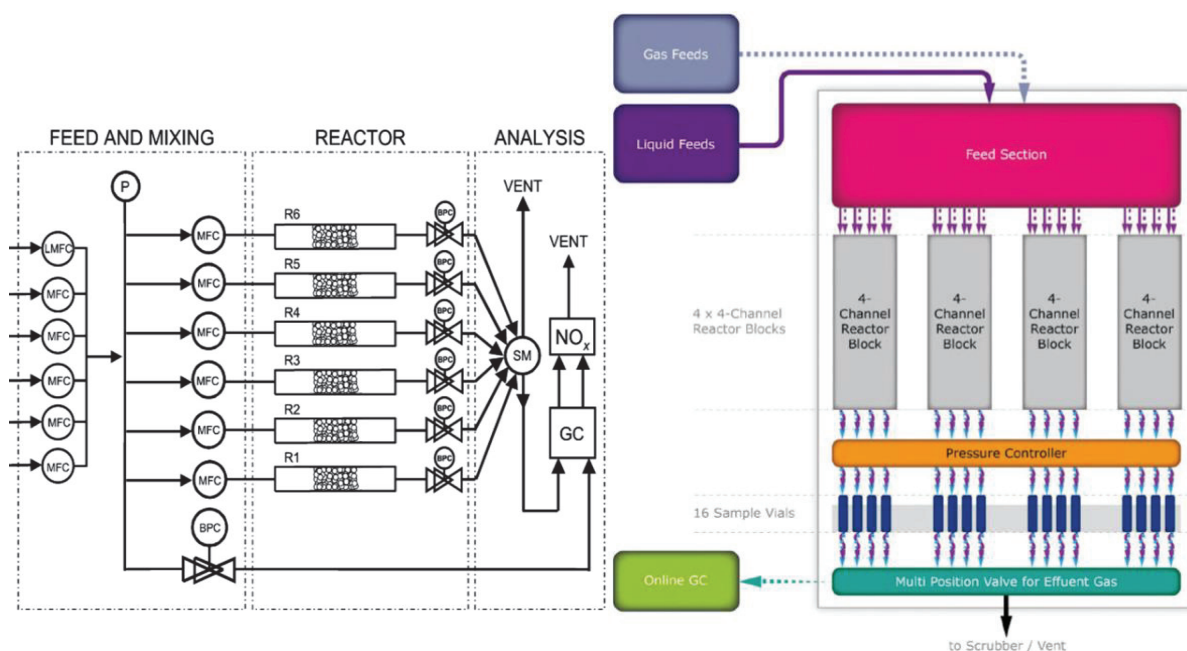


Figure 3. Examples of parallel reactor systems. Left: after [1], right: 16 reactors Avantium FLOWRENCE™ unit

It must be mentioned here that parallel reactor systems have also some drawbacks. For small reactors, only the total flow rate can be precisely controlled but not individual ones: the distribution is performed using pressure drop driven splitters. In some cases (Avantium technology) an additional tuning can be added by regulating a capillary temperature based on the readings of flow rate indicators. The systems are far from perfect and sensible to fouling. This means that, also considering the risks in operating such small reactors, the High Throughput Experimentation units may not (and often do not) give the same results in all reactors. Another drawback is that the G or LHSV between the reactors can only be changed by varying the catalyst mass in the reactors.

1.4 Thesis context

The downscaling has led to screening reactors with diameters of a few millimeters (packed bed millireactors [1, 3, 3, 5–7, 10–14]). These reactors proved to be beneficial for screening purposes.

Due to their much cheaper cost compared to higher scale units, a current question is to investigate their potential for the detailed investigation stage. Can they be used to speed-up the catalysts kinetic measurements through parallelization? As mentioned earlier, the risks are related to the reduced size of the reactors and the reduced superficial velocities that can lead to different flow physics and non-ideality of the reactors. So current questions are:

- What is the behavior of the hydrodynamic descriptors of packed bed millireactors? Are they ideal? Do we need reactor models?
- What is the best way to operate them: what is the effect of particle size, reactor diameter, bed length and porosity filler use?

The thesis will try to answer these questions. The field of interest is the following:

- Reactor diameters $D_r < 7.75$ mm, $L < 25$ cm;
- Catalyst pellets: cylinders, spheres;
- Operation with and without porosity filler;
- Gas-solid (G/S) and gas-liquid-solid (G/L/S);
 - Downflow co-current operating mode.

These ranges have been chosen to focus on an area still unknown or not well explored in the literature, as will be seen in chapter §3. Before presenting the detailed thesis program, we will present a short summary of the physics and models of packed beds and the literature state of the art.

2 Physics and modeling of packed beds

2.1 The particles disposition in packed bed reactors and millireactors

Packed beds are reactors packed with solid catalyst particles (Figure 4). Packed bed millireactors are packed beds with diameters smaller than 1 cm. Considering that the dimensions of the catalyst particles are in the order of a few millimeters, a packed bed millireactor is usually operated with values of $\delta = D_r/d_p$ (reactor/particle diameter) between 1 and 10 while traditional packed beds have bigger values (>1000 for industrial fixed beds).



Figure 4. Packed bed representation

The ratio $\delta = D_r/d_p$ (reactor/particle diameter) is critical to determinate the disposition of the particles in the reactor (Figure 5, spheres case). Different situations can be mainly distinguished according to the D_r/d_p value.

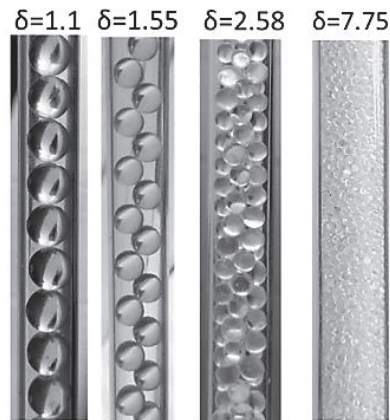


Figure 5. Examples of beads positioning depending on δ

For the smallest values of δ the preferential paths will drive most of the flow. When increasing the value of δ there are fewer preferential paths and dead-zones due to the stochastic position of the particles. This can also be seen when plotting the average porosity profiles along the bed radius (Figure 6). Near the wall, there is a higher average void fraction and hence higher flow rate. This effect goes under the name of “wall effects”. The contribution of “wall effects” is more important for small values of δ [15, 16].

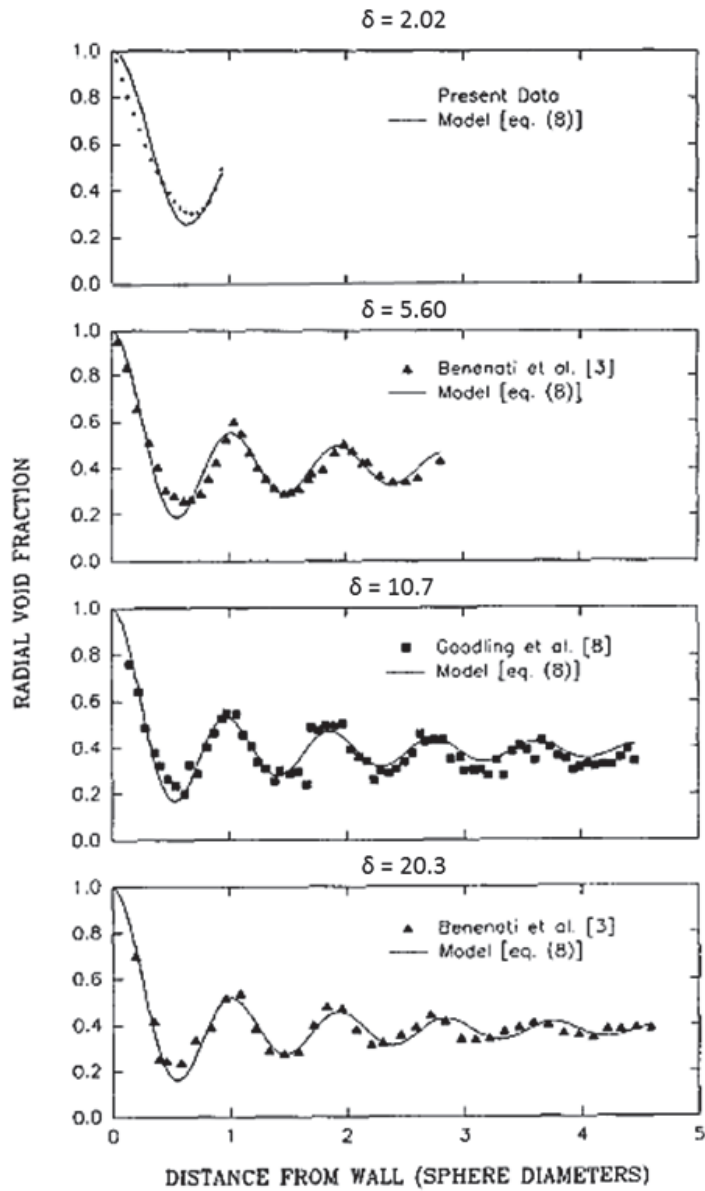


Figure 6. Variation of the porosity profile with the distance from the wall expressed in particle diameters, after [15]

The Equation 2 represented in Figure 6 represents the correlation proposed by Mueller [15, 16] to predict the average radial porosity profiles of packed bed reactors with $\delta > 2.02$:

$$\varepsilon(r^*) = \varepsilon_b + (1 - \varepsilon_b) \cdot J_0(ar^*) \cdot e^{-br^*} \quad \text{Equation 2}$$

in which ε_b is the bulk bed porosity (estimated by the authors as $0.365+0.22/\delta$), J_0 is the Bessel function of the first kind and order 0 and r^* is the dimensionless radial coordinate (the radial coordinate r/d_p). The parameters a and b are expressed as:

$$a = 7.45 - \frac{3.15}{\delta} \text{ for } 2.02 < \delta < 13 \quad \text{Equation 3}$$

$$a = 7.45 - \frac{11.25}{\delta} \text{ for } \delta > 13$$

$$b = 0.315 - \frac{0.725}{\delta} \quad \text{Equation 4}$$

In case of cylinders, the situation is similar. Defining ψ as the ratio between the cylinders length and the reactor diameter and δ' as the ratio between the reactor diameter and the cylinders diameter we have that when ψ is larger than 1 the cylinders align themselves along the reactor axis: this leads to beds with preferential passages between the cylinders and the walls. When ψ is smaller than 1 the cylinders can randomly position themselves in any direction including horizontally (Figure 7). This randomness leads to more uniform beds with less important preferential passages.

$\Psi=1.93$ $\Psi=0.64$



Figure 7. Examples of cylinders positioning depending on ψ

2.1.1 The importance of a reproducible packing

Literature describes the difficulty to achieve a reproducible packing. First, depending on how the pellets are introduced and the reactor vibrated, significant differences can be observed on void fraction. Literature speaks of “loose” and “dense” packings [17, 18]. It is not clearly understood if any difference on void fraction may have an effect on apparent kinetics, neither if identical void fraction packings may have different apparent kinetics due to local random differences [19]. In practice, to minimize risks, the loading procedures aim at a constant void fraction, so that the dense packings are usually recommended in literature.

When fine inert powder is used to fill the porosity left by catalyst particles, as mentioned in paragraph §1.3.1, two families of procedures have been proposed:

- Pack the catalyst pellets, then fill the empty spaces with fine powder [20];
- Fill the reactor with both particle types at the same time [20, 21] with vibrations. Sometimes the filling is done in small increments.

The first method has some variants: blocking the catalyst pellet or not. Both methods have advantages and drawbacks. The first one demands that the fine powder can flow inside the catalyst bed, requiring fine powders (60-200 μm maximum) with the potential risk of blocking some passages (bridges) and not filling up all cavities. The second one allows to use any fine powder granulometry but with the risk that the powder separates from catalyst particles during the free fall [22].

A last aspect worthy to mention, often neglected in literature, is the influence of the bed length/particle diameter ratio on the global void fraction for the reactors with high values of δ (>20). Short and long beds, packed in the same way (loose or dense) and having the same value of

δ , may have a different global void fraction. In particular for the longer bed the global void fraction is likely to be lower [23].

2.2 Packed beds modeling

Packed bed models must consider different physics that can be decoupled:

- Hydrodynamics;
 - Deviation from ideal plug flow behavior;
 - Liquid holdup ε_l : in case of presence of both liquid and gas phase, it is defined as:

$$\varepsilon_l = \frac{V_l}{V_r} \quad \text{Equation 5}$$

in which: V_l is the volume occupied by the liquid [mL] and V_r the volume of the empty reactor [mL]. It represents the fraction of volume occupied by the liquid in the reactor. It gives an indication also of the particles wetting;

- Pressure drop ΔP : the difference of pressure between the inlet and outlet of the reactor. It represents the energy required, per fluid volume unit, to allow the circulation of the fluid;
- Mass transfer;
- Heat transfer.

The pressure drop in millireactors is usually in the order of few kPa, and its effect is considered negligible on possible velocity and density variations. Also the deviation from isothermal operation, that is much smaller than the one in larger reactors [24], is considered negligible. Consequently, in this thesis, these aspects will be not discussed.

2.2.1 Deviation from the ideal plug flow: the axial dispersion model

Packed bed reactors usually exhibit flow behavior close to ideal plug flow. In an ideal plug flow reactor (PFR) all the reactant molecules have the same residence time in the reactor. In the reality, there is always some degree of dispersion due to the diffusion of the molecules and the tortuous path of the fluid flow around the solid particles. The net effect is a residence time distribution for the reactant molecules in the reactor. This affects the apparent performance of the reactor as the longer a molecule stays in the reactor, the more likely it will react.

To consider this dispersion effect, a mass balance equation considering a convective term and a dispersive term is used:

$$\frac{\partial C}{\partial t} = D_{ax} \frac{\partial^2 C}{\partial z^2} - \frac{u}{\varepsilon} \frac{\partial C}{\partial z} \quad \text{Equation 6}$$

in which: C is the concentration [mol/m^3], t is the time [s], D_{ax} is the axial dispersion coefficient [m^2/s], z is the spatial axial coordinate [m], u is the superficial velocity of the fluid [m/s] and ε is the global bed porosity. Closed system boundary conditions are a common choice for the inlet and outlet of the reactor.

The hypotheses behind this model are: 1D geometry and uniform values of velocity and void fraction in the whole reactor. What can happen with packed bed millireactors is that the 1D model may not be pertinent as void fraction distribution is quite different inside the reactor, particularly in the radial direction. An improvement could come from the consideration of two different components of the dispersion: one axial and one radial. Moreover it's worth mentioning that the validity of this model has been assessed for values of bed length/reactor diameter $L/D_r > 20$ [25], so that an eventual application for shorter packed beds has to be confirmed.

It is important to mark the concept that the axial dispersion coefficient should not be confused with the amount of dispersion. The latter is in fact quantified in terms of the dimensionless Peclet (Pe) and/or Bodenstein (Bo) numbers:

$$Pe = \frac{u_i \cdot L}{D_{ax}} \quad Bo = \frac{u_i \cdot d_p}{D_{ax}} \quad \text{Equation 7}$$

in which: u_i is the interstitial velocity (u/ε) [m/s], L is the catalyst bed length [m] and d_p is the catalyst particle diameter [m]. The Peclet number compares the convection and the dispersion in the reactor at the reactor scale. The higher the Peclet number of a system, the closer it is to ideal plug flow. The Bo number has the same meaning at the particle scale.

Many criteria have been proposed to evaluate the importance/negligibility of the dispersion in packed beds. A quite common one is the rule-of-thumb criterion of $Pe > Pe_{min}$ to consider the dispersion negligible. Depending on application, Pe_{min} can be 40, up to 1000 for separation for example. A widely used criterion has been proposed by Mears and then modified by Gierman [26] by looking at the Pe number that would lead to a 10% maximum error in the kinetic parameters estimation:

$$Pe > 8 \cdot n_r \cdot \ln \frac{1}{1-X} \quad \text{Equation 8}$$

in which: n_r is the reaction order and X the desired conversion. This criterion implies that to reach higher conversion higher Pe numbers are required (Figure 8).

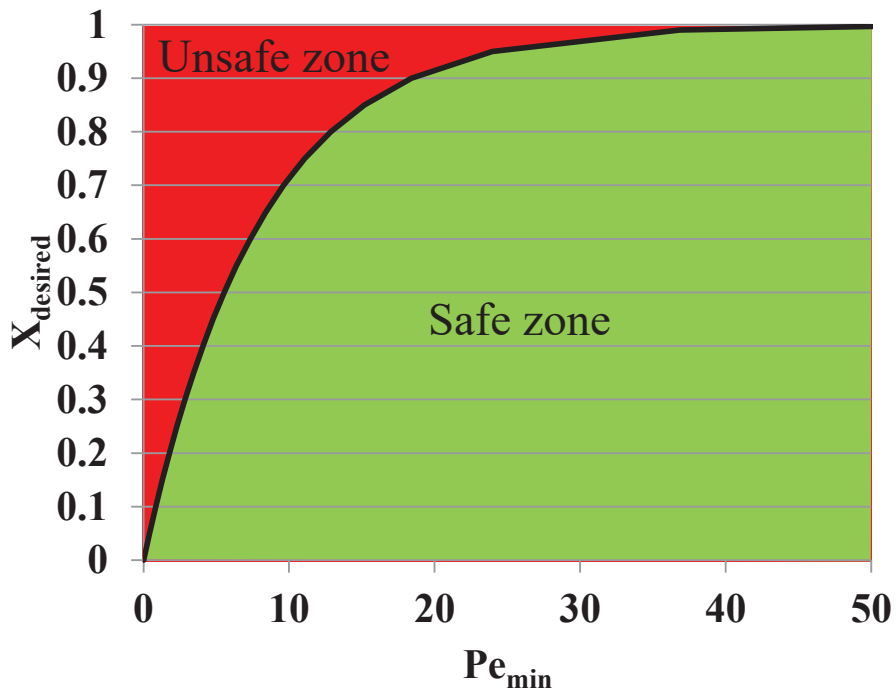


Figure 8. Minimum Pe number for the different levels of desired conversion according to the Mears-Gierman criterion [26] (first order reaction)

2.2.2 External mass transfer limitations

External mass transfer limitations denote the case when the kinetics is so fast (or when the mass transport is slow) that the reaction rate is limited by the transport of reactants from the fluid phase to the catalyst. Mass transfer limitations usually occur between liquid-solid and gas-solid phases, but they can also occur when a reactant needs to pass from the gas to liquid phase. The mass transfer flow is usually modeled by a simple equation, assuming concentration boundary layers called “film” (film theory [27], example in Figure 9).

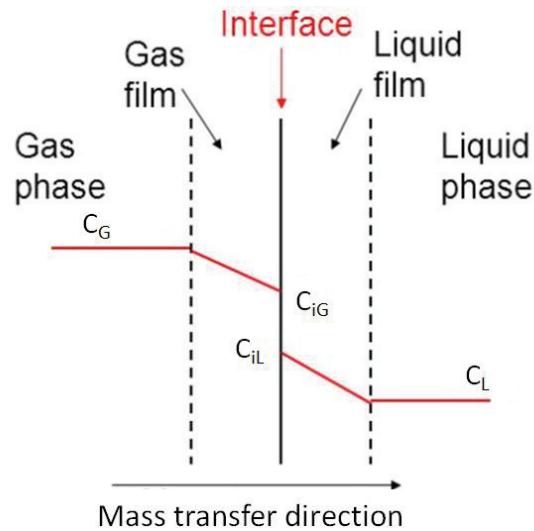


Figure 9. Example of gas-liquid mass transfer scheme

The mass flow is proportional to the concentration gradient and the interfacial area between the two phases. The concentration at the interface for the phases is the one at thermodynamic equilibrium (i.e. Henry equation for gas-liquid mass transfer). The equations can be expressed in the following form:

$$F = k_{ij} \cdot a_c \cdot \Delta C \quad \text{Equation 9}$$

in which: F is the molar flux between the two phases [$\text{mol}/(\text{m}^2 \cdot \text{s})$], k_{ij} is the mass transfer coefficient [m/s], a_c is the interfacial area between the two phases [m^2/m^3] and ΔC is the difference of concentration at the interface between the two phases [mol/m^3] that represents the driving force.

Some empiric correlations have been formulated to evaluate the mass transfer coefficients. They usually correlate the following dimensionless numbers:

- $Re = \frac{\rho \cdot u_i \cdot d_p}{\mu}$, the Reynolds number;
- $Sc = \frac{\mu}{\rho \cdot D_m}$, the Schmidt number;
- $Sh = \frac{k_{ij} \cdot d_p}{D_m}$, the Sherwood number.

in which: ρ is the fluid density [kg/m³], μ the fluid viscosity [kg/(m·s)] and D_m the molecular diffusion coefficient [m²/s]. One of the most used is the Ranz-Marshall equation [28]:

$$Sh = 2 + 0.6 \cdot Re^{0.5} Sc^{0.33} \quad \text{Equation 10}$$

2.2.2.1 Film theory applicability for packed bed millireactors

The Ranz-Marshall equation and other similar correlations have been validated in larger packed beds, but their use is questionable for packed bed millireactors. The film theory supposes that the film thickness is much finer than the characteristic dimension of free flow of the fluid. In packed beds the film thickness (valuable in first approximation as D_m/k_{ij}) is larger or similar to the empty space between two catalyst pellets (or also between the catalyst pellets and the wall in case of packed bed millireactors). In gas-solid conditions, considering two “extreme” flow situations ($Re=0$ and 20), this characteristic length varies between $\sim d_p/2$ and $\sim d_p/5$ (0.2-1.5 mm according to the particles size). The typical values of k_{ls} are, instead, in the range of 10^{-6} - 10^{-5} m/s. Considering $D_m=10^{-9}$ m²/s, the characteristic length of mass transfer is 0.1-1 mm. The characteristic dimension of free flow of the fluid in packed beds is instead on the order of $d_p/6$ (0.2-0.5 mm according to the particles size). The film theory in such cases applies on averaged fields, assuming that the concentration is uniform in a control volume. For larger packed beds it is possible to identify a control volume while for packed bed millireactors significant gradients are present, particularly in the radial direction. In such cases the model may not be applicable [19].

The powder addition to the catalytic bed to fill the remaining porosity in the reactor can improve the situation, reducing the space between the grains. In that case, the model would be applicable, but then new questions arise:

- What is the particle diameter to consider in that case?

- Which are the flow/mass transfer conditions far from the catalyst pellets?

3 Literature review on packed beds

3.1 Introduction

Hydrodynamics in packed bed reactors has been measured and correlated extensively for liquid and gaseous systems over the past few decades. More recently, the attention is focusing on packed bed millireactors. Different types of reactors and packings have been used in order to carry out these studies (examples in Figure 10).

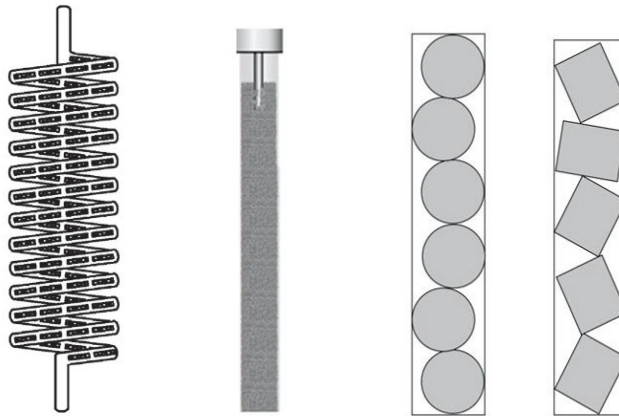


Figure 10. Examples of packed bed millireactors studied by (left to right): Papayannakos et al. [29], Marquez et al. [22], Šolcova and Schneider [13]

In this chapter, we will first resume the flow regimes encountered in packed bed reactors and millireactors. Then the methods for the measurement of dispersion and holdup will be presented. In the end, the relevant literature on dispersion, holdup and inert powder use in packed beds will be resumed. The attention will be focused on packed bed reactors and millireactors operated under gas-solid and gas-liquid-solid co-current downflow conditions.

3.2 Flow in packed bed reactors and millireactors

3.2.1 Single-phase flows

As already explained in paragraph §1.3.1, the small size of packed bed millireactors obliges to operate these reactors at superficial velocities much lower than those of larger packed beds. For this reason, in case of single-phase flows, the flow regimes are mainly laminar while for larger packed beds they are mostly turbulent.

Laminar flow is characterized by fluid particles following smooth paths in layers, with each layer moving smoothly past the adjacent layers with little or no mixing. There are no crosscurrents perpendicular to the direction of flow, nor eddies or swirls of fluids. When increasing the velocity, the flow starts to become turbulent. The transition is usually determined by the value of the Reynolds number (Re , presented in paragraph §2.2.2), which also depends on the viscosity and density of the fluid and the characteristic length of the flow. Depending on the expression of the Re number (different choices are made in literature about the characteristic length of the flow and/or the fluid velocity) pure laminar flow is considered until values around 10. When increasing the Re number at values > 10 we encounter a transition area until a fully turbulent flow is reached. Turbulent flow is a less orderly flow regime, characterized by eddies or swirling packets of fluid particles.

3.2.2 Gas-liquid co-current downflow

For the reactions carried out in gas-liquid phase in the presence of a solid catalyst, the flows are complex and result from a balance between the different physical forces involved: gravity, inertia,

viscosity, and capillarity. The nature of the flow determines how the catalyst will be wetted and fed with the reactants.

A classic typology of co-current gas-liquid flow for large packed beds is the one described by Reinecke [30] and shown in Figure 11. Some regimes appear in upflow and downflow, others only in downflow.

The trickle flow (a) corresponds to a majority of gas phase, with the liquid flowing in the form of a “film” over the catalyst grains. This regime is characterized by a strong inertia of the gas phase and drainage of the liquid by gravity (downflow). The bubble regime, bubble flow, (d) corresponds to a continuous and majority liquid phase and a gas flow in the form of bubbles. This regime is encountered either in upflow, or in downflow with a high flow of liquid. Between these two regimes, there is the pulsed regime (b): large gas bubbles which alternate with caps of liquid. Starting from the trickle flow, when the gas velocity increases, instabilities (waves) develop on the surface of the liquid “film”. This regime (not shown in Figure 11) is called "wavy" regime. When the gas velocity becomes strong enough to tear droplets of liquid from the “film”, the spray regime (c) occurs, and part of the liquid is then dispersed.

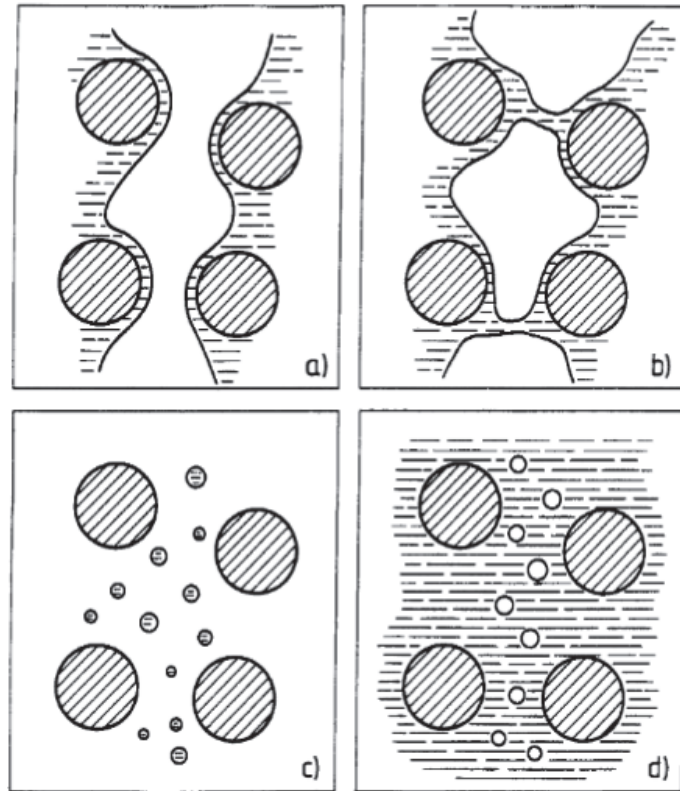


Figure 11. Gas-liquid flow regimes in packed beds [30]

However, packed bed millireactors are operated at velocities much lower than those used in larger packed bed reactors. In addition, the effect of the reactor walls starts to become important, due the much lower values of δ . In these conditions, the flow regimes may be different from those usually observed in larger packed beds. Some studies have focused on the identification of these regimes, but they concern only reactors packed with micrometric particles in which the capillary forces are likely to be predominant.

A first work by Van Herk et al. [31], performed in a 2 mm diameter tube filled with spherical particles of 100 μm over a height of 50 cm, proposes two flow regimes in order to interpret their residence time measurement results:

- A “segregated” regime where the gas phase is continuous and crosses the bed in a shorter time than the liquid;
- A “bubble” regime when increasing the liquid flow, where the gas and liquid phases alternately pass through the porosity of the bed in the form of packets.

Marquez et al. [22] did not observe transition between these two regimes. This can be due to the higher superficial velocities explored by Van Herk et al [31]. According to liquid phase dispersion measurements, a weak interaction between the gas and liquid phases has been observed. The gas phase would then be continuous from one end to the other of the reactor, which is similar to the "segregated" flow described by Van Herk et al [31].

In the work of Matthieu Rolland [19], the observation of the internal part of a packed bed millireactors was carried out via μ -tomography, in order to better understand the arrangement of the liquid and gas phases in this type of reactors. A 6 mm diameter tube, packed with 60 μm diameter glass beads, was firstly immersed in *n*-heptane before being exposed to a small nitrogen flow. The reactor was therefore closed for the measurement. The result is shown in Figure 12. In this figure, the glass beads appear in white, the heptane in grey and the gas in black. There are areas of high porosity in the image, where the glass beads are more widely spaced, mainly filled with gas. On the contrary the areas where the glass beads are more densely packed are mainly occupied by the liquid. The liquid occupies all the dense areas and walls, where the spheres are arranged very regularly. In these areas, the passages size is too small for the gas to "open" the passages.



Figure 12. Packed bed millireactor section obtained via μ -tomography [19]. The glass beads appear in white, the heptane in grey and the gas in black

3.3 The measurement of dispersion and liquid holdup

In this paragraph, the measurement techniques for dispersion and liquid holdup will be presented.

3.3.1 Dispersion measurement techniques

The dispersion is not measured directly but deduced from measurements by applying a model. The measure of the amount of dispersion in the reactors is performed by analyzing the temporal concentration profiles at the inlet and outlet of the reactor when a step or pulse change of a species is performed (Figure 13).

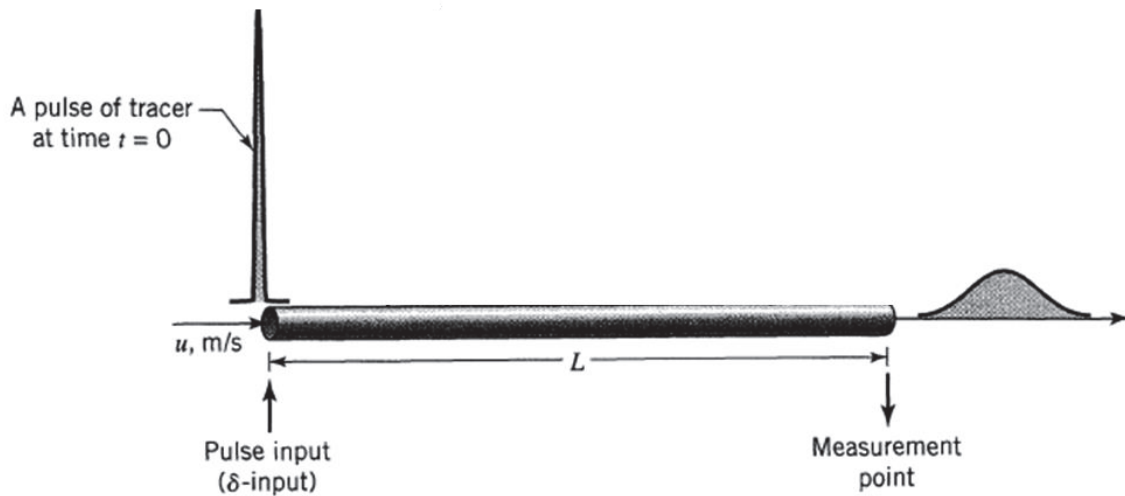


Figure 13. Difference between the inlet and outlet concentration profiles caused by dispersion [32]

Models are then used to predict the outlet curve from the inlet curve. If the axial dispersion model is used, the model parameters D_{ax} (axial dispersion coefficient) and ε (void fraction) are tuned so that the simulated outlet curve matches the experimental one. From them, it is possible to calculate the amount of dispersion in the reactors (Pe and Bo numbers).

Many experimental methods are available. The first choice is the type of tracer to use. This tracer must have some physical property different from the carrier species to be able to quantify accurately its presence while not changing too much the fluid properties when being injected. The detector response must be faster than the signal change. Residence time distributions have been measured on liquids by following the electric conductivity of the liquid [9, 29, 33], the refractive index [34] or colorimetry/absorbance [31]. For gases, mass spectrometry is the most common technique [12]. The tracer, as already said, can be injected by pulse [9, 13, 22, 31, 33, 35, 36] or by step change [12, 29]. If the injection is perfect, there is no need to measure the inlet curve [9, 24, 31]. In practice

the inlet profiles are not perfect and should be measured [33–35]. Measurements are never made exactly at the reactor inlet and outlet and the experimental procedure needs to account for the additional piping and connectors. A more rigorous method is to measure the signal using a shorter reactor or the circuit without reactor [12, 13, 22, 29]. In this way, it is possible to account for the contribution of the rest of the circuit on the signal measured with the reactor of interest.

3.3.2 Liquid holdup measurement techniques

As already said in the paragraph §2.2 the liquid holdup, in gas-liquid-solid operating mode, is the fraction of volume occupied by the liquid in the reactor. It can be divided in two components: external and internal liquid holdup. The internal liquid holdup is the ratio of the volume of the liquid in the pores of porous catalysts to the reactor volume, while the external liquid holdup is the ratio of the volume of the liquid outside the catalyst partially occupying the void volume of the bed to the reactor volume.

The external liquid holdup can be divided into dynamic and static liquid holdup. The dynamic liquid holdup is the free-flowing fraction of the liquid in the reactor. The static liquid holdup is the volume fraction of stagnant liquid and liquid retained between and around the contact points of the catalyst particles after draining. The measurement of the liquid holdup can be based on different techniques. The main ones are:

- Draining method: the dynamic liquid holdup is measured by draining the liquid after inlets and outlets of the reactor are shut off simultaneously [9, 20, 22, 37, 38]. The collected liquid mass is converted to a volume compared to reactor volume;
- Weighing method: the liquid holdup is measured by weighing the reactor while liquid flows through it and subtracting the weight of the dry bed to obtain total holdup or the weight of

the drained bed to obtain dynamic holdup. Subtracting the weight of the drained bed to the weight of the dry bed it is possible to obtain the static holdup + the internal holdup [9, 20, 37, 38];

- Tracer Method: the liquid holdup is measured by measuring the liquid residence time distribution's mean to obtain the total holdup [24, 29, 34, 39].

3.4 Dispersion in packed beds

In this paragraph, the relevant literature on the dispersion in packed bed reactors and millireactors will be presented, analyzing the effects of different parameters.

3.4.1 Effect of the fluid velocity

Single-phase flow reactors

To understand the influence of the fluid velocity on the dispersion, it is useful to consider the limiting case where $u \rightarrow 0$. In this limit condition, the dispersion is determined by the molecular diffusion D_m , more exactly by D_m/τ (with τ being the tortuosity factor). As the velocity of the fluid is increased, the contribution of convective dispersion becomes dominant over that of molecular diffusion and evaluable as $\frac{u_i \cdot d_p}{Bo(\infty)}$ with $Bo(\infty)=2$ [40]. Assuming that the diffusive and convective components of dispersion are additive we obtain:

$$D_{ax} = \frac{D_m}{\tau} + \frac{u_i \cdot d_p}{2} \quad \text{Equation 11}$$

This equation is expected to give the correct asymptotic behavior, in gas and liquid flow through packed beds, at high and low values of velocity. A lot of experimental points have been collected for different reactors, packings and types of fluids and often represented in form of Bodenstein

number against Reynolds number or molecular Peclet number ($Pe_m = \frac{u_i d_p}{D_m}$). For gases, the experimental points obtained for large packed beds ($\delta > 15$) seem to match pretty well with the theoretical curve at low velocities/particle diameters (low Pe_m , Figure 14) while for liquids (Figure 15), the data do not match very well.

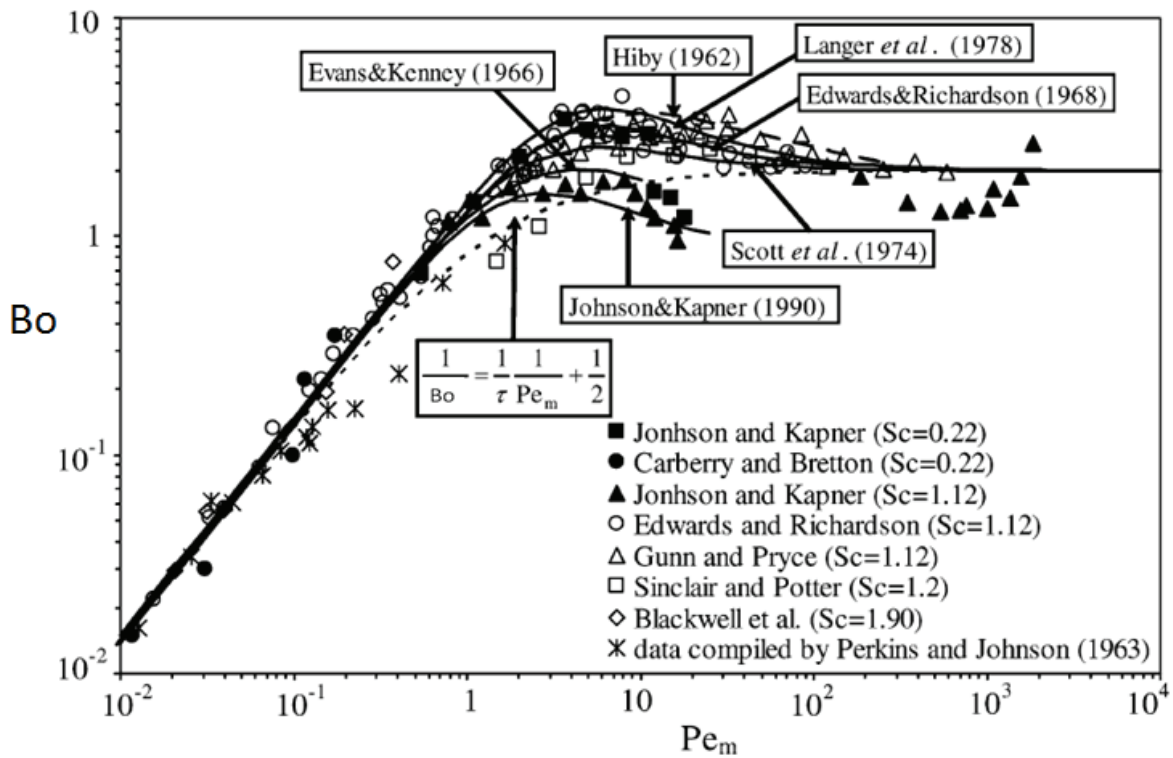


Figure 14. Experimental data on axial dispersion for gas flow, Delgado et al. [25]. The dotted line represents Equation 11

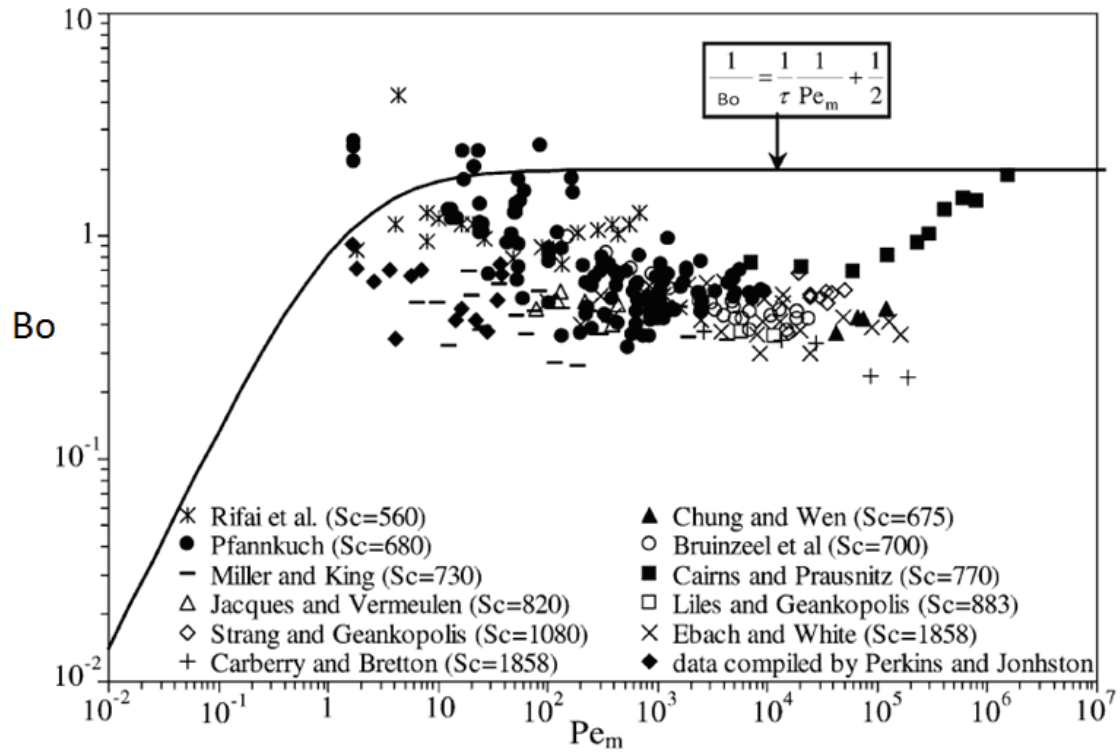


Figure 15. Experimental data on axial dispersion for liquid flow, Delgado et al. [25]. The continuous line represents Equation 11

For the gas-solid case, as it is also possible to see from the Figure 14, some authors have tried to formulate equations to predict the experimental data obtained in the “transition” area ($1 < Pe_m < 100$). These equations seem not to be justified by a particular physical concept but formulated mainly to fit the experimental data. Edward and Richardson [41] have, for example, proposed a model based on the following equation:

$$\frac{1}{Bo} = \frac{0.7}{Pe_m} + \frac{0.5}{1 + \beta/Pe_m} \quad \text{Equation 12}$$

in which β is a constant estimated by fitting the experimental data. This equation has also been used by Scott et al. [42], with a recalculation of the coefficients, to describe the results of their

reactors with $1.1 < \delta < 1.4$. Šolcova and Schneider [13], in order to predict their experimental data, have furtherly modified this equation, proposing the following relationship:

$$\frac{1}{Bo} = \frac{\gamma}{Pe_m} + \frac{\lambda_0 [1 - \lambda_1(d_p/D_r)[1 + \lambda_2(1 - \varphi)]] Pe_m}{\beta + Pe_m} \quad \text{Equation 13}$$

in which: D_r is the reactor diameter [mm], ϕ represents the sphericity of the particles and γ - β - λ_0 - λ_1 - λ_2 are constants estimated by fitting with experimental data. The sphericity is defined, for cylinders, by the following relationship:

$$\varphi = \left(\frac{18(L_{cyl}/D_{cyl})^2}{(1 + 2(L_{cyl}/D_{cyl}))^3} \right)^{1/3} \quad \text{Equation 14}$$

in which L_{cyl} [m] is the cylinder length and D_{cyl} [m] is the cylinder diameter.

The correspondence between the equation and the experimental points seems to be quite accurate (Figure 16).

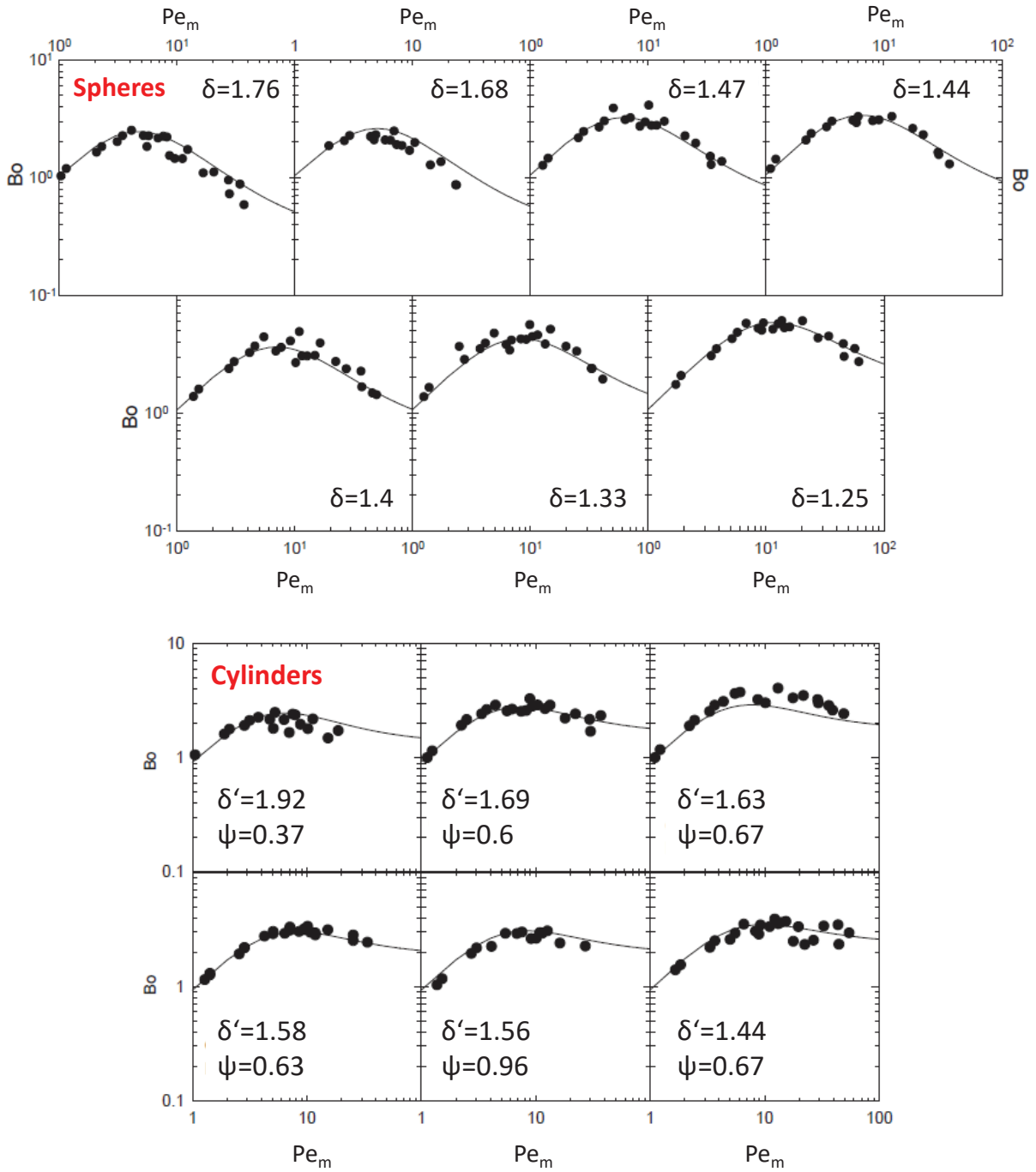


Figure 16. Model and experimental points matching for Šolcova and Schneider: spheres and cylinders case [13]

Gas-liquid co-current downflow reactors

Marquez et al. [22] performed RTD measurements in a packed bed millireactor of internal diameter 2 mm, packed with glass particles of 100 μm . Nitrogen was used as gas phase while methylstearate (tracer) and tetradecane (carrier) were chosen as liquids. Using small gas flow rates (<1 mL/min) and a liquid flow rate of 20 $\mu\text{L}/\text{min}$, they found no effect of the gas superficial velocity on the Bo number.

Other studies have been performed by Papayannakos et al. [29] and Van Herk et al. [31]. In [29] Papayannakos et al. studied the fluid dynamic features of a “string” reactor in spiral form with $D_r=2.5$ mm and bed length 4 m packed with non-porous extrudates of 1.4 mm diameter. Nitrogen was used as gas phase and two aqueous solutions as liquid phase (a carrier and a tracer). Van Herk et al. [31], instead, used a “cold-flow” setup consisting in a column of $D_r=2$ mm, packed with glass spherical particles of 100 μm . Ethanol has been used as liquid phase and nitrogen as gas phase while an injection of 10 μL of colored dye tracer pulse has been used for the dispersion measurement. From these RTD studies it was noticed that the u_g/u_l ratio affected the Peclet number, in particular in the region of low (<30) u_g/u_l values (Figure 17).

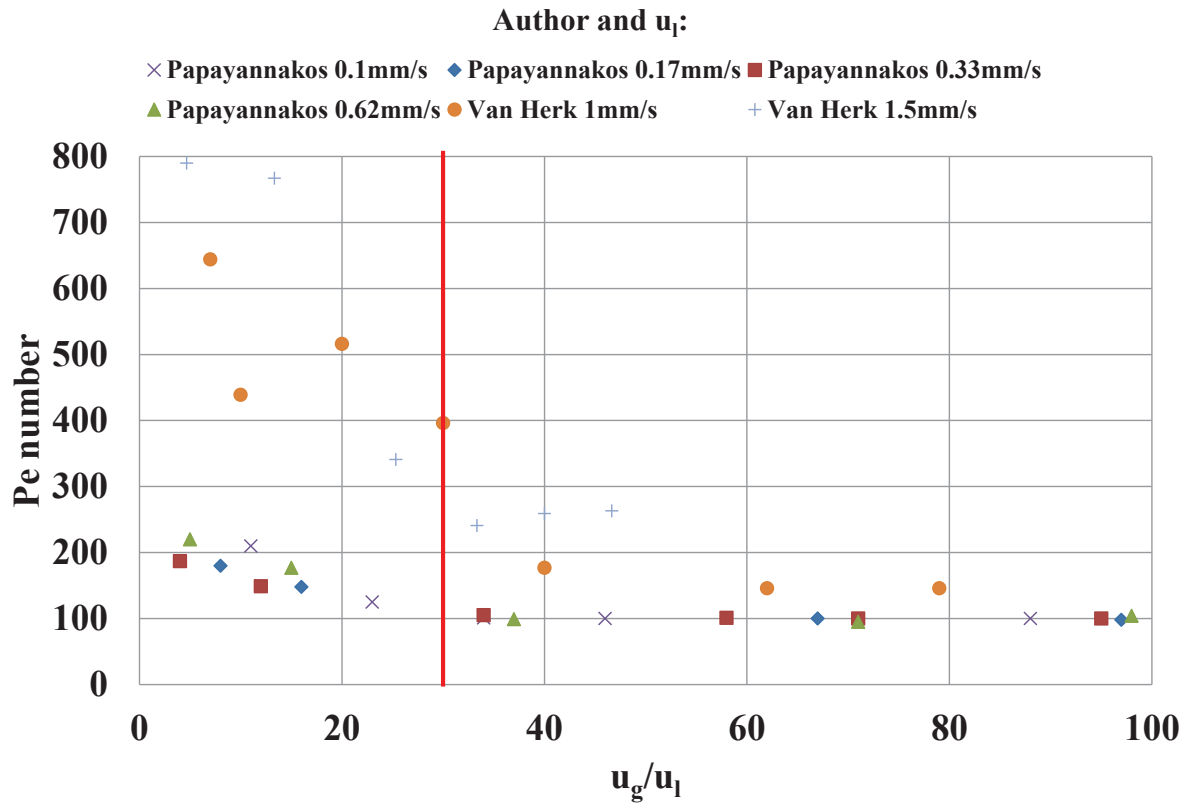


Figure 17. Estimated Pe number versus the gas to liquid superficial velocity ratio [29, 31]. The values reported in the legend are the liquid superficial velocities

The high Pe number values reported in these studies are probably justified by the length of the reactor from Papayannakos et al. (4 m) and by the high flow rates/small particles used from Van Herk et al..

3.4.2 Effect of the reactor/particle diameter ratio

As already mentioned in the paragraph §2.1, the reactor/particle diameter ratio δ is determinant for the disposition of the particles inside the reactor. This ratio also determines the radial profile of the reactor porosity. Wall effects are more important for reactors with small values of δ . For values of δ higher than 15 it is usually considered that the flow is plug flow [43]. That is because, in these

conditions, the wall effects inside the reactors are not anymore influent. However, as already said, in case of packed bed millireactors the typical values are $1 < \delta < 10$. In this domain, published hydrodynamic studies are less abundant and only in the single-phase gas flow domain. Moreover, they often do not compare or do not correctly compare the estimated dispersion by varying the value of δ . The length and the diameters of the reactors studied often exceed the ones of the reactors used in HTE (<30 cm), to which we are interested.

It is possible to mainly distinguish the studies based on the reactor's type they examined: Single Pellet String Reactors (SPSR, $1 < \delta < 2$) or not ($\delta > 2$).

Scott et al. [42] studied the hydrodynamics of a SPSR packed bed reactor with $D_r = 0.94$ cm, $L = 50$ cm and using H_2 , He and N_2 as carrier/tracer gases. They explored the area of $1.1 < \delta < 1.4$ using spheres of different diameter and different surface roughness, concluding that the reactor's behavior is close to the one observed in literature. Also Šolcova and Schneider [13] studied the dispersion in SPSRs packed with non-porous spherical and cylindrical particles (carrier gas: N_2 , tracer gases: H_2 , He, Ar, C_2H_6). Two internal column diameters ($D_r = 7-8$ mm) and a column length of $L = 50$ cm have been tested. They concluded that the value of δ for spheres and δ' and ψ for cylinders were discriminant in terms of estimated dispersion in the reactors, but they did not detail their arguments.

Hsiang et al. [36] carried out experiments on a packed bed reactor with $D_r = 1.72$ cm, $L = 152$ cm, using N_2 as carrier gas and He as tracer. They observed that, using non-porous spherical particles, the behavior of the reactors with $\delta = 1.13$ (SPSR) was less dispersive compared to those of reactors with higher values of δ (no SPSR) where higher dispersion was observed. The comparison was based on the Bodenstein number. When comparing different reactors in this δ range, keeping the same D_r and varying d_p , the comparison of the Bodenstein number (in which d_p is present in the

expression) is not necessarily a correct choice while it's more appropriate to compare the values of Peclet number.

Johnson and Kapner [35] have, instead, studied the effect of δ between 4 and very high values, above 100, on the dispersion of a reactor with $D_r=10$ cm and $L=30.5$ cm, using Ar as carrier gas and He as tracer. They concluded that the larger the δ value the lower the dispersion observed.

A last study that is worth mentioning is the one from Fernengel et al. [44]. Contrarily to the other studies, this work has been carried out via CFD simulations with OpenFOAM[®]. A single-phase gas flow in a SPSR packed with spheres has been simulated exploring the range $1.125 < \delta < 1.75$ ($D_r=0.9$ - 1.4 mm, $d_p=0.8$ mm) imposing a residence time of 1 s for all the reactors. They found a behavior closer to plug flow for the smallest reactor/particle diameter ratio (1.125).

3.5 Liquid holdup

In this paragraph, the relevant literature on the effects of different parameters on the liquid holdup in packed bed reactors and millireactors will be presented.

3.5.1 Effect of the fluid velocities

The effect of the fluid velocities on the liquid holdup has been analyzed by Al-Dahhan et al. [37] in a packed bed with $D_r=2.2$ cm, $L=57.15$ cm, $\delta=14.6$. The results are shown in Figure 18. In the case of $P=3.1$ bar it can be observed that the gas velocity has a very slight decreasing effect on the liquid holdup while the liquid one clearly improves it. When increasing the pressure to $P=35.5$ bar, it can be observed that the gas velocity effect starts to be more important.

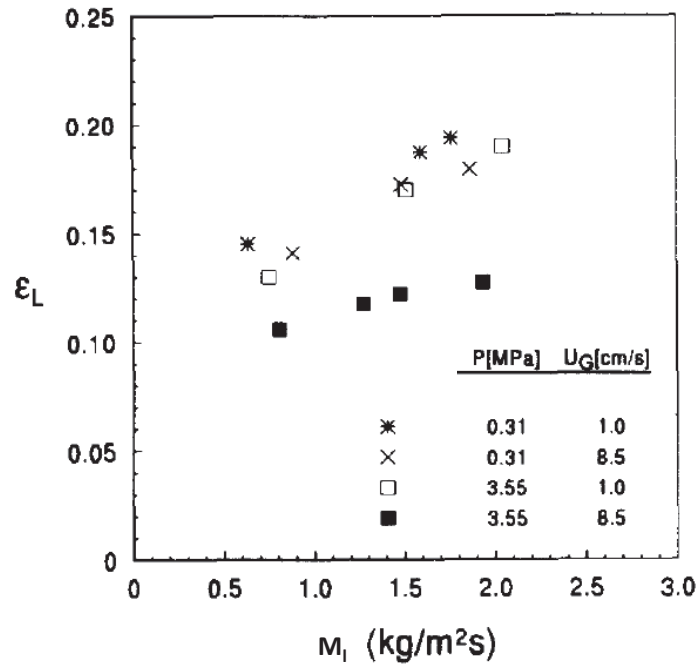


Figure 18. Effect of gas and liquid flow rates/velocities on the liquid holdup. System: hexane/nitrogen, porous spherical silica shell, $P=3.1$ and 35.5 bar [37]

Similar effects of the fluid velocities in packed beds have been found by other authors [20, 22, 29, 45]. It's interesting to mention that the effect of increasing the liquid flow rate is positive also on the catalyst wetting efficiency [45, 46], probably due to the increase of the liquid holdup. However, on the gas flow rate effect there is no unanimous consensus in literature. Herskowitz and Mosseri [47] observed a decrease of the wetting efficiency when increasing the gas flow rate, while Al-Dahhan and Dudukovic [46], Pironti et al. [48] and Kundu et al. [49] found the opposite trend, especially at elevated pressures, as the consequence of an improved spreading of the liquid film around the solid particles despite a lower liquid holdup.

Márquez et al. [22] also observed an increase of the liquid holdup due to the increase of the liquid flow rate in a packed bed millireactor of $D_r=2$ mm packed with 0.1 mm glass particles. It is

interesting to notice that, operating the reactor at very low gas and liquid velocities, they observed larger values of ε_l than those observed in larger packed beds (0.28-0.37 against 0.1-0.2).

For the calculation of the liquid holdup, the correlation of Colombo et al. [50] is generally accepted:

$$\varepsilon_l = 3.86\varepsilon(Re_L \cdot \varepsilon)^{0.565}(Ga_L)^{-0.42} \left(\frac{a_s \cdot d_p}{\varepsilon} \right)^{0.65} \quad \text{Equation 15}$$

in which: ε is the void fraction of the reactor, Re_L is the Reynolds number for the liquid, Ga_L is the Galileo number for the liquid $\left(\frac{\rho^2 \cdot g \cdot d_p^3}{\mu^2} \right)$, a_s is the specific area of the bed [m^2/m^3] and d_p is the particle diameter [mm]. The main drawback of this correlation is that it does not consider the impact of gas flow rate on liquid retention, even if often in literature it has been found small/negligible compared to the liquid flow rate.

3.6 Addition of inert powder

As already explained in paragraph §1.3.1, inert powder addition between millimetric catalyst pellets is a common practice in order to improve the flow distribution and the wetting inside the reactors. This practice is in fact mainly adopted for two-phase (gas and liquid) packed bed reactors. The powder can be used only as porosity filler or, when used in excess, as diluent to improve the heat diffusion and removal (in this case it increases the bed length).

In this paragraph, the literature on the effects of the use of inert powder between millimetric catalyst pellets on dispersion, liquid holdup, and reactive performances in packed bed reactors and millireactors will be presented.

3.6.1 Effect on the dispersion

Studies in single-phase flow reactors are scarce. One of them is the one from Fernengel et al. [44], carried out via CFD simulations with OpenFOAM[®]. A single-phase gas flow in a SPSR has been simulated for a reactor with internal diameter $D_r=1$ mm, packed with spherical particles of $d_p=0.8$ mm with the porosity of the bed filled with spheres 5 times finer. They found, keeping a residence time in the reactor equal to 1 s for both cases, a behavior closest to plug flow when using the fine particles.

Most of the studies are focused on dilution of traditional packed beds in gas-liquid-solid conditions. These studies agree that the use of inert powder improves the hydrodynamics of the reactors. Chander et al. [9] used a reactor of $D_r=2.5$ cm and 70 cm of length, packed with cylindrical pellets of α -alumina of 1.2 mm of diameter. Diluting the catalyst bed, they observed that the smaller is the size of the fines used (SiC, silicon carbide, in this study) the larger is resulting Pe number (Figure 19).

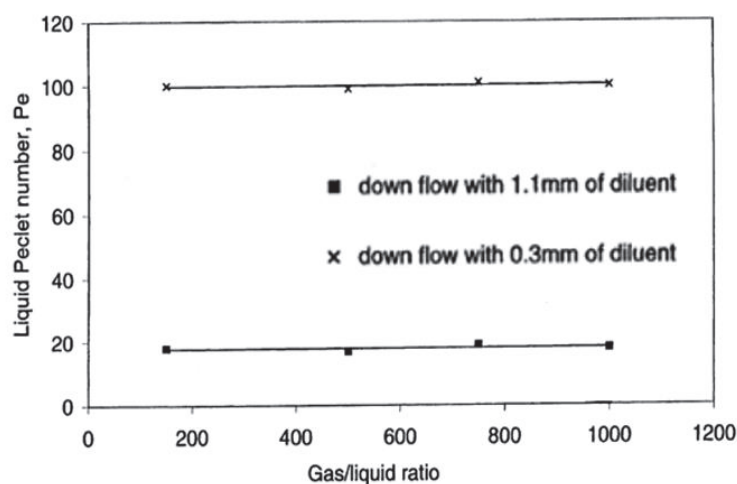


Figure 19. Variation of the liquid Pe number at different gas/liquid ratios (constant LHSV of 0.75 h^{-1}) and two different size of fines (ratio catalyst-diluent 1:1), after [9]

Other studies from Kulkarni et al. and Van Klinken and Van Dongen [38, 51] concluded the same.

The results in literature suggest, as also put forward by Sie [2], that when fine powder is added to a bed of supported catalyst the smaller particle's diameter is the one determining the hydrodynamics.

3.6.2 Effect on the liquid holdup

Al-Dahhan et al. [20] studied the effect of the catalyst dilution with inert powder on the liquid holdup. Porous extrudates of $d_p=1.57 \times 4.3$ mm have been diluted with 0.21 mm inert SiC particles in a reactor of $D_r=2.2$ cm. The fine powder clearly improved the liquid holdup. In particular, as we can see from Figure 20, the higher is the amount of fines used the higher the gain in liquid holdup. In another study [52] they equally observed an increasing particles wetting efficiency when using fines.

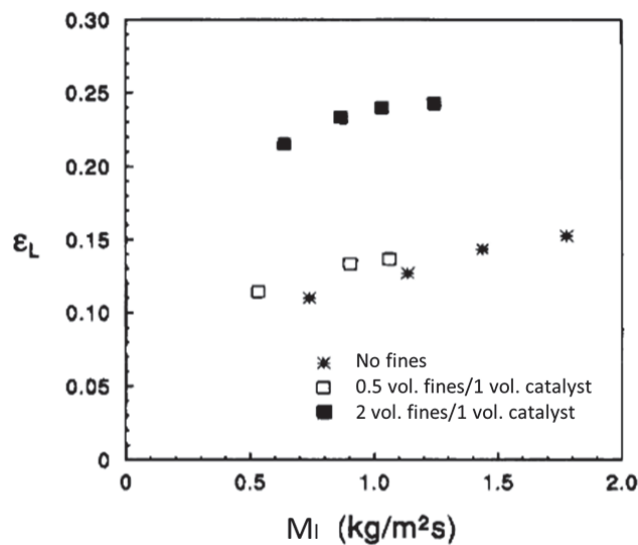


Figure 20. Effect of fines adding in different proportions on the liquid holdup for different liquid mass flow rates ($u_g=1$ cm/s, $P=3.1$ bar) [20]

Also Chander et al. [9], using a reactor of $D_r=2.5$ cm and $L=70$ cm packed with cylindrical pellets of α -alumina ($d_p=1.2$ mm of diameter), experienced an increased liquid holdup value with the use of a smaller size of particles (Figure 21).

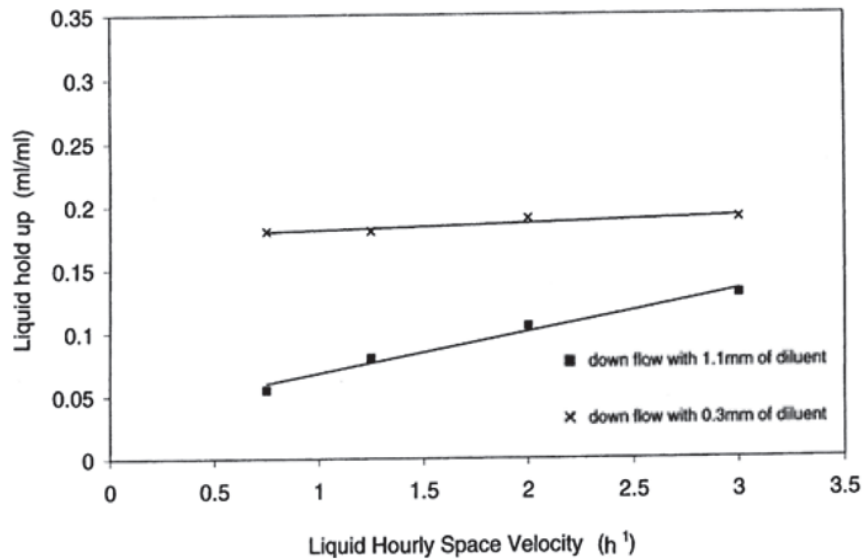


Figure 21. Variation of the liquid holdup with the liquid velocity for two different inert particle size (G/L volume feed ratio=500) [9]

Several works from other authors [9, 38, 45, 51] confirmed these effects and concluded the same.

Also in this case the results in literature suggest, as also put forward by Sie [2], that when fine powder is added to a bed of supported catalyst the smaller particle's diameter is the one determining the hydrodynamics.

3.6.3 Effect on the reactive performances of packed bed millireactors

Single gas flow reactors

Studies in case of single-phase flows in packed bed millireactors are scarce. One of them is the study of Fernengel et al. [44] performed through CFD simulations with OpenFOAM[®]. They

explored the effect of using porosity fillers in a reactor packed with bigger particles on the conversion of an isothermal, irreversible hypothetical first order reaction taking place at the catalytic particles surface. The reactor was a SPSR with internal diameter $D_r=1$ mm, packed with spherical particles of $d_p=0.8$ mm. The porosity of the bed was in one case filled with spheres 5 times smaller than the bigger particles. They found, keeping a residence time in the reactor equal to 1 s for both cases, that the conversion was reduced in the reactor packed with the porosity filler.

Two-phase (gas-liquid) flow reactors

Most of the studies have explored the reactive performances of gas-liquid-solid packed bed millireactors. Using millimetric catalyst particles, they compared the results obtained with and without use of inert powder as porosity filler. The hydrodesulphurization (HDS) reaction of gasoil (slow and exothermic) has been chosen in all the cases here presented.

Moonen et al. [6] used a small-scale 16 parallel-packed bed millireactors system (Avantium FLOWRENCETM unit) to evaluate the performance of a commercial HDS catalyst. Cylindrical catalyst extrudates (1.3x3-5 mm) were loaded as a single string in the reactor tubes (Single Pellet String Reactor, Figure 22). The reactor was made of a tube of $D_r=2$ mm with a length of 55 cm, including a conditioning zone at the top of the reactor. The bed length has been varied between $L=7.5$ and 30 cm corresponding to catalyst bed volumes between 0.3 and 0.6 mL. An inert diluent material was used as a porosity filler for a selection of the beds with extrudates (non-porous ceramic beads, diameter 0.07 mm). This material was added to the reactors after loading the extrudates. Gentle tapping of the tube distributed the inert material over the complete length of the reactor tube, surrounding all the extrudates.



Figure 22. Example of the Single Pellet String Reactor packing [6]

The results showed that there was a small contribution on the performances by adding the porosity fillers (Figure 23).

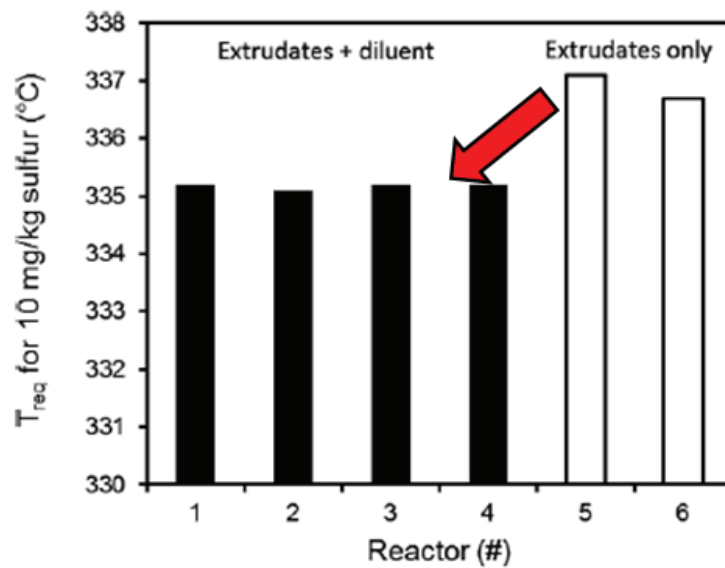


Figure 23. Temperatures to reach 10 mg sulfur/kg with and without inert powder in the bed, after [6]

The temperature necessary to reach 10 mg sulfur/kg was found lower for the reactors with inert powder added, indicating that the reactor performance is better in that case.

A similar result has been found by Bellos et al. [53]. The HDS reaction was studied with a commercial catalyst in cylindrical form with a mean diameter of 1.15 mm, in reactors with $D_r=8$ mm. Diluted and non-diluted beds have been tested, with the use of SiC fine particles with a mean diameter of 0.25 mm. The bed height of the non-diluted and the diluted bed was 14 and 16.9 cm, respectively, while both beds were loaded with 5.5 g of catalyst extrudates. In Figure 24 it can be seen that the bed dilution with inert fines improves the catalytic activity, resulting in a lower outlet sulfur concentration.

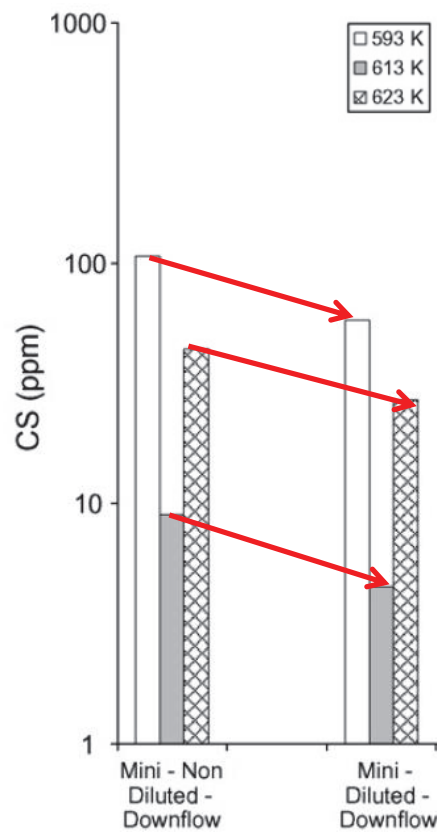


Figure 24. Exit sulfur concentrations for diluted/non-diluted beds at different temperatures, after [53]

A last interesting work is the one of Bej et al. [8] that studied the effect, on the performances of the gasoil HDS reaction, of adding inert silicon carbide (SiC) particles of different size in the catalytic

bed. They used a reactor of $D_r=1.3$ cm, packed with commercial Co-Mo/alumina catalyst trilobes of $d_p=1.5$ mm and length of 4.5-6 mm. The catalyst volume tested was 5 mL. They observed that the value of the apparent rate constant for the HDS reaction increased with the decrease in SiC size. In particular, the effect of diluent size on the apparent rate constant was more prominent for low values of the LHSV (Figure 25).

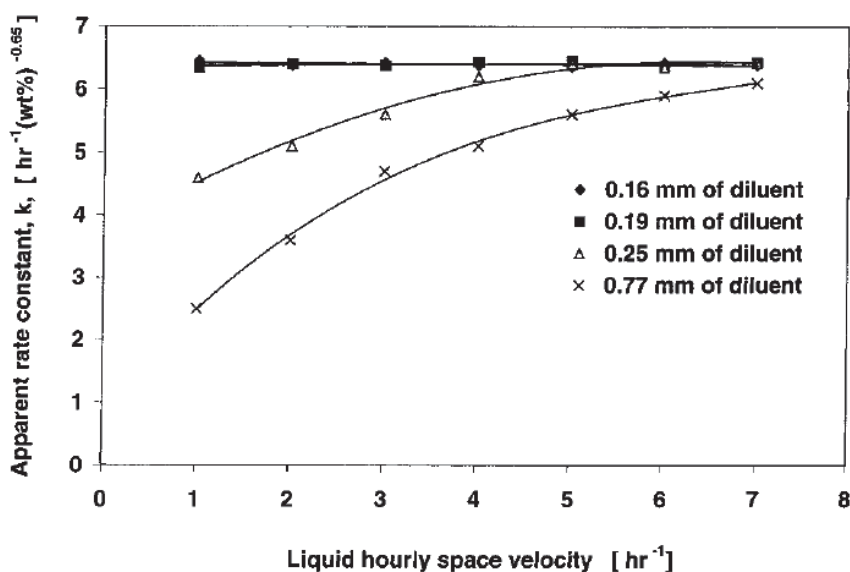


Figure 25. Effect of LHSV on the apparent rate constant of HDS for different sizes of diluents. $T=340^{\circ}\text{C}$, $\text{H}_2/\text{gasoil ratio}=500$ L/L [8]

The size effect is explained by the fact that when the size of SiC particles was about 0.2 mm, the particles could fill up all the void spaces in the catalyst bed. When a larger size of diluent (0.25 mm and above) was used, it could not correctly access the void spaces between catalyst particles. Therefore, the finest SiC particles filled up the void spaces increasing the liquid holdup of the bed. The higher liquid holdup helped in higher wetting, and hence, better use of catalysts. The LHSV effect instead suggest that for low values the drawbacks as channeling, axial back mixing, and wall effect reducing the reactor performance, were eliminated when very fine size of diluent was used.

Overall, it has to be considered that the addition of inert powder changes also the external mass and thermal transfer properties, not only the hydrodynamic properties of the reactors. This means that the different performances cannot be explained by a single reason but that further investigations are needed.

3.7 Literature summary

The studies presented in the literature review allow an understanding of the main parameters affecting the hydrodynamics of packed bed reactors and millireactors and their reactive performances.

The level of knowledge and the missing points in literature are summarized in the following Table 1 and Table 2. The numerical legend in Table 1 and Table 2 corresponds to the degree of knowledge evaluated for the literature analyzed: 0 means no works, 1 means one work, 2 means some studies and 3 means abundant literature.

As already mentioned, in Table 1, for the gas-liquid-solid part, only the studies in downflow co-current operating mode have been considered.

Table 1. Summary of the effects of the different parameters on dispersion and liquid holdup. G/S: gas-solid, G/L/S: gas-liquid-solid. 0 means no works, 1 means one work, 2 means some studies and 3 means abundant literature

	Fluid velocities	δ	Inert powder addition
G/S Dispersion	3	2	1 (CFD)
	<u>Missing knowledge:</u> Incoherent data for high velocities	<u>Missing knowledge:</u> Characterization/comparison for $1 < \delta < 8$	<u>Missing knowledge:</u> No experimental studies found
G/L/S Dispersion	3	0	2
		<u>Missing knowledge:</u> Characterization/comparison for $1 < \delta < 8$	<u>Missing knowledge:</u> Use as porosity filler? Porosity filler size and shape effect?
G/L/S Liquid holdup	3	2	3
		<u>Missing knowledge:</u> Characterization/comparison missing for $1 < \delta < 8$	<u>Missing knowledge:</u> Use as porosity filler? Porosity filler size and shape effect?

Table 2. Summary of the effects of porosity fillers on reactive performances. G/S: gas-solid, G/L/S: gas-liquid-solid. 0 means no works, 1 means one work, 2 means some studies and 3 means abundant literature

		G/S reactors	G/L/S reactors
Porosity filler effect on reactive performances	1	2	
	<u>Missing knowledge:</u> No experimental studies found	<u>Missing knowledge:</u> Physics of the effects? Has the catalyst particles disposition an impact? Porosity filler shape effect?	

In conclusion, the literature presents some aspects not or not completely investigated. Often the works do not concern packed bed millireactors ($D_r < 1$ cm) in the typical range $1 < \delta < 8$. Globally it is also interesting to observe that studies in packed bed millireactors packed with millimetric particles are absent in case of gas-liquid flows.

From these observations comes the need in exploring this area, to better understand and characterize the behavior of these millireactors.

4 Computation Fluid Dynamics in packed beds

Computational fluid dynamics (CFD) uses computers to solve momentum and volume conservation equations. CFD is currently applied to a wide range of research and engineering problems in many fields of study and in industries.

Direct numerical simulation (DNS) is a class of CFD that solve the Navier–Stokes equations with no other assumptions (no closure term for example). DNS is a powerful tool to study packed beds with single-phase laminar flow as it can offer local information on the hydrodynamics and reactive flow, and its use has progressed enormously in the last two decades.

In this chapter, we will analyse the workflow that leads to the simulation of the fluid flows in packed beds and a short review of the actual state of the art.

4.1 The packed bed generation

The first step is the generation of the packed bed. The objective is to predict the position and orientation of all the particles in the bed. Two main families of methods are available:

- The methods that produce packings based on geometric considerations: starting from a random arrangement of points, the principle is to move all the points until the distance between all points is above the particle diameter. This method only works for spheres;
- The mechanical methods, whose the most popular is the discrete element method (DEM), which aims at modeling the particles pouring and settling process by solving the trajectories and rotation of all particles in the simulation using the unsteady equations of the solids dynamics and considering inelastic collisions.

The numerical packed beds produced agree with experimental knowledge, notably the void fraction. The simulations are even able to reproduce the increase of void fraction seen

experimentally when pouring faster the particles. As DEM can manage non-spherical particles, it is the most common way of generating packings [54–56].

The key aspect in DEM is to detect collisions and compute the contact forces (direction and module). At each time step the particle position is updated, and the detection algorithm is run. If two particles are in collision, a force is applied whose module is proportional to the particle overlap. Time steps ought to be small enough so that overlap remains small enough to produce “acceptable forces”. For spherical particles, the collision detection is straightforward, and the force direction is the normal at the contact point. For convex particles, the detection of the contact is done by discretizing the particles (or the surface). The force direction is an issue, and a solution has been proposed by Gilbert, Johnson and Keerthi [57]. The idea is to expand slightly one of the particles and use the direction of motion of the overlapping volume center. Handling non-convex particles is the most complex case, as multiple contacts points must be handled. Complex particle shapes are thus treated as a collection of simpler particles tied together (glued sphere and glued convex [58]).

Many DEM solvers have been developed. Among the open-source ones, we can quote LMGC90 (open source but not user-friendly) or the bullet library of Blender as used by the group of Boccardo et al. [59]. The StarCCM++ package commercialized by Siemens includes a DEM module.

With advances in computing power and numerical algorithms, it has become possible to numerically simulate millions of particles on a single processor. In practice, DEM requires short time steps to prevent excessive particle overlap. That is why using DEM for packed beds of more than 1000 particles is very long.

4.2 Mean age theory and Pe number calculation

CFD can be used to estimate Pe numbers in a very clever way (Liu and Tilton [60, 61]). The method will be presented hereafter.

Residence Time Distribution (RTD) and the degree of mixing (see Danckwerts [62] and Zwietering [63]) are widely used indicators in chemical processes for steady incompressible single-phase flows. As already discussed in paragraph §3.3.1 in an opened reactor, i.e. in a system with an inlet and an outlet, time distribution data are generally obtained by measuring the outlet concentration response following a tracer input.

Experimentally RTD measurements are thus transient experiments. Considering $C_{in}(t)$ the inlet concentration of the tracer and $C_{out}(t)$ the outlet concentration, $C_{in}(t)$ and $C_{out}(t)$ are the computed molar flow weighted averages of the local concentration $C(x, t)$ on the inlet and outlet surfaces.

We note as $E(t)$ the normalized response at the exit plane to a Dirac function $\Delta(t-t_0)$, taking the value $+\infty$ for $t = t_0$ and 0 elsewhere. $F(t)$ is instead defined as the normalized response at the exit plane to a Heaviside function $H(t-t_0)$ taking the value C_0 for $t \geq t_0$ and 0 elsewhere. $E(t)$ is called the Residence Time Distribution (RTD) and $F(t)$ the cumulative RTD:

$$E(t) = \frac{c_{out}(t)}{\int_0^{+\infty} c_{out}(t) dt} \quad \text{Equation 16}$$

$$F(t) = \frac{c_{out}(t)}{C_{out\infty}} \quad \text{Equation 17}$$

where $C_{out\infty}$ represents the concentration at exit at time $t = \infty$. If a Dirac function is used at inlet, then $C_{out\infty} = 0$. If a step function is used, then $C_{out\infty} = C_0$.

As the step function is the primitive of the Dirac function, the step and Dirac responses of a reactor are related by the following relationship:

$$E(t) = \frac{dF(t)}{dt} \quad \text{Equation 18}$$

The mean residence time at the exit is the first moment of E(t):

$$M_{1,out} = \int_0^{+\infty} t \cdot E(t) dt = \int_0^{+\infty} (1 - F(t)) dt \quad \text{Equation 19}$$

Higher moments of E(t) at the exit write as:

$$M_{n,out} = \int_0^{+\infty} t^n \cdot E(t) dt = \int_0^{+\infty} n \cdot t^{n-1} (1 - F(t)) dt \quad \text{Equation 20}$$

The variance σ_{out}^2 between the inlet and outlet is a parameter of importance in the design of chemical reactors, as it provides a measure of the dispersion of the RTD curves. A null variance corresponds to plug flow. It is defined as:

$$\sigma_{out}^2 = (M_{2,out} - M_{1,out}^2) - (M_{2,in} - M_{1,in}^2) \quad \text{Equation 21}$$

Danckwerts [62] showed that similar equations can be applied locally, at any point in the reactor, so that local concentration measurements could be performed to obtain a spatially resolved RTD.

So for a Dirac input response, Equation 20 can be generalized to:

$$M_{n,out} = \frac{\int_0^{+\infty} t^n \cdot C(x, t) dt}{\int_0^{+\infty} C(x, t) dt}$$

Then, following the approach of Sandberg [64] and Spalding [65], Liu and Tilton [60, 61] demonstrated that the n-th moment follows a steady state convection/diffusion equation similar to momentum, energy or species:

$$\nabla \cdot (\mathbf{v}M_n) = \nabla \cdot (D_m \nabla M_n) + nM_{n-1} \quad \text{Equation 22}$$

in which \mathbf{v} is the velocity vector and the term of molecular diffusion D_m is valid in case of laminar flow.

Consequently, we have to consider that the Pe number can be calculated using the following relationship:

$$Pe = 2 \frac{\bar{t}^2}{\sigma^2} = 2 \frac{(M_{1,out} - M_{1,in})^2}{(M_{2,out} - M_{1,out}^2) - (M_{2,in} - M_{1,in}^2)} \quad \text{Equation 23}$$

in which: \bar{t} is the mean residence time [s], σ^2 is the variance [s^2] and M_1 and M_2 are the velocity weighted averages of the first and second moment of the age distribution [s and s^2 respectively]. This means that the Pe number can be computed in any given couple of planes perpendicular to the mean flow.

This method makes it very straightforward to numerically compute the Pe number at a reasonable cost, using only steady state simulations.

4.3 Literature on DNS in packed beds

Most of the research is, at present, based on single-phase flows and reasonably low Reynolds numbers. In the beginning, it has been used by several teams to study pressure drops inside fixed beds in relation to randomness in the packing with a pioneering work of Freund and al. [66]. Works that are more recent focus the coupling of thermal and chemical aspects with internal mass and heat transfer limitations. For example, Partopour and Dixon [67] conducted a resolved CFD simulation on *n*-butane partial oxidation in a fixed bed. They proved that changing the bed configuration could lead to different temperature profiles and different local selectivity patterns. Minhua et al. [55] conducted CFD simulation modeling the coupling reaction-diffusion phenomenon inside fixed beds. The authors also proved a strong heterogeneity of flow field inside the bed (like dead zones behind particles and high-speed channels) and of the radial temperature profile. Another interesting study is the one from Fernengel et al. [44]. They computed the flow in

a Single Pellet String Reactor (SPSR, $1.125 < \delta < 1.75$) to obtain the RTD curves of these reactors (unsteady simulations) and to obtain information on the conversions of a isothermal, irreversible hypothetical first order reaction taking place at the catalytic particles surface (steady simulations).

CFD simulations have been mostly conducted using custom or proprietary codes, but some work has also been done using the OpenFOAM[®] package [44, 54, 59]. Boccardo et al. [59] demonstrated that OpenFOAM[®] is a robust tool to simulate packed bed reactors as the numerical results of the void fraction (bulk and radial distribution) reproduced the experimental data under the operating conditions tested and the pressure drop simulated matched those predicted with the Ergun law. The reason for choosing OpenFOAM[®] is that it is portable, and it offers great parallelization capabilities.

4.4 Synthesis on CFD

Recently the workflow packing generation + CFD has been widely used and validated not only for the prediction of the packing properties but also for the simulation of the fluid flows in packed beds. This means that we can access local information on the flow fields, more difficult to obtain in case of experiments.

We propose to use CFD to calculate Pe numbers in geometries that were not possible to simulate experimentally (lack of variety in particle size).

In our work, the coupling DEM + DNS with OpenFOAM[®] has been chosen. The DEM solver is Grains3D, originally developed by IFPEN and currently by UBC (University of British Columbia, Vancouver). After validation against experimental points, this tool will be used to analyze the $\delta = D_T/d_p$ ratio, fluid velocity, molecular diffusivity, and porosity filler effects on the hydrodynamics of packed bed millireactors.

5 Thesis strategy

The trend in catalyst testing is going towards the miniaturization of the reactors, until reactor diameters of size comparable to the catalyst pellets (packed bed millireactors). Extending the use of the data from these reactors from the screening phase of the catalyst development cycle to more detailed studies (kinetics, scale-up, etc.) is very attractive but the hydrodynamic conditions in these small reactors have not been well explored yet in chemical engineering.

A more detailed characterization is required to improve our knowledge on packed bed millireactors. We will focus on reactors with values of $1 < \delta < 8$ under G/S and G/L/S downflow co-current conditions. The aspects to investigate will be:

- Hydrodynamic features;
- Mass transfer properties;
- Effect of porosity filler addition.

To fulfill these requirements, the strategy of the work has been the following:

- For single-phase gas flow:
 - Residence Time Distribution (RTD) experiments to characterize the dispersion of the packed bed millireactors packed with non-porous spherical and cylindrical particles. Investigation of the effects of bed length, reactor/particle diameter ratio and inert powder addition as porosity filler;
 - Reactive experiments to check the effect of the use of inert powder as porosity filler on the mass transfer properties of these reactors;
 - Computational Fluid Dynamics (CFD) simulations to obtain local information on flow and mass transfer of the packed bed millireactors packed with spherical

particles. Investigation of the effects of bed length, reactor/particle diameter ratio, fluid velocity, molecular diffusivity, and inert powder addition as porosity filler.

- Gas-liquid two-phase flow (downflow):
 - Residence Time Distribution (RTD) experiments to characterize the liquid dispersion, the holdup, and the flow regimes of the packed bed millireactors packed with non-porous spherical and cylindrical particles. Investigation of the effects: fluid velocities, reactor/particle diameter ratio, particles material, and inert powder addition as porosity filler;
 - Reactive experiments to check the effect of the use of inert powder as porosity filler on the mass transfer properties of these reactors.

6 Gas-solid case

In this section, we will explore the use packed bed millireactors for gas-solid applications.

We start with a presentation of the High Throughput Experimentation (HTE) bench that we used to perform reactive tests and that will be our reference in the quest to use screening data to model kinetics.

Next, we include the latest version of a paper submitted to Chemical Engineering Science in July 2020 that includes the experimental work. This work is divided in two parts: a hydrodynamic study through residence time distribution (RTD) experiments and reactive tests aiming at establishing good practices regarding the packing procedures.

In the end, we will present CFD simulations of packed bed millireactors. We first explored their behavior in absence of fine particles, aiming at accurate predictions of Pe numbers. This part is presented under the form of a paper draft to be submitted to Chemical Engineering Science, after review from the other co-authors. A second part deals with the effect of fine particles used as porosity filler on the Pe number and mass transfer.

Other information of interest is included in appendix:

- Vaporization problems in the HTE reactors;
- Deviations from the axial dispersion model in presence of porosity fillers.

6.1 High Throughput Experimentation (HTE) unit presentation

In this work, the reactive tests are performed on the T1504 Avantium FLOWRENCE™ unit, an 8-parallel reactor system (Figure 26). The unit has a common gas and liquid supply for the 8 reactors. The gas supply (H₂, He and N₂) is ensured by Bronkhorst® mass flow controllers (one for each gas). Helium is introduced in the reactors as inert species, to check the gas flow distribution in the reactors during the experiments. A glass chip with capillary channels, all identical in length and internal diameter, creates a pressure drop (>10 bar) that ensures a good distribution of the flows in each one of the 8 reactors. Similarly, the liquid feedstock is pumped from a tank to a Coriolis mass flow controller and then split, by a glass chip, into 8 identical fluxes. The liquid and gas phases are mixed at inlet of the reactors.

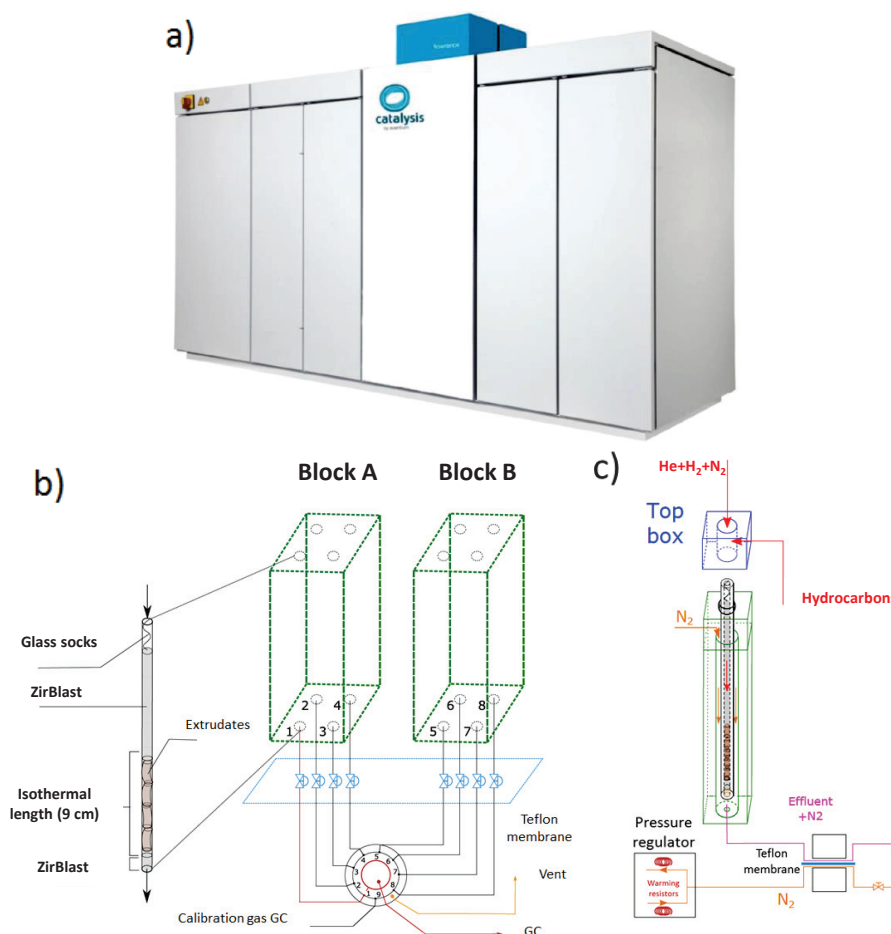


Figure 26. Avantium FLOWRENCE™ unit T1504: a) External view, b) Unit arrangement, c) Single line sketch

The reactors are in quartz, with an external diameter of 6 mm and internal diameters from 2 to 4 mm. The total reactor length is 30 cm, with an isothermal zone¹ of 9 cm where the catalytic bed should be placed. The flow in the reactors is downflow. The reactors are placed in two heating blocks, each of which accommodates four reactors. Thanks to the use of quartz, temperatures up to 750°C can be achieved. Each block is regulated by two thermocouples located one on the top and one on the bottom zone of the reactors.

¹ The isothermal length and location is given by the vendor and was not measured in this thesis.

The vendor recommends using the catalyst in presence of an inert ceramic porosity filler such as ZirBlast/MicroBlast[®] spheres. The reactor part before the catalytic bed may be filled (totally or in part) with inert powder or glass socks (or both) to ensure pre-heating, evaporation of the liquid and homogeneous flow distribution. The vendor also recommends filling the bottom of the reactors with inert powder (to correctly place the catalyst bed in the isothermal zone).

Outside of each reactor, a flow of pressurized nitrogen (N₂) allows for a dilution of the effluents going to the analysis, also preventing an eventual condensation. The pressure is thus identical inside and outside of the reactor which allows the use of brittle materials (quartz) and avoids being impacted by the pressurized equipment regulations. The N₂ flow also enhances heat transfer from the block to the reactors.

The effluent section is temperature controlled to a maximum of 200°C by an oven. Inside the oven there are a parallel pressure regulator and a sample/waste valve. The oven holds the entire effluent section.

The regulation of the reactor inlet pressures is performed with a Teflon membrane system, located downstream of the reactors (after the N₂ dilution). The effluent of each reactor passes on one side of the membrane while a counter-pressure is exerted by a nitrogen stream on the other side. In case the counter-pressure is identical for all reactors an identical outlet pressure for all the reactors is obtained. To obtain identical inlet pressures the counter-pressure is regulated reactor by reactor to account for potential different reactor pressure drops. This individual pressure control is based on changing the pressure of the back-pressure nitrogen stream through a thermal regulation. The thermal regulation allows for a change of the viscosity and thus of the pressure drop. The reactor pressures can be regulated between 0 and 20 barg.

A sampling valve selects the reactor effluent that will be then sent to the gas chromatograph (GC, Agilent Technologies 7890B). Therefore, during an analysis and at a given time t , the effluent (mixed with the nitrogen of the dilution) of only one of the eight reactors is analyzed, the rest is sent to waste. The analysis of the effluents for each reactor takes 30 minutes for the two gas-solid performed reactions (*n*-heptane reforming and methylcyclohexane dehydrogenation) while 27 minutes for the α -methylstyrene hydrogenation.

To summarize, the unit allows for:

- Independent thermal regulation for each of the 2 blocks of 4 reactors;
- Identical flow rate for all the reactors;
- Identical inlet pressure for all the reactors.

Individual flow rates in the reactors are not measured but they are assumed to be identical and steady. The unit seems to be more designed to test identical amounts of different catalysts than to test one catalyst under different operating conditions (all the reactors are exposed to the same flow rates). One may think of using various amount of catalyst in each reactor to change the residence times but that would lead to shorter than 9 cm long reactors. Is that always sufficient?

In this work, the liquid feedstock is composed by hydrocarbons (*n*-heptane, methylcyclohexane or α -methylstyrene).

6.2 Hydrodynamic and reactive experimental tests

Paper submitted to Chemical Engineering Science: “Choosing the right packing in packed bed millireactors under single phase gas flow”

Choosing the right packing in packed bed millireactors under single phase gas flow

Vittorio Petrazzuoli^{1,2}, Matthieu Rolland¹, Adrien Mekki-Berrada¹, Olivier Said-Aizpuru¹, Yves Schuurman^{2*}

1 IFP Energies nouvelles, Rond-point de l'échangeur de Solaize, BP 3, 69360 Solaize - France

2 Univ Lyon, Université Claude Bernard Lyon 1, CNRS, IRCELYON, 2 Avenue Albert Einstein F-69626, Villeurbanne, France

**Corresponding author: yves.schuurman@irceylon.univ-lyon1.fr*

Highlights

- Focus on packed beds with diameter < 1 cm packed with millimetric catalyst;
- Study of hydrodynamics and mass transfer with spherical beads and extrudates;
- Criterion for dispersion effects negligibility in packed bed millireactors;
- Positive effect of the porosity fillers that are recommended in all cases;
- Spherical porosity fillers recommended as they yield lower void fraction.

Abstract

Packed bed reactors with diameters below 1 cm, packed bed millireactors hereafter, are often used to test catalysts. The prospect of using these reactors for catalytic kinetic measurements is quite attractive, but it requires a better knowledge of the flow characteristics of these reactors. This study focuses on the main hydrodynamic features of packed bed millireactors in single phase gas flow. The effects of the bed length, gas velocity, reactor/particle diameter ratio (δ) and use of fine inert

powder as porosity filler are investigated via residence time distribution measurements and reactive tests. When using spherical particles, for values of reactor/particle diameter ratios between $1 < \delta < 3$ the behavior of the Peclet number, Pe , is not monotonous, with risk of lower values for specific values of δ corresponding to large void spaces between the particles and/or between the particles and the walls. For values of $\delta > 3$ higher Pe numbers are observed, in particular at high gas velocities, due to the transition to more uniform packings in which the walls are no more the major constraint. When using cylindrical particles, higher dispersion is observed when the cylinders align on each other along the reactor axis compared to when they are randomly arranged in the reactor. A criterion to calculate the maximum conversion that can be achieved neglecting dispersion effects has been proposed, highlighting the situations in which it has to be used with caution. The dispersion in these reactors can often be neglected. In case the criterion is not fulfilled, filling the porosity of the beds with powder reduces the dispersion. Using porosity fillers in reactors with internal diameters between 2 to 4 mm equally showed an improvement of the conversions for *n*-heptane reforming and methylcyclohexane dehydrogenation reactions, improvement that is attributed to an external mass transfer improvement. Fine and spherical powders fill better the porosity and yield lower dispersion and higher mass transfer.

Keywords: *Fixed bed gas phase hydrodynamics; High-Throughput Experimentation; Single Pellet String Reactor; Residence Time Distribution; Axial dispersion; n-heptane reforming*

6.2.1 Introduction

The development cycle of a catalyst begins with a broad screening of many catalyst formulations, which is followed by a detailed investigation of a selection of the best candidates aiming at gathering sufficient knowledge to design an industrial process and guarantee its performance. The industrial catalyst development is preferably based on the final millimetric size catalyst pellet rather than the powder sample for several reasons. As impregnation may depend on catalyst size, especially if impregnation solutions are very viscous, all catalysts must be prepared with millimetric size pellets to avoid up-scaling the impregnation procedure from powder to pellet. Testing powders requires an additional step of crushing or grinding, which may introduce some variability (i.e. small changes in the powder size distribution, pollution of metallic parts, etc.). A powder catalyst may perform differently in terms of conversion and selectivity in presence of internal mass and/or heat transfer limitations so that a model coupling kinetic and mass and/or heat transport is necessary to predict the millimetric size catalyst performances [2], introducing more uncertainty in the process design. Due to the high financial stakes in the performance guarantees, the model validation on millimetric size catalysts will be anyway performed and it is much more efficient to perform only millimetric catalyst testing than both millimetric and powder testing. Experimental tests on pellets are thus mandatory.

Over decades, packed bed reactors for catalyst testing have faced a reduction in size and have now diameters commonly below 1 cm, the limit being the catalyst pellet size (~1-3 mm). The advantages are the reduction of the development costs and delays: less catalyst [1], lower amount of feedstock and waste [4, 5], better temperature control (higher surface to volume ratio) [5], easier implementation of parallel reactor systems [6] yielding more reactors per unit area and per man-hour and reduced safety issues [6]. The experimentation performed using parallel reactor systems

is known as High Throughput Experimentation (HTE). Recent HTE systems offer 8 or more reactors in parallel for the cost of a single unit. The reactors share most of the essential functions like analyzers, mass flow controllers, utilities, furnaces, feedstock tanks or back-pressure controllers, leading to cheaper units with smaller footprints. An interesting consequence of HTE is the possibility of replication/determination of the statistical significance of the results with reasonable costs and delays.

Packed bed millireactors, like their predecessors, are operated keeping the L- or G-HSV (Liquid or Gas Hourly Space Velocity) similar to those on an industrial scale. This leads to a reduction of gas and liquid superficial velocities by a factor of 10 to 100 compared to industrial reactors which results in an increase in mass and heat transfer resistances, reactors deviating from plug flow behavior and, for gas-liquid flows, in changes of the flow patterns, phase distributions, and catalyst wetting [2].

Additional risks in operating reactors on the order of millimeters of diameter are: accuracy of small catalyst mass measurement, sampling bias when using a very small number of pellets [68], accurate mass flow control (equipment are used in their lower operating range, often a splitter is necessary to achieve low flow rates), lower effluents amounts which may be limiting for analysis and potential packing issues (local reactor porosities, grain size differences and orientation).

As packed bed millireactors produce a large amount of data cheaply, it is quite tempting to use these units for up-scaling purposes. These reactors were validated for catalyst screening, where the important information is the ranking and some indication of the performance gains; in this case it is admissible that the information depends on the reactor size. In these systems, the hydrodynamics is not really an issue as long as the ranking are correct and uncertainties under control. On the opposite, for up-scaling tests, it is preferred that the information is independent of the reactor used.

Even if the reactor characterizations and models can explain and correct the differences, no reactor model is perfect. Any reactor model imperfection will introduce uncertainties in the kinetic model optimization, uncertainties that will propagate in the final industrial design. It is therefore preferred by process engineering that the experimental raw data can be used directly without any reactor model. The goal of this paper is to explore the hydrodynamics and mass transfer performances of packed bed millireactors and give insight on when experimental kinetic results can be upscaled without models.

The reactors used in HTE consist of packed bed reactors with diameters smaller than 1 cm and lengths that usually do not exceed the 20-30 cm. As the catalyst particles are on the order of a few millimeters, a packed bed millireactor is usually operated with values of $\delta = D_r/d_p$ (reactor/particle diameter ratio) between 1 and 5, possibly 10, while traditional packed beds have much higher value (> 1000 for industrial packed beds). In packed bed millireactors, the ratio $\delta = D_r/d_p$ governs the disposition of the particles in the reactor (example in Figure 27 for spheres). For large values of δ there are few preferential paths and dead-zones due to the stochastic position of the particles at the center of the bed and the higher packing density [69, 70], while for the low δ values occurring in packed bed millireactors the global void fraction is higher and radially non-uniform [15] and preferential paths near the walls are important enough to drive most of the flow.

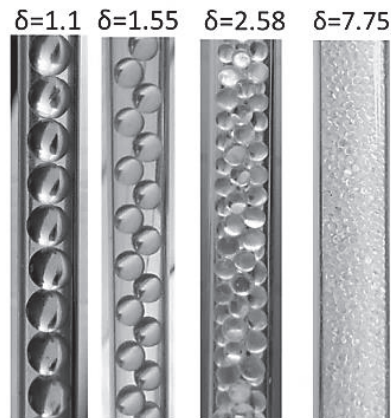


Figure 27. Examples of spherical particles positioning for different δ (D_r/d_p) values

Although the hydrodynamics in gas-solid fixed beds has been measured and correlated extensively in large reactors, the literature for millireactors is significantly less abundant. The packed bed reactor hydrodynamics is usually well described by the axial dispersion model that assumes some degree of dispersion, a quantity physically analog to the diffusion of molecules but augmented by mixing induced by the flow. A common rule-of-thumb [25] recommends values of δ higher than ~ 15 , so that the radial porosity fluctuations near the walls have less impact on the average flow and the packing can be considered as uniform in the radial direction. In this case variations of the fluid velocity, porosity and axial dispersion coefficient in the radial direction can be neglected. Packed bed millireactors do not respect this rule of thumb and another design criterion is required. A study from Johnson and Kapner using a large packed bed ($D_r=10$ cm) [35] analyzed the effect of the δ values ($4 < \delta < 128$) on the hydrodynamics, and concluded that the dispersion decreases with increasing δ . Other studies from Šolcova and Schneider [13], Scott et al. [42] and Hsiang and Haynes [36] showed that low values of dispersion, comparable to larger packed beds, are achieved when δ is below 2.

Another important aspect for correct reactor upscaling is the absence of mass and/or heat transfer limitations during kinetic measurements in lab-scale reactors. External mass transfer in gas phase reactors can be evaluated experimentally by measuring apparent performances under conditions where the reaction rate is governed by mass transfer. This process requires knowledge of the kinetics, which can only be deduced in absence of mass transfer limitations. To circumvent this loophole, the usual way is to measure the kinetics in another type of reactor, like stirred-tank reactors. In this study, we opted to study the effect of the packing on mass transfer by changing the hydrodynamics through the filling of the reactor's void space with fine powder. This approach will help to answer other pending questions about HTE reactors: should we use porosity filler? And what type (size and shape)?

In this experimental work we report the effect of different parameters on the hydrodynamics of packed bed millireactors: bed length (L), gas superficial velocity (u), reactor diameter (D_r), reactor/particle diameter ratio (δ) and the use of porosity filler. We then propose a criterion to estimate the maximum conversion that can be achieved neglecting dispersion effects. In a second part the influence of a porosity filler on the performance of gas-solid reactions is investigated.

6.2.2 Materials and methods

In this part, we present the materials and methods for both the residence time distribution (RTD) measurement and the reactive tests.

6.2.2.1 RTD measurements

Axial dispersion model

The axial dispersion model is an adequate description of single phase flow in semi-infinite packed beds [25] ($L/D_r > 20$). One of the objectives is to assess if this model is suitable to describe the hydrodynamics of packed bed millireactors with small values of δ and $L/D_r < 20$.

The model consists of a 1D mass balance equation corrected with a dispersion term (Equation 24):

$$\frac{\partial C}{\partial t} = D_{ax} \frac{\partial^2 C}{\partial z^2} - \frac{u}{\epsilon} \frac{\partial C}{\partial z} \quad \text{Equation 24}$$

in which z is the axial coordinate along the bed [m], C is the concentration of the gas phase species [mol/m^3], D_{ax} the axial dispersion coefficient [m^2/s], u the superficial gas velocity [m/s], ϵ the void fraction of the reactor and t the clock time [s]. Closed system boundary conditions have been chosen for inlet and outlet of the reactor.

The “amount” of dispersion is quantified in terms of the dimensionless Peclet (Pe) and/or Bodenstein (Bo) numbers:

$$Pe = \frac{u_i \cdot L}{D_{ax}} \quad Bo = \frac{u_i \cdot d_p}{D_{ax}} \quad \text{Equation 25}$$

in which $u_i = u/\epsilon$ is the gas interstitial velocity [m/s], L the bed length [m] and d_p the particles diameter [m]. The Peclet number compares the convection and the dispersion in the reactor at the reactor scale. The higher the value of the Peclet number, the better the reactor can be described by (ideal) plug flow in which all the molecules have the same residence time in the reactor. The Bo number has the same meaning at the particle scale.

For cylinders d_p is instead the equivalent volume/surface ratio sphere diameter (Equation 26).

$$d_p = \frac{3D_{cyl}L_{cyl}}{D_{cyl} + 2L_{cyl}} \quad \text{Equation 26}$$

in which D_{cyl} is the cylinder diameter [m] and L_{cyl} the cylinder length [m]. When using powder as porosity filler the particle diameter d_p is the powder diameter as it governs the hydrodynamics [2].

RTD set-up

We estimated the axial dispersion coefficient in the reactors by analyzing the transient concentration profiles of a tracer species after a step change. Blank profiles have been measured without the reactors, in order to take into account the dispersion coming from the upstream and downstream equipment in the future analysis [13, 22]. The tracer is helium in nitrogen with a step change from pure nitrogen to a 50-50% mixture (vol) of helium and nitrogen. The gas concentration is measured using mass spectrometry (MS), a very common technique for gas phase RTD measurements [12].

The flow diagram of the RTD setup is shown in Figure 28. A remote controlled 4-way valve (Vici valve from Valco Instruments Co. Inc.) switches the gas flow through the reactor from nitrogen (circuit B) to a mixture of 50% vol. nitrogen and 50% vol. helium (circuit A). The gases are delivered by mass flow controllers (Brooks Instrument). A needle valve is used on the vent gas line to match the reactor pressure drop to eliminate the overshoot in the transient response. A mass spectrometer (INFICON) measures the temporal concentration profile of the tracer. The valve position change ($t=0$) is recorded by the mass spectrometer with a time resolution of 85 ms. At the end of the test, the temporal concentration profiles and the switching time are available on the same time track. The exact switching time will be the recorded time, with a time lag of maximum 85 ms.

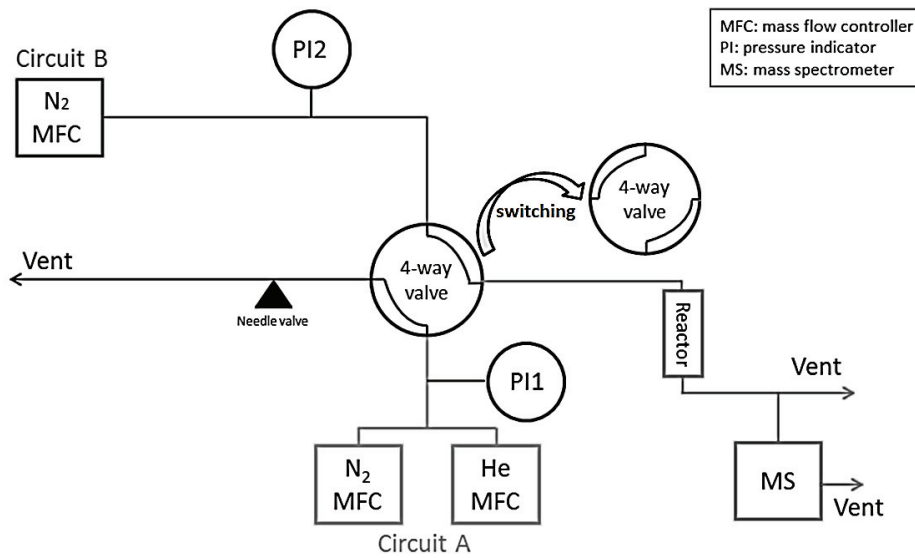


Figure 28. RTD experimental setup scheme

In this setup, the temporal concentration profiles also account for dispersion of the lines, the valve, and the MS inlet device. As their contribution to the dispersion does not depend on their order, we measure the system response without reactors and use these temporal profiles, called “blanks” afterwards, as the inlet profile for the axial dispersion model.

To improve the accuracy of the measurements, the mass flow controllers and mass spectrometer signal were regularly calibrated. The calibration has been performed using mixtures with known proportions of helium and nitrogen (from 0 to 50 % in volume of helium) and recording the signal variations. Then, an interpolating curve is used to calculate the helium molar fraction according to the MS signal value. The mass to charge ratios analyzed for helium and nitrogen are respectively 4 and 28 m/z.

RTD measurements without reactors have been repeated regularly during the test campaign and showed no significant deviation. All RTD measurements have been repeated 5 times (Figure 29).

The curves were found to be identical except for a time lag induced by the MS time resolution (85 ms). In the model analysis, the median curve has been retained. The helium MS response signals presented some noise at high concentration levels.

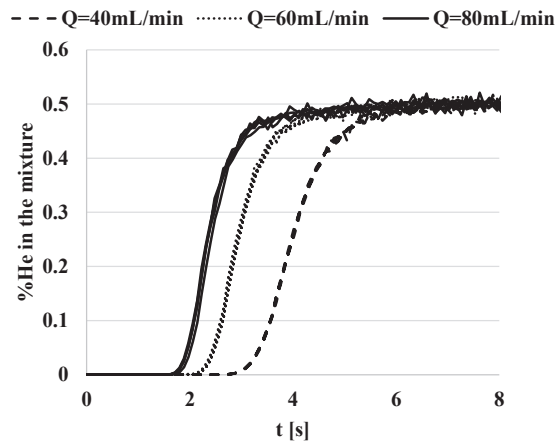


Figure 29. Evolution of the %He measured at the reactor outlet after a step change: three flow rates and five measurements for each flow rate. Reactor with $L=8.8$ cm, $D_r=5.8$ mm and $d_p=2 \times 5$ mm glass cylinders

RTD data analysis

The convection – dispersion equation (Equation 24) was solved in a numerical model used to propagate the inlet tracer concentration profiles through the reactor and predict the outlet tracer concentration profiles. The model uses finite differences and an adaptive Runge-Kutta solver. Grid size and time step have been refined to ensure grid and time step independence.

For each reactor configuration and condition, the model is used to fit the two unknown parameters: D_{ax} , the axial dispersion coefficient, and ε , the void fraction. They have been fitted so that the simulation output matches the experimental “reactor” outlet temporal profiles when inputting the blank temporal profiles (Figure 30).

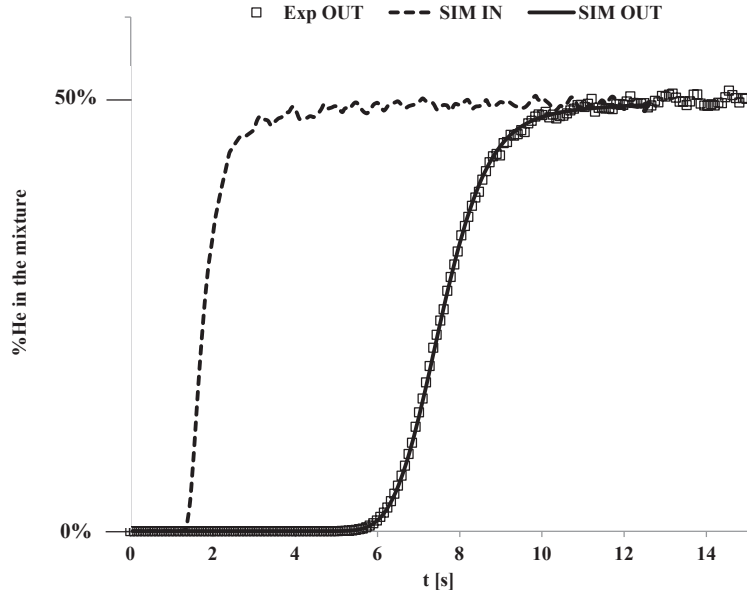


Figure 30. Fit of a reactor experimental curve using the axial dispersion model

More precisely, the value ε has been first estimated at the lowest flow rate (the longest residence time), to ensure the highest accuracy and this value has been used for the other flow rates of this particular reactor. The value of D_{ax} is estimated by minimizing the relative square error (RSE) between experimental and numerical output (Equation 27).

$$\sum_i \frac{(y_i^{mod} - y_i^{exp})^2}{y_i^{exp2}} \quad \text{Equation 27}$$

in which y_i is the helium molar fraction at the time i . The summation in Equation 27 is considered for helium mol fractions between 0.05% and 25%. The 0.05% threshold aims at reducing the impact of the “background MS noise” at very low concentration. The upper limit at 50% of the concentration change is used to reduce the noise observed at high concentration (see signal’s tail in Figure 29). We have defined (arbitrarily) the uncertainty range of D_{ax} as the upper and lower

values of D_{ax} such that the value of the maximum relative error on any single point is lower than 20%, so $\max_i \left(\frac{y_i^{mod} - y_i^{exp}}{y_i^{exp}} \right) \leq 20\%$.

Operating conditions

The following conditions have been used to measure the dispersion in gas-solid packed bed millireactors:

- The reactor diameters varied from 2.0 to 7.75 mm and the lengths from 8.7 to 25 cm;
- The gas flow rates varied from 40 to 120 mL/min at 28°C. The corresponding inlet superficial velocities are from 0.014 to 0.21 m/s;
- Glass or ceramic non-porous catalyst pellets with cylindrical and spherical shape (1-7 mm) were used to pack the reactors;
- Inert powders (silicon carbide and commercial ZirBlast/MicroBlast® ceramic powders [71]) of different sizes were added in some cases to fill the porosity of the beds.

A thin layer of glass wool has been used at the top and bottom of the reactor to keep the particles in position inside the reactor.

6.2.2.2 Reactive tests: unit description and experimental conditions

The reactive tests have been conducted in a high-throughput catalytic testing setup (Avantium FLOWRENCE™) equipped with 8 parallel fixed bed reactors between 2 and 4 mm internal diameter and a catalyst capacity of around 100 mg per reactor. The products composition has been measured via on-line gas phase chromatography. Helium has been introduced in the reactors as an internal standard to check the outlet flow rates. Conversions have been calculated as $X(\%_{mol}) = 100 * (1 - F_{out}/F_{in})$, where X is the conversion and F is the molar flow rate of the reagent.

Tests have been performed on two reactions with different thermicity:

- *n*-heptane (nC7) reforming, almost a-thermic ($\Delta H_0 \approx 0$ kJ/mol);
- methylcyclohexane (MCH) dehydrogenation, highly endothermic ($\Delta H_0 = 204.8$ kJ/mol [72]).

Both reactions involve the transformation of a C-7 molecule at the surface of a naphtha reforming catalyst. The same catalyst has been used for both reactions. Extrudates Pt/ γ -Al₂O₃-Cl and spherical beads Pt-Sn/ γ -Al₂O₃-Cl have been tested. The extrudates have a diameter of 1.4 mm and a length of 5±2 mm. The beads have a mean diameter of 1.8 mm. The catalysts have been reduced *in situ* for two hours at 500°C under H₂ flow before exposition to the gaseous feedstock.

The following powders were used as porosity fillers: 60 μ m SiC, 150 - 200 μ m SiC, 60 μ m MicroBlast®, 150 - 200 μ m ZirBlast® and 300 - 400 μ m ZirBlast®. We will refer to the 60 μ m MicroBlast® powder as ZirBlast® for convenience, as it is the same material. Experiments over the extrudates or beads and the equivalent packing with porosity filler were always run in parallel. This allowed to minimize the effect of catalyst activation or deactivation on the results, as the difference in conversion between two packings is analyzed, which was always rather small (< 6-7 conversion points).

The experimental conditions for the two reactions are presented in Table 3 and Table 4.

Table 3. Ranges of operating conditions explored in the nC7 reforming

Condition	Range	Unit
Reactor diameter	2;3;4	mm
Temperature	450-515	°C
Total pressure	10	barg
H ₂ /nC7	10	mol/mol
WHSV	5-15	g _{nC7} /(h·g _{cat})
Conversion	45-90	%

Table 4. Ranges of operating conditions explored in the MCH dehydrogenation

Condition	Range	Unit
Reactor diameter	2;4	mm
Temperature	330-350	°C
Total pressure	10	barg
H ₂ /MCH	5	mol/mol
N ₂ /H ₂	1	mol/mol
WHSV	5-17.5	g _{MCH} /(h·g _{cat})
Conversion	40-80	%

To explore external mass transfer limitations, we have chosen conditions in which the reaction kinetics is fast, mainly high temperature.

6.2.3 Results and discussion: RTD experiments

6.2.3.1 Plug flow behavior

The analysis of the temporal concentration profiles of the RTD measurements has confirmed that the axial dispersion model is adequate for the description of the hydrodynamics of packed bed millireactors with small values of δ (Figure 30). The experimental data collected using different reactors and particles, under different flow rates, spanning a range of δ from 1.1 to 7.75, are in line with the literature already published for larger packed beds (Figure 31).

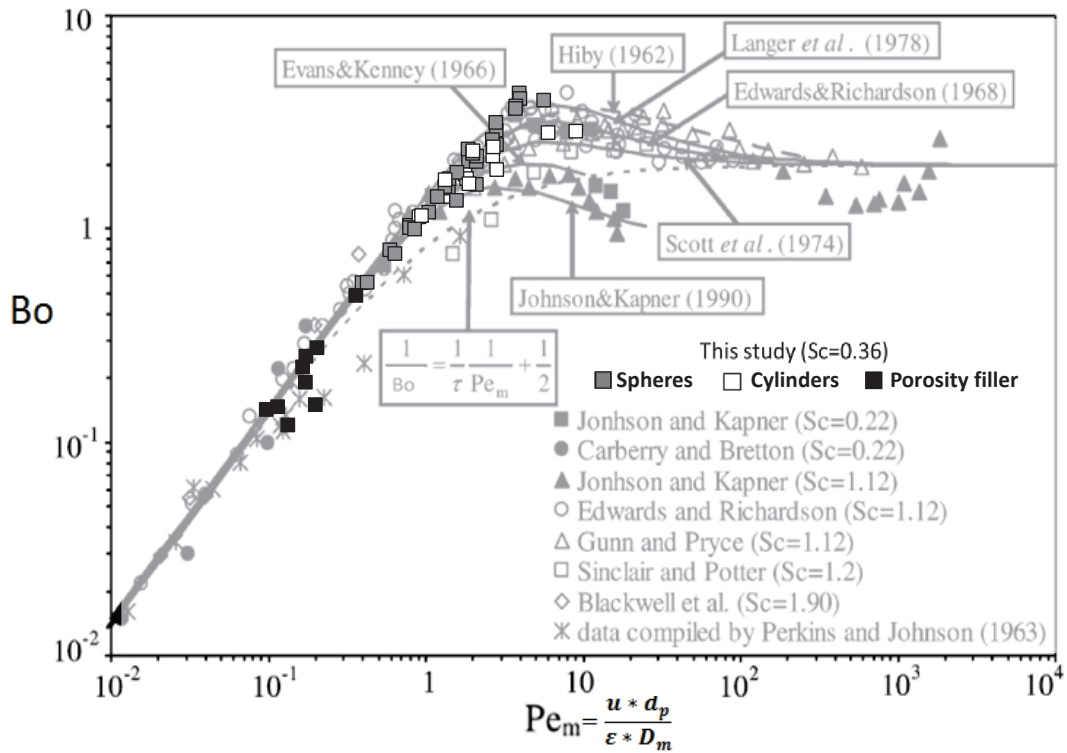


Figure 31. Summary of the literature data on dispersion in packed beds from Delgado [25], with the addition of our experimental data points. Grey: spheres, white: cylinders, black: spheres or cylinders + porosity filler

In Figure 31, Delgado included a theoretical curve derived by assuming additive contribution of two asymptotic dispersions: at very low velocity, the dispersion is equal to molecular diffusion divided by the tortuosity of the packed bed, while at high velocity each particle acts as a perfect mixer so that $Bo(\infty)=2$ [40]. This leads to Equation 28 and Equation 29:

$$D_{ax} = \frac{D_m}{\tau} + \frac{u \cdot d_p}{\varepsilon \cdot 2} \quad \text{Equation 28}$$

$$\frac{1}{Bo} = \frac{1}{\tau} \frac{1}{Pe_m} + \frac{1}{2} \quad \text{Equation 29}$$

At low $Pe_m \left(\frac{u_i \cdot d_p}{D_m} \right)$ number values, the dispersion is mostly due to diffusion corrected by the bed tortuosity. In all the experimental literature, measurements of Bo numbers overestimate this asymptotic behavior for intermediate values of the Pe_m number ($Pe_m \sim 1-10$). Our measurements are in both the molecular diffusion zone and in the overestimation zone. We measured high values of Bo ($Bo > 3$) for reactors with low values of δ . This is in line with the values reported, for higher gas velocities, by Šolcova and Schneider [13], Scott et al. [42] and Hsiang and Haynes [36].

Some authors have modified the Equation 29 in order to predict their experimental data, in particular for the overestimation zone (i.e. Edwards and Richardson [73], Scott et al. [42] or Šolcova and Schneider [13]).

6.2.3.2 Effect of the bed length

In the explored experimental domain, Bo and thus D_{ax} are independent from the length of the reactor (example in Figure 32): the Pe number is proportional to the length. For larger packed beds, Han et al. [74] found the same result for values of $Pe_m \leq \sim 700$ (but for values of $L/D_r > 70$).

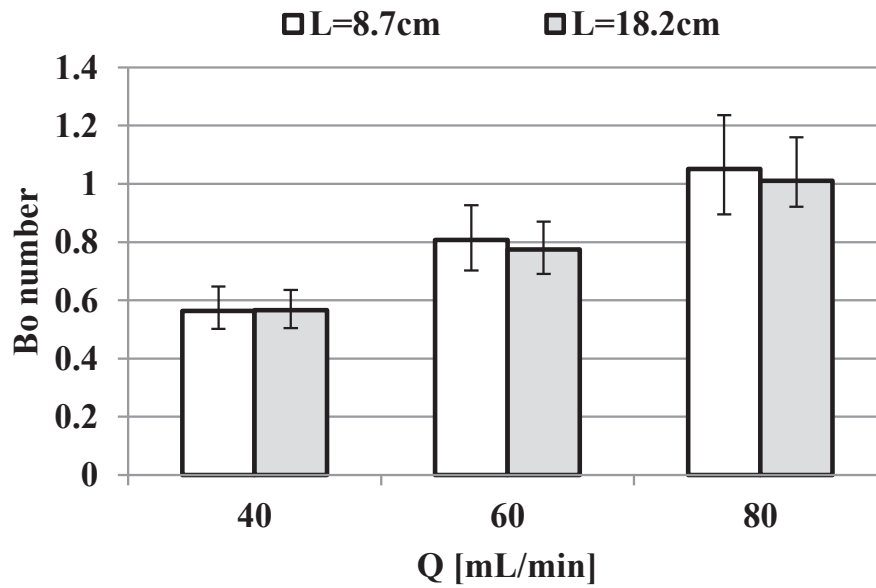


Figure 32. Variation of the Bo number for reactors with $D_r=7.75$ mm and $d_p=1$ mm spheres, all other parameters identical

6.2.3.3 Effect of reactor/particle diameter ratio

Several RTD measurements have been performed in the same reactor ($D_r=7.75$ mm, $L=18.2$ cm), filled with spherical particles of diameters ranging from 1 to 7 mm. The values of Pe number and ϵ are shown in Figure 33 for two values of the superficial gas velocity: 0.014 m/s and 0.028 m/s. The value of the Pe number is increased but not doubled when doubling the gas velocity.

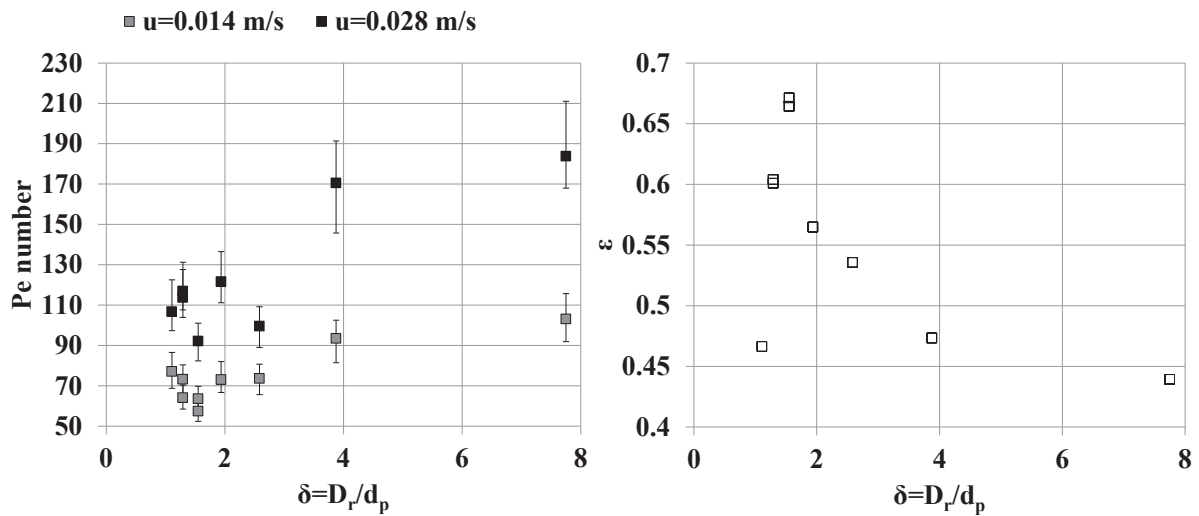


Figure 33. Estimated Pe number and ϵ for different values of δ . Reactors with $D_r=7.75$ mm, $L=18.2$ cm filled with spheres of different size. Grey: Pe number values for $u=0.014$ m/s. Black: Pe number values for $u=0.028$ m/s. White: ϵ values.

The Pe number evolution as a function of δ is complex and not monotonous for $\delta < 3$. At both gas velocities, the Pe number presents a minimum for $\delta = 1.55$, corresponding to the reactor that has the largest void fraction. In that reactor, the beds arrange in a vertical plane leaving large empty spaces on their side (Figure 27). This structure is prone to bypass, which explains the drop in the Pe number. Another minimum is present at $\delta = 2.58$ but only for the highest velocity ($u = 0.028$ m/s). At that value, the beads arrange in a circular manner, all touching the reactor wall and leaving a large empty passage in the reactor center, promoting a severe bypass of the bed and a drop in the Pe number compared to structures with not too different δ . Clearly, our experimental sampling of δ is not sufficient to capture the complete curve. We will report in more detail the trend by using numerical tools in another paper.

A pronounced increase in the Pe number occurs when $\delta > 3$, especially at the highest velocity. This corresponds to a transition towards beds where the packing is less influenced by the presence of

the reactor walls and more “uniform”. This extends Johnson and Kapner’s results [35] towards lower values of δ .

In the case of cylindrical particles, we define ψ as the ratio between the particle length and the reactor diameter and δ' the ratio between the reactor diameter and the particle diameter. Higher Pe numbers have been observed when cylinders are arranged randomly than when they align on each other along the reactor axis (Figure 34). Visual observations confirmed that when ψ is larger than 1 the cylindrical particles align along the reactor axis: this leads to structured beds with potential preferential passages between the cylindrical particles and the walls. When ψ is smaller than 1 the cylinders can position themselves in any direction including horizontally. This promotes a more random and more uniform structure with fewer bypasses.

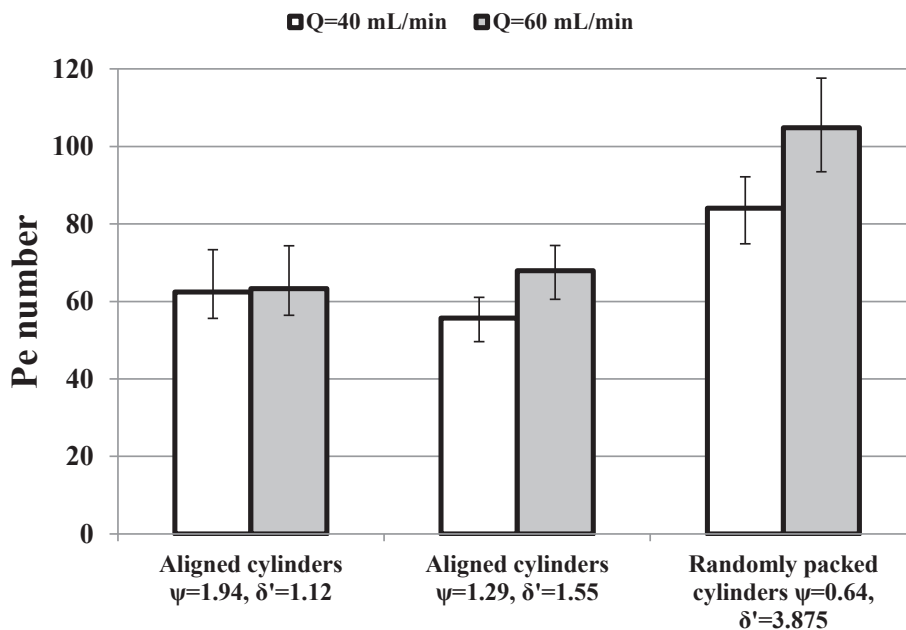


Figure 34. Pe number for aligned/randomly packed cylinders in a reactor with $D_r=7.75$ mm, $L=18.2$ cm and for two flow rates: 40 and 60 mL/min

6.2.3.4 Effect of superficial gas velocity

In the case of spheres, in a 7.75 mm diameter reactor, both the axial dispersion coefficient (Figure 35 left) and Pe number (Figure 35 right) increase with increasing gas velocity. This is expected as our experiments are in the range $0.1 < Pe_m < 10$, area where an increase of velocity corresponds to an increase of the Bo number and, consequently, of the Pe number (see Figure 31). For higher values of the Pe_m number an increase of the velocity could result in a decrease of the Bo number (see Figure 31 and [13, 36, 42]).

D_{ax} increases less than linearly with the gas velocity and it converges to D_m/τ at low velocities (see Figure 31, in the region of $Pe_m < 1$).

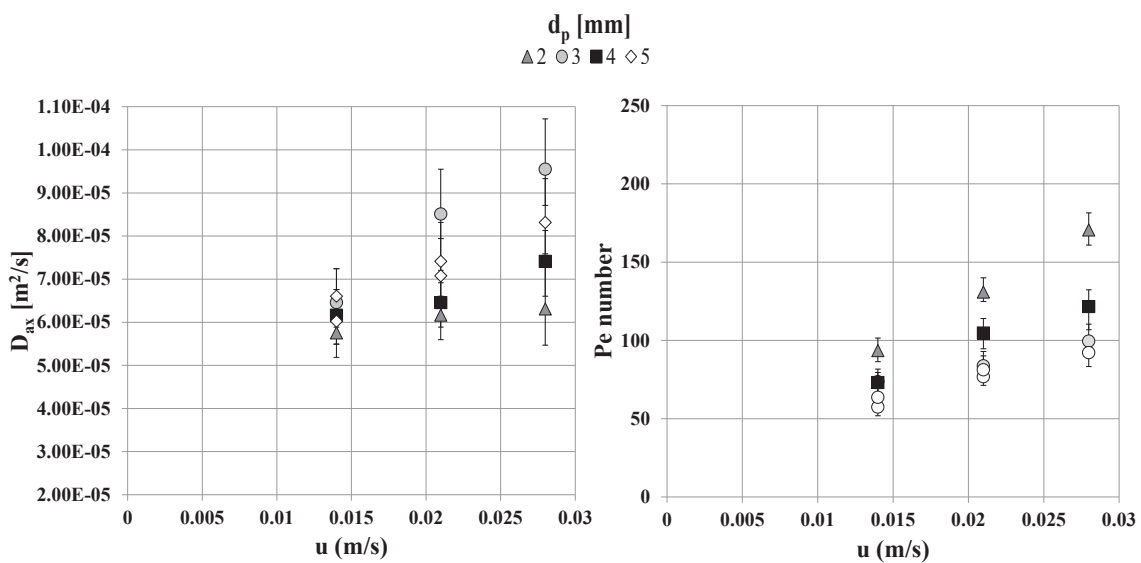


Figure 35. Variation of D_{ax} (left) and Pe number (right) as a function of the gas superficial velocity. Reactors with $L=18.2$ cm and $D_r=7.75$ mm, packed with spheres of different size

The molecular diffusivity of helium in nitrogen is $\sim 7.5 \times 10^{-5} \text{ m}^2/\text{s}$ at 25°C . Assuming $\tau = \frac{1}{\sqrt{\varepsilon}}$ [75], the tortuosity values for the data shown in Figure 35 vary between 1.23 and 1.52 and the values of D_m/τ between ~ 4.9 and $6.1 \times 10^{-5} \text{ m}^2/\text{s}$, which corresponds indeed to the lower end of the D_{ax} values (Figure 35, left).

This means that at low velocities the Pe number values are mainly driven by the global reactor void fraction, which influences the interstitial velocity (see Figure 33, $u=0.014 \text{ m/s}$, where the Pe number behavior is inversely proportional to the void fraction). By increasing the velocity, the flow is no longer only governed by the molecular diffusivity but bypasses inside the structures.

6.2.3.5 Effect of inert powder addition as porosity filler

Experimental data have been acquired with a reactor with $D_r=7.75 \text{ mm}$, $L=18.2 \text{ cm}$, $u=0.014 \text{ m/s}$ and packed with glass beads of 5 mm . Silicon carbide (SiC), mean $d_p=0.2, 0.8 \text{ mm}$ and sieved between $d_p=0.3-0.4 \text{ mm}$, and ZirBlast[®] (ZB), sieved between $d_p=0.3-0.4 \text{ mm}$ have been then added to these reactors as porosity fillers. The pressure drop for these reactors has been measured and was found to be insignificant, avoiding any effect on the data analysis.

The porosity fillers are inserted in the beds following a precise protocol:

- 1) The reactor is initially packed with the millimetric particles;
- 2) Powder is added up to the reactor top;
- 3) Gentle tapping during 25 s is performed. The void created by the rearrangement of the fine powder is filled again with fine powder. This operation is repeated twice.

In one experiment with SiC $0.3-0.4 \text{ mm}$, we repeated the step 3 of the packing protocol three times, instead of two, which reduced the void fraction from 0.39 to 0.37 .

The use of porosity fillers increases significantly the Pe number and this increase is mainly driven by the decrease of the bed void fraction of the reactor (Figure 36).

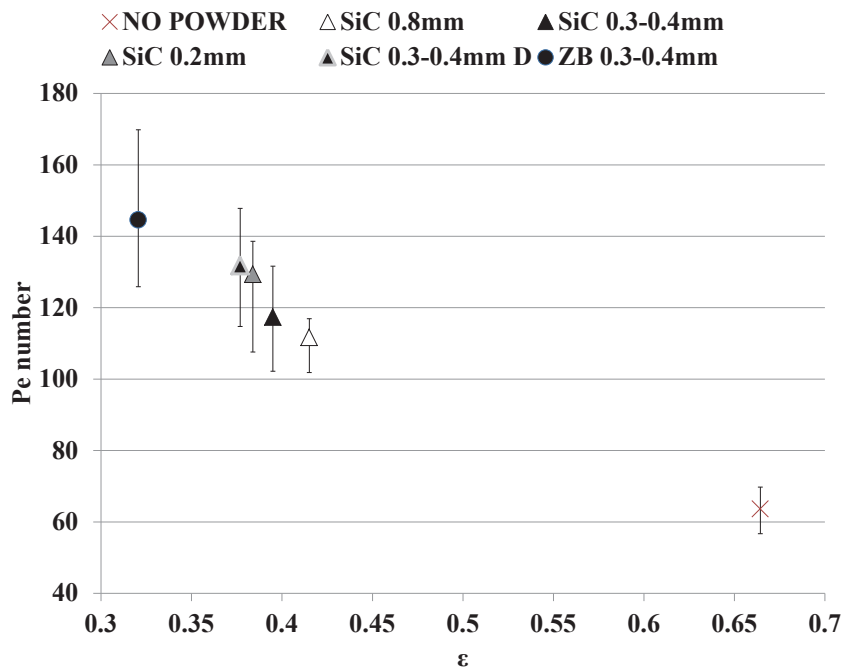


Figure 36. Pe number against void fraction. Reactors with $D_r=7.75$ mm, $L=18.2$ cm, $u=0.014$ m/s and packed with spheres of 5 mm and different types of porosity fillers. D means “dense packing”, obtained repeating three times the step 3 of the packing protocol

Another effect of the porosity fillers addition to a bed of millimetric particles is that the size governing the hydrodynamics becomes the porosity filler diameter. The Pe_m number is thus lower and most certainly in the range where Bo is proportional to Pe_m , even increasing the velocity (see Figure 31).

For the same powder size (0.3-0.4 mm), ZB powder enhances more the Pe number than SiC powder, but this is a direct effect of the void fraction: 0.39 for bed filled with SiC vs 0.32 for the bed filled with ZB. This void fraction difference is most likely caused by the shape of the two

powders: while the ZB powder is spherical and flows very well, the SiC particles have irregular forms and do not fill up the void fraction as the ZB powder (Figure 37).

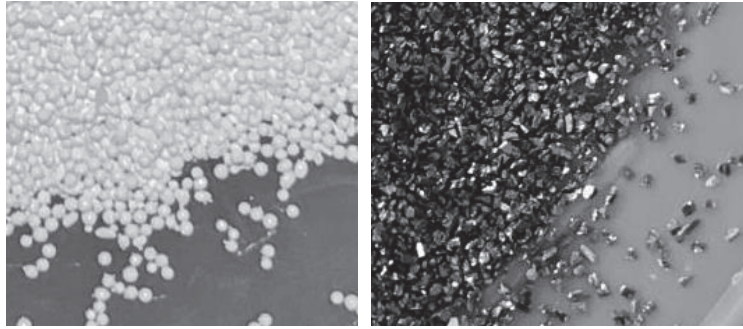


Figure 37. Pictures of ZirBlast® on the left, SiC on the right

Other experiments performed with the same reactor ($D_r=7.75$ mm) but different particles ($d_p=7$ mm spheres and 5x10 mm cylinders) confirm the positive effect of the powder on the Pe number (Figure 38).

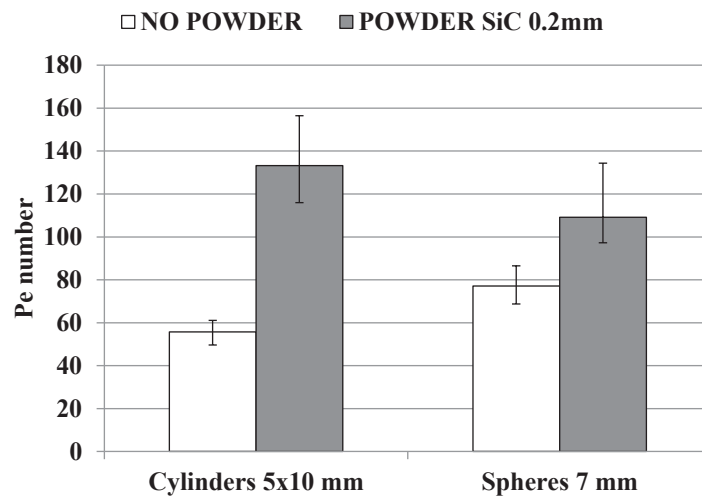


Figure 38. Porosity filler effect on the Pe number. Reactor with $D_r=7.75$ mm, $L=18.2$ cm and d_p indicated in the x axis. $Q=40$ mL/min

6.2.3.6 Criterion for axial dispersion limitations

In this paragraph, we define a criterion for deciding if axial dispersion effects can be neglected for a given reactor, catalyst, and kinetic study. Our derivation is based the Mears-Gierman criterion [26] combined with a correlation describing our experiments. The Mears-Gierman criterion [26] gives a minimum Pe number allowing to neglect axial dispersion effects without degrading kinetic constant evaluation by more than 10% (Equation 30):

$$Pe > 8 \cdot n_r \cdot \ln \frac{1}{1-X} \quad \text{Equation 30}$$

in which n is the reaction order and X the desired conversion. We can notice that for a first order reaction and a desired conversion of 99%, a Pe number of 40 is enough to neglect the effect of the dispersion on the conversion.

To correlate our data, we adopted the correlation proposed by Šolcova and Schneider [13] (Equation 31):

$$\frac{1}{Bo} = \frac{\gamma}{Pe_m} + \frac{\lambda_0 \left[1 - \lambda_1 (d_p/D_r) [1 + \lambda_2 (1 - \phi)] \right] Pe_m}{\beta + Pe_m} \quad \text{Equation 31}$$

in which: ϕ represents the particles sphericity γ - λ_0 - λ_1 - λ_2 - β are constants estimated by fitting with experimental data. The sphericity is defined as the ratio of the surface area of the sphere of the same volume as the particle and the surface area of particle. Thus, for spherical particles $\phi=1$ while for cylindrical particles it is given as:

$$\phi = \left(\frac{18(L_{cyl}/D_{cyl})^2}{(1 + 2(L_{cyl}/D_{cyl}))^3} \right)^{1/3} \quad \text{Equation 32}$$

This correlation has been tested on both spherical and cylindrical particles and it has been found valuable for different carrier-tracer systems. However, Šolcova and Schneider studied single pellet string reactors with $1.25 < \delta < 1.76$, $1.43 < \delta' < 1.75$ and $0.44 < \beta < 0.86$ and their correlation does not fit our data points adequately. To fit our experimental points that span a larger range of δ , δ' and β , we adjusted the γ - λ_0 - λ_1 - λ_2 coefficients, while keeping the original value of β .

Experimental data from two reactor configurations are not well predicted by this model:

- 1) $\delta=2.58$. This point represents a geometry that is characterized by a pronounced preferential passage and a very low Pe number value so that the prediction is not accurate. We do not recommend operating reactors with δ values close to this one;
- 2) $\delta=1.1 + \text{SiC } 0.2 \text{ mm}$. This is the only reactor that has a small ε value without porosity filler (lower than 0.5 while higher than 0.6 for the others). In this reactor, the passages between the walls and the catalyst are quite narrow and the fine powder structure itself is affected by the presence of the walls. The characteristic dimension for the hydrodynamics is probably not the size of the fine powder.

For all other reactor configurations, we consider the model as an adequate representation of the experimental data.

Minimizing the root mean square error (RMSE) of the relative difference of the experimental data and the model prediction allowed to estimate the values of the coefficients γ - λ_i (denoted as best fit) with a good accuracy. However, the correlation with these values overestimates half of experimental data points and some by up to 18%. We propose another set of constants γ - λ_i (denoted as conservative), with a lower prediction accuracy but it never overestimates Bo.

All sets of constants and the original one from Šolcova and Schneider are shown in Table 5.

Table 5. The two set of constants (best fit and conservative fit) for the model in Equation 31

	γ	λ_0	λ_1	λ_2	β	RMSE
Šolcova and Schneider	1.142	5.311	1.169	2.296	39.76	
Best fit (min RMSE)	0.763	1.786	0.629	3.708	39.76	0.07
Conservative fit	0.934	1.605	0.639	4.420	39.76	0.17

So, our criterion is based on the following steps:

- 1) Use Equation 31 to estimate the Bo number for the packed bed millireactor using the set of conservative values from Table 5;
- 2) Use Equation 33 to compute the maximum acceptable conversion. This equation is a direct rewriting of Equation 30.

$$X_{max} = 1 - e^{-\frac{L \cdot Bo}{8n_r d_p}} \quad \text{Equation 33}$$

6.2.4 Results and discussion: reactive tests

Reactive tests have been performed to explore the effect of adding powders as porosity fillers in packed bed millireactors on the external mass transfer. We rank the performances in terms of conversion and assess the effect of the different porosity fillers. We did not wait for stabilization of the catalyst activity because we are interested in the differences between the reactors and not in their absolute values.

The 95% confidence interval on the differences in conversion is estimated at $\pm 1\%$. It was estimated through a statistical analysis on the average of the differences of conversion observed in replicated reactors. Both the data on *n*-heptane reforming and methylcyclohexane dehydrogenation were considered in this analysis.

6.2.4.1 Check of thermal transfer and axial dispersion limitations

In this section, we check the absence of thermal transfer and axial dispersion limitations.

Mears developed a criterion [76] to predict the presence of radial temperature gradients in large fixed beds in the case where only the wall temperature is known and not the center temperature (which is our case). Radial thermal transfer limitations in a packed bed can be neglected if the condition in Equation 34 is respected:

$$\Delta T_{rad} = \left(1 + \frac{8}{\frac{\alpha_w \cdot D_r}{\lambda}} \right) \cdot \left| \frac{\Delta H_0 \cdot R_v \cdot d_p^2 \cdot (1 - \epsilon)}{32 \cdot \lambda} \right| < \frac{0.05 \cdot R \cdot T^2}{E_a} \quad \text{Equation 34}$$

in which α_w is the wall heat transfer coefficient [W/(m²·K)], λ is the thermal conductivity of the packed bed [W/(m·K)], ΔH_0 is the reaction enthalpy [J/mol], R_v the volumetric reaction rate [mol/m³_{catalyst}·s] and T the absolute temperature [K]. This criterion is usually stricter than the one for axial thermal transfer [77]. This means that, if this Mears radial criterion is fulfilled, the axial thermal transfer is also negligible. In practice, the Mears radial criterion is at most indicative as it requires the estimation of two unknown quantities, the wall heat transfer coefficient α_w and the thermal conductivity λ , for which the correlations in literature [78–84], give a wide range of estimations. Those correlations have been developed for large packed beds reactors and their validity for packed bed millireactors with low values of δ is unknown.

According to our calculations, considering the cases at the highest temperature, the criterion is always fulfilled for *n*-heptane reforming. For the methylcyclohexane dehydrogenation, which is highly endothermic, most, but not all correlations used for predicting α_w and λ allowed to fulfill the criterion.

For this reason, we performed an experimental check on the isothermicity of the methylcyclohexane dehydrogenation by comparing runs with a single bed of catalyst and a reactor, denoted diluted, whose catalyst bed has been split into two parts separated by a bed of highly conductive inert SiC particles. The inert layer will promote reheating of the fluid at the inlet of the second catalytic bed. In the case of heat transfer limitations, we expect higher conversion in the diluted reactor. The conversion in the diluted reactor was in fact lower.

Equation 31 and Equation 33, using the “conservative fit”, showed that in our operating conditions dispersion effects can be neglected. We confirmed this conclusion using the analytical solution for a first order reaction in absence of mass transfer limitations. Conversion differences when adding porosity fillers can only be attributed to changes in mass transfer.

6.2.4.2 Porosity filler effect on the conversion: *n*-heptane reforming reaction

In this part, we will compare the apparent conversions of the reactors packed with and without porosity filler for the *n*-heptane reforming reaction. We have measured, for different operating conditions, the difference $\Delta X = X_{\text{filler},i} - X_{\text{no_filler}}$ where $X_{\text{filler},i}$ represents the conversion with the porosity filler *i*, while $X_{\text{no_filler}}$ the conversion without porosity filler. For each test we consider the average of the different ΔX calculated to assess the effect of the porosity filler and compare it to the 95% confidence interval. The effect on the conversion is indicated with a “+” if adding the porosity filler increases the conversion compared to the case without porosity filler. If a reactor has a duplicate in a test, the *X* values retained are the mean of the measured conversions for each particular condition.

Catalyst extrudates

The differences in conversion between the reactors packed with and without porosity filler for some of the operating conditions are shown in Figure 39 (5 tests) while Table 6 summarizes the effects observed for all the results. The addition of porosity fillers had always a beneficial effect on the conversion.

As discussed above, the conversion gains are necessarily due to changes in the external mass transfer. A likely explanation is the decrease of the void fraction and thus the increase of the interstitial velocity, which is known to improve the external mass transfer. Mass transfer coefficient correlations in the literature, for example that of Ranz-Marshall [28], usually relate the external mass transfer coefficient k_{gs} [m/s] and the fluid velocity with a relationship in the form of Equation 35:

$$k_{gs} \propto a + b \cdot u_i^c \quad \text{Equation 35}$$

where a, b and c are constants. In most correlation, the value of a is such that the Sh number $\left(\frac{k_{gs} \cdot d_p}{D_m}\right)$ equals 2 for $u_i=0$, which is the theoretical asymptotic value for a creeping flow around a single sphere. The value of the exponent c is in literature in the range of 0.5-0.6 [28, 85]. So, the external mass transfer coefficient increases with increasing interstitial velocity.

nC7 reforming

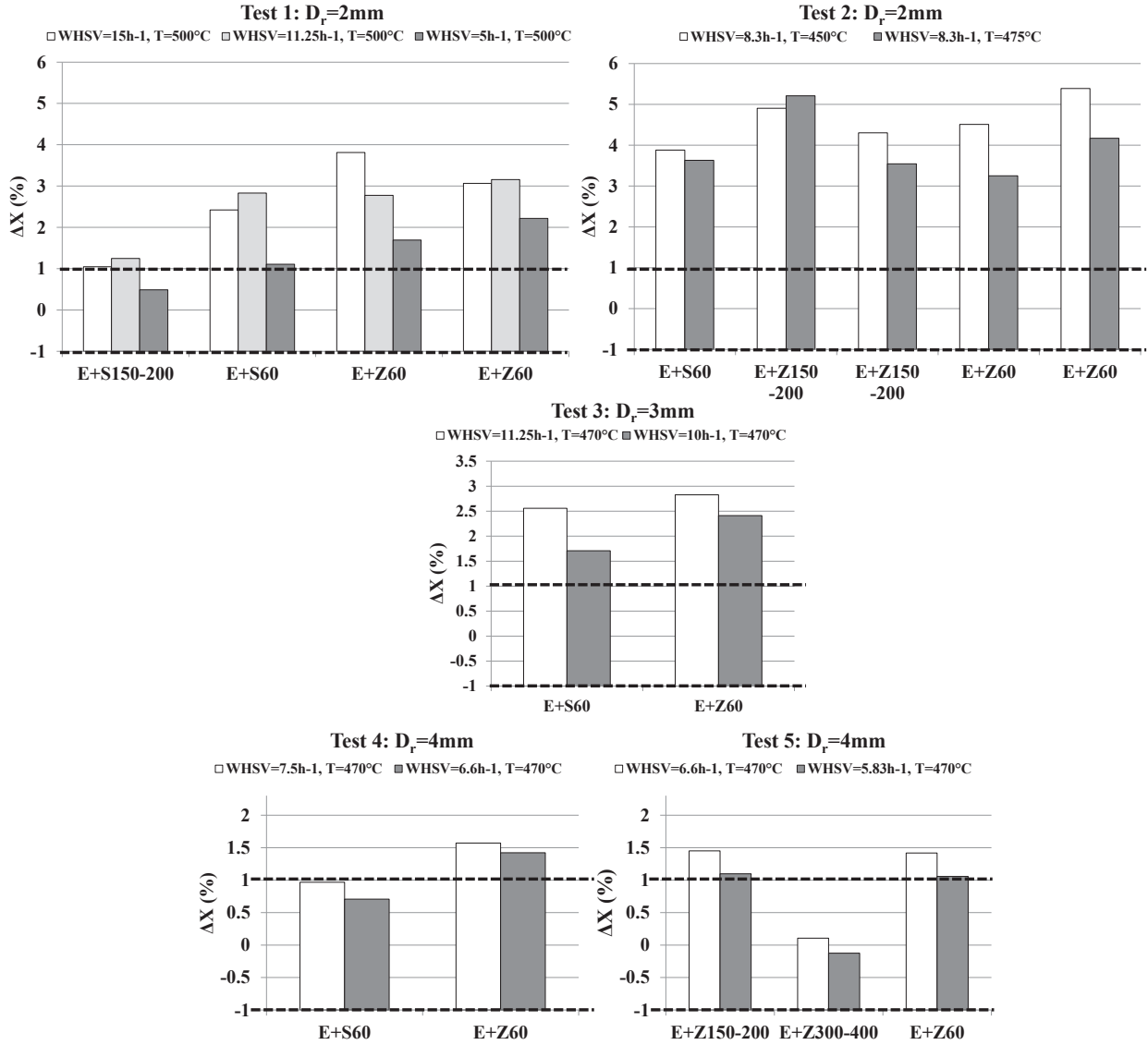


Figure 39. Differences in conversions between the reactors packed with catalyst extrudates + porosity filler and the reactors packed with only catalyst extrudates. n-heptane reforming, $D_r=2, 3$ and 4 mm. E=Extrudates, S=SiC, Z=ZirBlast[®]. The dotted line indicates the confidence interval ($\pm 1.0\%$)

Table 6. Results for *n*-heptane reforming performed with catalyst extrudates. Reference: packing without powders. Empty cells mean no test. +: statistically significant increase in conversion when adding this type of powder

<i>n</i> -heptane reforming		ZirBlast [®]			SiC	
		60 μm	150-200 μm	300-400 μm	60 μm	150-200 μm
Test 1 and 2: D_r=2 mm	WHSV=5-15 h ⁻¹	+	+		+	+
Test 3: D_r=3 mm	WHSV=8.8-11.25 h ⁻¹	+			+	
Test 4 and 5: D_r=4 mm	WHSV=5.83-6.6 h ⁻¹	+	+	No effect	No effect	

The effect of porosity fillers on the conversion is more pronounced for the smaller reactors. The extrudates catalysts have a 1.4 mm diameter and a 5±2 mm length. The extrudates particles are vertically aligned in the reactor of D_r=2 mm but are randomly oriented in the reactor of D_r=4 mm. The enhancement of mass transfer induced by the porosity filler is thus lower when the reactor structure was random and presented a lesser risk of bypass before the porosity filling.

Another trend is that increasing the WHSV tends to increase the gains in conversion when adding porosity fillers. As we operate at constant catalyst mass, increasing the WHSV is equivalent to increasing the gas velocity. If the formalism in Equation 35 applies, this indicates that, the exponent obtained using porosity fillers is higher than the one obtained with millimetric particles only.

Catalyst beads

The effect of the porosity fillers on the conversion with spherical beads is presented in Figure 40 for some operating conditions. All the results are summarized in Table 7. The effect of the porosity fillers using beads is less pronounced than for extrudates, not always significantly changing the conversion. The catalyst beads have a mean diameter $d_p=1.8$ mm, not always perfectly spherical, and they have been tested in reactors with internal diameters of 3 and 4 mm. In the 3 mm reactor ($\delta=1.67$), the catalyst beads are positioned in a planar manner with large passages on the side. In the 4 mm reactor ($\delta=2.22$), the catalyst beads are arranged irregularly due to the shape and the size distribution of the particles, generating a structure with few bypasses.

The higher effect of the porosity filler in the 3 mm case is probably due to the presence of bypasses between the catalyst particles and the wall. The conversion levels with the spherical beads are consistently higher than extrudates. At this point, as the catalyst formulation is different, it is impossible to decouple between kinetic or mass transfer.

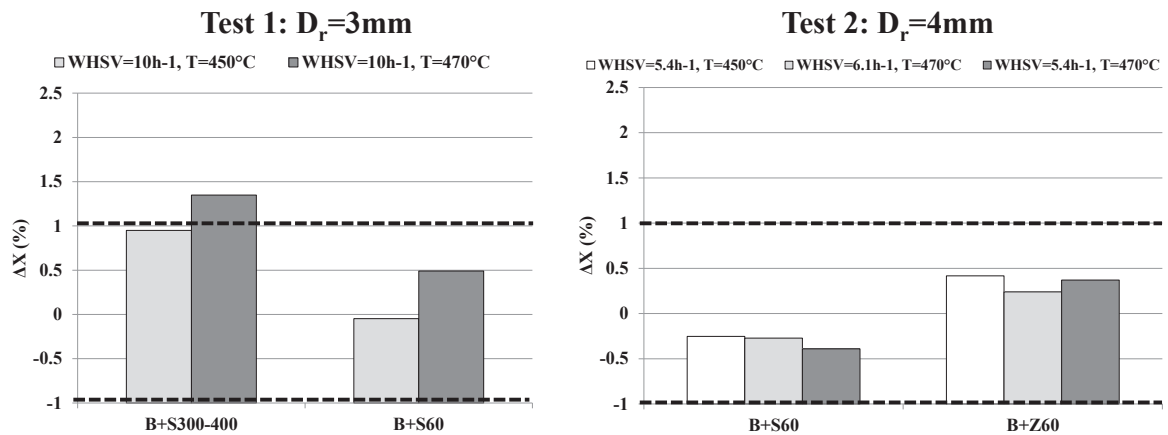


Figure 40. Differences in conversions between the reactors packed with catalyst beads + porosity filler and the reactors packed with only catalyst beads. *n*-heptane reforming, $D_r=3$ and 4 mm. B=Beads, S=SiC, Z=ZirBlast[®], the number indicates the powder size in μm . The black dotted line indicates the confidence interval ($\pm 1.0\%$)

Table 7. Results for *n*-heptane reforming with spherical catalyst. Reference: packing without powders. Empty cells mean no test. +: statistically significant increase in conversion when adding this type of powder

<i>n</i> -heptane reforming		ZirBlast [®]	SiC	
		60 μm	60 μm	300-400 μm
Test 1: $D_r=3$ mm $\delta=1.67$	WHSV=8.8-11.25 h ⁻¹		No effect	+
Test 2: $D_r=4$ mm $\delta=2.22$	WHSV=5.4-6.1 h ⁻¹	No effect	No effect	

Porosity filler size and shape effect

The effect of the porosity filler type (SiC or ZirBlast[®]) was studied by calculating differences in conversion $\Delta X_{\text{powders}} = X_{\text{ZirBlast},i} - X_{\text{SiC},i}$ where $X_{\text{ZirBlast},i}$ or $X_{\text{SiC},i}$ represents the conversion of the packings with the porosity filler ZirBlast[®] or SiC of size *i*. In most cases, the use of ZirBlast[®]

results in higher conversions, +0.5 points of conversion in average. The difference for each individual test is not statistically significant but the effect has been observed repeatedly and it is on average significant (the confidence interval on the average is divided by the square root of the number of repetitions).

This higher performance of ZirBlast[®] was also observed on the Pe number and explained by a better filling of the porosity. We propose that the slight mass transfer enhancement also results from a reduced void fraction through resulting in a higher interstitial velocity and higher mass transfer when filling the porosity with ZirBlast[®] than with SiC. ZirBlast[®] powder, which is spherical, flows better and fills better the void spaces than SiC powder that is angular.

The effect of powder size is not statistically significant in our experiments. The safe conclusion is that the powder size shows no or very small effect. A detailed look at Table 6 and Table 7 combined with our remarks on bypasses in the reactors hint that large porosity filler increase the performance in presence of large passages whereas fine porosity filler are more performant in structures with smaller passages. So, the optimal powder size probably depends on the bypasses size.

6.2.4.3 Porosity filler effect on the conversion: methylcyclohexane dehydrogenation reaction

Extrudates catalyst particles have also been used for methylcyclohexane dehydrogenation in reactors of internal diameters of 2 and 4 mm.

For the the methylcyclohexane dehydrogenation, the differences in conversion between the reactors packed with and without porosity filler are summarized in Table 8 (2 tests) and in Figure 41 for some operating conditions. The addition of porosity fillers has always a beneficial effect on the conversion with a higher effect in the 2 mm reactor.

MCH dehydrogenation

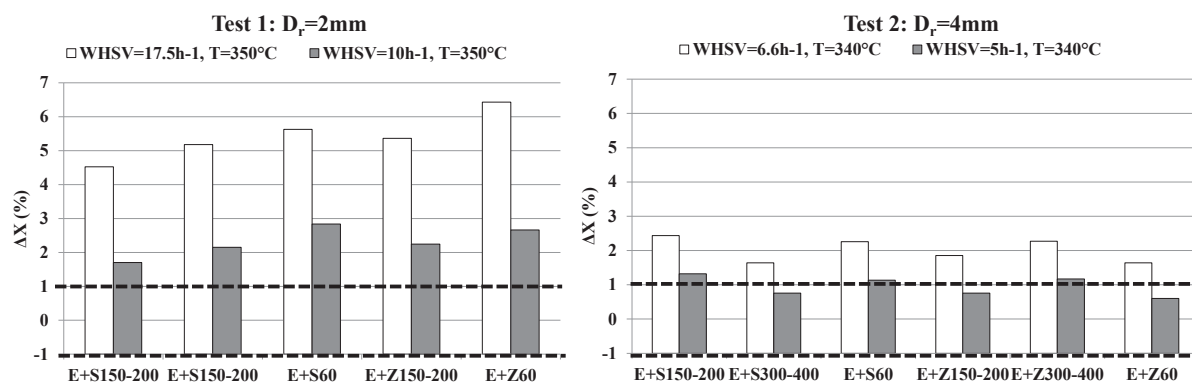


Figure 41. Differences in conversions between the reactors packed with catalyst extrudates + porosity filler and the reactors packed with only catalyst extrudates. Methylcyclohexane dehydrogenation, $D_r=2$ and 4 mm. E=Extrudates, S=SiC, Z=ZirBlast[®], the number indicates the powder size in μm . The black dotted line indicates the confidence interval ($\pm 1.0\%$)

Comparing to the *n*-heptane reforming case, we observe the same trends: a larger mass transfer enhancement when increasing the velocity (WHSV) and no clear effect of powder size. The SiC/Zirblast[®] difference is, however, not observed.

Table 8. Results for methylcyclohexane dehydrogenation with catalyst extrudates. Reference: packing without powders. Empty cells mean no test. +: statistically significant increase in conversion when adding this type of powder

Methylcyclohexane dehydrogenation		ZirBlast [®]			SiC		
		60 μm	150-200 μm	300-400 μm	60 μm	150-200 μm	300-400 μm
Test 1: $D_r=2$ mm	WHSV=7.5-17.5 h^{-1}	+	+		+	+	
Test 2: $D_r=4$ mm	WHSV=5-6.67 h^{-1}	+	+	+	+	+	+

6.2.5 Conclusions

Gas-solid RTD experiments and reactive tests on *n*-heptane reforming and methylcyclohexane dehydrogenation reactions have been performed in packed bed millireactors with low values of the reactor/particle diameter ratio ($1 < \delta < 8$) in order to assess the hydrodynamic and mass transfer characteristics of these reactors.

The axial dispersion model was found adequate to model the RTD curves of these reactors. The dispersion values were found in the range of traditional packed bed reactors for the area explored ($0.1 < Pe_m < 10$) except that the linear relationship between Pe_m and Bo extends until Bo higher than 3. For both cylinders and spheres, the reduction of the particle size has a significant impact on the packing structure and Pe number values. For spheres, the experimental resolution on δ was not sufficient to capture the complex dependency of the Pe number with δ (that also depends on the gas velocity). The Pe number values present minima when the structure is prone to create bypasses. It increases when $\delta > 3$. A CFD study is ongoing to explore the range $1 < \delta < 3$. For cylinders, the Pe number is lower when the cylinders are constrained to align vertically compared to when they can lay horizontally and form a random structure ($\psi > 1$).

Adding fine inert powder to fill the porosity increases the Pe number through a reduction of the void fraction and the velocity increase. Additionally, as the hydrodynamic characteristic diameter is much reduced, the Pe_m is low enough for Bo to remain proportional to Pe_m , even at high velocities. The best porosity filler is the one that better fills up the entire void fraction, especially near the contact points: it is preferably round (better flowability) and as small as possible (better access to stranded zones near particles contact points). Overall packed bed millireactors have shown, in most cases, quite good hydrodynamics for most applications. A criterion to calculate, in a conservative manner, the maximum conversion that can be achieved neglecting the dispersion

effects is proposed. Some cases where this model is not predictive have been found (at least two identified here: $\delta=2.58$ and for $\delta=1.1$ + porosity filler).

Reactive tests showed that using porosity filler can increase the external gas-solid mass transfer which we think is due to the lower void fraction that leads to a higher interstitial gas velocity. Spherical powders are again recommended as they yield lower void fractions for a given grain size. The effect of the powder diameter is below our experimental capabilities, but we do not recommend too fine grain sizes, but the one small enough to correctly fill the bed porosity.

At last, our work also shows that the data reproducibility for HTE systems may be limiting types of kinetic studies investigating very small differences, except at the cost of repeating the tests several times. The weak points appear to be the flow distribution control, which is quite difficult for small flow rates, and the very small amounts of catalyst tested that raise questions about the catalyst sample uniformity.

6.3 CFD simulations in absence of porosity fillers

Paper draft to submit to Chemical Engineering Science: “Numerical prediction of Pe numbers in small fixed bed reactors of spheres”

Numerical prediction of Pe numbers in small fixed bed reactors of spheres

Vittorio Petrazzuoli¹, Matthieu ROLLAND¹, Vasileios Sassanis¹, Vincent Ngu¹, Yves Schuurman², Lionel Gamet¹

1 Process Intensification dept, IFP Energies Nouvelles, Rond-point de l'échangeur A7, 69360 Solaize, France

2 IRCELyon

**Corresponding author: matthieu.rolland@ifpen.fr*

Highlights

- DEM-OpenFOAM[®] workflow to compute Pe number in packed beds of spheres in laminar flow;
- Workflow faster and more informative than experiments;
- Complex influence of the reactor to sphere diameter ratio on Pe number;
- Pe number uncertainty decreases as a function of a power -0.5 of the reactor length.

Abstract

Accurate predictions of Pe numbers have been performed in small fixed bed reactors using DNS (Direct Numerical Simulations) in single phase laminar flow. The fixed bed structure is obtained using a Discrete Element Method (DEM) code (Grains3D), and the Pe numbers are computed from steady state simulations of the moments of the age distribution using the open source OpenFOAM[®]

framework. Results are close to the experimental data. The DEM-OpenFOAM[®] workflow is efficient enough to produce local and global results with a good control of the parameters, and it is faster than an experimental approach.

We first explored the relationship of the Pe number as a function of δ ($\delta < 4$), fluid velocity and molecular diffusivity. The behavior proved much more complex than any previous report, and it can be qualitatively explained by looking at the packing structure.

Then, we used the DEM-OpenFOAM[®] workflow to quantify the uncertainty when repeating the packing of a $\delta=4$ fixed bed reactor.

In the end we propose that the uncertainty on the Pe number decreases with a power -0.5 of the reactor length.

Key words (max 6): Computational Fluid Dynamics; small fixed beds; Péclet number; packing geometry; Direct Numerical Simulations; laminar flow

6.3.1 Introduction

6.3.1.1 Fixed bed downscaling

Over the decades, fixed bed reactors for catalyst testing have faced a reduction in size and now they commonly have diameters below 1 cm, the limit being the catalyst pellet size (~1-3 mm). The advantages of these reactors are numerous: less catalyst used, less amount of reactant used and of wastes produced, better temperature control, reduced safety risks and easier implementation of parallel reactor systems [1]. Those reactors were designed for catalyst screening, so that the hydrodynamics was not really an issue if the ranking and uncertainties were correct. As those reactors produce a large amount of data, a new question arises: can we use those results to build

models for catalyst performance prediction? One of the limiting factors might be the hydrodynamic quality of the flow. This work aims at improving our understanding of the hydrodynamics inside these small reactors using CFD tools.

Downscaling of fixed beds reactors is usually performed by keeping the ratio of flow rate (Q) to the catalyst amount (V_{cat}) constant, usually denoted as Hourly Spaced Velocity or HSV. In the literature, it is reported the notation LHSV for liquids and GHSV for gases. This ratio can be seen as the inverse of the contact time. When expressing the catalyst amount as a volume, the HSV is the ratio of the superficial velocity (u_s) to the reactor length (L) (Equation 36). Laboratory reactors are typically 10-50 cm long so that the velocities are 100 times smaller than in industrial reactors (~10 meters in length).

$$HSV = \frac{Q}{V_{cat}} = \frac{u_s}{L} \quad \text{Equation 36}$$

For a wide range of reactions in biorefinery, biochemistry, petrochemistry, and refining, the velocities in laboratory reactors are so low that the flow regime is often laminar with Reynolds numbers < 10 . For this reason, in the rest of the paper we focus on single phase laminar flows.

Currently the reactors used in heterogeneous catalyst testing have arrived until diameter values smaller than 1 cm and lengths that usually do not exceed the 20-30 cm. As the catalyst particles are on the order of a few millimeters, a packed bed millireactor is usually operated with values of $\delta = D_r/d_p$ (reactor/particle diameter ratio) between 1 and 5, possibly 10, while traditional packed beds have much higher value (> 1000 for industrial packed beds). In packed bed millireactors, the ratio $\delta = D_r/d_p$ governs the disposition of the particles in the reactor. For large values of δ there are few preferential paths and dead-zones due to the stochastic position of the particles at the center of the bed and the higher packing density [69, 70], while for the low δ values occurring in packed bed

millireactors the global void fraction is higher and radially non-uniform [15] and preferential paths near the walls are important enough to drive most of the flow.

6.3.1.2 Plug flow behavior

To perform kinetic studies, the results of experiments must express the kinetic behavior of the catalyst rather than the hydrodynamics of the reactor. In a fixed bed, the ideal flow is plug flow with high heat and mass transfer coefficients. If these conditions are not met, the usual approach is to characterize those features building a reactor model that accounts for them and then optimize a kinetic model coupled with the reactor model. An example of this process can be found in [53]. In this paper, we focus on the plug flow behavior of the fixed bed reactors that is very well described by the classical convection equation augmented with an axial dispersion term (Equation 6) [25]:

$$\frac{\partial c}{\partial t} = D_{ax} \frac{\partial^2 c}{\partial z^2} - \frac{u}{\varepsilon} \frac{\partial c}{\partial z} \quad \text{Equation 6}$$

in which z is the axial coordinate along the bed [m], C is the concentration of the species [mol/m³], D_{ax} the axial dispersion coefficient [m²/s], u_s the superficial gas velocity [m/s], ε the void fraction of the reactor and t the time [s]. If the axial dispersion coefficient, D_{ax} , is sufficiently small, the axial dispersion can be neglected, which greatly simplifies the models. At this point, it is worth introducing the Pe number that compares dispersion time scales to convective time scales. The higher the Pe number, the closer the reactor is to ideal plug flow. In kinetic studies, it is very interesting to operate reactors with Pe number high enough that they can be considered as ideal; “high enough” depending on the conversion level of the reaction as proposed by Mears [76].

To experimentally evaluate the dispersion in the reactors, transient experiments are required. Usually a tracer is injected, and its concentration temporal evolution is recorded at the reactor inlet and outlet. When the inlet is a Dirac function, the outlet curve is the residence time distribution

(RTD) denoted as $E(t)$. This is the reason why these types of experiments are often called RTD measurements. In practice, the inlet is never exactly a Dirac function so that a measurement of the reactor inlet is recommended.

The axial dispersion coefficient can be deduced from the reactor outlet and inlet temporal tracer concentration profiles solving the axial dispersion model equation [13, 29, 43, 73, 86]. For example, Equation 6 can be solved using the inlet temporal profile for the inlet boundary conditions. The axial dispersion coefficient and void fraction values are optimized to match the simulated and experimental concentration temporal profiles at the reactor outlet.

Another method to evaluate the dispersion is to compute the first two moments of each signal (inlet and outlet) [9, 22, 31, 36, 42]:

$$M_{1,x} = \frac{\int_0^{+\infty} t \cdot c_x(t) \cdot dt}{\int_0^{+\infty} c_x(t) dt}, \quad x = \text{inlet or outlet} \quad \text{Equation 37}$$

$$M_{2,x} = \frac{\int_0^{+\infty} t^2 \cdot c_x(t) \cdot dt}{\int_0^{+\infty} c_x(t) dt}, \quad x = \text{inlet or outlet} \quad \text{Equation 38}$$

and compute the Pe number as:

$$Pe = 2 \frac{\bar{t}^2}{\sigma^2} = 2 \frac{(M_{1,outlet} - M_{1,inlet})^2}{(M_{2,outlet} - M_{1,outlet}^2) - (M_{2,inlet} - M_{1,inlet}^2)} \quad \text{Equation 23}$$

in which \bar{t} is the mean residence time, σ^2 is the variance and M_1 and M_2 are the first and second order moments of the residence time distribution curves.

A fine control of the experimental setup is necessary to achieve a good accuracy on the axial dispersion measurements [87], which is time consuming. Besides that, not all experimental conditions can be tested: spherical beads are only available in limited number of diameters, same for the reactor diameters. Fluid and tracer choice are limited by the analyzer's capabilities. For

these reasons, we developed a numerical workflow to compute Pe numbers and be able to perform all the simulations required to get a better understanding of the underlying physics.

Plug flow behavior studies in packed bed millireactors are scarce, and they focus mainly on experimental studies. A common rule-of-thumb [25] recommends values of δ higher than ~ 15 , so that the radial porosity fluctuations near the walls have less impact on the average flow and the packing can be considered as uniform in the radial direction. In this case variations of the fluid velocity, porosity and axial dispersion coefficient in the radial direction can be neglected. Packed bed millireactors do not respect this rule of thumb and another design criterion is required.

Experimental studies from Šolcova and Schneider [13], Scott et al. [42] and Hsiang and Haynes [36] showed that low values of dispersion, comparable to larger packed beds, are achieved when δ is below 2.

A CFD study simulating residence time curves from Müller et al. [88] on a Single Pellet String Reactor (cylindrical reactor and spherical particles, $\delta=1.2$ and $L=0.1$ m) concluded plug flow behavior for all the conditions tested, ranging from laminar to turbulent flow. Fernengel et al. [44] performed a similar study but ranging the δ value between 1.25 and 1.75. Non-diffusive numerical tracer simulations revealed that the reactors have plug flow behavior. They also simulated a heterogeneously catalyzed isothermal and isomolar gas-phase reaction with no change in gas density that showed conversions deviating less than 5% from plug flow.

However, a study that reports and compares the effects of different parameters on the hydrodynamics of packed bed millireactors like bed length, fluid superficial velocity, reactor diameter and reactor/particle diameter ratio for values higher than 1.75 is missing.

6.3.1.3 Pe number evaluation using CFD

Direct numerical simulation of reactive flows in fixed beds has progressed enormously in the last decade with velocity, concentration and temperature 3D profiles [89–91]. Many papers present workflows to solve CFD problems in random packed beds of complex shapes, some of them using open source solvers like OpenFOAM® [54, 59]. The computational resources are now sufficient to perform successfully CFD simulations of packed bed High Throughput Experimentation reactors for non-reactive single-phase flows.

A very interesting advance comes from the work of Liu [60] that showed that the moments of the age distribution could be computed using steady-state simulations. Let us first introduce the notion of age distribution: at any point of the reactor, the age of the molecules $a(x,t)$ since the reactor entrance follows a distribution, which is generally unknown but can be characterized by its moments (Equation 39).

$$M_n(x) = \frac{\int_0^{+\infty} t^n \cdot a(x, t) dt}{\int_0^{+\infty} a(x, t) dt} \quad \text{Equation 39}$$

Following the works of Spalding [65], Danckwerts [62] and Zwietering [63], Liu and Tilton [60] demonstrated that the n -th moment of the age distribution follows a steady state convection/diffusion equation similar to momentum, energy or species:

$$\nabla \cdot (\mathbf{v}M_1) = \nabla \cdot (D_m \nabla M_1) + 1 \quad \text{Equation 40}$$

$$\nabla \cdot (\mathbf{v}M_n) = \nabla \cdot (D_m \nabla M_n) + nM_{n-1}, \quad n > 1 \quad \text{Equation 41}$$

in which \mathbf{v} is the velocity vector [m/s] and D_m the molecular diffusion coefficient [m²/s]. The boundary conditions are: $M_i = 0$ at inlet, no fluxes at the reactor walls and outlet. The equation for the first moment is quite easy to understand. The first moment of age follows a classical convection

diffusion equation and its rate of change is unity. Those equations are valid for any open reactor and are easy to implement and solve in steady-state CFD solvers. Liu also demonstrated that a mass flux integration of the M_1 and M_2 fields over the inlet and outlet (Equation 42) yields $M_{1,x}$ and $M_{2,x}$. The Pe number is then calculated using Equation 23.

$$M_{i,x} = \frac{\int_x u \cdot M_i \cdot dS}{\int_x u \cdot dS}, \text{ i=1 or 2, x = inlet or outlet} \quad \text{Equation 42}$$

The integrals of the moments can also be easily computed in cross-sections of the reactor located at various axial position z ($z = 0$ at inlet, $z = L$ at outlet). In this way, considering the first and second order moments integrals, it is possible to obtain the profile of the Pe number along the bed axis using Equation 23.

6.3.2 Aim of the work

We want to calculate Pe numbers in small fixed beds and study the effects of different physical and process parameters on the hydrodynamics as a post-treatment of a combined DEM packing & CFD workflow. The CFD is simple: laminar flow (Navier-Stokes equations) augmented with two convection – diffusion equations. In the following sections, we will present the workflow in detail as well as its validation, and we will investigate two open questions in small size fixed bed design: one being the Pe number behavior in small reactors, the other the uncertainty on the Pe number induced by the packing.

6.3.3 Materials and methods

6.3.3.1 Detailed simulation Workflow

The simulation workflow starts with the reproduction of the particle's arrangement using Discrete Element Method. The DEM method [92] is a Lagrangian particle tracking method which computes the velocity, trajectory and orientation of each individual particle in the system. The simulation accounts for the collisions of each particle with other particles and with the system walls. A key feature of any DEM tool is its ability to detect collisions, determine the contact point(s) and compute the resulting contact forces. Our DEM code Grains3D is based on the Gilbert-Johnson-Keerthi algorithm for collision detections [57]. Detailed information about our code Grains3D, its DEM and parallel computing features including the contact force model and the extension to non-convex shapes can be found in another publication by Wachs et al. [93]. In this work we use Grains3D to compute packing of spheres in a cylindrical reactor. Simulations for this work were run on a single CPU and lasted a few hours at most.

Meshing is performed using the sequence of `blockMesh` and `snappyHexMesh` utilities. `blockMesh` computes a coarse background mesh. Its output is a mesh consisting of near cubic blocks with curved edges to match the reactor cylindrical shape. The block size is a very influential parameter on the simulation results. In this paper, we present results in terms of “density”, which is the number of blocks per diameter of reactor (bpd).

`snappyHexMesh` computes a refined mesh that matches the solid interfaces. The solid particles are defined using the “searchable object” feature that is an analytical definition of the objects. Local refinement can be specified on solid surfaces, small gaps, and global geometry. The output mesh consists in quadrangle and tetrahedra. The interested reader can refer to the OpenFOAM® online

user-guide [94]. The suitable set of parameters has been chosen to achieve mesh convergence with the minimum mesh size. This is detailed in the mesh convergence section.

The next step in our workflow is to compute the velocity and the first two moments of age distribution in the porosity of the packed beds. We use the open source OpenFOAM[®] suite as other teams [54, 59]. The solver is `SimpleFoam` [95] augmented with two convection diffusion equations for the moments with a source term as described earlier. Our implementation of the mean age equations was validated against the 2D test case detailed in Liu and Tilton [60] but this is not presented here. Boundary conditions are defined as follows: velocity is uniform on the inlet surface, pressure is uniform on the outlet surface, first and second moments are uniform and equal to 0 on the inlet surface and with no gradient on the outlet surface. On the reactor walls and particles, we assumed no-slip condition for the velocity and no gradient for the moments of the age distribution.

Last, the integrals of the moments are computed during post-treatment using a user defined function that computes the mass flux weighted integrals of the moments over cross sections at various positions along the axial direction of the reactor.

6.3.3.2 Mesh convergence

The mesh quality is evaluated by checking the accuracy of the simulation on known quantities such as fluid flow rate conservation, total particles volume, and mean residence time. Those numbers are correlated. We next check the mesh convergence for pressure and Pe number. A parametric search shows that for our problem, the optimal mesh is obtained with a fine background mesh (high mesh density) and moderate additional refinement (level 1 in the `snappyHexMesh` terminology) near the solid surfaces and in the small gaps (Figure 42). This is expected for our problem where we need to capture the velocity gradients near the solid surfaces and the concentration gradients

everywhere in the volume. As a last remark, `snappyHexMesh` has a feature to build “boundary layers” made only with quadrangles on surfaces (particles and walls) but this proved unnecessary and even inefficient in our case.

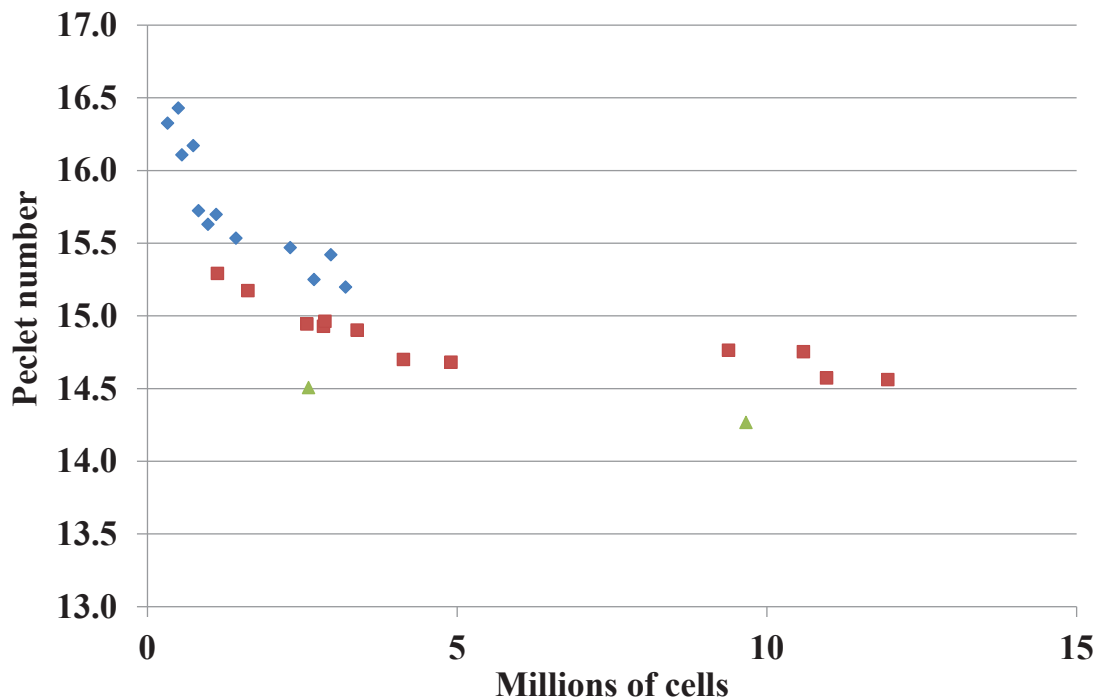


Figure 42. Mesh convergence on the *Pe* number as a function of the millions of cells for three background cell densities. $L = 50$ mm, $D_r = 7.75$ mm, $d_p = 4$ mm, $u = 0.0272$ m/s and $D_m = 10^{-6}$ m²/s. Blue diamonds: 27 bpd, red squares: 54 bpd, green triangles: 80 bpd. All the points of the same color and shape correspond to meshes of same bpd but different level of refinement on particles, walls and in small gaps. Chosen mesh: green triangle with the smallest number of cells

The chosen mesh is the one with 80 blocks per reactor diameter with only a moderate additional refinement (level 1 in the `snappyHexMesh` terminology) near the solid surfaces and in the small gaps. This corresponds to the green triangle with the lowest number of cells in Figure 42. The mesh is presented in Figure 43. The mesh convergence has been checked on 4 geometries: $D_r=7.75$ mm

and particles $d_p=7.5$ mm, $d_p=4$ mm, $d_p=3$ mm and $d_p=2.4$ mm for each fluid velocity and molecular diffusivity tested.

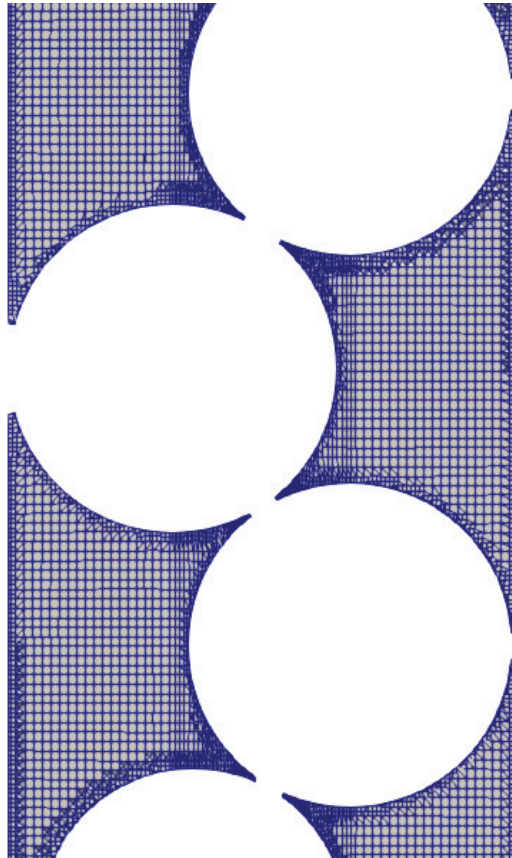


Figure 43. Cut of the mesh obtained with the final meshing strategy. $D_r=7.75$ mm, $d_p=5$ mm

Mesh convergence proved easier than expected. Numerical convection - diffusion problems can be quite stiff, requiring fine mesh near the catalyst pellets. In our case, the mean age evolves almost linearly from the entrance to the outlet while the second moment presents a quadratic shape (Figure 44). The problem is numerically quite smooth and the mesh reasonable in size. A typical simulation of the flow and moments would last 10 hours on 48 CPUs.

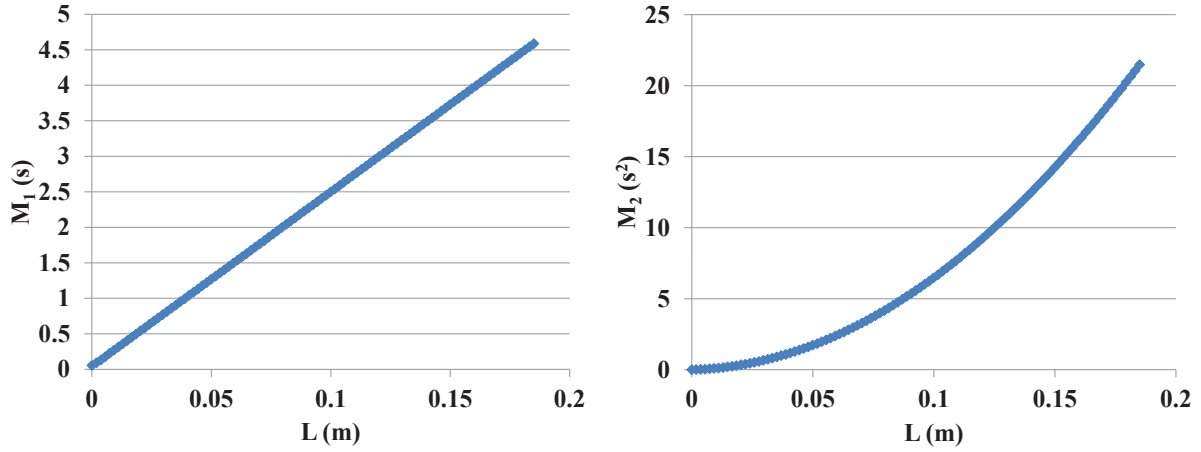


Figure 44. Example of M_1 and M_2 evolution along the bed. $D_r = 7.75$ mm, $d_p = 5$ mm, $u = 0.0272$ m/s and $D_m = 7.5 \times 10^{-5}$ m²/s

6.3.3.3 Workflow Validation

We validated the predictive ability of our workflow (DEM+CFD with OpenFOAM[®]) with a comparison of the Bo numbers that we measured in a 7.75 mm diameter reactor. Apparatus and procedures are described in detail in the paragraph §6.2.2. Numerical simulations are performed using corresponding operating conditions and physical properties: $0.014 < u < 0.028$ m/s, $D_r = 7.75$ mm, $D_m = 7.5 \times 10^{-5}$ m²/s (helium-nitrogen diffusivity), $\rho = 1.2$ kg/m³, $\mu = 1.85 \times 10^{-5}$ m²/s (nitrogen properties) for various particle diameters. We define δ as the ratio of reactor diameter to the particle diameter.

The agreement is good (Figure 45), except for the points corresponding to the reactor with $\delta = 1.1$. The experimental points have been confirmed, repeating them twice, while a mesh refinement confirmed the CFD results. It is not clear how to consider this difference. A difference between the

experiments and the CFD is that in the experiments a viscosity change occurs when performing the step change. Moreover, small differences between experimental and numerical geometries will express more in that case than in the others (local deviation of reactor diameter, circularity, particle diameter and sphericity...).

A last comment can be that OpenFOAM[®] may not solve the right equations because of high Reynolds number values so that the flow is no longer laminar. The Reynolds number, calculated with the particle diameter as characteristic length, is 26 for the points that do not match.

We do not know exactly if the problem is coming from the geometry or the high velocities (or both). We decide to present anyway the data obtained, keeping in mind that for very low values of δ (<1.2) the experimental-CFD matching is probably less accurate.

However, CFD is able to capture changes in trend near $\delta=2$ as we will see later. In fact, the CFD work confirmed that the experimental data were correct and made us stop looking for loopholes in our experimental setup.

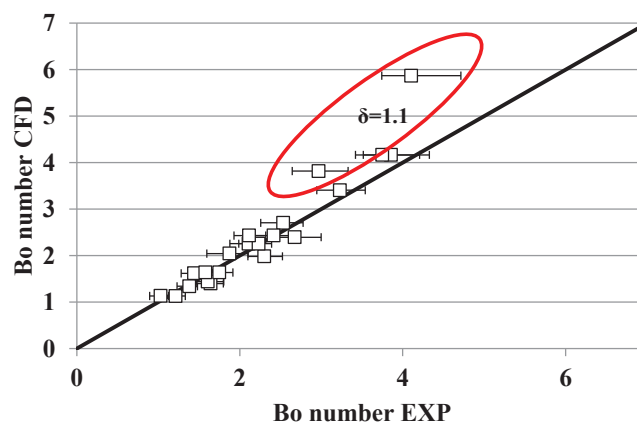


Figure 45. Validation of the workflow by comparing the Bo number values of simulations and experimental work. $D_r = 7.75$ mm. Comparison for different values of u and δ

Another validation was performed against the experimental data from Šolcova and Schneider ([13], Figure 46). The agreement is good. We observe a small overestimation of the Bo numbers, particularly for high Pe_m numbers.

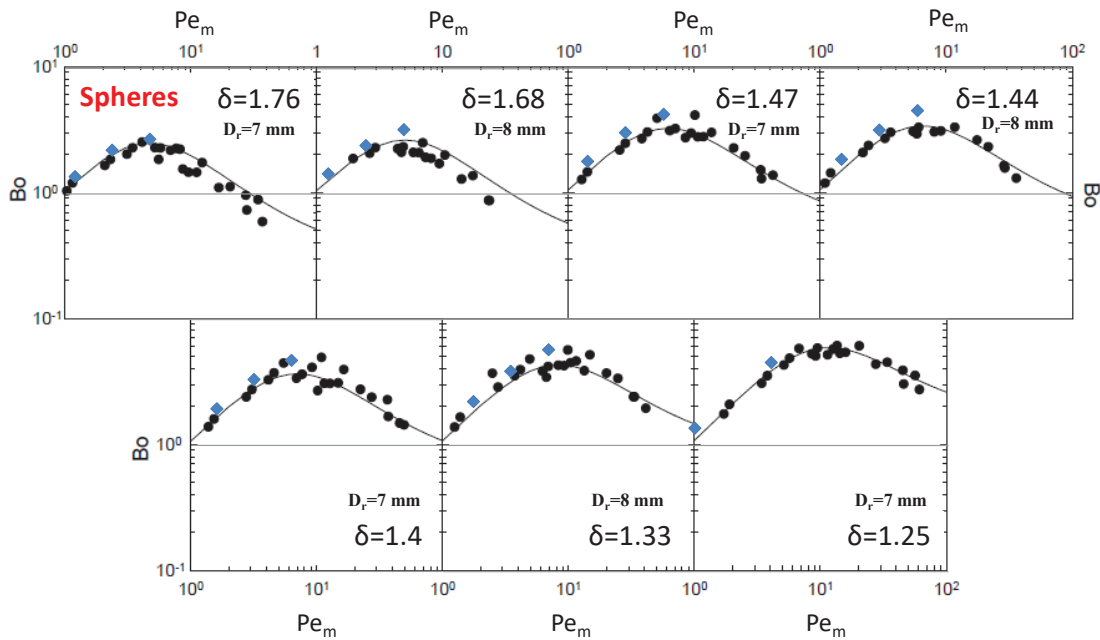


Figure 46. Our CFD results (in blue) compared to Šolcova and Schneider (in black) [13]

We conclude that our workflow correctly predicts the Bo numbers, except for small δ values in which we risk overestimations. Our CFD simulations take less than 24 hours and can be fully automated with scripts. Through parallelization, they yield results faster than experiments. An additional benefit of the DEM + CFD workflow is that we have a good control of the simulation parameters, especially dimensions and fluid properties.

6.3.4 Results

We used the CFD simulations to gain a better understanding about two crucial questions in heterogeneous catalyst testing. The first issue deals with the evolution of the Pe number as a function of δ in small reactors filled with spherical beads. The experimental data presented in §6.2 show a complex behavior with δ and we wanted to explore this in detail. We used *in silico* experiments to estimate Pe numbers for different values of δ and other physical parameters (molecular diffusivity) and process (fluid velocity, particles diameter, reactor diameter and length) parameters. We report this in section §6.3.4.1.

The second issue is about the repeatability of the Pe number when repeating the packing. In previous work we showed that 10% variability on void fraction has to be expected [96] when repeating the packing with the same particles. What is the effect of a random packing on the Pe number? We use our predictive capability to repeat the simulation starting from the packing generation using another random seed. This is explored in section §6.3.4.2.

6.3.4.1 Pe number in narrow reactors

Pe number evolution along the bed

The Pe number increases along the bed axis. However, depending on the value of the molecular diffusivity D_m , the Pe number evolution is slightly different.

For higher values of molecular diffusivity ($>10^{-5}$ m²/s) the Pe number tends to follow almost perfectly a straight line (example in Figure 47, A), while for lower values ($<10^{-5}$ m²/s) the behavior presents some “stairs” around the linear trend (example in Figure 47, B). However, when computing the overall bed Pe number, it will tend to be proportional to bed length as experimentally observed (see paragraph §6.2.3).

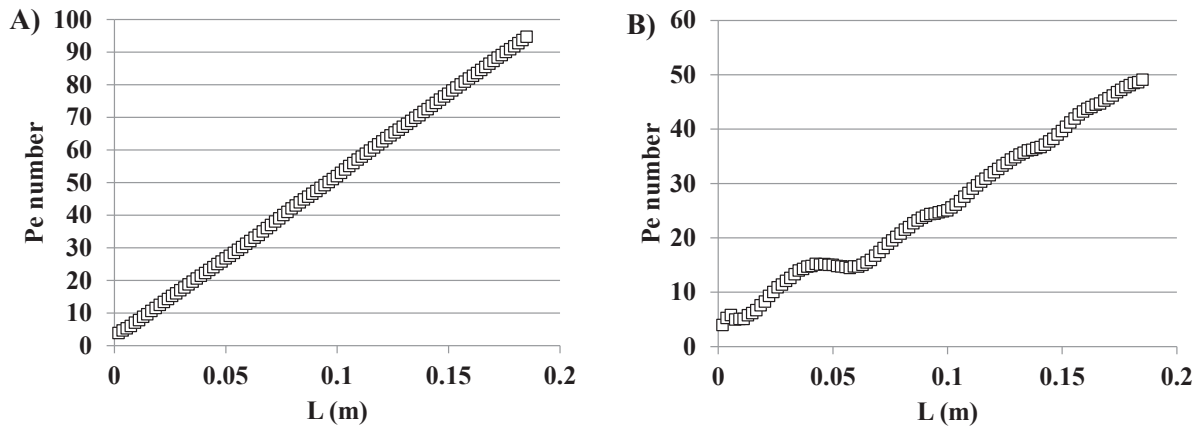


Figure 47. Pe number evolution along the bed axis for two different molecular diffusivity values: A) $D_m = 8 \times 10^{-5} \text{ m}^2/\text{s}$, B) $D_m = 10^{-6} \text{ m}^2/\text{s}$. $D_r = 7.75 \text{ mm}$, $d_p = 5 \text{ mm}$




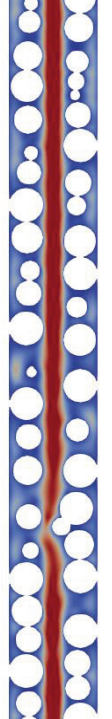
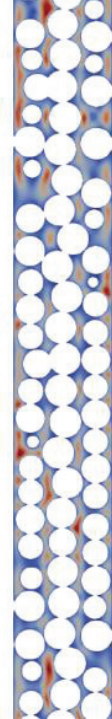
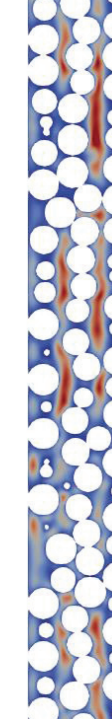
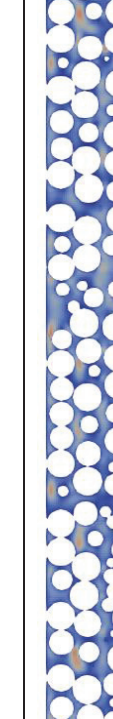
A look at the local packing structures

Table 9 shows the packing structures used for the CFD simulations. For $\delta < \delta_c$, with $\delta_c = 1 + \sqrt{3}/2 = 1.87$, a particle touches the wall and 2 other particles (one above, one below); the particles arrange in a planar and alternate way. Two side passages are present on the side of the particles. At the critical value $\delta = \delta_c$, the reactor is wide enough that the particle has now 5 contact points: the wall, two particles above, and two particles below. The arrangement is still planar. For $\delta > \delta_c$, the arrangement stops to be planar and the particles arrange in a spiral. Our DEM packings present in some cases deviation from ideal packings that can arise during the pouring process when a particle is blocked by another one before reaching its equilibrium position.

For larger δ , the arrangement tends to be more and more random although some structures can appear. For example, for $\delta > 2$, the particles can form rings and the packing presents a “hole” in the center whose size is maximum near $\delta = 2.6$. The hole in the center disappears for higher δ as the probability of a particle being stable in the center increases which prevents regular rings formation.

The same rings and holes structure occur for $\delta \sim 3.4$. The reactor to particle diameter δ governs the packing and small changes of its value can lead to significantly different arrangements.

Table 9. Packing structures for chosen values of δ . Particles are in white and the fluid zone is colored by velocity magnitude (red = fastest flow, blue = slowest flow, the scale is different for each case)

δ	1.06	1.72	2.21	2.58	3.1	3.37	3.875
Structure	Almost planar with passages on the side		Ring and hole in the center		Uniform	Some preferential passages	Uniform
Reactor's cut in the central vertical plane							

A consequence of this non monotonous behavior is that great care must be taken when using literature correlations near “geometric” transitions. Figure 48 compares the void fraction measured from our DEM simulations to the void fraction predicted from the correlation proposed by Dixon for spheres [97]. As we can see there is a good matching until $\delta \sim 1.87$, then for higher values the

correlation is not able to capture packing defects. For $\delta > 1.87$ the correlation shows a stable decreasing in ϵ while the data from DEM present some “rebound” due to packing imperfections.

The correlation that predicts the radial void fraction deviates for some specific values of δ . For example, the correlations proposed by Mueller ([15], see Equation 2) do not predict a hole ($\epsilon=1$) in reactor center for $\delta \sim 2.6$ (Figure 49). In that case, some experimental data is present in the literature [98].

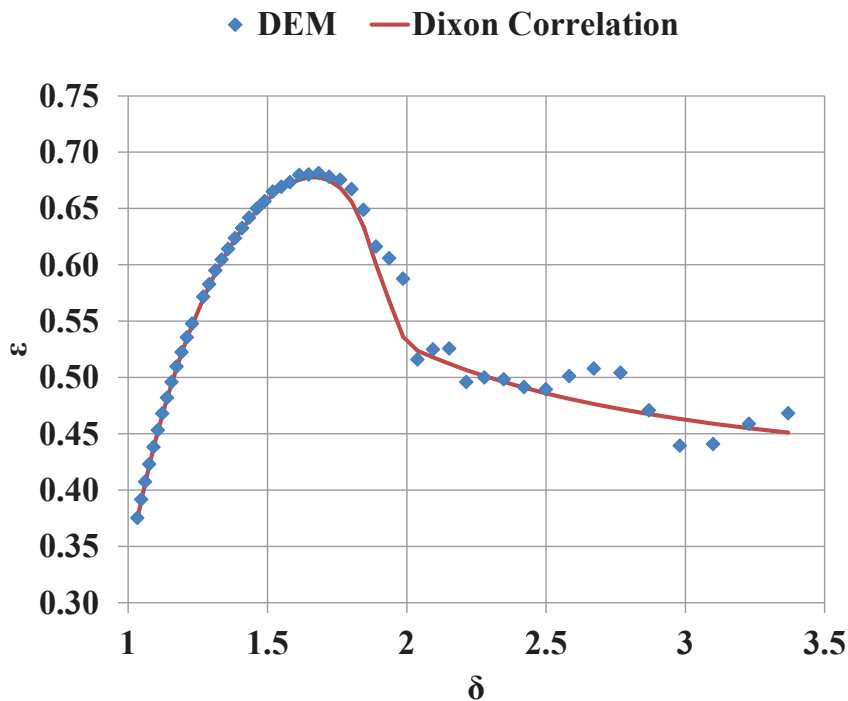


Figure 48. Void fraction as a function of δ in packed beds of spheres measured by DEM (blue diamonds) compared to the Dixon correlation (red straight line) [15]

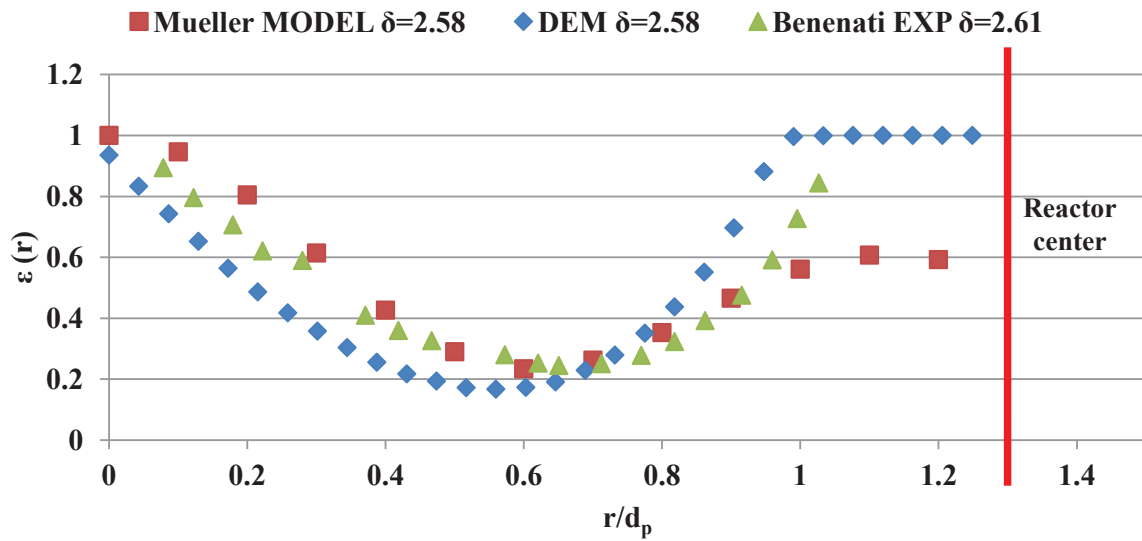


Figure 49. Comparison between radial void fraction profiles measured experimentally [98], Mueller correlation ([15], Equation 2) and our DEM results

From our DEM work, we conclude that classical correlations on void overall and radial fraction should be used very carefully for values of $\delta > 1.87$ and in particular near geometrical transitions located at $\delta = \delta_c$, $\delta \sim 2.6$ (single ring), and for the values of δ leading to other ring formations ($\delta \sim 3.4$).

Results in narrow reactors for a set reactor length

In this part, we use our DEM + CFD workflow to predict Pe numbers in narrow reactors filled with spherical particles varying the geometry through the particles size, the velocities and molecular diffusion. The reactor diameter is set to 7.75 mm and the length to 107.3 mm.

The Pe number profiles against δ are presented in Figure 50 for various combinations of velocity and molecular diffusion. The profile is more complex than it could be expected from our experimental work and depends both on δ and on the combination of velocity and molecular diffusion.

First comment is that for the largest part of experimental conditions explored (specifically $Pe_m < 3-4$) doubling the velocity or halving the molecular diffusivity coefficient has the same effect on the Pe/Bo number values. This suggests u/D_m as invariant. However, this is not true for higher values of the Pe_m number because of the intervention of a Schmidt number effect (see Annex C and [25]).

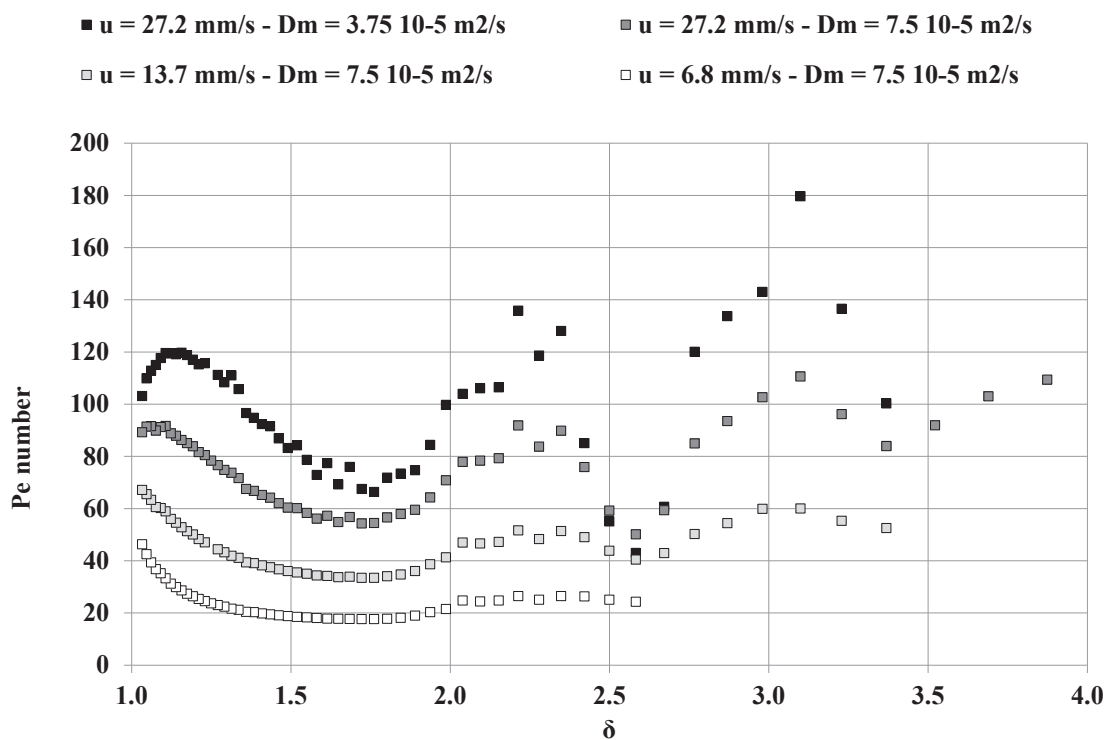


Figure 50. Evolution of Pe number against δ for various superficial velocities and molecular diffusivity values. $D_r = 7.75 \text{ mm}$, $L = 10.73 \text{ cm}$

Let us first explore in detail the profile of the top curves of Figure 50 (highest velocity and lowest molecular diffusivity, dark points). Starting from δ just above 1, the Pe evolution presents a smooth evolution as the geometrical constraints prevent random packing defects. The reactor Pe number value starts at a high value, increases to a maximum ($\delta \sim 1.2$) and then decreases toward a minimum

located near $\delta = 1.75$, which is slightly less than the critical value. We explain the gradual decrease of Pe with δ by the progressive increase of the passages on the particle sides that act as bypasses. As seen in Table 9, the packings are not ideal for $\delta = 1.72$ with a change in the orientation of the particle settling planes due to packing “defects”. Those random effects explain why the Pe starts to increase for $\delta < \delta_c$, in other words before the transition to “spiral” packing that present less opportunities for bypass. For $\delta > \delta_c$, the Pe number increases until the hole at the center of the geometry becomes large enough to create a significant bypass whose consequence on the Pe number depends on velocity and molecular diffusion. The Pe number reaches a minimum near $\delta = 2.6$. The “irregularities” in the curve are due to defects in the packing that locally create or prevent bypasses. For larger δ , the Pe number increases again due to a more random arrangement less likely to create by-passes. The rest of the curve is a repetition of the latter part: decrease due to a significant preferential passage in the center ($\delta \sim 3.4$) and increase due to a more random and uniform arrangements and less bypasses.

When the ratio fluid velocity to molecular diffusion decreases, the Pe number values are shifted downward. The curves are smoother and the oscillations are dampened (Figure 50). The smoothing and dampening are explained by a higher contribution of molecular diffusion compare to velocity. Molecules have more time to diffuse in and out of the bypass. Two length scales are governing the physics: one in the axial direction (particle size or reactor length), one in the radial direction (fluid passage size).

The behavior of string pellet reactors for δ very close to 1 ($1 < \delta < 1.3$) is also different: there is a maximum that is shifted towards lower δ values and it is less pronounced when reducing the fluid velocity (or increasing the molecular diffusivity). In that range of delta, the particles are in a plane. The flow lines are of two types: one type that flows outside of the particles plane (and that become

more important for larger delta) and one type that flows in-plane, going from one side of the reactor to the other around the particles. As we can see from Figure 51 for $\delta=1.1$, most of the flow lines are in-plane while increasing δ (1.5 in Figure 51) the flow lines become more out of plane.

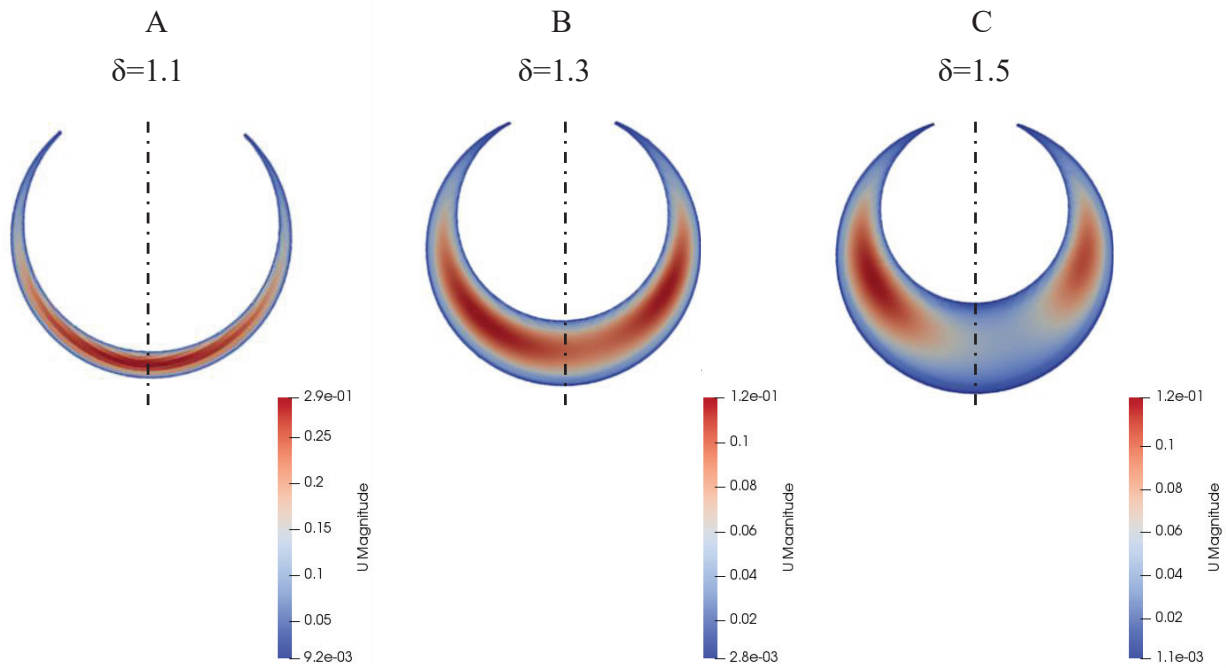


Figure 51. Velocity magnitude in cross sections as function of the δ value. The cross sections pass through a sphere center. The symmetry plane is indicated with a dashed line. $u=0.0272$ m/s, $D_r=7.75$ mm, $D_m=7.5 \times 10^{-5}$ m²/s. Red = fastest flow, blue = slowest flow

We propose that the change in behavior with velocities and molecular diffusion is due to a relative change in the importance (and interaction) of those two systems of flow lines.

Comparison with literature on larger packed beds

In the literature the results are traditionally representation of the results is $Bo=f(Pe_m)$ (see definitions in §3.4.1), which scales all dimensions to particles diameter. In Figure 52, we plot the results reported by Delgado [25] for single phase gas flow as well as our results.

For clarity, we decided to split our results in three groups. The first group (Figure 52-A) corresponds to reactors whose Bo numbers are in line with the literature. This group corresponds to $\delta > \delta_c=1.87$ except for the reactors with holes in the center.

The next group (Figure 52-B) corresponds to reactors with a hole in the center ($2.4 < \delta < 2.7$, $\delta=3.37$). At low Pe_m number values ($Pe_m < 2$), in the molecular diffusion driven dispersion zone, those reactors present a similar behavior as group A. But when Pe_m increases, the Bo number of those reactors falls under that of group A: Pe_m is large enough that the preferential paths in the reactor's center lower the Bo number.

The last group (Figure 52-C) encompasses all reactors with $\delta < \delta_c=1.87$ that we will denote as Single Pellet String Reactors (SPSR). Those SPSRs present high Bo number values (>5), particularly for the reactors with $\delta < 1.3$. Our values are similar to those of Šolcova and Schneider [13] (experimental study) for $\delta=1.25$, as discussed in §6.3.3.3. We think that those high values result mostly from the dimension scaling that is based on the particle diameters (quite large in our simulations and Šolcova and Schneider [13] experiments, $d_p > 7$ mm). A more physical scaling based on fluid passage size (hydraulic diameter for example) would bring those points closer to the group A. For larger δ , the passage size is a weaker function of the void fraction and the scaling by particle diameter offsets the curve by a constant amount.

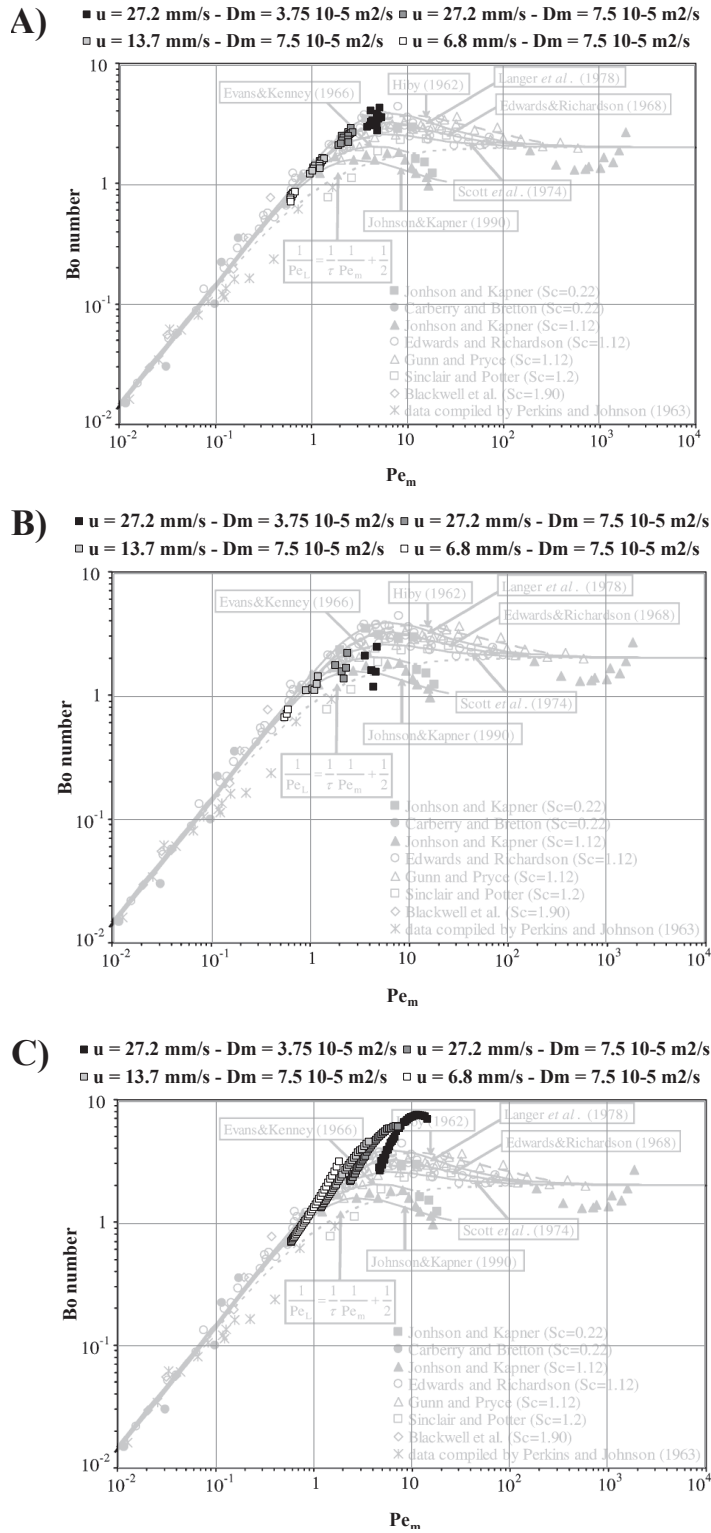


Figure 52. Evolution of the Bo number against Pe_m for various superficial velocities, molecular diffusivities, and bed geometries. A) $1.87 < \delta < 2.4 + 2.7 < \delta < 3.3$, B) $2.4 < \delta < 2.7 + \delta = 3.37$, C) $1.03 < \delta < 1.87$. $D_r = 7.75 \text{ mm}$

A practical case: choosing the right reactor diameter for a given particle size

Previously, we presented the results for reactors with the same length. In the real catalyst development practices, the catalytic tests are performed for a given mass or volume of catalyst and a target range of LHSV. The particle diameter is usually that of the industrial reactor [86].

We will now develop a real-life case in which we are designing a new catalyst testing unit and we want to decide the best reactor diameter. In this case, for a given catalyst mass and LHSV, the flow rate is known ($8 \times 10^{-7} \text{ m}^3/\text{s}$ in our study case). The catalyst diameter is also set (3 mm in our study case). Changing the reactor diameter means changing the fluid velocities (through the reactor cross-section). The catalyst volume conservation yields the following expression for the length of the bed:

$$L \sim \left(\frac{1}{\delta^2} \right) \cdot \frac{1}{1 - \epsilon} \quad \text{Equation 43}$$

We then simulated various reactor diameter cases using our workflow and adjusted the bed length to have the same number of particles in the reactor (100 in this study case). The resulting Pe numbers are presented in Figure 53. The best reactors are the narrowest ones. In practice, catalytic grains may not have a perfect spherical shape nor all exactly the same size and it is recommended to avoid too narrow reactors (δ too close to 1).

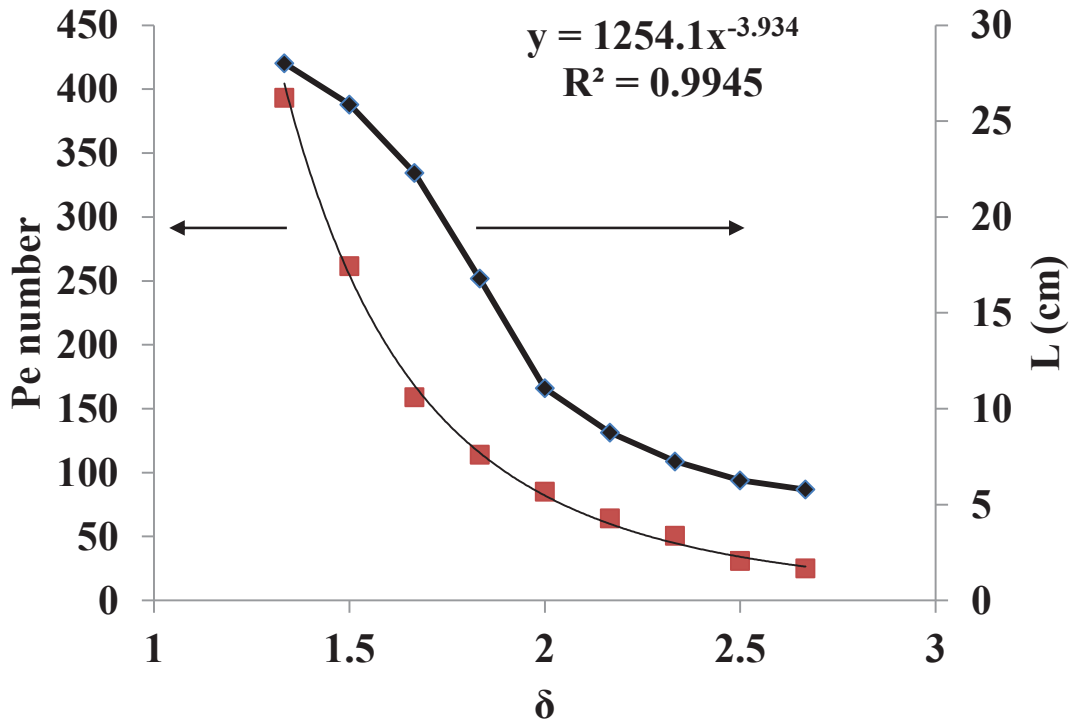


Figure 53. Evolution of the Pe number and bed length against δ for reactors made of 100 particles of diameter $d_p=3$ mm and for a flow rate 8×10^{-7} m³/s. The equation shown in the figure is a power law interpolating curve of the Pe number points

The Pe number points can be fitted with a power law of exponent very close to -4, which can be easily explained as follows. Noticing that the reactor cross section scales as δ^2 , using the expression for the bed length given above ($L \sim \left(\frac{1}{\delta^2}\right) \frac{1}{1-\epsilon}$) and substituting the interstitial velocity as $\frac{Q}{S^* \epsilon}$, we can write the Pe number as:

$$Pe = \frac{u_i \cdot L}{D_{ax}} \sim \left(\frac{1}{\delta^4}\right) \frac{1}{\epsilon} \frac{1}{1-\epsilon} \frac{1}{D_{ax}} \quad \text{Equation 44}$$

The Pe_m values vary between 1.24 and 4.25: in this range the molecular diffusion governs the axial dispersion and it is reasonable to approximate D_{ax} by D_m/τ . Assuming then $\tau \sim 1/\varepsilon^{0.5}$ [75] we obtain a final estimate of the Pe number:

$$Pe \sim \left(\frac{1}{\delta^4}\right) \frac{1}{\varepsilon^{1.5}(1-\varepsilon)} \frac{1}{D_m} \quad \text{Equation 45}$$

In the range of ε explored ($0.489 < \varepsilon < 0.677$), the product $\varepsilon^{1.5}(1-\varepsilon)$ is almost constant (max variation 6%). We conclude that the Pe number follows a $1/\delta^4$ evolution. For higher LHSV, D_{ax} could not be estimated so easily, but we expect the best choice would still be the narrowest reactor.

This ends this section about the Pe number evaluation in narrow reactors and we will pass now to the study of the repeatability of the packings.

6.3.4.2 Repeatability of the Pe number profiles in narrow reactors

Methods

In this part, we are interested in the variability in random packed beds and we will compare the Pe number profiles against the reactor length for beds packed with the same set of particles but loaded differently through a different set of initial conditions (random seed). In the end, the bed structure is different due to the stochastic loading while the particles composing the bed are the same.

As seen earlier, the Pe number curves for small δ are smooth as the geometrical constraints limit the probability of defects occurring during packing. We now study larger fixed beds made with 3 mm diameter spheres packed in a 12 mm diameter reactor ($\delta=4$). We repeated six times the workflow (DEM-CFD) from scratch, obtained six different packings and checked that the packings

were really all different and not a rotated version of one another. In our opinion, the easiest way to check this is to sort particles by their center's height (z_i), plot z_i against their rank and check that the curves are not identical. One may also compare void fraction on several slices.

Pe number profiles in repeated packed beds

The Pe number evolution with the reactor length follows a linear overall trend consistent with an axial dispersion independent on the length (Figure 54). It presents small variations around this trend and these variations are different in all packings. In the cases presented in Figure 54, there is almost no difference at $z = 10$ cm, while a difference in Pe number of 10 is measured at $z = 7$ cm. Such a difference can yield significant differences in the apparent reactor performance for high conversion reactions if the Pe number is low ($Pe < 40$ for example). It depends on the reaction desired conversion [76].

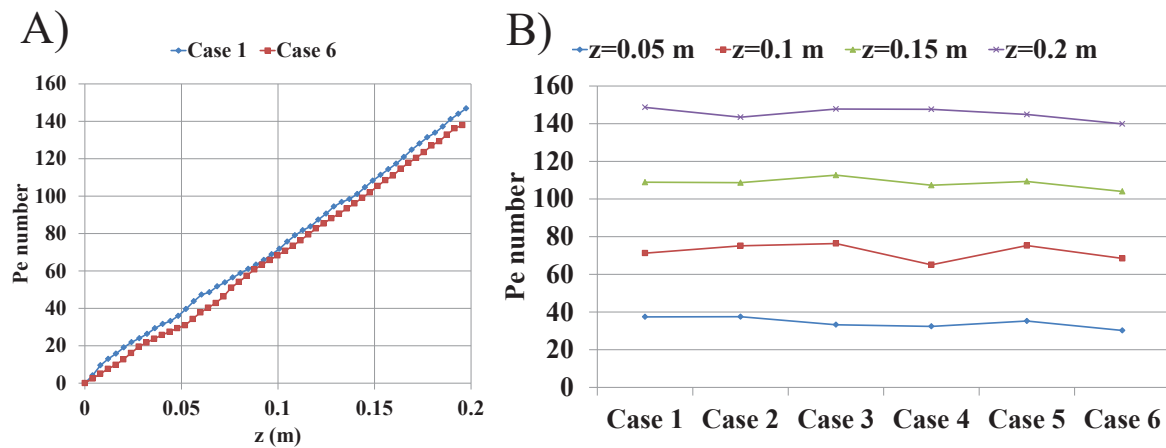


Figure 54. A) Plots of Pe number as function of the length in the reactor for two repeats of the same numerical experiment (both beds are made with the same beads and are different). B) Pe number variation for the six cases and for four bed lengths. $D_m=10^{-6} \text{ m}^2/\text{s}$

A better view of the variability is achieved when plotting the Pe number increments (ΔPe) from plane to plane as done in Figure 55 for the case 2 that presents a locally flat evolution of the Pe number. The ΔPe value depends of course on the distance between two cut planes dz (here $dz = 4$ mm). Pe number increments in that case are mostly between 1.5 and 2 with slightly higher values but significantly lower values. Lower values (as near $z = 0.13$ m) are due to a hole in the packing and a resulting preferential path of fluid.

We will now propose a method to quantify this variability as a function of length which can be useful to design reactors.

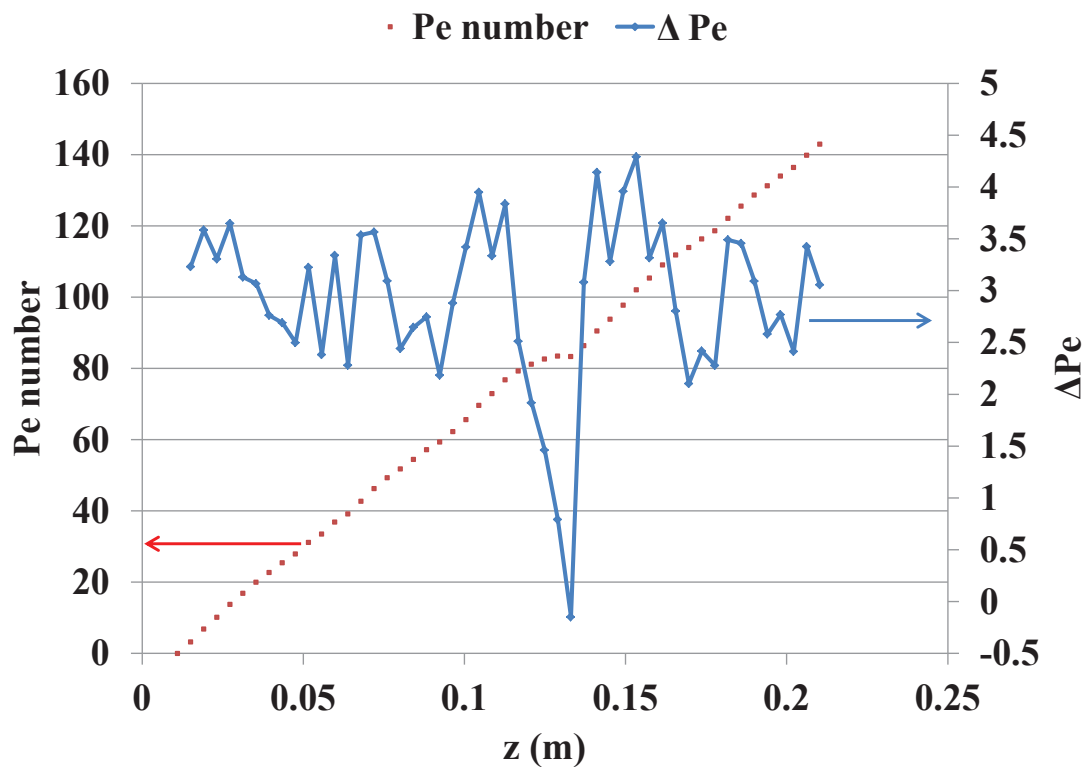


Figure 55. Case 2 - Left axis (red, dashed line): Pe number evolution. Right axis (blue): Evolution of the Pe number increment ΔPe as a function of reactor length ($dz = 4$ mm). $D_m = 10^{-6} \text{ m}^2/\text{s}$

The Pe number uncertainty as a function of the reactor length

We will now propose a method to quantify the variability of the reactor Pe number as a function of the bed length, which can be useful to design reactors.

We assume that ΔPe is a random variable with a probability density. We can then estimate the Pe numbers for a reactor of a given length L as the sum of N realizations of the ΔPe random variable, N being the number of Pe number increment (L/dz). This assumes that the realizations are independent from each other, which is equivalent to say that the sources of variation in one layer would not affect another layer. This assumption is of course not true, but it is probably correct if the distance between two cut planes dz is large compared to the packing defects and the reactor area large enough to average out the defects.

The central limit theorem shows that the sum of any random variable will behave as a Gaussian law for a large number of terms. For this reason, we will then assume that the Pe increment follows a Gaussian law of mean m and standard deviation s . This assumption let us conclude that the Pe number then follows a Gaussian law of mean $m_{Pe} = N \cdot m$ and standard deviation $s_{Pe} = s\sqrt{N}$. The relative uncertainty of the Pe number with a 95% confidence level $U_{95\%}$ is by definition given by Equation 46. As L is proportional to N , $U_{95\%}$ is proportional to $\frac{1}{\sqrt{L}}$ (Equation 47).

$$U_{95\%} = 1.96 \frac{s_{Pe}}{m_{Pe}} \quad \text{Equation 46}$$

$$U_{95\%} = 1.96 \frac{s\sqrt{N}}{N \cdot m} \sim 1.96 \frac{s\sqrt{L}}{L \cdot m} \sim \frac{1}{\sqrt{L}} \quad \text{Equation 47}$$

The relative uncertainty on the Pe number due to random packing decreases as the inverse of the square root of the reactor length. Short reactors are thus likely to give both small Pe numbers and large variations of Pe number values and are thus not recommended for kinetic studies.

6.3.5 Conclusions and perspectives

Combining recent advances in fixed bed simulation and Liu's moment theories, we were able to compute accurate values of Pe numbers in fixed bed reactors packed with spheres in presence of a single-phase laminar flow. The whole workflow is fully automated and requires less than 1 day per case (geometry creation, meshing, CFD simulation and post-treatment). This workflow is now faster than experiments and with a perfect control on parameters. It gives access to local information as would be given by complex experimental tools like μ PIV or tomography.

We first used this capability to explore the relationship of the Pe number as a function of δ for narrow reactors ($\delta < 4$), fluid velocity and molecular diffusivity. This relationship proves to be quite complex and it can be qualitatively explained by looking at the packing structures. At low δ ($\delta < \delta_c \sim 1.87$), the packed beds are structured (string pellet string reactors) and the Pe number evolution, for a fixed bed length, is mainly explained by the increasing size of the preferential passages between the spheres and the walls. For larger δ , the packed beds are more random and start to behave like larger fixed beds except when δ values correspond to a structured case (ex : structuration in several circles of spheres with a hole in the center $\delta \sim 2.6, 3.4, \dots$). We also notice that average reactor void fraction present steep changes against δ that are not captured by literature correlations that tend to be too "smooth".

We then presented a real-life case study when, for a fixed catalyst mass and flow rate, we have to choose the optimal reactor diameter or particle diameter to adopt. In both cases we recommend

avoiding δ around 2.58 (hole in the center). Single Pellet String Reactors are a good option but from a practical point of view δ values very close to 1 are to avoid because of the potential blockage of particles during the reactor loading if the particles are not perfectly spherical or present a size distribution.

In the end, we use the digital twin workflow to quantify the packing uncertainty in a $\delta=4$ fixed bed reactor. While, as already known, the Pe number increases on average linearly with the length, we propose that the uncertainty on the Pe number decreases with a power of -0.5 of the reactor length.

Perspectives are to perform the same work with cylindrical pellets where we expect smoother evolution of the Pe number as a function of reactor diameter due to a more random packing. Another perspective is to extend the workflow for a study of local mass transfer quantification which will be more challenging due to very steep gradient near the particles: a finer mesh will probably be necessary to capture those gradients, especially for liquids. In the end it could be interesting to study the effect of porosity fillers. Here the limitations will be the computational load as the DEM simulation are very long (months) and the parallelization does not reduce significantly the simulation time.

6.4 CFD simulations exploring the effect of porosity fillers

CFD simulations are performed using the same workflow as presented in the section §6.3. The main differences are in the geometry and the mesh convergence.

6.4.1 Case description

The base geometry is a reactor of internal diameter 4 mm, filled with four spherical beads of diameter 3 mm. DEM was used to prepare that base geometry and, in a subsequent step, the porosity filler was added. The DEM simulations lasted about 40 days and were performed by a former IFPEN student (Anais Devouassous). Two DEM simulations were completed, one with a 328 μm diameter spherical porosity filler and the other with 160 μm . Cuts across the packing indicate that the 328 μm porosity filler was not able to fill up all the void fraction in a uniform manner (see Figure 56).

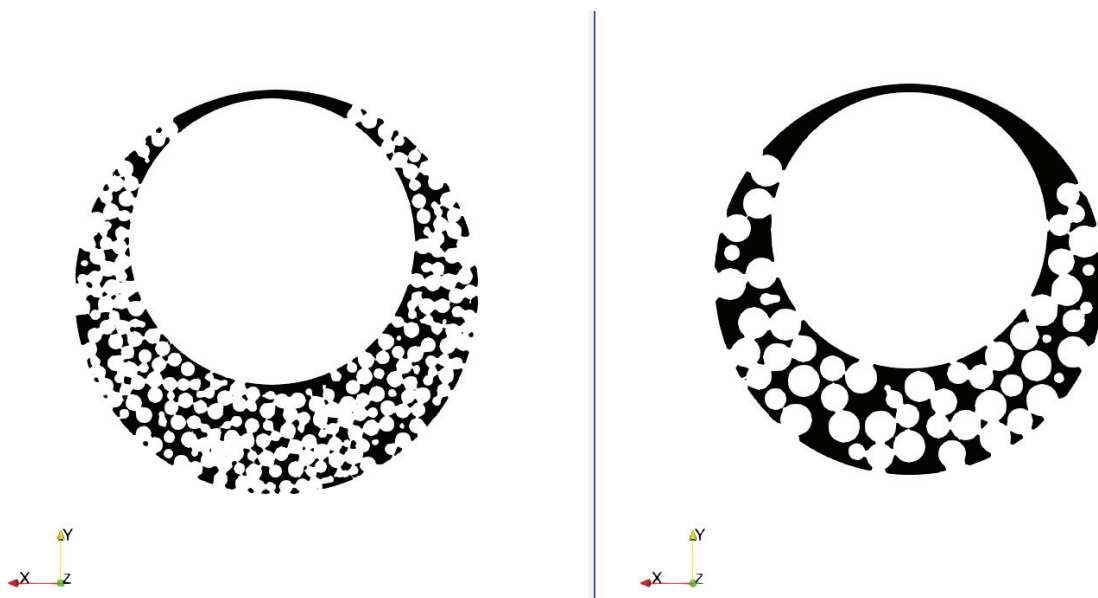


Figure 56. Comparison of packings when using porosity fillers of 160 μm (left) and 328 μm (right) in diameter

CFD simulations were only performed with the largest porosity filler. We added empty reactor length of 3 mm before the first large bead and 12.5 mm after the last one to limit the effect of inlet and outlet boundary conditions on the simulation.

6.4.2 Pe number with and without porosity filler

6.4.2.1 Mesh convergence

For the packing without porosity filler, the background average mesh cell size has been fixed at 55 μm per single cell, that is highly sufficient for the mesh convergence (in the cases presented in §6.3.3.2 it was 96 μm for the reactor of 7.75 mm). With porosity filler the fluid passages are smaller, and a mesh convergence study has been done for the packings (Figure 57), varying the background average mesh cell size.

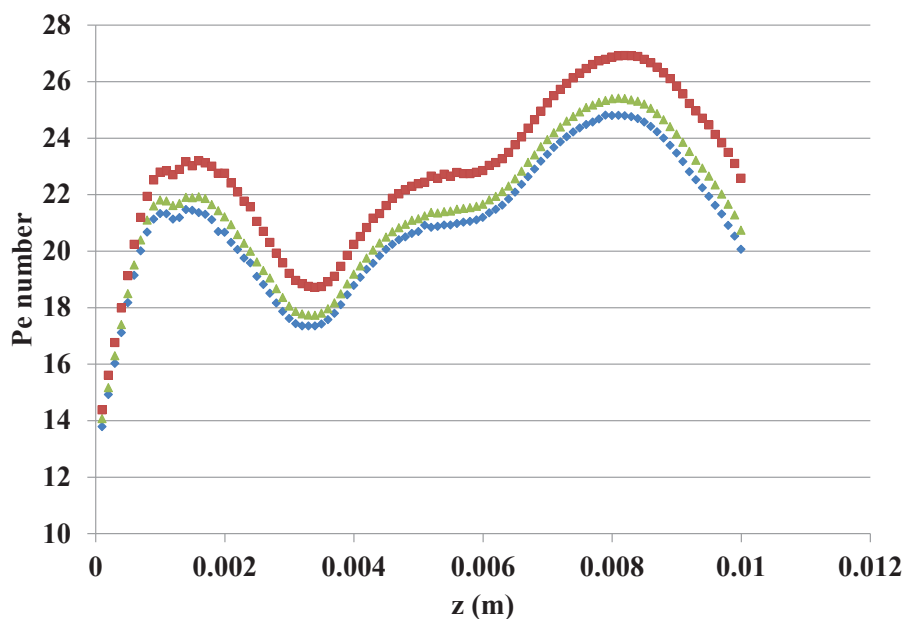


Figure 57. Comparison of three different background average mesh cell size (55 μm : red squares, 37 μm : green triangles, 27.5 μm : blue diamonds) based on the Pe number profile along the bed

The chosen mesh is the one with 27.5 μm background average mesh cell size. The simulations take around 30 hours for 25 million of cells.

An image of the final mesh is shown in Figure 58:

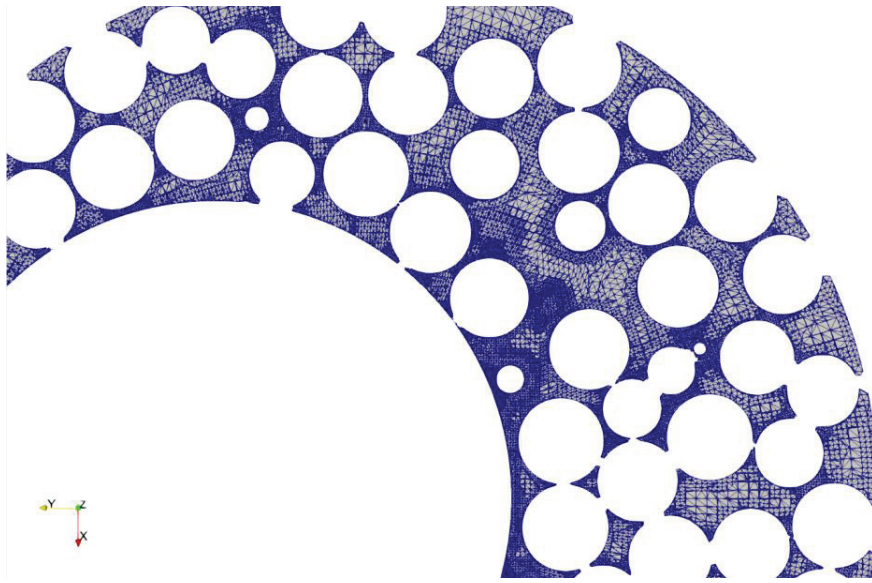


Figure 58. Mesh resolution in presence of porosity filler

6.4.2.2 Different flow patterns

Without porosity filler, the flow before the beads evolves as a Poiseuille flow, and then it is fully deviated through the porosity between the first sphere and the wall (Figure 59).

With porosity filler, the flow before the packed bed is more uniform. When the packed bed begins, the flow distribution is quite uniform, with passages visible in specific areas corresponding to zones with relatively “larger” spaces, for example at the contact points of the spheres with the reactor wall (Figure 59).

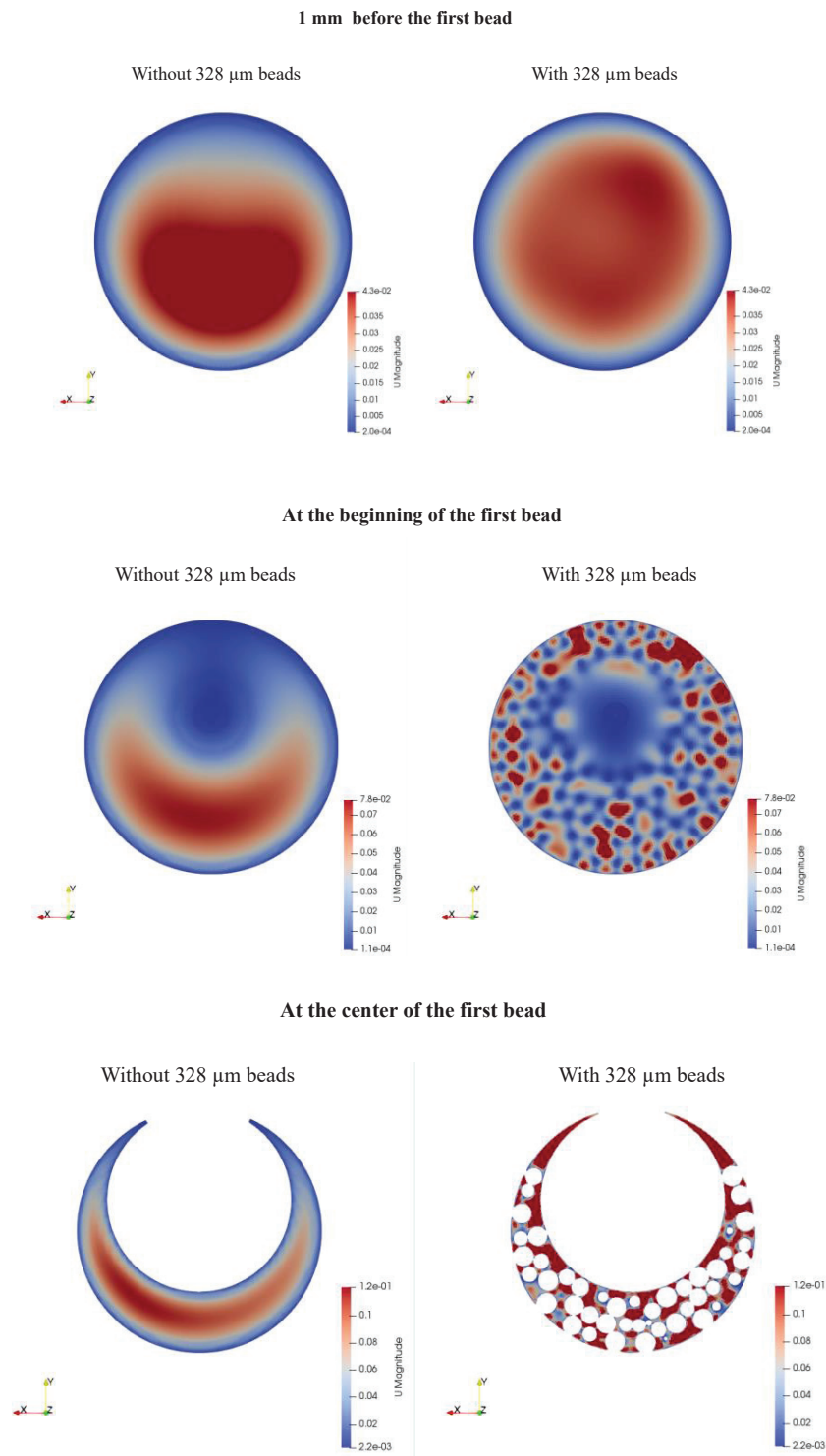


Figure 59. Velocity fields with and without porosity filler in different cross sections of the bed

6.4.2.3 Pe number profiles along the bed

With such different flow patterns, it is not surprising to observe significant differences on the Pe number profiles along the bed (Figure 60).

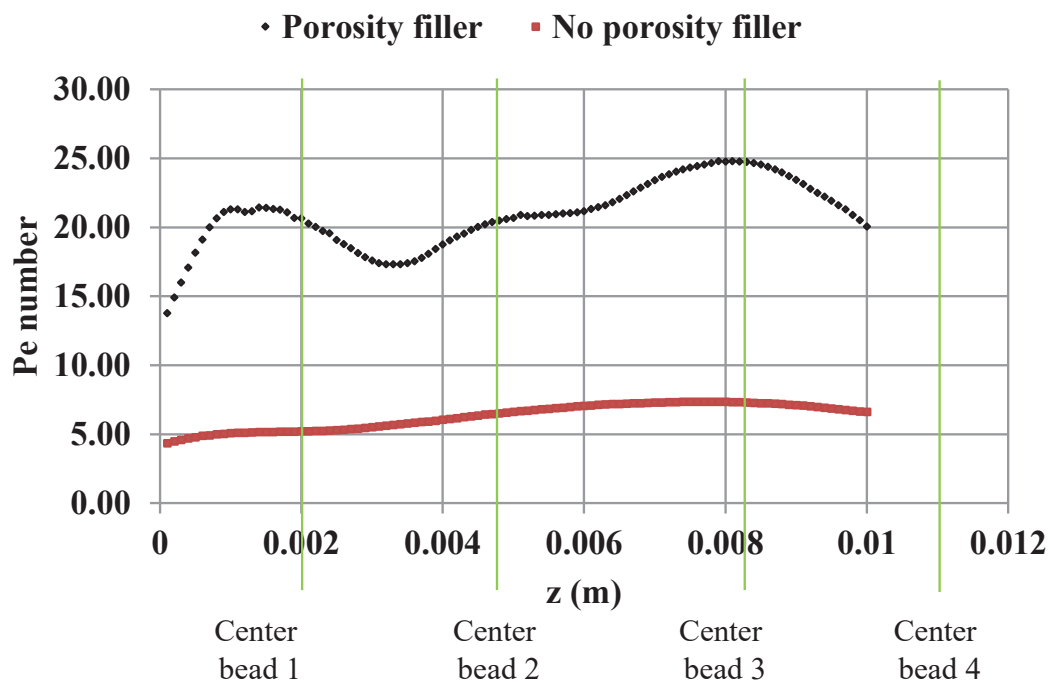


Figure 60. Pe number profiles in the reactor with and without porosity filler. $z = 0$ is 1 mm before the first sphere. The green vertical lines indicate the larger bead centers

A first observation is that the Pe number is much higher in presence of porosity filler starting already from the beginning ($z \sim 0$). This results from the developing Poiseuille flow in absence of porosity filler that causes dispersion.

Another observation is that the Pe number profiles for both cases present the same overall shape: a maximum around the first bead, a steady increase and a decrease near the end, but with a dampened evolution in absence of porosity filler.

The decrease of the Pe number around $z=2$ mm for the reactor with porosity filler is explained by bypasses near the larger beads – reactor contact points where porosity filler cannot access (Figure 61). This effect is more visible at the level of the first bead compared to the second, probably because the flow around the first bead is affected by the inlet flow.

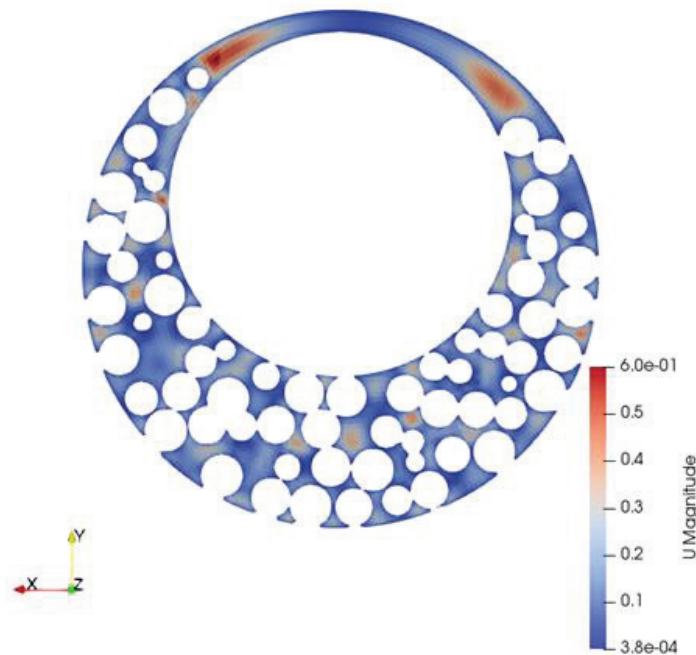
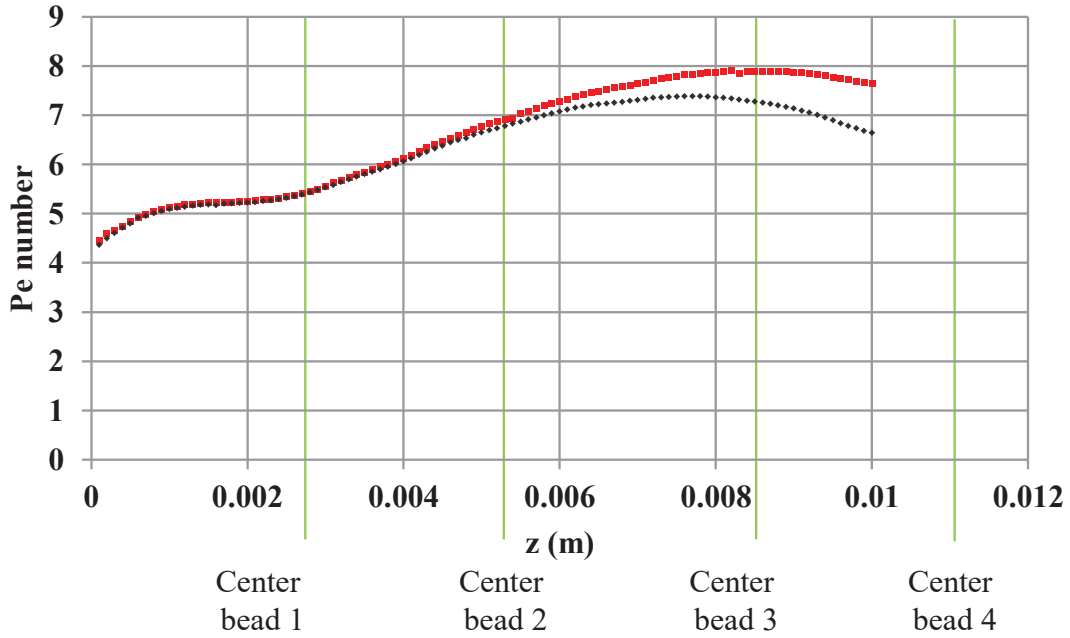


Figure 61. Velocity field in a transverse reactor section showing bypasses near the contact points. $z=1.8$ mm

We explored the effect of the size of the empty domain after the fixed bed (Figure 62). In absence of porosity filler, the effect of the empty length downflow of the catalyst bed on Pe number extend almost back to the first bead. At this point, it is unclear which case yields the most physical results. With porosity filler, the effect of the empty length only extends to the third bead and it is reasonable to think we have a physical solution.

A) No porosity filler



B) Porosity filler

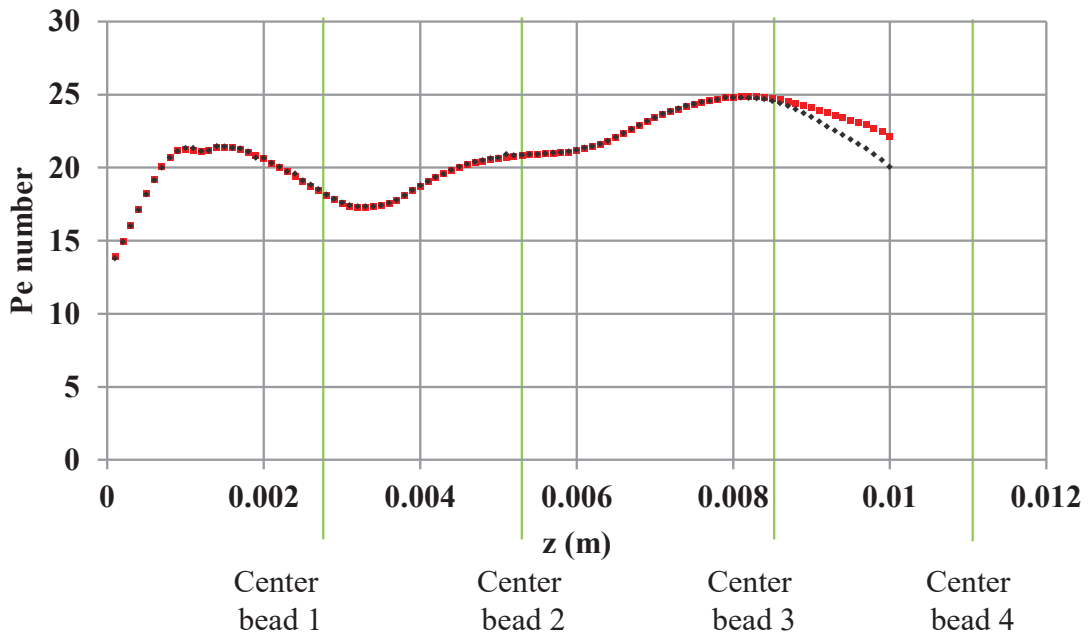


Figure 62. Effect of the empty length after the packing on the Pe number evolution in the bed. A) Without porosity filler, B) with porosity filler. Red squares: 0.55 cm of void, black diamonds: 1.25 cm of void

A further comparison is performed with a longer geometry (24 cm of packing) obtained previously, for the work presented in §6.3, with $D_r=4$ mm and $d_p=3$ mm. As we can see in Figure 63, even using the data from the geometry with only 0.55 cm of empty space after the packed bed, the difference of values is quite important. For this reason, in the paragraph §6.3 we always computed Pe numbers on bed length shorter than the simulated ones.

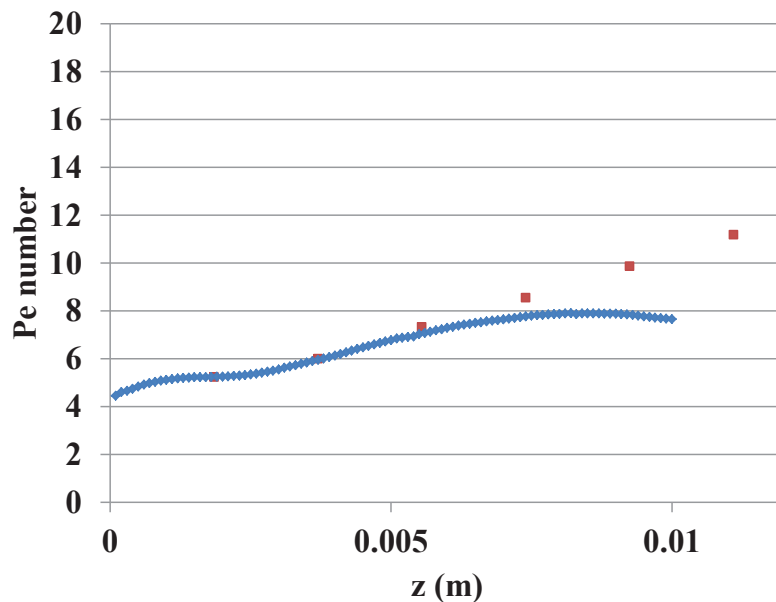


Figure 63. Pe number evolution along the bed length for a reactor $D_r=4$ mm packed with 3 mm particles. Blue diamonds: bed composed of only four beads, red squares: longer bed. The empty domain downflow the bed composed by the four beads is 0.55 cm.

To compare quantitatively the reactors with and without porosity filler, we calculate the slope of the Pe number evolution along the bed axis between 3.7 and 7.4 mm, a zone that in theory is not or less affected by the inlet-outlet effects on the flow. We obtain a value of 2.5 considering for the

case without porosity filler not the geometry with only four beads but the longer one whose results are shown in Figure 63.

Experimentally, in the work presented in §6.2, we found a ratio of around 2 but for another type of reactor.

To gain reliability, further work should deal with longer geometries, but this will significantly increase the computational cost of the simulations.

6.4.3 Mass transfer

Mass transfer is evaluated by coupling a classical transport equation to the CFD solver and computing the concentration profile of a tracer whose concentration is set to 0 at the reactor inlet and to 1 on the active particle surfaces (the beads). The boundary condition on the other particles is “no concentration flux”. This approach is analog to a “dissolution experiment” (for example β -naphthol dissolution or ice vaporization in hot air) with the advantage that the particle diameter does not change during the simulation. The overall mass transfer is evaluated during post processing through the calculation of the mixing cup concentration (velocity weighted average) in planes perpendicular to the reactor axis. CFD also gives information on local transfer. Using CFD we varied the number of active particles, the fluid velocity, and the molecular diffusion coefficient.

The mesh convergence has been performed on a single bead geometry without porosity filler and testing the following background cell size: 50, 33.3, 25, 20 and 16.7 μm . The tracer concentration profiles along the bed axis (Figure 64) show that between the meshes with 20 and 16.7 μm base cell size the difference is negligible so that the former is adopted for future tests. The mesh convergence has not been repeated on geometries with porosity filler (328 μm beads) for two

reasons. The first is the high computational cost, the second is that we already concluded that the geometries were too short to ensure a developed flow. The results will remain indicative.

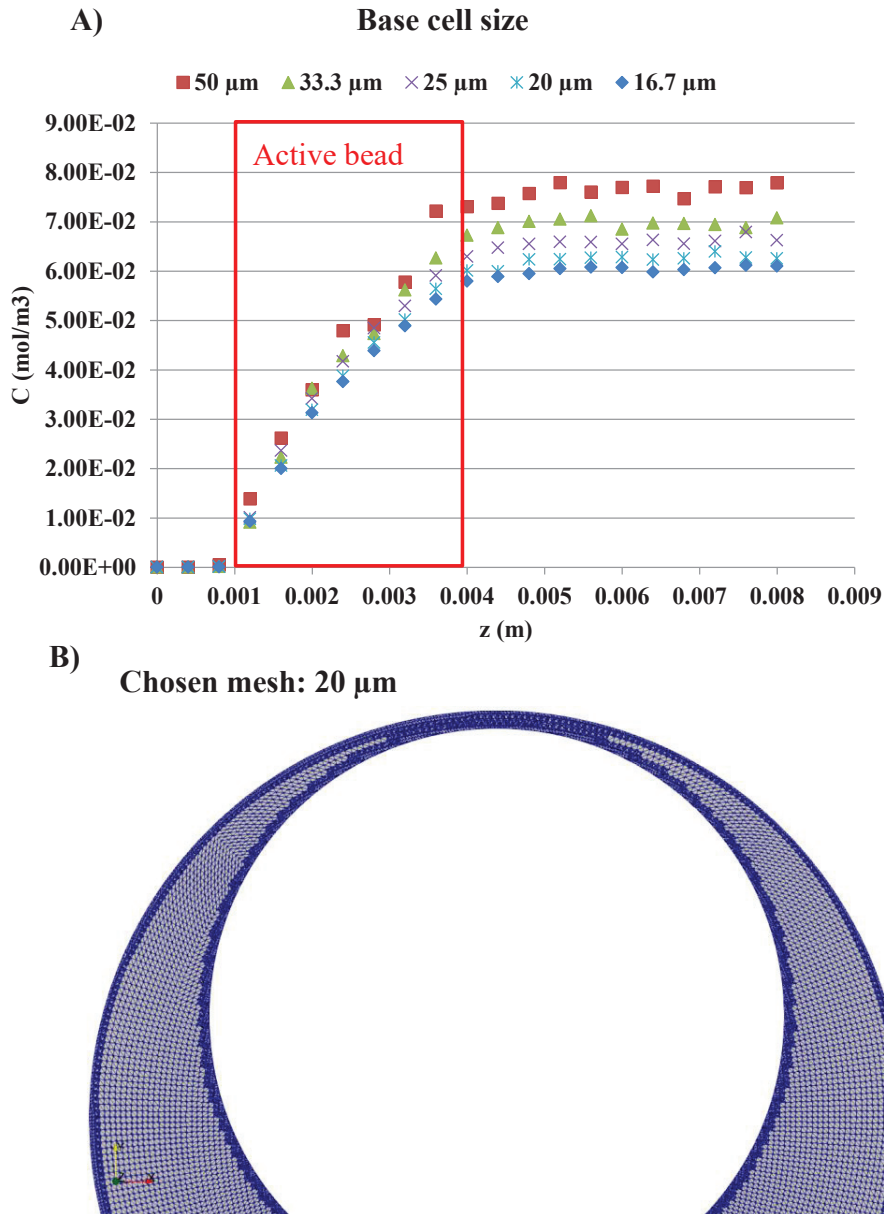


Figure 64. A) Comparison of five different background average mesh cell size mesh: averaged concentration profiles along the bed. B) Representation of the chosen mesh (20 μm)

For the geometry with the four beads, the porosity filler, and an empty space of 0.55 cm after the packing, we have a mesh of 28.5 million cells. The simulations take around 10-12 hours splitting the convergence process in two steps: first the hydrodynamics (velocity field), then the concentration field. The strategy reduced the memory and the CPU load.

6.4.3.1 Porosity filler effect on mass transfer

One active bead

When a single particle is active (the second on the four), the mass transfer is much higher using porosity fillers (Figure 65 Right). A detailed analysis of the concentration evolution in transverse cuts (Figure 65 Left) indicate that, in presence of fine particles, the concentration near the active particle decreases faster when the distance to the particle increases. The concentration gradients are thus higher and transfer faster. We think this is due to the higher interstitial velocity. Interestingly, when looking in transverse cut, the concentration fronts are steeper in presence of powder. The tracer is localized exactly downstream of the active particle and is not as well mixed as in the case without powder.

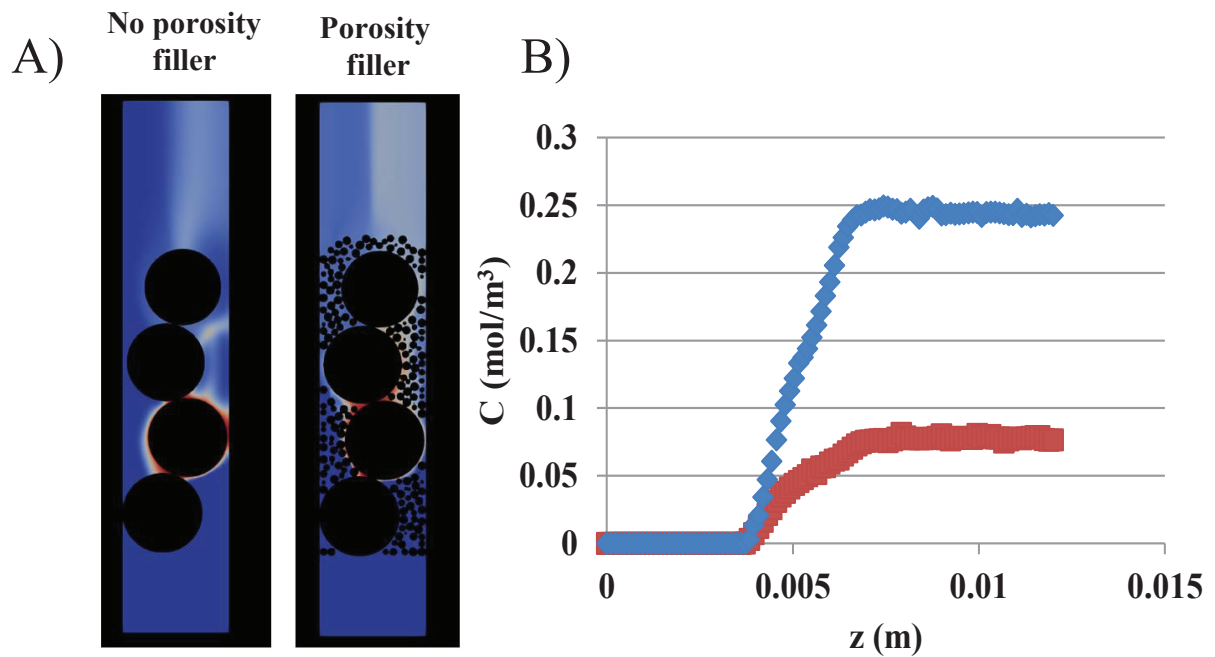


Figure 65. Concentration profiles. Only the second bead is « active ». $D_m=10^{-7}$ m²/s, $u=0.0272$ m/s. A) Axial cuts. Dark blue $c=0$, red $c=1$. B) Averaged concentration profiles (blue diamonds: porosity filler, red squares: no porosity filler)

Varying the molecular diffusivity, we can see that the positive effect of the porosity filler is reduced at high molecular diffusion coefficients (Figure 66).

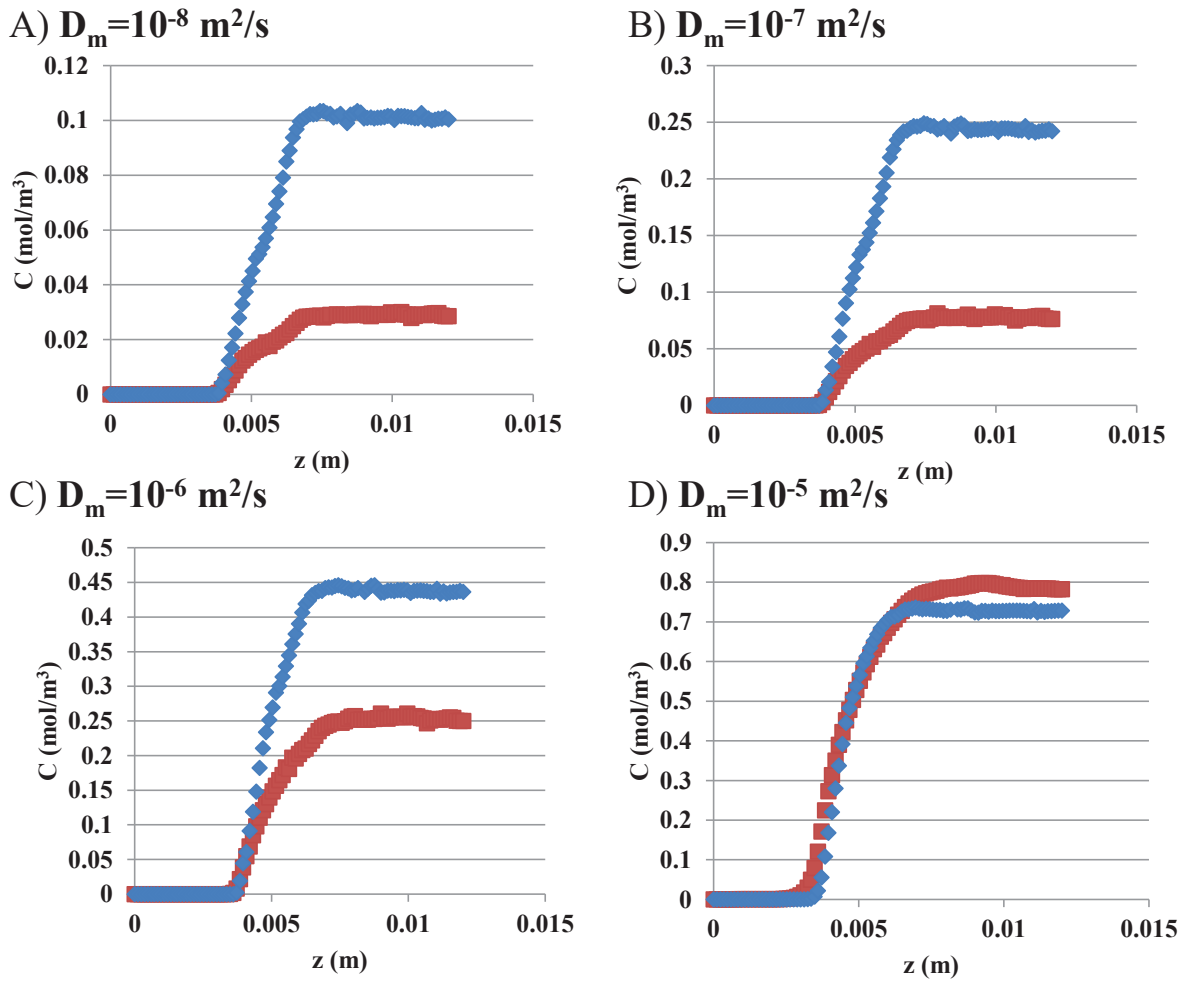


Figure 66. Averaged concentration profiles for four values of molecular diffusivity. $u=0.0272$ m/s, only one bead active. Blue diamonds: porosity filler, red squares: no porosity filler

When increasing the velocity for the case $D_m=10^{-5}$ m²/s we see that porosity filler shows again a beneficial effect (Figure 67). This means that porosity fillers improve mass transfer when convection dominates over diffusion.

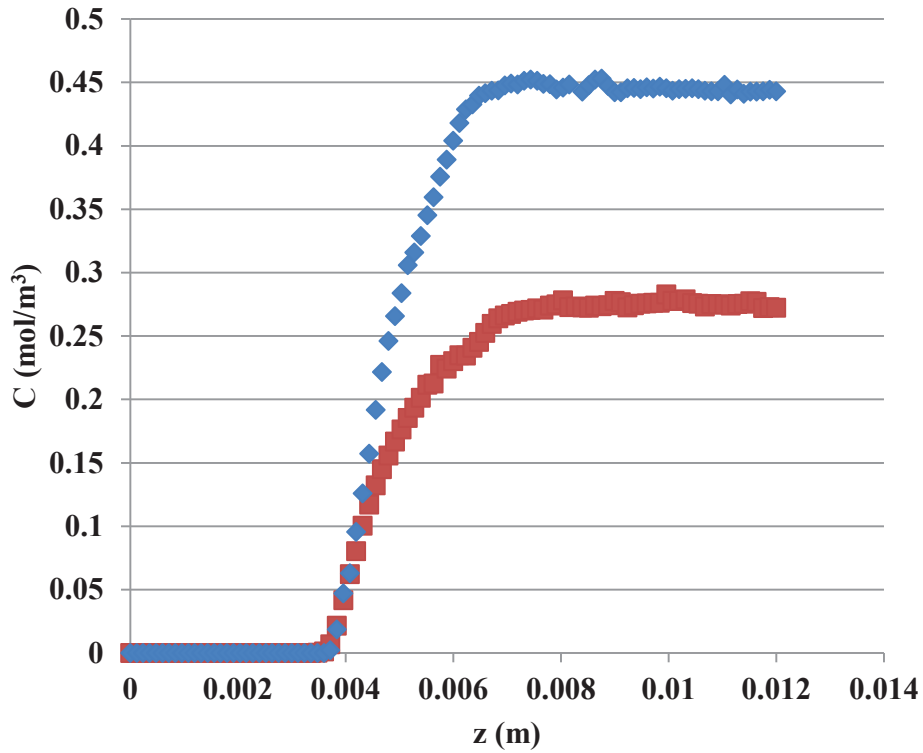


Figure 67. Averaged concentration profiles for $D_m=10^{-5} \text{ m}^2/\text{s}$ and $u=0.272 \text{ m/s}$. Only one bead active. Blue diamonds: porosity filler, red squares: no porosity filler

We will now present the values of overall gas-solid mass transfer coefficient k_{gs} [m/s] and Sh number that we computed with the following equations:

$$k_{gs} = \frac{Q \cdot C_{out}}{A \cdot (C_{sat} - C_{in})} \quad \text{Equation 48}$$

$$Sh = \frac{k_{gs} \cdot d_p}{D_m} \quad \text{Equation 49}$$

in which Q is the fluid flow rate [m^3/s], C_{out} is the concentration at the reactor outlet [mol/m^3], A is the surface exchange area (πd_p^2 in the case of a single sphere) [m^2], C_{sat} is the saturation concentration [mol/m^3 , 1 in our case], and C_{in} the concentration at the reactor inlet [mol/m^3 , 0 in our case]. The term $Q \cdot C_{out}$ indicate the molar flux at the reactor's exit, and it represents the overall mass transfer flux from the packing to the fluid. In the Sh number, the particle diameter is always

represented by the diameter of the large particles, which are the “active” particles for the mass transfer.

We observe (Figure 68) that k_{gs} increases with the molecular diffusivity, with the flow velocity and when using porosity fillers (confirming our experimental deductions in §6.2). At high molecular diffusion and low velocities, the packing effect disappears: in this regime, the molecular diffusion is fast enough to homogenize the concentration profiles whatever the flow pattern.

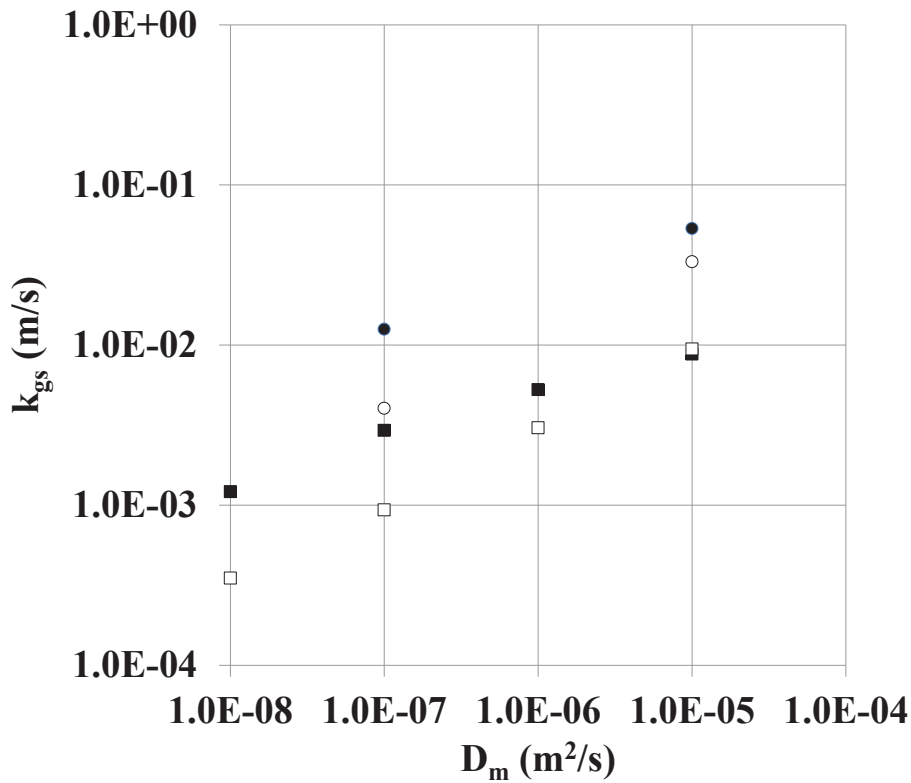


Figure 68. k_{gs} as a function of D_m when only the 2nd bead is active. Packings with (black points) and without (white points) porosity filler. Two superficial velocities tested: 0.272 m/s (circles) and 0.0272 m/s (squares)

The same comments are valid for the evolution of the Sh number (Figure 69), with the exception that it decreases with the molecular diffusivity instead of increasing (because D_m is in the denominator of the expression of the Sh number and k_{gs} increases less than linearly with D_m).

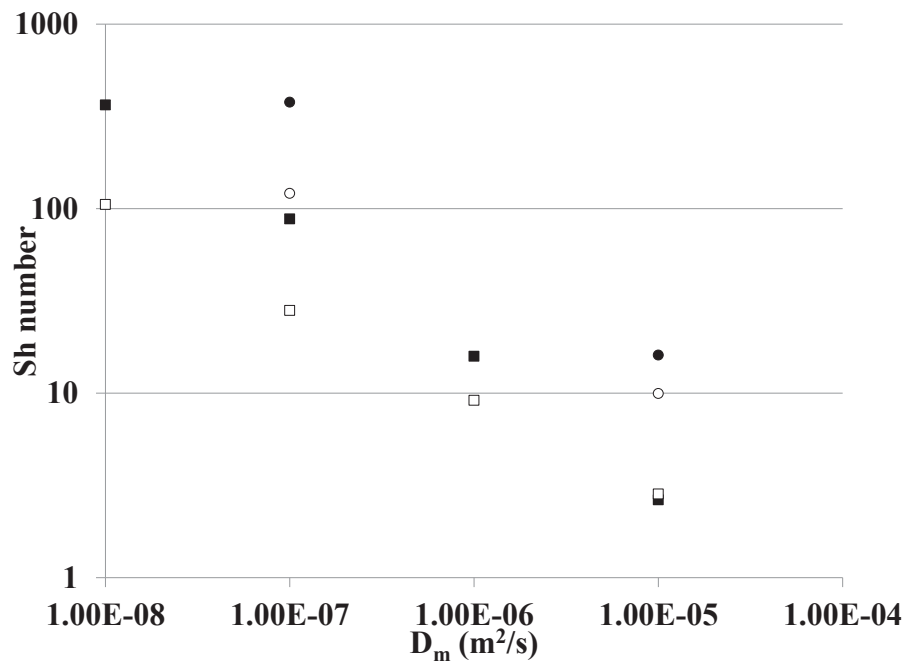


Figure 69. Sh number as a function of D_m when only the 2nd bead is active. Packings with (black points) and without (white points) porosity filler. Two superficial velocities tested: 0.272 m/s (circles) and 0.0272 m/s (squares)

A last comment is that the effect of increasing u or decreasing D_m is almost equivalent. This is expected as the common relationship in literature show that the Sh number is dependent from the Reynolds number (u in the numerator) and Schmidt number (D_m in the denominator) with a slight different powers (usually 0.5-0.6 and 0.33 respectively, i.e. [28, 85]).

Two active beads

Further simulations have been performed with two beads active (the 2nd and the 3rd) for a fluid velocity 0.0272 m/s and two values of molecular diffusivity: 10^{-7} and 10^{-5} m²/s. For $D_m=10^{-5}$ m²/s we saturate the flow and reach the maximum concentration (~ 1) so that only the points at $D_m=10^{-7}$ m²/s will be presented.

The presence of porosity fillers is still beneficial. But if we compare this case with the case of only one bead active, the k_{gs} and Sh number are slightly decreased (Table 10). This indicates that probably the transfer is affected by the reduction of the “driving force” between the beads and the fluid when the fluid meets the second bead.

Table 10. Sh number and k_{gs} compared when 1 or 2 beads are « active »

Sh number	k_{gs} (m/s)	Porosity filler	N° active beads
28.08	9.36×10^{-4}	NO	1
27.20	9.07×10^{-4}	NO	2
88.03	2.93×10^{-3}	YES	1
73.79	2.46×10^{-3}	YES	2

Although the bed length is probably too short to have a fully developed flow, these results are interesting as they give interesting trends that should be confirmed in further work.

Comparison with the Ranz-Marshall model

The Sh number computed in the case of only one bead active will now be compared with the Ranz-Marshall equation ([28], see Equation 10), using the coefficients optimized by Wakao et al. [85]:

$$Sh = 2 + 1.1Re^{0.6}Sc^{0.33} \quad \text{Equation 50}$$

in which Re is the Reynolds number $\left(\frac{\rho \cdot u_i \cdot d_p}{\mu}\right)$ and Sc the Schmidt number $\left(\frac{\mu}{\rho \cdot D_m}\right)$. The characteristic dimension (d_p) is the active bead diameter for the Sh number while for the Re number it is the smallest diameter of the particles (catalyst diameter in absence of porosity filler or filler diameter if present). The correlation describes correctly the CFD derived Sh numbers in the case without porosity filler but severely overestimates the Sh in presence of presence of porosity filler (Figure 70).

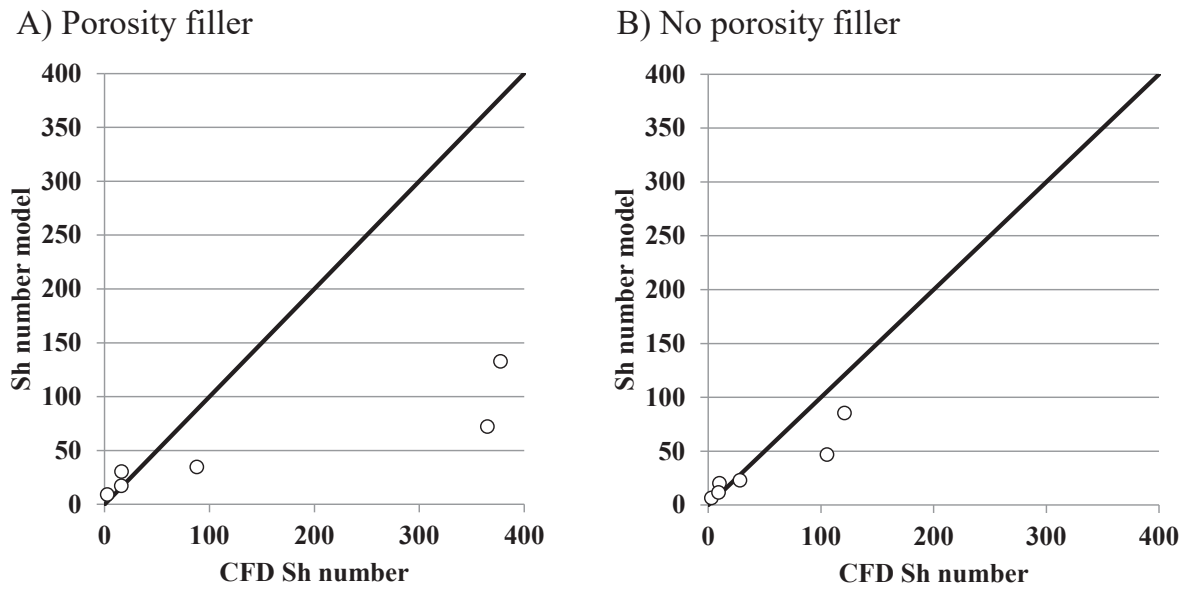


Figure 70. CFD derived Sh numbers compared those obtained with the equation of Wakao et al. [85]

A better fit can be obtained if we change the exponents of the Re and Sc numbers (Table 11 and Figure 71). This re-optimization leads to high exponents for the Sc numbers and one can argue on their physical meaning. We are not able to understand if this results from a too coarse mesh, a too short bed or from the peculiar geometry of Single Pellet String Reactors. Further work is required but CFD appears promising to explain mass transfer in SPSRs and to optimize packings.

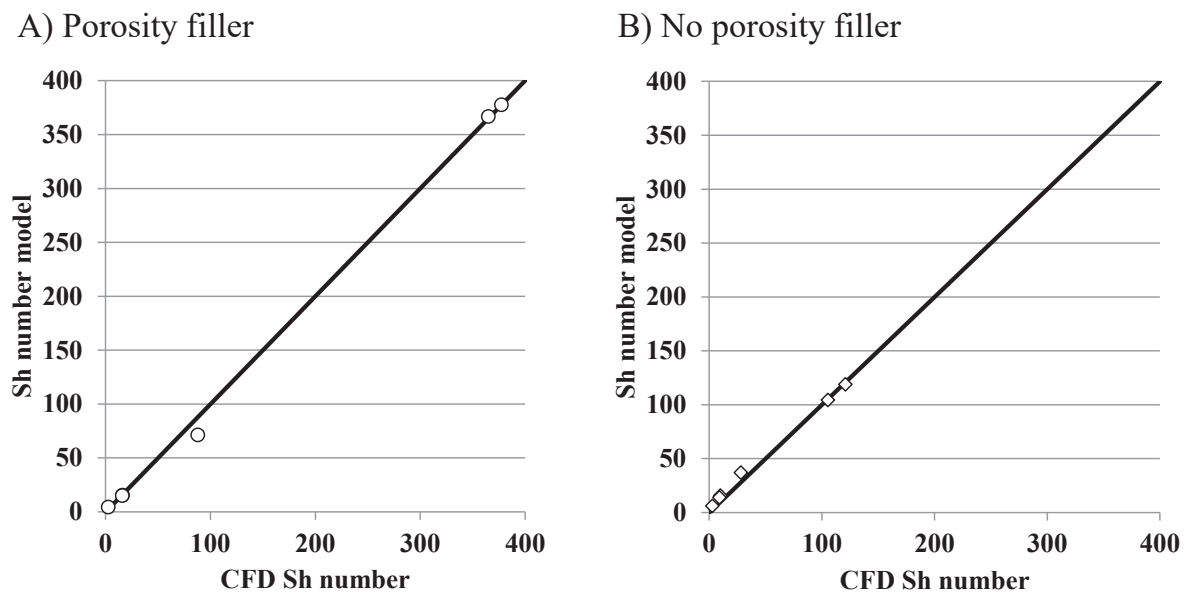


Figure 71. CFD derived Sh numbers compared those obtained with the Ranz-Marshall equation [28] and re-optimized coefficients for the Re and Sc number

Table 11. Recalculated exponents for the Re and Sc number

	Wakao et al.	No porosity filler	Porosity filler
Re number exponent	0.6	0.522	0.734
Sc number exponent	0.33	0.464	0.721

6.4.4 Conclusion on CFD with porosity filler

The workflow described in §6.3 has been used for a Single Pellet String Reactor filled with 4 spheres of 3 mm, packed in a tube of diameter 4 mm. 328 μm spheres have been used as porosity filler. One conclusion is that the geometries are probably too short to be predictive, but the CFD simulations gave anyway an insight of the physics. Adding the 328 μm spheres as porosity fillers makes the flow more uniform and faster (void fraction effect). Some bypasses still exist near the large particle to reactor contact points where the porosity filler cannot fit in. Both the Pe number and the mass transfer are increased by the presence of the porosity filler. The mass transfer enhancement is likely to be due to an increase of the interstitial velocity that conveys the tracer away faster and thus increases the gradient and hence the fluxes. The computed Sh numbers in absence of porosity filler, contrarily to those computed in their presence, are close to the values that can be calculated using the models available in literature. The cause may be a not sufficiently refined mesh in case of packings with porosity fillers, but further simulations are needed to explain the difference observed.

We recommend for future work to prepare longer geometries which will be very long to create using DEM (~ 100 days) as those simulations do not gain in parallelization. To avoid this, an idea could be to “repeat” the packing geometry obtained with the four spheres and translate it to obtain that the two packings are consecutive. This can be done using “periodic packings” or by accepting some discontinuity on the fine powder packing.

7 Gas-liquid-solid case

The bibliographic study presented in §3 shows a lack of knowledge on packed bed millireactors operated in gas-liquid-solid conditions and packed with millimetric particles. To fill this lack, the following strategy is adopted:

- Flow regime visualization and residence time distribution (RTD) experiments are carried out to understand the hydrodynamics of these reactors;
- Reactive experiments, aiming at evaluating the porosity filler effect on the conversion, are carried out in the same unit used for the gas-solid reactive tests and presented in §6.1.

7.1 Hydrodynamic experiments

7.1.1 Strategy and scope of the tests

Hydrodynamic experiments are performed to study the effect of the packing type on the flow regimes, liquid dispersion and holdup in G/L/S packed bed millireactors. We remind here that, as defined in §2.2, in our work the liquid holdup is the ratio between the volume occupied by the liquid and the volume of the empty reactor. The parameters of interest are the $\delta=D_r/d_p$ ratio, the bed length, the fluid velocities, the particle material, and the porosity filler effect. The following conditions are tested:

- The reactor diameters vary from 2 to 4 mm and the lengths from 9 to 17.9 cm;
- The gas flow rates vary from 26.75 to 294.72 NmL/h;
- The liquid flow rates vary between 1.07 and 11.79 mL/h, corresponding to liquid superficial velocities from 10.7 to 93.82 cm/h;

- The G/L flow rate ratio varies between 5 and 60 NmL/mL;
- Non-porous pellets in form of cylinders/spheres (1-3 mm) in glass, ceramic or metal material are used;
- Fine inert powders of different sizes (SiC or ZirBlast[®]) are added in some cases to fill the remaining porosity of the beds.

The particle size and the inert powders used are the same as those used for the G/S reactive tests (see §6.2).

A thin layer of glass wool is used to keep the particles in position inside the bed. The gas and liquid flow rates, as also the G/L ratios, have been chosen to include the range of experimental conditions explored in the reactive tests.

7.1.2 Experimental bench description

Both flow visualization and RTD experiments are performed on the same bench (Figure 72). The reactors are in transparent glass, so that it is possible to visualize the flow, at least near the walls.

To measure the liquid residence time distribution curves of the packed bed millireactors, a set volume of a liquid tracer (~63 μ L) is injected at the inlet of the reactor. In this work *n*-heptane (nC7) is used as carrier and iso-hexadecane (iC16: 2,2,4,4,6,8,8-heptamethylnonane) as tracer. The properties of the two liquids are resumed in Table 12. The tracer has been chosen due to a good mixing with the *n*-heptane, low vapor pressure (to avoid evaporation) and a refractive index significantly different from *n*-heptane.

Table 12. *n*C7 and *i*C16 properties

Property	<i>n</i> C7	<i>i</i> C16
Viscosity (15°C) [mPa·s]	0.435	4.206
Density (15°C) [kg/m ³]	689.92	787.76
Vapor pressure (15°C) [Pa]	3607.98	2.62
Surface tension (20°C) [N/m]	0.0203	0.0244

Two syringe pumps are used to feed the two liquid species (Harvard PHD ultra 4400 for the *n*-heptane and Harvard PHD 2000 for the *i*C16). Both pumps run continuously, and the tracer injection is obtained by switching the position of a 6-way valve (Vici valve from Valco Instruments Co. Inc.). At the switching, the *i*C16 volume enclosed in the loop is pushed by the *n*-heptane into the reactor: we have a “pulse” of *i*C16 in *n*C7. The gas phase is nitrogen, delivered by a mass flow controller (Brooks Instrument). The *n*-heptane evaporation is estimated negligible in presence of nitrogen. A manometer is installed on the nitrogen line to check the pressure drop.

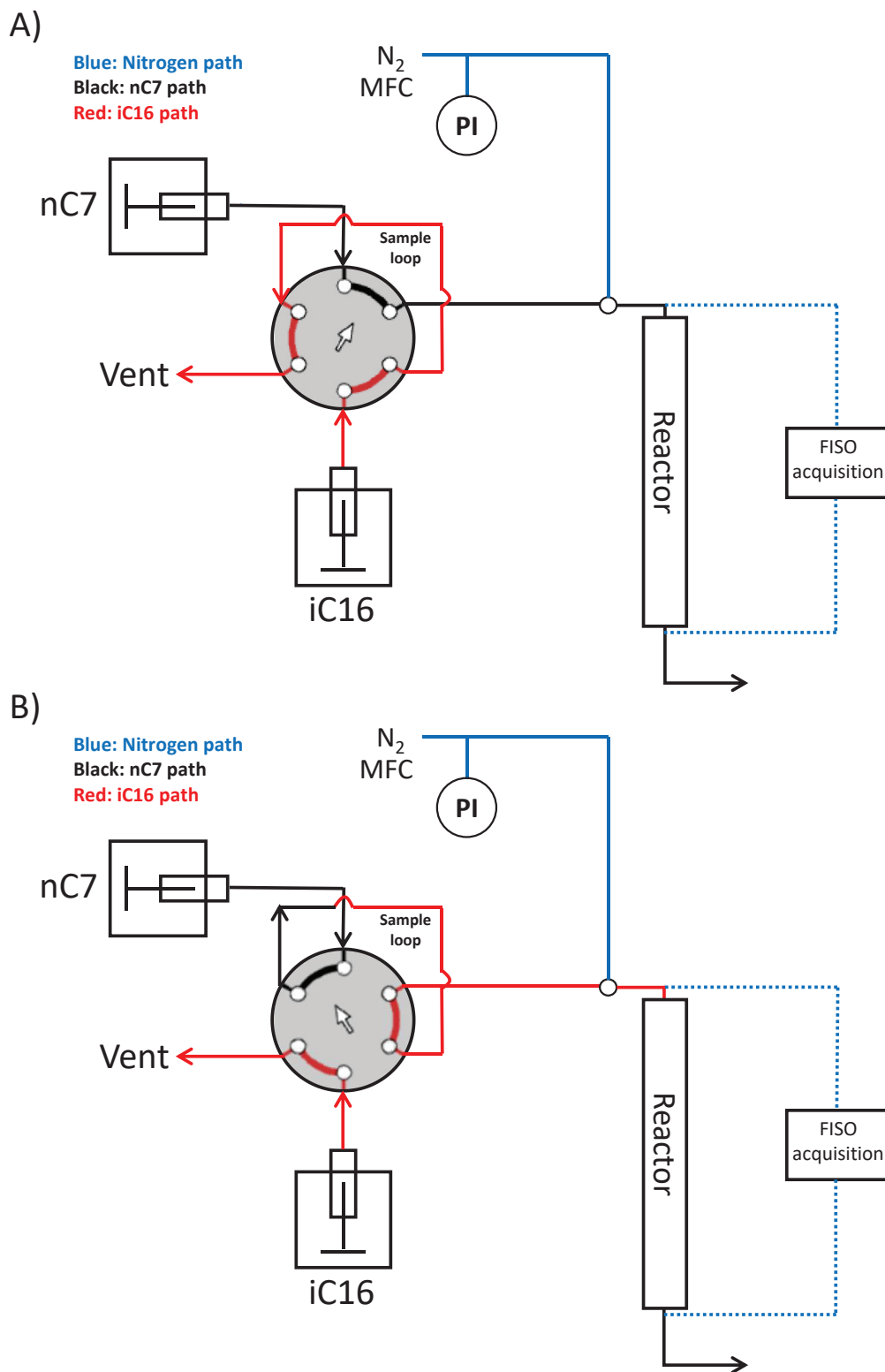


Figure 72. G/L/S experimental setup scheme: A) Before the switching B) After the switching

The gas and the liquid phase get in contact in a T-junction positioned before the reactor inlet. The flow at the exit of the T-junction is a train of gas bubbles and liquid slugs (Taylor flow). The connecting tube between the T-junction and the reactor inlet is in fused silica (internal diameter 0.53 mm). Contrarily to PTFE or PFE tubes, it has better wetting properties and provides for more stable bubble trains.

The tracer detection is performed by measuring the refractive index of the liquid phase using micro-probes (FISO) located at the inlet and outlet of the reactor in presence also of the gas phase. Surface tension keeps the prisms at the tip of the probe constantly surrounded by liquid and the measurement is not impacted by the bubbles [24]. The bubble passages are in fact helping to sweep the fluid and prevent stagnant liquid at the probe tip. This choice is different compared to the one of Marquez et al. [22], that separate the two phases after the reactor exit but before the measurements. The risk is to generate dispersion when separating the two phases, dispersion that has to be not too high and easily modellable. The time resolution of the acquisitions is 80 ms.

The fluid coming out of the reactor is sent to a waste bottle where gas and liquid phases separate.

Conversion of refractive index to concentration is performed through a calibration curve resulting from measurements at various concentrations. The calibration curves are different for each probe (Figure 73) and proved to be linear. Even if the absolute signal values change a little bit from one calibration to another, the difference between the signals corresponding to pure *n*-heptane and pure iso-hexadecane is constant.

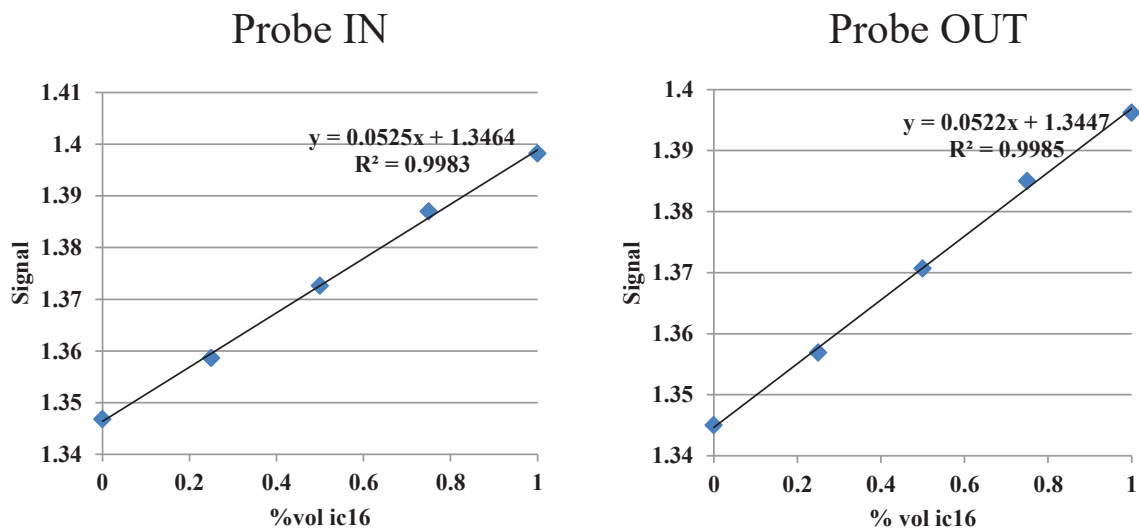


Figure 73. Refractive index variation with the %vol of iC16 in the mixture

7.1.3 Experimental protocol

To maximize the repeatability of the measurements and reduce the uncertainties, the following protocol has been optimized:

- The flow through the packed bed millireactors is started at least 1 hour before performing the tracer injections, to ensure that the hydrodynamic regime is well stabilized;
- The calibration has been regularly checked and a linear relation has always been found. Due to temperature changes, the absolute signal values changed a little bit from one calibration to another, but the difference between the signals corresponding to pure *n*-heptane and pure iso-hexadecane is constant and likewise the slope. The signal at the beginning of each test (nC7 only) is used to adjust the potential offset;
- For each condition, at least two consecutive acquisitions are performed.

All the experiments are performed at room temperature ($\sim 20^\circ\text{C}$) and atmospheric pressure.

7.1.4 Data interpretation: from the concentrations to Pe number

Two methods can be used to compute the Pe numbers. We recall that amount of dispersion, as already presented in paragraph §2.2.1, is quantified in terms of dimensionless Peclet (Pe) and/or Bodenstein (Bo) numbers:

$$Pe = \frac{u_{i,L} \cdot L}{D_{ax}} \quad Bo = \frac{u_{i,L} \cdot d_p}{D_{ax}} \quad \text{Equation 7}$$

in which $u_{i,L}$ is the liquid interstitial velocity (so u_L/ϵ_l).

A first method consists in using the axial dispersion model, as done for the gas-solid case. We remind here that it consists of a 1D mass balance equation with a dispersion term and closed system boundary conditions for the inlet and outlet of the reactor:

$$\frac{\partial C}{\partial t} = D_{ax} \frac{\partial^2 C}{\partial z^2} - \frac{u_l}{\epsilon_l} \frac{\partial C}{\partial z} \quad \text{Equation 6}$$

The model has been implemented in a FORTRAN program called using an Excel interface. For each reactor, the unknowns are D_{ax} , the axial dispersion coefficient, and ϵ_l , the liquid holdup. They are optimized in order that, running the model using the data obtained with the inlet probe as input data, the predicted concentration curve matches the recorded reactor outlet concentration curve. The model uses finite differences and an adaptive Runge-Kutta solver. Grid size and time step have been refined to ensure grid and time step independence.

First, ϵ_l is estimated by matching the experimental mean residence time with the simulated one. The experimental mean residence time is calculated as the difference between the outlet and inlet curves first moments of the normalized concentration.

$$\bar{t} = M_{1,out} - M_{1,in} \quad \text{Equation 51}$$

where $M_{1,out}$ and $M_{1,in}$ are respectively the inlet and outlet first order moments of the normalized concentration curves.

Next, the value of D_{ax} is optimized minimizing the relative difference between the experimental and simulated curve:

$$\sum_i \frac{|c_{out,i}^{mod} - c_{out,i}^{exp}|}{c_{out,i}^{exp}} \quad \text{Equation 52}$$

in which: $c_{out,i}^{mod}$ is the value of iC16 molar concentration at the instant t calculated with the model and $c_{out,i}^{exp}$ is the value of iC16 molar concentration at the same instant coming from the experimental curve. Due to experimental noise, the parts of the curve with values below 0.5% vol of tracer are not considered.

An example of the result of the optimization process is shown in Figure 74.

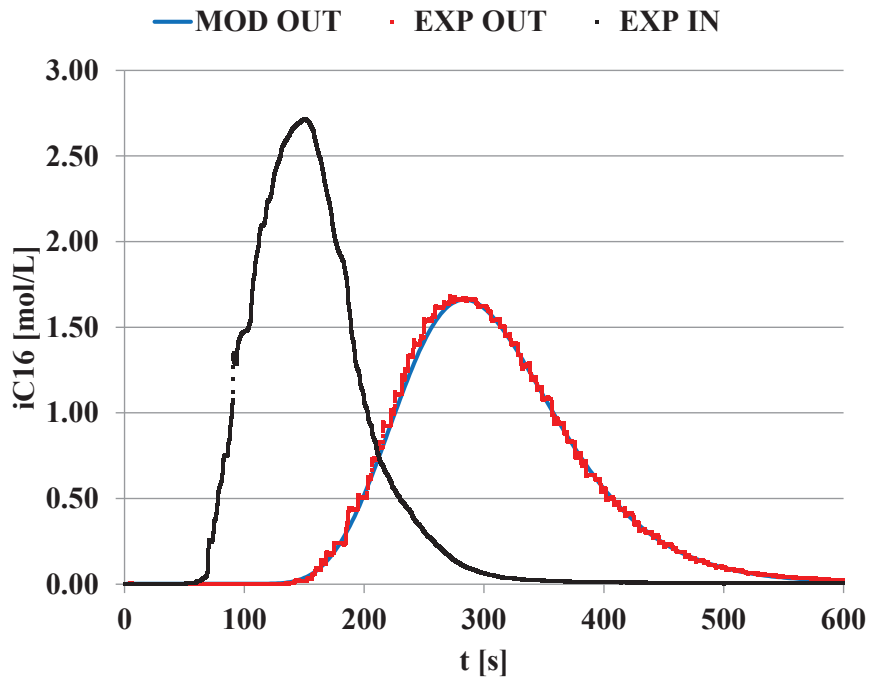


Figure 74. Result of the axial dispersion coefficient optimization method. $D_r=3$ mm, $d_p=2$ mm glass beads, $L=9$ cm, $Q_f=2.92$ mL/h, G/L ratio=60

Having access to the concentration profile at the reactor inlet makes it possible to use another method based on the moments of the concentration curves (reactor inlet and outlet) to calculate the Pe number:

$$Pe = 2 \frac{\bar{t}^2}{\sigma^2} = 2 \frac{(M_{1,out} - M_{1,in})^2}{(M_{2,out} - M_{1,out}^2) - (M_{2,in} - M_{1,in}^2)} \quad \text{Equation 23}$$

in which: σ^2 is the variance and M_1 and M_2 are the first and second order moments of the residence time distribution curves.

As we will see, the results of these two Pe number calculation methods are very close except for the cases that we will discuss now.

7.1.5 Differing inlet and outlet curves integrals

During the experimental campaign, the reactor inlet curves are stable, and their integrals return correctly the expected value: the number of moles of the tracer injected (\pm an experimental error) divided by the flow rate. An acceptable difference is fixed at $\pm 5\%$. We observed that, in some cases, the reactor outlet integrals are not always equal to the inlet:

- When the flow regime is highly pulsed, the integral of the outlet curve is higher than the one of the inlet curve (from +5 to +10%);
- When fine powder is used as porosity filler, the integral of the outlet curve is smaller than the one of the inlet curve (from -5 to -15%).

The Pe number calculated with the moments of the residence time distribution curves is not affected by this difference of the integrals because the moments are calculated using normalized curves. On the contrary, the Pe number calculated with the axial dispersion model is affected by this difference

because the fitting of the axial dispersion coefficient is performed directly on the concentration curves.

In pulsed flow (Figure 75), the measured concentration curves present a peculiarity on the rising side: they increase quickly, and then decrease to remain stable for some time, and so on. A plateau corresponds to stagnant liquid. An opposite pattern is observed on the decreasing side of the concentration curves.

The integral of the concentration is a simplification of the mass balance that assumes a constant velocity. The concentration peak before the plateau is probably sign of reverse flow due to capillary forces. The velocity at the reactor outlet is probably not constant and the integrals have no physical meaning.

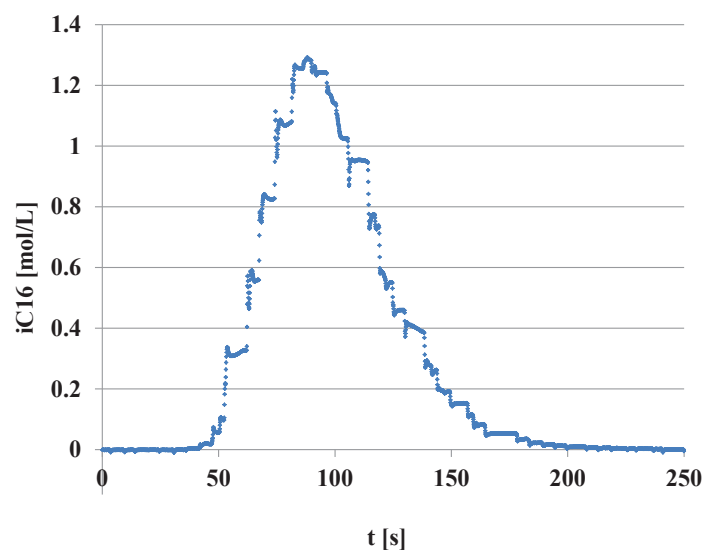


Figure 75. Example of a reactor experimental outlet curve obtained in case of pulsed flow.
 $D_r=4$ mm, $d_p=3$ mm, $L=9$ cm, $Q_f=10.72$ mL/h, G/L ratio=25

We will now explore in detail the “loss” of integrals for cases where the flow is stable (Table 13). As the phenomenon occurs only when using porosity fillers, it is not related to the measurement method or the equipment. When the porosity filler is smaller than 800 μm , integral losses until $\sim 10\%$ are measured for SiC particles and until $\sim 15\%$ for ZirBlast[®] powder (ZB). The particle shape plays a role, and we suspect capillary effects. Both the SiC and ZB particles are non-porous. They are not known to have some specific interaction with branched alkanes.

Table 13. Inlet-outlet integrals losses. $D_r=3\text{ mm}$, $L=9\text{ cm}$, $d_p=2\times 5\text{ mm}$ glass cylinders, $Q_I=2.92\text{ mL/h}$, $G/L\text{ ratio}=30$. In yellow, the points in which the difference is between -5 and -10%, in red the points in which the difference is above -10%

Porosity filler	% difference IN/OUT	Comments
No	+7.4	1 st pulse, pulsed flow
No	+8.6	2 nd pulse, pulsed flow
SiC 800 μm	+0.6	1 st pulse
SiC 800 μm	+0.2	2 nd pulse
SiC 300-400 μm	-9.3	1 st pulse
SiC 300-400 μm	-11.2	2 nd pulse
ZB 300-400 μm	-13.7	1 st pulse
ZB 300-400 μm	-15.6	2 nd pulse
SiC 150-200 μm	-8.1	1 st pulse, $\Delta P=10\text{ mbar}$
SiC 150-200 μm	-7.8	2 nd pulse, $\Delta P=10\text{ mbar}$

In order to better investigate this phenomenon, specific tests are performed filling a reactor only with ZirBlast[®] powder 300-400 μm (so without millimetric particles) into two reactors with different internal diameter, 3 and 4 mm, but same length, 9 cm. In the 4 mm diameter reactor, repeating the pulses at various time intervals (Figure 76) indicate that the repeatability of the outlet integral compared to the inlet is quite low (from -6.1% to +5.4%). A particularity of these outlet

curves, never seen otherwise, is the “staircase” behavior on the decreasing side of the curves (Figure 77), as if the flow was pulsed on the decreasing side but much less on the increasing side.

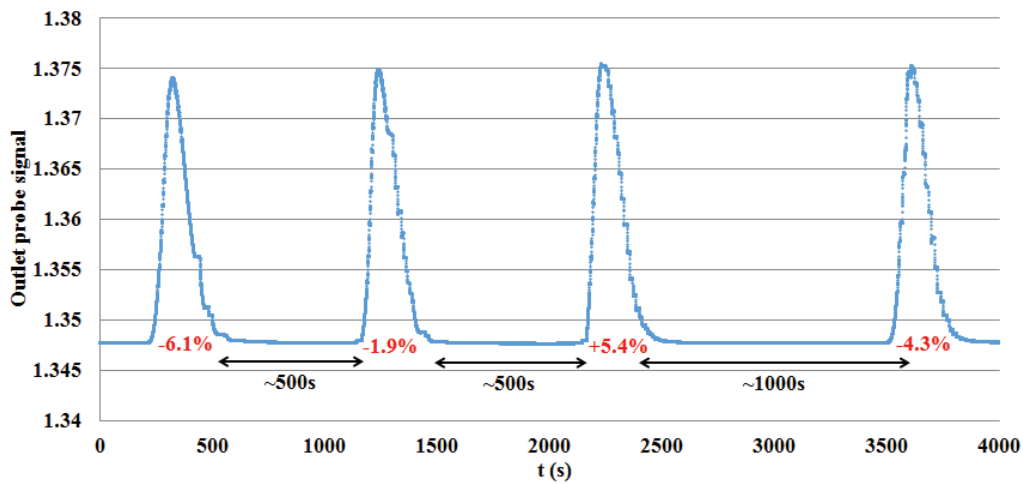


Figure 76. Experimental data of four consecutive pulses performed on a reactor with $D_r=4$ mm, $L=9$ cm, $Q_f=2.92$ mL/h, G/L ratio=30 and packed with ZirBlast® powder 300-400 μ m. The numbers in red indicate the % of difference of the integrals of the outlet and inlet experimental curves

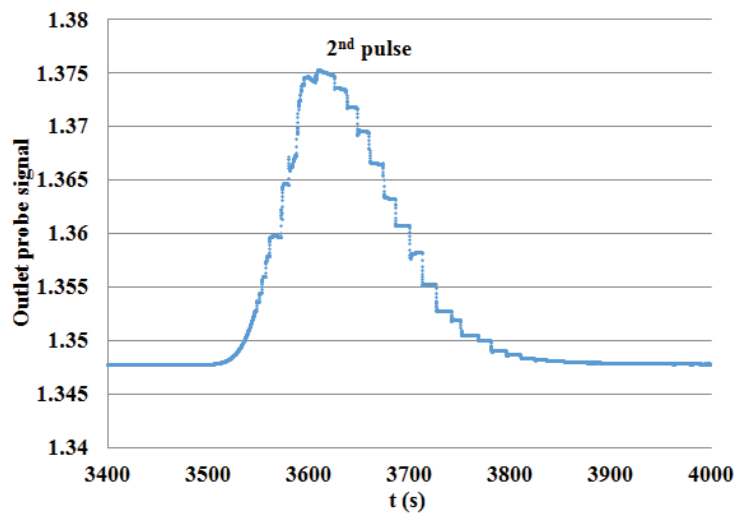


Figure 77. Zoom on the second pulse performed on a reactor with $D_r=4$ mm, $L=9$ cm, $Q_f=2.92$ mL/h, G/L ratio=30 and packed with ZirBlast® powder 300-400 μ m

Repeating the pulses in the 3 mm diameter reactor with the same flow rates (and hence with higher velocities) yields a different picture (Figure 78). More tracer is getting out of the bed when repeating the pulses. The integral loss decreases when repeating the experiment three times.

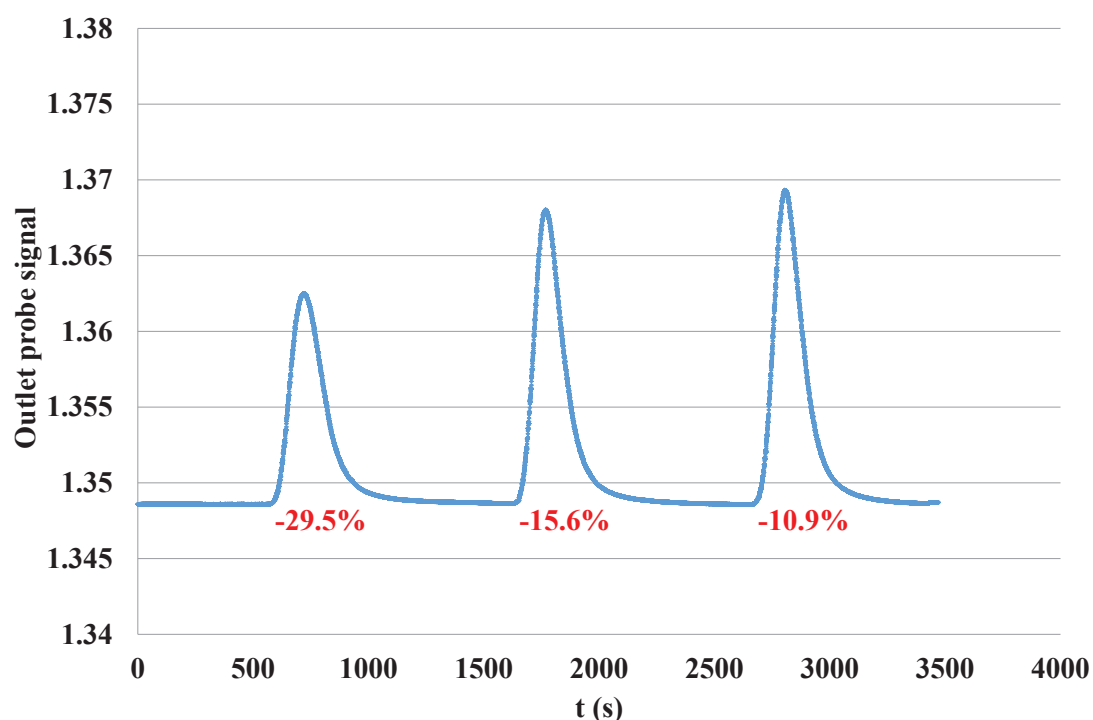
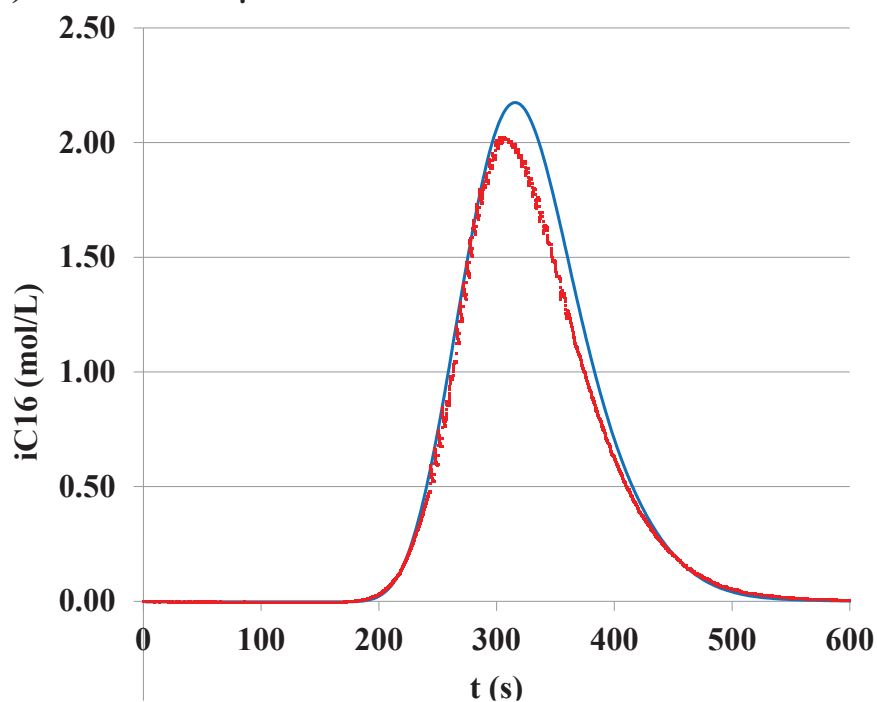


Figure 78. Experimental data of three consecutive pulses performed on a reactor with $D_r=3$ mm, $L=9$ cm, $Q_f=2.92$ mL/h, G/L ratio=30 and packed with ZirBlast[®] powder 300-400 μ m. The numbers in red indicate the % of difference of the integrals of outlet and inlet experimental curves

Another interesting fact is that, when using the powders as porosity fillers, the experimental curves are not well predicted by the axial dispersion model (see Figure 79). We remind that the liquid holdup is adjusted so that the experimental and model outlet curves have the same residence time. The experimental curve is skewed to the left, suggesting the presence of a desorption.

A) SiC 300-400 μm



B) ZB 300-400 μm

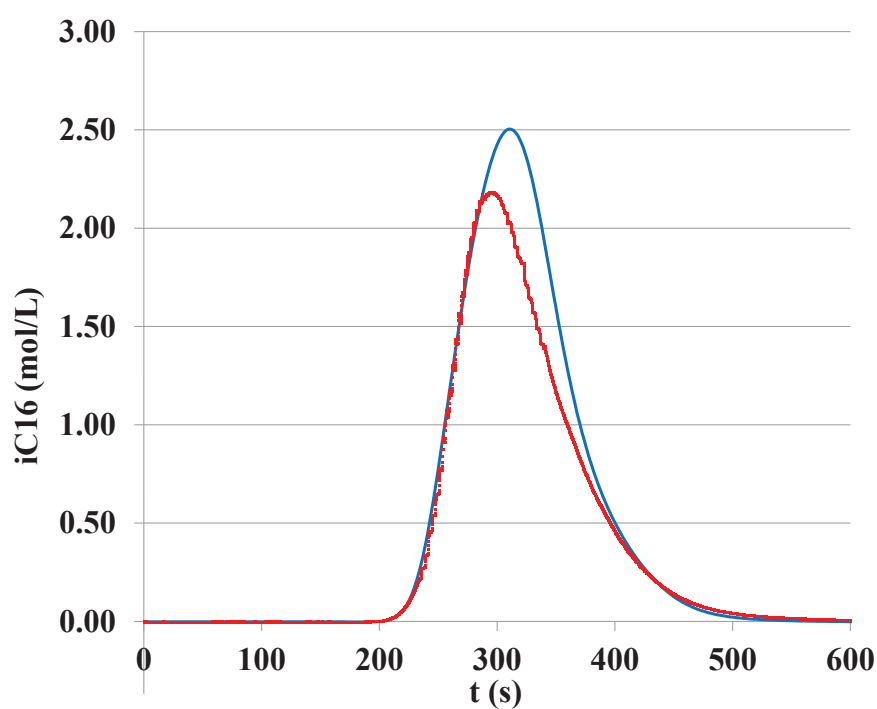


Figure 79. Example of fitting of the axial dispersion model when porosity fillers are used. Red curve: experimental points, blue curve: model. A) SiC 300-400 μm B) ZirBlast[®] 300-400 μm . The model output has a higher “integral” but the same average residence time as the experimental one

We propose an explanation of those integral losses based on the high viscosity difference between the carrier and the tracer. Before the iC16 injection, the flow of nC7 liquid and the gas is steady with stable interfaces. When the viscous tracer is injected, the pressure in the liquid increases due to the higher viscosity and the gas-liquid interfaces move (higher liquid holdup). After the pulse, nC7 is injected again and does not replace the tracer in all liquid patches. The reactor is thus filled with three types of fluids: gas (N_2) / more viscous liquid (iC16) / less viscous liquid (nC7). With the time, the tracer diffuses back to the nC7 main flow (continuous) and interfaces are settling back to their original position in a step-by-step irregular way. Indeed, the motion of an interface in a porous media occurs by sudden drainage of pores. This would explain the staircase behavior seen in Figure 77. Therefore, we propose a rapid accumulation of tracer in some pores in the rising side and a slow drainage in the decreasing side of the RTD experiments with a long tail. Some “stranded pores” probably remain filled with iC16 for long enough time not to see nC7 again during the experiment. The more irregular SiC has a higher void fraction and the pore throats are larger which makes the interface more stable and the integral loss lower compared to the spherical powder. At high velocities (3 mm reactor case), the viscous drag increase is higher and the interface motion more important. This mechanism explains the skewness of the experimental curves compared to the axial dispersion model output.

All the experiments performed with porosity filler, which will be presented later, have liquid superficial velocities comparable to the case of 3 mm of diameter.

Concentration integral losses are around 5-15%, which is sufficiently low to have a limited impact on our estimation of the Pe number. The Pe numbers calculated from the two methods (moments and model) are often different with porosity filler as the integral loss affects the optimization of the model but not the moment calculation (done on normalized concentrations by construction). As we

will see, the method of the moments yields more stable and lower Pe number values, and it is probably a more trustworthy evaluation for a reactor design targeting high conversions.

7.1.6 Repeating the pulses

In this paragraph, the results coming from consecutive measurements are compared (Table 14).

While the liquid holdup values seem to be quite stable, the Pe numbers present a higher variability.

The Pe number calculated using the method of the moments of the residence time distribution curves seems more stable. This is expected, as the method is based on normalized concentration and is not affected by integral differences between inlet and outlet of the reactors.

Table 14. Results of the reproducibility of consecutive pulses

Reactor	Operating conditions		ϵ_1	Pe (model)	Pe (moments)
$D_r=3$ mm $d_p=2$ mm $L=9$ cm	$Q_I=2.92$ mL/h $G/L=60$	<u>Pulse 1</u>	0.192	15.2	15.5
		<u>Pulse 2</u>	0.192	17.0	14.4
		<u>Pulse 3</u>	0.196	13.3	13.2
		<i>Mean</i>	0.193	15.2	14.4
		<i>Relative error</i>	1.2%	12.2%	8%
$D_r=3$ mm $d_p=2 \times 5$ mm $L=9$ cm	$Q_I=2.92$ mL/h $G/L=60$	<u>Pulse 1</u>	0.120	8.8	10.9
		<u>Pulse 2</u>	0.117	8.8	11.2
		<u>Pulse 3</u>	0.120	8.6	10.5
		<i>Mean</i>	0.119	8.7	10.9
		<i>Relative error</i>	1.5%	1.3%	3.2%
$D_r=4$ mm $d_p=2$ mm $L=15.5$ cm	$Q_I=2.92$ mL/h $G/L=30$	<u>Pulse 1</u>	0.061	9.3	11.4
		<u>Pulse 2</u>	0.061	12.9	13.0
		<u>Pulse 3</u>	0.059	9.6	12.0
		<i>Mean</i>	0.06	10.6	12.1
		<i>Relative error</i>	1.9%	18.8%	6.7%

We therefore decide to use the test with the best matching INLET/OUTLET integral curves.

7.1.7 Results: The flow regimes observation

Three types of flow regime are observed:

- Gravity driven flow: an alternation of gas bubbles and liquid slugs is observed inside the reactors. The RTD curves present steps;
- Stable flow: there is a continuous and stable flow of both gas and liquid phases;
- Intermediate regime: a continuous and stable flow of both gas and liquid phases is periodically interrupted by the passage of gas bubbles in specific areas of the packed bed millireactor.

These regimes are different to those observed in larger packed bed reactors, mainly trickle and pulsed flow, because of the reduced size of the reactors.

Flow regime in gas-liquid fixed beds of small sizes has been studied by Matthieu Rolland in his PhD thesis [19] and we follow his approach. The physical forces considered are: capillary forces, viscous forces and gravity. Inertia is not considered because of the small liquid Reynolds numbers of the flows tested (<1). The following two independent dimensionless numbers are relevant:

- Capillary number: $Ca = \frac{\mu_l u_l}{\sigma} = \frac{\text{viscous forces}}{\text{capillary forces}}$, quite common in porous media;
- Irrigation number: $I = \frac{\mu_l u_l}{(\rho_l - \rho_g) g d_p^2} = \frac{\text{viscous forces}}{\text{gravity}}$, that defines how much the gravity destabilizes the flow [19, 99].

Using the physical properties of the *n*-heptane (Table 12), we plot our observations in a (Ca, I) diagram (in Figure 80 the results when using glass spheres). When powder is used as porosity filler,

the mean particle diameter d_p is the powder diameter (or the mean between the sieving extremes in case the powder is sieved), which we think is the one that governs the hydrodynamics [2].

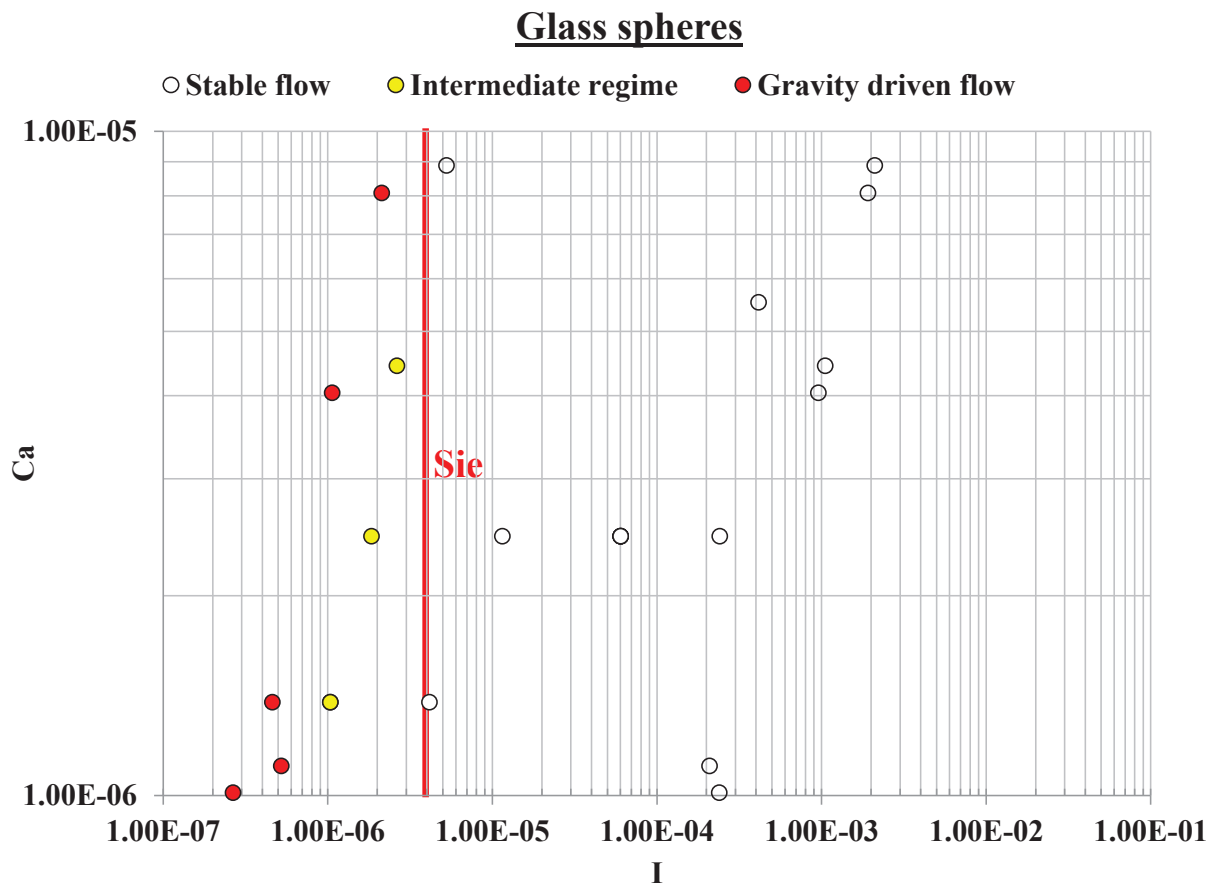


Figure 80. Flow chart for packed bed millireactors packed with glass spheres. The vertical red line represents the threshold of the Sie criterion [99]

The flow regime is highly dependent on the value of the Irrigation number (I).

For glass spheres, a transition between the gravity driven and the stable flow is observed for values of the Irrigation number between 10^{-6} and 4×10^{-6} (Figure 80).

It is interesting to notice that the value of 4×10^{-6} has already been proposed by Sie [99] for the transition between a gravity driven flow (poor particles wetting) and trickle flow (good particles wetting). This means that for the reactors in which the flow is gravity driven, a poor catalyst wetting is expected.

For spheres in ceramic material (ZirBlast[®]), no pulses are observed for $I=8 \times 10^{-7}$. We suspect that different wetting properties of the ceramic material compared to glass explain the difference. Glass being more hydrophilic would be less wetted and easily de-wetted favoring slug flow. ZirBlast[®] would, on the opposite, favor stable films on the particles. An effect of the particle nature on liquid holdup has also been observed (see §7.1.8.3, the material effect part).

We think that the transition can shift also if the particles shape changes. When using glass cylinders, it seems to occur for slightly higher values of the Irrigation number (a pulsed flow is observed for $I=2.36 \times 10^{-6}$), even if the data collected do not allow us to establish exactly the transition.

In conclusion, if we are in presence of pulsed flow, we can stabilize it by reducing the particle diameter (for example using porosity fillers) and/or increasing the liquid flow rate.

7.1.8 Results on liquid holdup and plug flow behavior

7.1.8.1 Comparison with literature

Plug flow behavior

The analysis of the temporal concentration profiles of the RTD measurements has confirmed that the axial dispersion model is not always completely adequate for the description of the hydrodynamics of packed bed millireactors with small values of δ , in particular in presence of powders as porosity fillers (see §7.1.5).

The experimental data collected using different reactors and particles and under different flow rates returned Bo numbers between 0.1 and 0.5 for Reynolds number values below 1 ($Re_L = \frac{\rho \cdot u_{i,L} \cdot d_p}{\mu}$). Gierman [26] reported, for larger packed beds, the values of Bo number for trickle flow gas-liquid reactors and single phase reactors (Figure 81, it is not specified which type of single flow it is nor the source of the data). Chander et al. [9] also found similar values as Gierman in a trickle flow reactor of $D_r=2.5$ cm.

Our values are thus in between the two regions proposed by Gierman in large reactors, closer to the single-phase flow values. Delgado [25] also, in his review, reports for single liquid phase flows Bo number values > 0.2 .

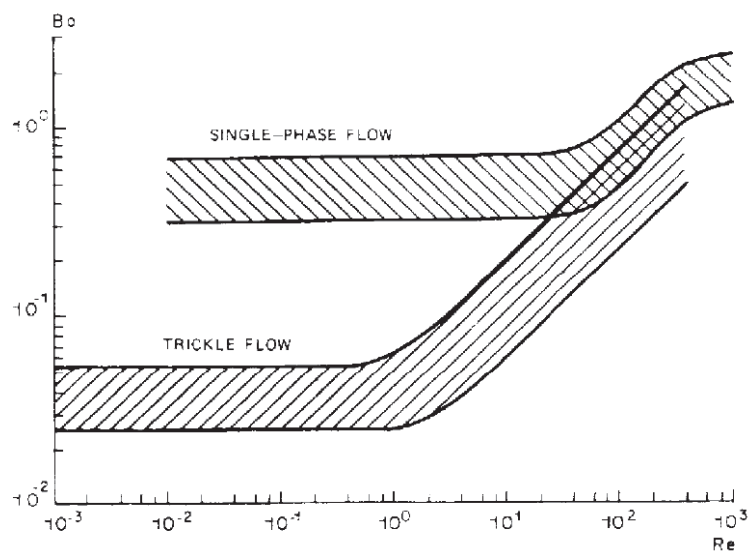


Figure 81. $Bo-Re_L$ expected correlation for trickle flows and single phase flows [26]

When using small particles (~ 0.1 mm) in packed bed millireactors, all authors (Marquez et al. [22], Van Herk et al. [31] and Charles Bonnin in his thesis work [24] – see Figure 82) found Bo number

values in the range 0.065 – 0.5 for Reynolds number values <1 , as we did.. This is yet another proof that flow in powders is not trickle bed, but rather capillary.

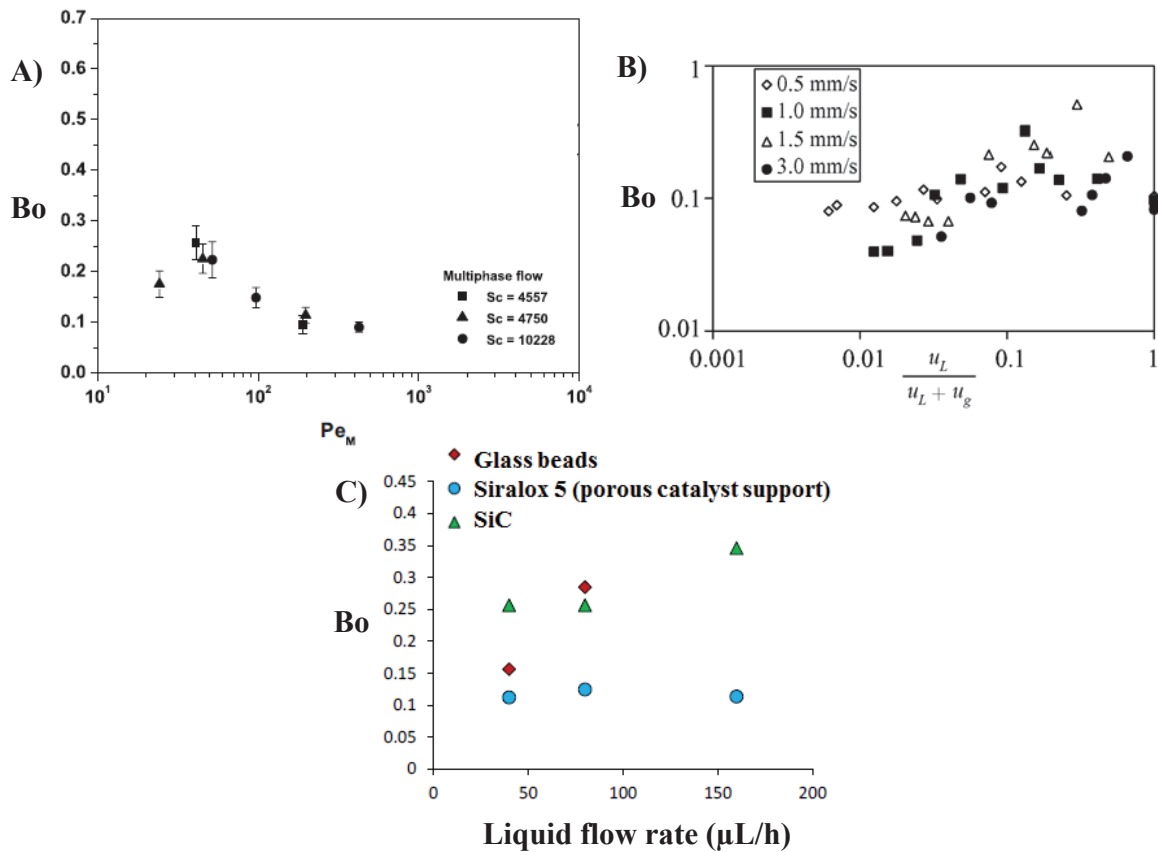


Figure 82. Examples of Bo numbers found in literature for packed bed millireactors. A) Marquez et al. [22], B) Van Herk et al. [31], C) Charles Bonnin thesis work [24]. $Re < 1$

Liquid fraction in the reactor

As others in the literature, we define the liquid retention as the ratio of volume occupied by the liquid in the reactor to the empty volume of the reactor after being packed.

Few studies have been performed in packed bed millireactors packed with millimetric particles. One of them by Kallinikos et al. [29] reported values of liquid retention around 0.3 for a spiraled Single Pellet String Reactor operated in downflow (but some sections of the reactor are almost horizontal). Our values in absence of porosity filler are lower, around 0.2. In presence of very small particles ($\sim 100 \mu\text{m}$) Marquez et al. [22] found liquid retention values between 0.65 and 0.85 while we found between 0.6 and almost 1.

Coming back to the liquid holdup, Charles Bonnin in his thesis work [24] reports liquid holdup values around 0.2-0.25, the same values we find when using porosity fillers.

7.1.8.2 An effect of the start-up procedure

As wetting may have an impact on the flow regime (Baussaron et al. [100], van Houwelingen et al. [101]), we investigated how the start-up protocol changes the hydrodynamics of our packed bed millireactors. Two start-up protocols are tested:

- Protocol 1: immersion of the bed. A pre-wetting of the packed bed millireactor is performed by closing the reactor outlet (bottom) and feeding only liquid. Once the filling is complete the outlet is opened, and the gas and liquid flows are set to the desired values;
- Protocol 2: starting from a dry bed, direct feed of the gas and liquid phases at the desired flow rates.

The results for a reactor of 3 mm internal diameter, 9 cm of length and packed with spherical glass beads of 2 mm, with and without SiC 300-400 μm porosity filler, are shown in Figure 83.

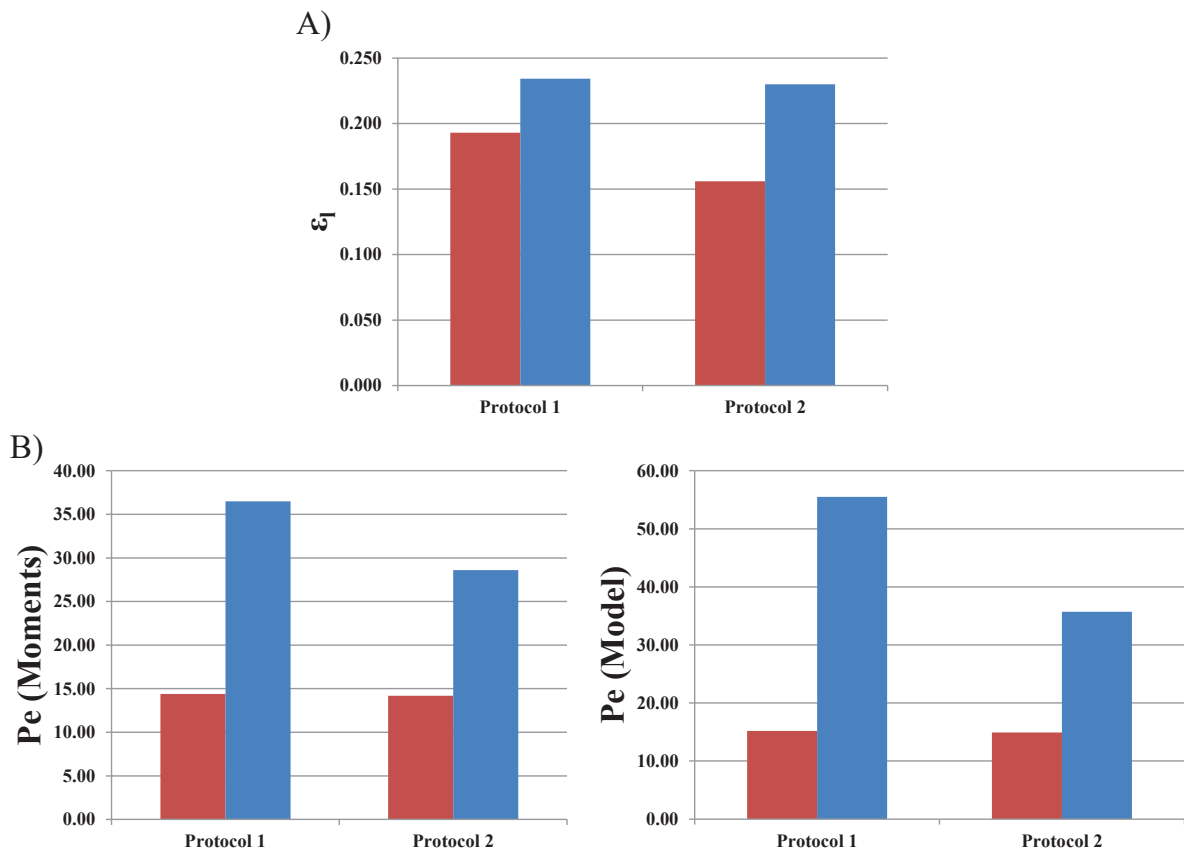


Figure 83. Start-up protocol effect on liquid holdup (A) and Pe number (B). Reactor with $D_r=3$ mm, $d_p=2$ mm spheres, $L=9$ cm. $Q_f=2.92$ mL/h, G/L ratio=60. Red: no porosity filler, blue: SiC 300-400 μm porosity filler

The start-up protocol has important effect (+24%) on the liquid holdup for the reactor with millimetric particles (without porosity filler). On the opposite, almost no effect is observed on the reactor packed with the porosity filler: capillary effects contribute to a good distribution of the liquid phase and yield a constant and probably uniform wetting regardless of the start-up conditions.

Despite the difference in liquid holdup, the Pe number is not affected by the start-up procedure in absence of porosity filler. On the contrary, when using porosity filler, the pre-wetting (protocol 1) yields higher Pe numbers.

The same is observed for cylinders (Figure 84). In this case, the increase in the holdup is slightly lower, around 18%. No remarkable effect is observed on the Pe number values (very low, <5).

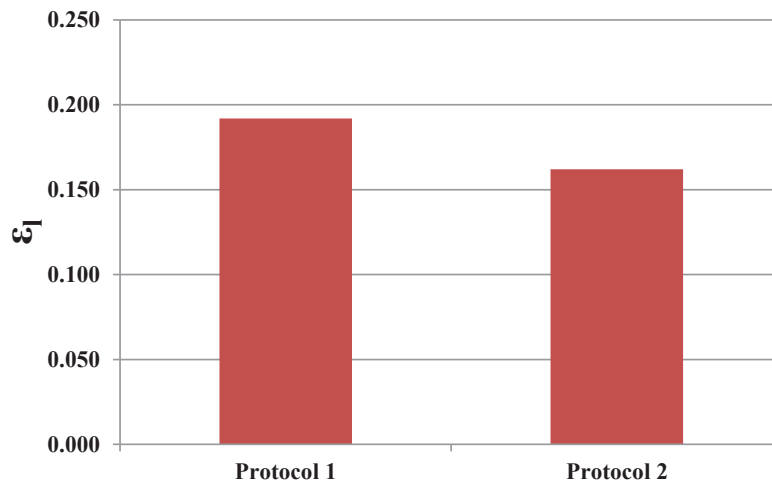


Figure 84. Start-up protocol effect on liquid holdup. Reactor with $D_r=2$ mm, $d_p=1.6 \times 5$ mm cylinders in metal, $L=9$ cm. $Q_r=2.92$ mL/h, G/L ratio=60

Going back to our main target, this means that the starting procedure of the catalytic test may change the liquid holdup and Pe number with some impact on catalytic results.

Considering that a pre-wetting is not performed on the reactive unit that is used for the reactive tests, we decided to acquire all our data using the Protocol 2 (no pre-wetting).

7.1.8.3 Hydrodynamics in absence of porosity filler

Fluid flow velocities and G/L ratio effect

The effect of the fluid velocities and of the G/L ratio is tested on two reactors (Table 15).

Table 15. Reactors and packings for the gas and liquid velocities effect exploration

	SPSR-Cyl	FB-Sph
Particle shape	Cylinders	Spheres
D_r (mm)	3	3.7
L (cm)	9	17.9
Particles size (mm)	2 (diameter) x 5 (length)	1
Packing structure	Large passages between particles and walls	Uniform with small side passages

SPSR: Single Pellet String Reactor, FB: Fixed bed

In both cases, the effect is explored starting from the lower liquid flow rate, and then increasing it, without performing a drying and a re-start.

In the range studied, the liquid holdup and the Pe number do not depend on the liquid flow rate (Figure 85), meaning that the axial dispersion coefficient D_{ax} is proportional to the liquid flow rate. The gas to liquid ratio has no impact on the Single Pellet String Reactor (SPSR-Cyl) bed properties (Figure 86) while for the bed packed with spheres (FB-Sph), an increase of the G/L ratio results in a slight decrease of holdup and increase of the Pe number.

Probably our results are affected from the fact that we are not repeating the experiments starting always from dried bed. The values for the higher liquid flow rates are influenced by the “history” of the bed at lower liquid flow rate values.

In literature some authors report, as us, liquid holdup values independent from the gas and liquid flow rates (Kallinikos et al. [29] with a Single Pellet String Reactor) while other report higher values for higher liquid flow rates (Charles Bonnin [24] and Marquez et al. [22] using fine particles). We do not think that the particle size is the reason of this difference. For the Pe number

values the authors agree that the gas flow rate is not influent, but usually a beneficial effect of liquid flow rate is observed [22, 24, 29].

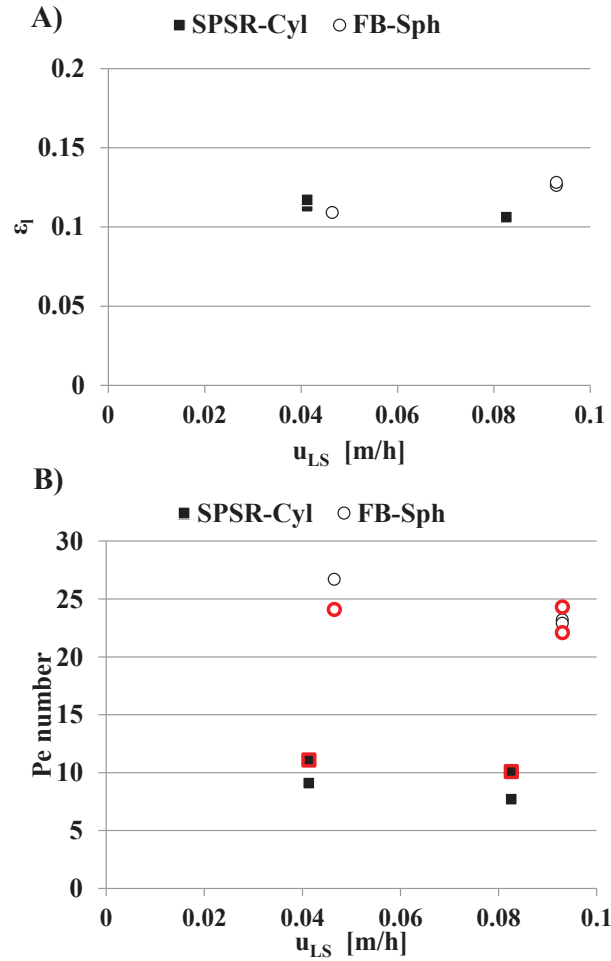


Figure 85. A) Liquid holdup and B) Pe number variation with the liquid superficial velocity. Various G/L ratios. In the graph B) the points marked with red borders represent the Pe number calculated with the first and second order moments method, the points not marked represent the Pe number calculated with the axial dispersion model

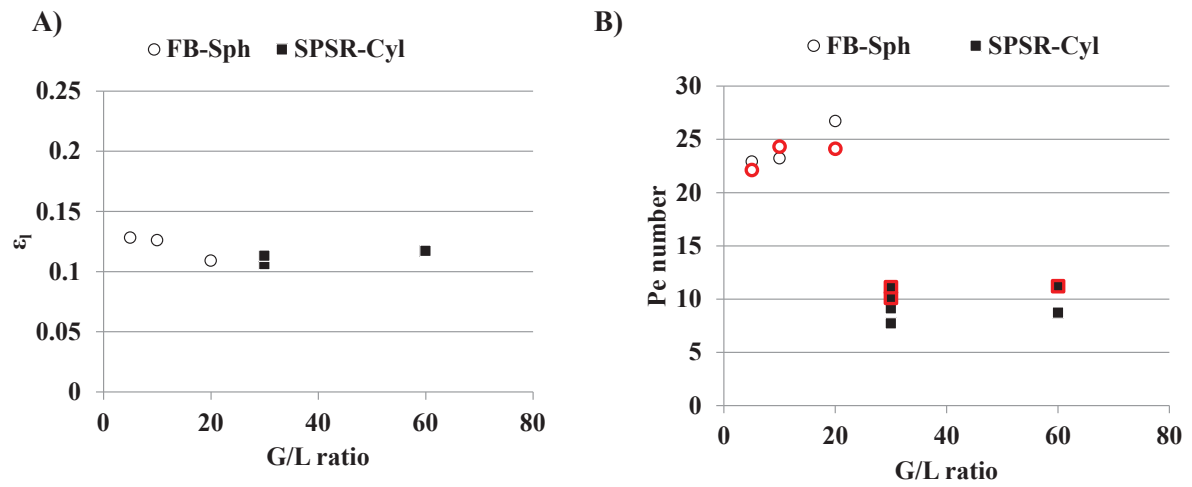


Figure 86. A) Liquid holdup and B) Pe number variation with the G/L ratio. Various liquid flow rates. In the graph B) the points marked with red borders represent the Pe number calculated with the first and second order moments method, the points not marked represent the Pe number calculated with the axial dispersion model

The effect of bed length

The bed length effect is investigated on a reactor with $D_r=4$ mm, $d_p=2$ mm and lengths of 9 and 15.5 cm (photo of the packing in Figure 87).



Figure 87. Photography of a reactor with internal diameter $D_r=4$ mm packed with glass spheres of $d_p=2$ mm

The results are shown in Figure 88. Unexpectedly, the reactor length has an impact on the average liquid holdup that decreases when increasing the reactor length. Even if the two values do not differ too much, a similar result has been obtained by Charles Bonnin in the works of his thesis [24] but using smaller particles (~ 100 μm). In our case, this could be explained by an acceleration of the liquid by gravity in case of the longer bed and thus an increasing liquid velocity.

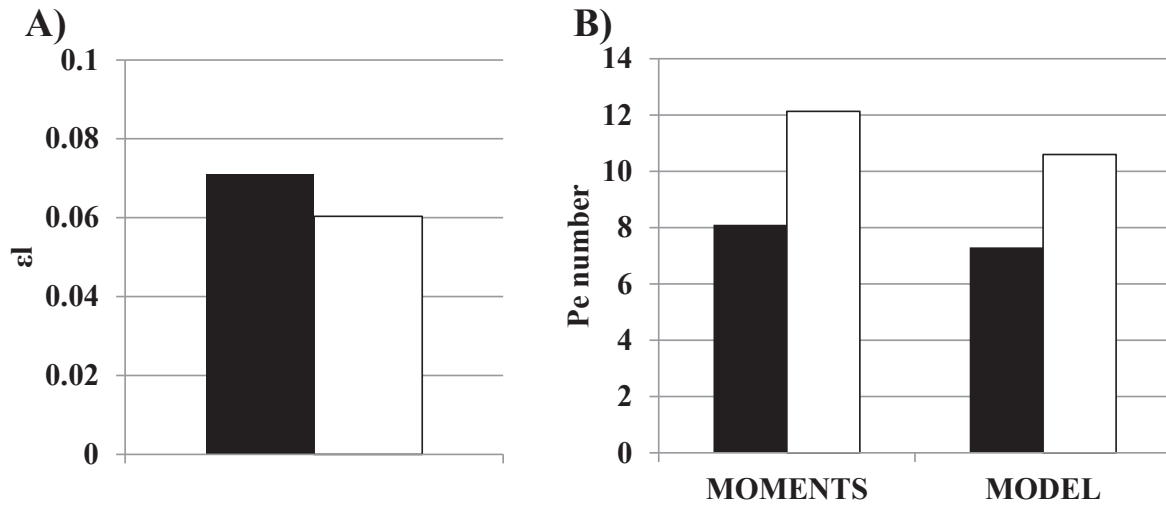


Figure 88. A) Liquid holdup and B) Pe number variation with the reactor length. Black: $L=9$ cm, white: $L=15.5$ cm. $D_r=4$ mm, $d_p=2$ mm, $Q_f=2.92$ mL/h, G/L ratio=30. MOMENTS: Pe number calculated with the method of the moments, MODEL: Pe number calculated with the axial dispersion model.

The liquid Pe number values are quite low and, as expected, the shorter reactor has the lower Pe number. The Pe numbers seem to follow the proportionality with the reactor length: ratio of length: 1.72, ratio of Pe(Moment)=1.52 and ratio of Pe(Model)=1.45. We conclude that the axial dispersion coefficient and the Bo number are independent from the bed length.

The δ reactor/particle diameter ratio effect and polydispersed packings

The reactor/particle diameter ratio effect is explored using a reactor of $D_r=4$ mm and $L=9$ cm. Glass spheres with diameters of 3, 2 and 1 mm are used (Figure 89). The flow is observed as pulsed for the reactors packed with the 2 and 3 mm glass spheres while stable when packed with the 1 mm glass spheres. A liquid flow rate of 2.92 mL/h and a G/L ratio of 30 are used.



Figure 89. Packed bed millireactors used for the study of the δ effect. $D_r=4$ mm, from left to right: $d_p=3, 2, 1$ mm

Figure 90 compares the three reactors on a liquid retention basis defined as the volume occupied by the liquid divided the empty volume of the reactor after being packed with the solid particles (ϵ_l/ϵ). The ϵ values used are calculated with the correlations proposed by Dixon [97] (we cannot take the values estimated in the G/S RTD campaign because the values of δ are different):

$$\begin{aligned}
 \epsilon &= 1 - \frac{0.667}{\delta^3} \cdot \left(\frac{2}{\delta} - 1\right)^{-0.5} \text{ for } \delta < 1.865 \\
 \epsilon &= 0.528 + 2.464 \cdot \left(\frac{1}{\delta} - 0.5\right) \text{ for } 1.865 < \delta < 2 \\
 \epsilon &= 0.4 + \frac{0.05}{\delta} + 0.412 \left(\frac{1}{\delta}\right)^2 \text{ for } \delta > 2
 \end{aligned}
 \tag{Equation 53}$$

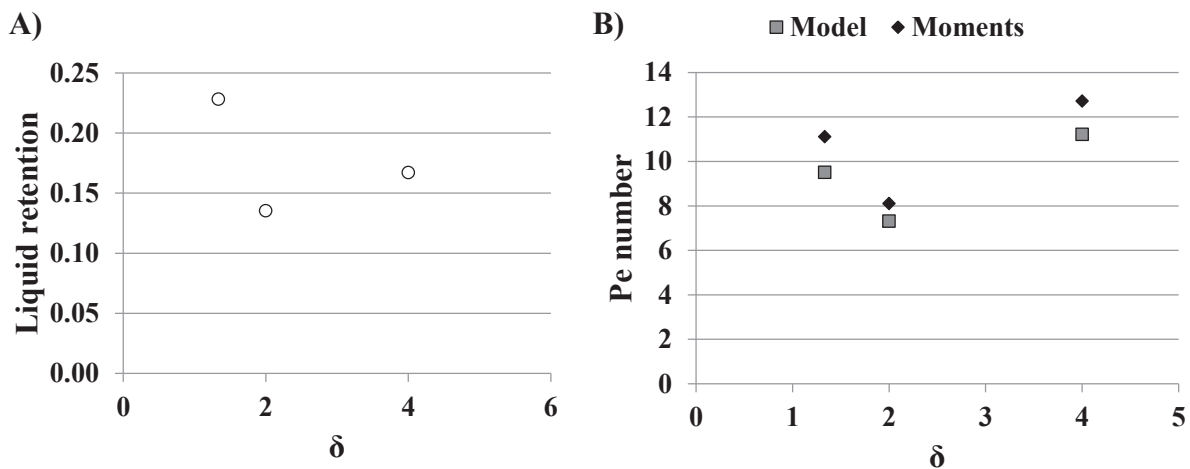


Figure 90. A) Liquid retention and B) Pe number variation with the δ =reactor/particle diameter ratio. Model: Pe number calculated with the axial dispersion model. Moments: Pe number calculated with the method of the moments. $L=9$ cm, $Q_I=2.92$ mL/h, G/L ratio=30

The single pellet string reactor ($\delta=1.33$) shows the highest liquid retention, while the reactor with $\delta=2$ shows the lowest one. The limited space between the particle and the walls makes it easier to form films. Similarly to what has been observed for the G/S RTD experiments, we have a decrease of the Pe number between 1 and 2 and then a new rise for $\delta=4$. Overall, Pe numbers are quite small and we decided not to explore further the effect of δ on the hydrodynamics of packings without porosity filler.

An experiment is also performed by testing a packing made of 3 types of spheres (glass spheres of 2 and 3 mm and 2.3 mm ZirBlast[®] spheres, Figure 91), inserted in the following repeated sequence: glass 2 mm, ZB 2.3 mm, glass 3 mm. The same operating conditions as for the δ effect experiments ($Q_I=2.92$ mL/h and G/L ratio=30) are tested. This packing shows the highest Pe number among those observed in this δ effect study (Pe=16).



Figure 91. The polydispersed spheres packing. $D_r=4$ mm, $d_p=2$ and 3 mm glass spheres and 2.3 mm ZirBlast[®] spheres

The material effect (glass/ZirBlast[®])

The effect of the non-porous particle material is explored performing tests on a reactor of 4 mm internal diameter, 9 cm of length and packed with 1 mm spheres in glass or ZirBlast[®] ceramic material (Figure 92). The ZirBlast[®] ceramic material is composed of 60 to 70% of zirconia (ZrO_2), 28 to 33% silica (SiO_2) and <10% of alumina (Al_2O_3). The operating conditions are: liquid flow rate 2.92 mL/h and G/L ratio 30.



Figure 92. Packed bed millireactors used for the study of the non-porous particle material effect ($D_r=4$ mm). On the left $d_p=1$ mm ZirBlast[®], on the right $d_p=1$ mm glass

The results are summarized in Table 16. The two reactors show almost the same Pe number (slightly lower for the ZirBlast[®] case) while the liquid holdup is significantly higher (+~50%) for the reactor packed with the ceramic particles. The ceramic material shows better wetting properties towards hydrocarbons that we explain by the hydrophilic nature of the glass that thus would repel *n*-heptane more than ceramic (see the flow regimes part §7.1.7).

Table 16. Liquid holdup and Pe number obtained varying the particle material. $D_r= 4$ mm, $d_p=1$ mm, $L=9$ cm. Liquid flow rate: 2.92 mL/h, G/L ratio=30

Particle	ϵ_l	Pe (Moments)	Pe (Model)
Glass	0.073	12.70	11.21
Ceramic (ZirBlast [®])	0.113	9.60	10.30

Conclusions on the hydrodynamics without porosity filler

In absence of porosity filler, the hydrodynamic properties (flow regime, liquid holdup and Pe number) are governed by the packing geometry, the particle nature (hydrophilic or not) but hardly

by the liquid and gas velocities, meaning that in the investigated area the axial dispersion coefficient is proportional to the liquid velocity.

The estimated liquid holdup values are lower than 0.15. The Pe numbers for 9 cm long reactors are quite small (<15) which is not acceptable for catalytic studies. The corresponding Bo numbers obtained range around 0.1-0.5. Compared to larger packed beds, these values are closer to the Bo number values observed in liquid-solid case (see Delgado et al. [25] and Gierman [26]) than those proposed by Gierman for three-phase reactors [26]. On the contrary, the literature on packed bed millireactors [22, 24, 31] reports Bo number values coherent with the ones we observed.

7.1.8.4 Hydrodynamics with porosity filler

The effect of the porosity fillers and their size and type is explored by using a reactor with $D_r=3$ mm, $L=9$ cm, packed with 2×5 mm glass cylinders (Figure 93) and different types of porosity fillers: SiC sieved between 150-200 μm or 300-400 μm , SiC with mean diameter 800 μm and ZirBlast[®] sieved between 300-400 μm . The operating conditions are: $Q_l=2.92$ mL/h and G/L ratio=30. Pressure drop is found negligible for all the reactors tested (few tens of mbars). In the cases presented hereafter, a pressure drop of 10 mbars is observed for the reactor packed with 150-200 μm powders.



Figure 93. The single pellet string reactor tested: $D_r=3$ mm, $d_p=2 \times 5$ mm glass cylinders and $L=9$ cm

The liquid holdup (Figure 94) increases when using porosity fillers and it increases when reducing the size of the porosity fillers. When comparing SiC and ZirBlast[®] with the same grain size it appears that the latter shows a lower liquid holdup. When taking into account the porosities of the beds, the bed whose porosity has been filled with ZirBlast[®] powder shows the higher liquid retention².

² The bed porosity without porosity filler has been fixed at 0.55, approximation obtained as $1 - \frac{d_p^2}{D_r^2}$. The bed porosities with porosity fillers have been obtained considering the ratios between the reactor's porosities obtained with/without porosity filler in the GS RTD experiments (see paragraph §6.2, the same powders are used except the SiC 150-200 μm that replaces the SiC 200 μm). The same ratios are applied here.

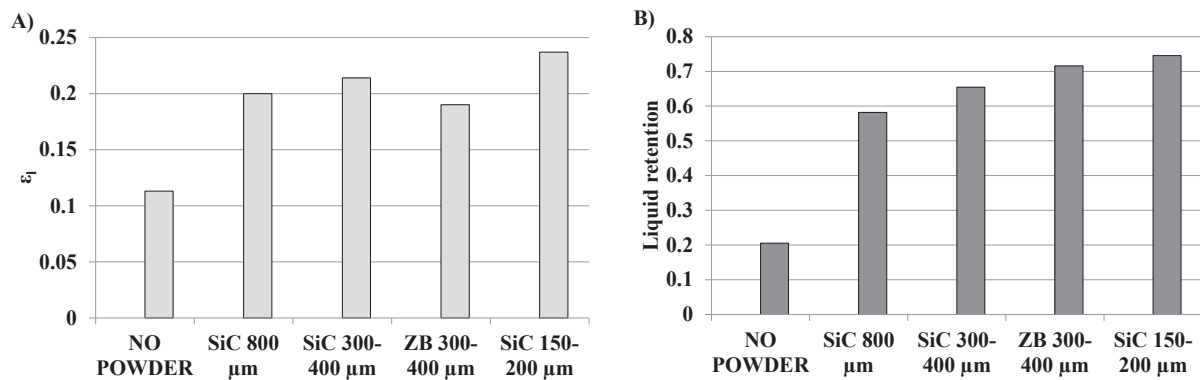


Figure 94. A) Liquid holdup and B) Liquid retention when adding porosity fillers. $D_r=3$ mm, $d_p=2 \times 5$ mm glass cylinders + porosity fillers, $Q_f=2.92$ mL/h, G/L ratio=30.

The Pe number increases with the addition of smaller porosity fillers (Figure 95). The reactor with ZirBlast® shows a higher Pe number than the same reactor filled with SiC.

A last comment is that the results of the data calculated with the method of the moments are more stable and reasonable compared to those obtained with the model.

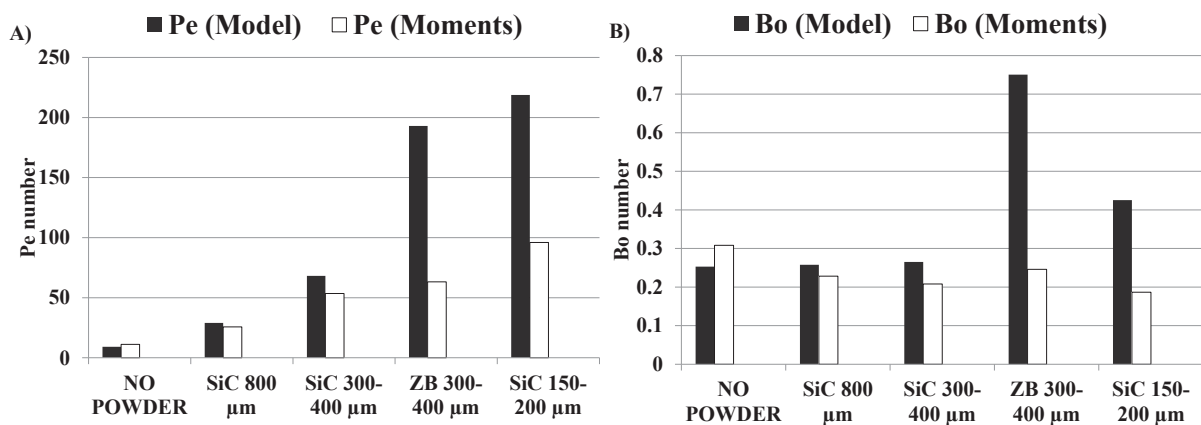


Figure 95. A) Pe number and B) Bo number variation when adding porosity fillers. $D_r=3$ mm, $d_p=2 \times 5$ mm glass cylinders + porosity fillers, $Q_f=2.92$ mL/h, G/L ratio=30.

The Bo numbers are ~0.2-0.3 for the conditions tested.

Positive effect of the porosity filler on liquid holdup and Pe number has also been observed in other two experiments performed. The data are shown in Table 17.

Table 17. Effect of porosity fillers on liquid holdup and Pe number

D_r (mm)	d_p (mm)	L (cm)	Q_l (mL/h)	G/L ratio	ε_l	Pe (Moments)	Pe (Model)
3	2	9	2.92	60	0.156	14.4	14.9
3	2 + SiC 0.3-0.4 mm	9	2.92	60	0.23	28.6	35.7
4	3	9	10.72	25	0.137	12.9	11.9
4	3 + SiC 0.1 mm	9	10.72	25	0.224	38.2	75.7

To conclude on the porosity filler experiments, a last result worthy to mention is that, even for these reactors, the effect of the fluid flow rates (this time keeping constant the G/L ratio) is found small/negligible (Table 18, consider always that the Pe number values obtained from the model are less reliable in case of porosity fillers):

Table 18. Effect of the liquid and gas flow rates on a reactor packed with porosity filler

D_r (mm)	d_p (mm)	L (cm)	Q_l (mL/h)	G/L ratio	ε_l	Pe (Moments)	Pe (Model)
4	3 + SiC 0.1 mm	9	10.72	25	0.224	38.2	75.7
4	3 + SiC 0.1 mm	9	5.36	25	0.223	43.5	47.8

7.1.9 Conclusions on the hydrodynamic experiments

Residence Time Distribution experiments performed on packed bed millireactors have been carried out to assess their hydrodynamic features and explore the effect of the different operating conditions and of the packing type.

Three flow regimes are encountered: a gravity driven flow, a stable flow and a transition flow between these two. The transition between the flows is governed by the Irrigation number, the particle surface properties and probably the particle shape. These regimes are different to those observed in larger packed bed reactors, mainly trickle and pulsed flow, because of the reduced size of the reactors.

The start-up protocol has an impact mainly on the liquid holdup. In case of pre-wetting of the bed the liquid holdup is enhanced in case we do not use any porosity filler. In case of use of porosity fillers, this impact becomes much smaller and negligible.

The hydrodynamic features of the packed bed millireactors tested are not influenced significantly by gas and liquid flow rates but slightly influenced by the bed structure ($\delta=D_r/d_p$ ratio). Lower liquid holdup and Pe number values have been found for $\delta=2$ while polydisperse packings seem to exhibit a good Pe number. Increasing the bed length appears to lower the liquid holdup, probably due to the gravity force that in case of longer beds causes an acceleration of the liquid to the reactor outlet. Anyway, it has no effect on the axial dispersion coefficient/Bo number and the Pe number is proportional to the bed length.

The liquid holdup and Pe numbers measured for the packed bed millireactors packed only with millimetric particles are quite low ($\epsilon_l < 0.15$, $Pe < 15$ for $L=9$ cm). These values are not suitable for kinetic studies so that the use of porosity fillers is recommended since they increase liquid holdup and Pe numbers ($\epsilon_l > 0.2$, $Pe > 30$ for $L=9$ cm). For the reactors and conditions tested, the Bo numbers range around $\sim 0.065-0.5$, similarly to what has been found by other authors in packed bed millireactors. But these values are lower than those observed for larger packed bed reactors, indicating that the flow behavior is different.

In the case of packed bed millireactors operated in presence of porosity fillers, a loss of tracer is often observed and explained by the high difference in viscosity of the two liquids. This limits the precision and reliability of the measured data, as well as the applicability of the axial dispersion model in these cases. For further RTD tests, we suggest that system nC7 – iC16 system should be changed: aromatics can be used for example to keep the refractive index difference and the evaporation phenomenon small.

7.2 Reactive tests

A gas-liquid-solid reaction is carried out in packed bed millireactors to investigate the effect of the porosity fillers on reactive performances. The porosity fillers size and shape effects will also be investigated.

The unit used to perform these tests is the same used for G/S reactive tests (see §6.1). The hydrogenation of α -methylstyrene (AMS) to cumene (Figure 96) has been chosen as reaction as it is very fast and likely limited by mass transfer.

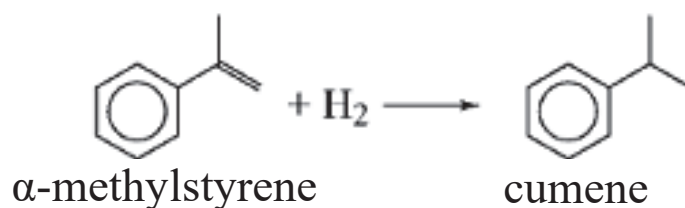


Figure 96. Representation of the α -methylstyrene (AMS) to cumene hydrogenation reaction

The reaction is exothermic: $\Delta H_0 = -109$ kJ/mol [102]. It is known in literature being of 1st order in hydrogen [103] and order 0 in α -methylstyrene [34, 104].

7.2.1 Materials and unit constraints

7.2.1.1 The catalyst

The hydrogenation is performed using a 0.5% Pd/ γ -Al₂O₃ catalyst. It is available in two shapes: 1.6x3-4 mm quadrilobe extrudates and 2-4 mm beads. The beads, using a sieve of size 2.8 mm, are separated into two categories: B- ($2 < d_p < 2.8$) and B+ ($2.8 < d_p < 4$).

The catalyst is reduced *in situ* under hydrogen flow, at atmospheric pressure and 150°C for 2 hours.

As the catalyst is sensitive to water, zeolite 4A pellets located in the liquid tank are used to capture the water content present in the feedstock.

Because of the use of millimetric catalyst particles, the amount of reactant is likely to decrease rapidly going from the catalyst surface to the internal structure. An apparent 1st order reaction is reasonable to be considered in further evaluations, as we will do to estimate the Pe number effect on the reactive conversion.

7.2.1.2 The reactors and loadings

Quartz reactors, available with an internal diameter of 2, 3 and 4 mm and a length of 30 cm are used for the tests. The reactors are operated in downflow mode. The isothermal zone where the catalyst particles are located is 9 cm long.

The bottom of the reactors (below the catalytic bed) is filled with ZirBlast[®] B20 (250-425 μm) or SiC 419 μm (in some cases for the reactors of 4 mm) for a length of 2-2.5 cm. The upper part of the reactors is filled with ZirBlast[®] B20 up to \sim 2 cm from the top to ensure a good pre-heating of the feed and a good liquid distribution inside the reactors. To prevent this powder to fall in the catalytic bed and fill up the porosity, we introduced a layer of 2-3 cm of “large” inert particles located between the catalytic bed and the pre-heating layer. The large particles consist of ZirBlast[®] 1 mm spheres for the $D_r=4$ mm reactors, SiC 800 μm for the $D_r=2$ mm reactors. In some cases of the $D_r=4$ mm reactors, the layer of large particles is replaced by a frit of 0.5 cm length and \sim 4 mm diameter.

The top part of the reactors (2 cm left) is then filled with glass socks.

This loading sequence ensures that the reactor’s performance changes are due to the inert powder in the catalytic bed and not due to fluid phases pre-heating or distribution on the reactor’s section.

7.2.1.3 The liquid feedstock

The feedstock is composed of a mixture 80 % weight *n*-heptane (purity=99.6%) and 20% weight α -methylstyrene (purity=99.5%). The purities have been measured via gas chromatography (Flame Ionization Detector, FID) at IFPEN.

7.2.1.4 Operating conditions and unit constraints

The choice of the operating conditions is limited by the unit constraints in terms of temperature and maximum liquid flow rate.

Usually the AMS hydrogenation is carried out at temperatures lower than 50°C [104, 105]. For our practice, the catalyst minimum temperature is 60°C. For set points lower than 60°C, the heat flow from the downstream oven is sufficient to heat the reactors above the required temperature with unknown effect on the thermal profiles. At this temperature, the reaction is very fast and near complete conversion is very likely to be achieved. To have the best analysis accuracy, an intermediate conversion is preferred (~40-90%) so that we needed to reduce the residence times.

The pump maximum mass flow rate is 24 g/h for all the reactors (3 g/h per reactor). However, 24 g/h is not recommended as in case of small flow rate fluctuations the maximum pressure allowed for the pump may be easily reached. For this reason, the flow rate of 20 g/h has been highly preferred during the experiments.

The only solution to avoid complete conversions is to operate short bed lengths (between 3 and 4 cm), having a strong impact on the results as we will see later.

The hydrogen on hydrocarbon ratio (H_2/HC), except if not differently indicated, is fixed at 250 NL/L. Helium is introduced in the reactors as inert species, to check the gas flow distribution in the reactors during the experiments. The chosen H_2/He ratio is 5. To lower the conversion levels,

dilutions of the gas feed with nitrogen is made (N_2/H_2 ratios between 0.25 and 1) to reduce the hydrogen partial pressure.

The unit used for the tests is not designed to operate liquid products. The equipment downstream of the reactor has to be used in absence of liquid. Flash simulation software Pro-II showed that keeping a temperature of 200°C after the N_2 dilution of the products was sufficient to ensure complete vaporization of the products at the operating pressure (5 barg). The temperature of the oven after the reactors is thus set at 200°C.

The total reactor inlet pressure is fixed at 5 barg. Higher pressures, during preliminary experiments, caused problems for the vaporization of the effluents downstream the reactors. Moreover, they would have resulted in an increase of the conversion levels that we are instead interested in reducing. Lower pressure could have been interesting to lower the H_2 concentration and thus conversion but at risk of liquid evaporation.

7.2.1.5 $D_r=2$ mm reactors isothermicity

An experiment is performed to check the isothermicity of the reactors by splitting in two parts the catalytic bed and using inert SiC particles to separate the two bed parts. In the reactors of $D_r=2$ mm, the conversion is not affected by the catalytic bed splitting in two parts (Figure 97), even if the reproducibility of the results is not good. Catalyst deactivation is observed but this will be discussed in the results part (§7.2.2)

We conclude that the reactors with $D_r=2$ mm without porosity filler are isothermal for reaction rates equals or lower than the ones observed in this experiment, that is $0.25 \text{ mol}_{AMS}/(\text{g}_{cat}\cdot\text{h})$ for the highest conversion values.

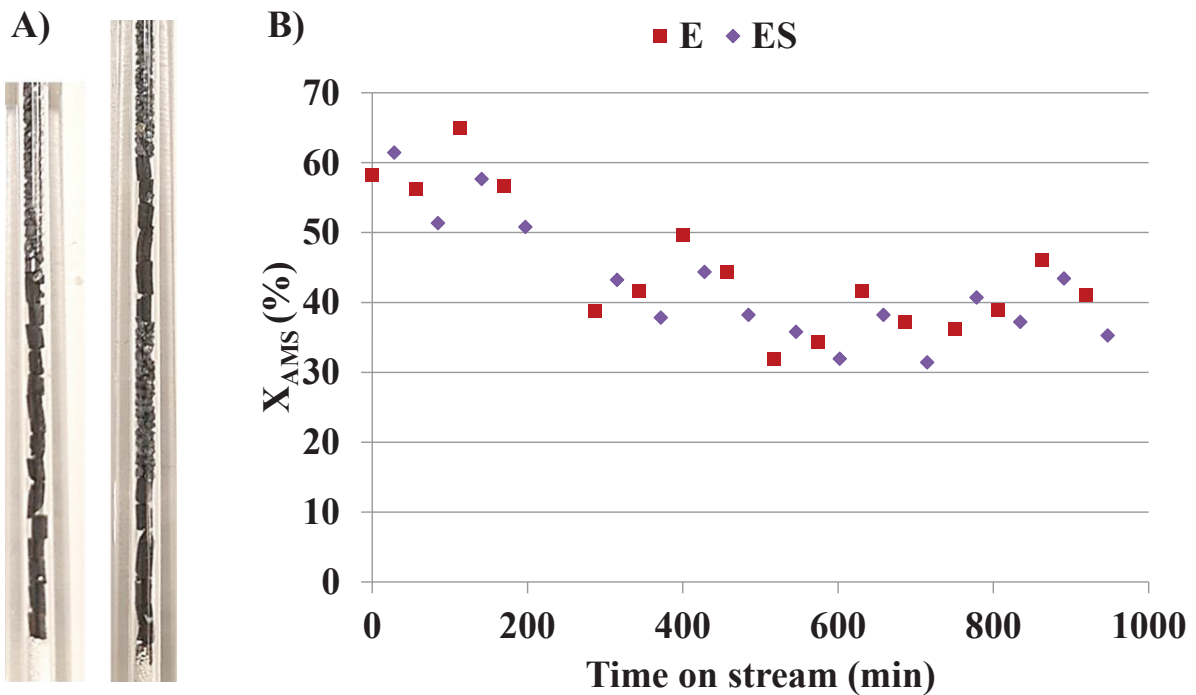


Figure 97. A) Reactors used for the isothermicity test B) Conversions for the single bed reactor (E = extrudates) and the split bed reactor (ES, S = split). Operating conditions: $T=60^{\circ}\text{C}$, $W_f=2.5\text{ g/h}$, $m=50\text{ mg}$, $N_2/H_2=0$

7.2.2 Results

First the experimental plan and the expected hydrodynamic conditions will be presented.

Then the catalyst deactivation phenomenon, the effect of temperature and of the hydrogen partial pressure on the reaction will be discussed.

In the end the porosity filler effect will be presented, separately for the reactors of 2 and 4 mm and for the two catalyst particles tested. In this part we will even perform a comparison of the reactors of 3 and 4 mm using the same catalyst particles. The tests will be named following the legend

DXY/Z where X indicate the reactor diameter in mm, Y the catalyst particles used (E: quadrilobe extrudates, B-: beads $2 < d_p < 2.8$ mm, B+: beads $2.8 < d_p < 4$ mm) and Z the test number.

7.2.2.1 The experimental plan

The experiments are carried out using the reactors and the particles described in §7.2.1. The following combinations are tested (Table 19):

Table 19. Reactors and particles tested in the AMS hydrogenation experiments. Green cells mean that the combination has been tested. E: quadrilobe extrudates, B-: beads $2 < d_p < 2.8$ mm, B+: beads $2.8 < d_p < 4$ mm

Reactor diameters and catalysts	Porosity fillers							
	No	Z60	S60	Z150-200	S150-200	Z300-400	S300-400	S800
$D_r=2$ mm*, E								
$D_r=3$ mm, B-								
$D_r=4$ mm*, E								
$D_r=4$ mm, B-								
$D_r=4$ mm, B+								

*in some tests, the bed length has been increased using inert alumina extrudates

7.2.2.2 Expected hydrodynamic conditions

The Irrigation numbers for catalyst beads are estimated using 2.4 and 3.4 mm as particle diameters for the B- and B+ groups respectively. The values fall in a range between 3.13×10^{-7} and 1.12×10^{-6} . They correspond, according to the flow observations performed and discussed in §7.1.7, to gravity driven flows. Only the value $I=1.12 \times 10^{-6}$ (estimated for the reactors of $D_r=3$ mm) may correspond to the intermediate regime between gravity driven and stable flow.

The Irrigation numbers in case of catalyst quadrilobes are estimated using an equivalent sphere diameter with the same volume/surface ratio (see paragraph §6.2.2, the quadrilobes are approximated to cylinders). The values fall in a range $1.18-3.88 \times 10^{-6}$. The lower value, found for the reactors of $D_r=4$ mm, corresponds, according to the flow observations, to a gravity driven flow. The higher value, found for the reactors of $D_r=2$ mm, corresponds to the intermediate regime between gravity driven and stable flow.

In case of use of porosity fillers, the flow is expected to be stable.

The liquid holdup values measured for the packed bed millireactors tested in the hydrodynamic experiments are quite low ($\epsilon_l < 0.15$). They vary with the bed length, the particles material and, slightly, with the gas and liquid flow rates. It would be difficult to attribute a specific value of the liquid holdup for the reactors used now in the reactive tests. However, what has to be kept in mind when comparing reactors with and without porosity filler, is that porosity fillers are found to nearly double (from $\times 1.5$ to $\times 2$) the liquid holdup and, consequently, the volume of liquid in the reactor.

In the same way, the Pe numbers measured for the packed bed millireactors tested in the hydrodynamic experiments are quite low ($Pe < 15$ for $L=9$ cm). These values are not suitable for kinetic studies so that the use of porosity fillers is recommended since they increase the Pe numbers ($Pe > 30$ for $L=9$ cm). For the bed lengths tested in the reactive tests, this would correspond to $Pe \sim < 5$ without porosity filler and $10 < Pe < 15$ with porosity filler. Case by case we will present the Pe numbers calculated for the geometries closest to the presented case, knowing that a perfect correspondence is not possible, first of all because of the variable particle size used in the reactive tests.

To resume, when porosity fillers are used the flow regimes are stabilized and in all the cases they are no longer governed by gravity. According to the Sie criterion [2], when the flow is driven by gravity a poor catalyst wetting is expected so that porosity fillers are necessary to enhance the catalyst wetting. In addition, porosity fillers are expected to double the liquid holdup values and to increase the Pe number values. All these observations lead to an expected higher reactive performance of the reactors packed with porosity filler.

7.2.2.3 Catalyst deactivation

Catalyst deactivation is observed during the experiments. Two hypotheses to explain the phenomenon are possible:

- The catalyst is highly sensitive to water content so that, even if zeolite 4A is used as molecular sieve, the cumulative residual amount of water dissolved in the hydrocarbons deactivates the catalyst;
- Coke formation.

When the reactors are operated in presence of porosity fillers, the deactivation rate is lower (Figure 98). When adding porosity fillers, we increase the liquid holdup and the catalyst wetting. We propose two explanations for the phenomenon:

- Big molecules like coke precursors cannot evaporate easily and thus they are more easily removed by the higher presence of liquid;
- The presence of the porosity filler ensures a more uniform liquid distribution and a more “homogeneous” catalyst usage that may result in a slower overall deactivation rate.

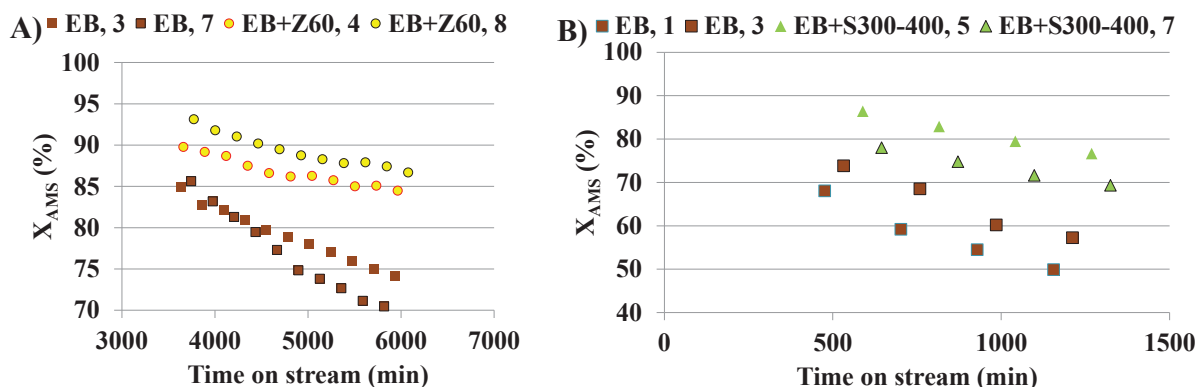


Figure 98. Conversion against time on stream for two experiments performed with catalyst quadrilobe extrudates. EB: extrudates elongated bed, S: SiC, Z: ZirBlast®. The numbers in the legend indicate the porosity filler size in μm (if present) and the reactor number in the unit

Consequently, the comparison of beds packed with or without porosity filler is only meaningful at the beginning of the tests.

7.2.2.4 Apparent activation energy estimations

Tests performed varying the temperature between 60 and 70°C (Figure 99) allowed for estimations of an apparent activation energy. In literature, it has been observed that the reaction is zero order on α -methylstyrene and first order on hydrogen [34, 104]. Considering that we are in large hydrogen excess, we estimate the apparent activation energy only on AMS and assuming a zero-order reaction kinetics.

In literature, the reported intrinsic reaction activation energy estimations do not agree on one specific value. This is probably because of differences between the operating conditions of the different studies [104] (i.e. catalyst deactivation by water, different internal diffusion limitations, etc.). We will use for reference the value of 40 kJ/mol reported by Meille et al. [104]. As we use

millimetric catalyst, we expect internal mass transfer limitations and an apparent activation energy of at most 20 kJ/mol. The apparent activation energies are mostly below 10 kJ/mol (Figure 100) indicating that the reaction rate is, as expected, also impacted by external mass transfer limitations.

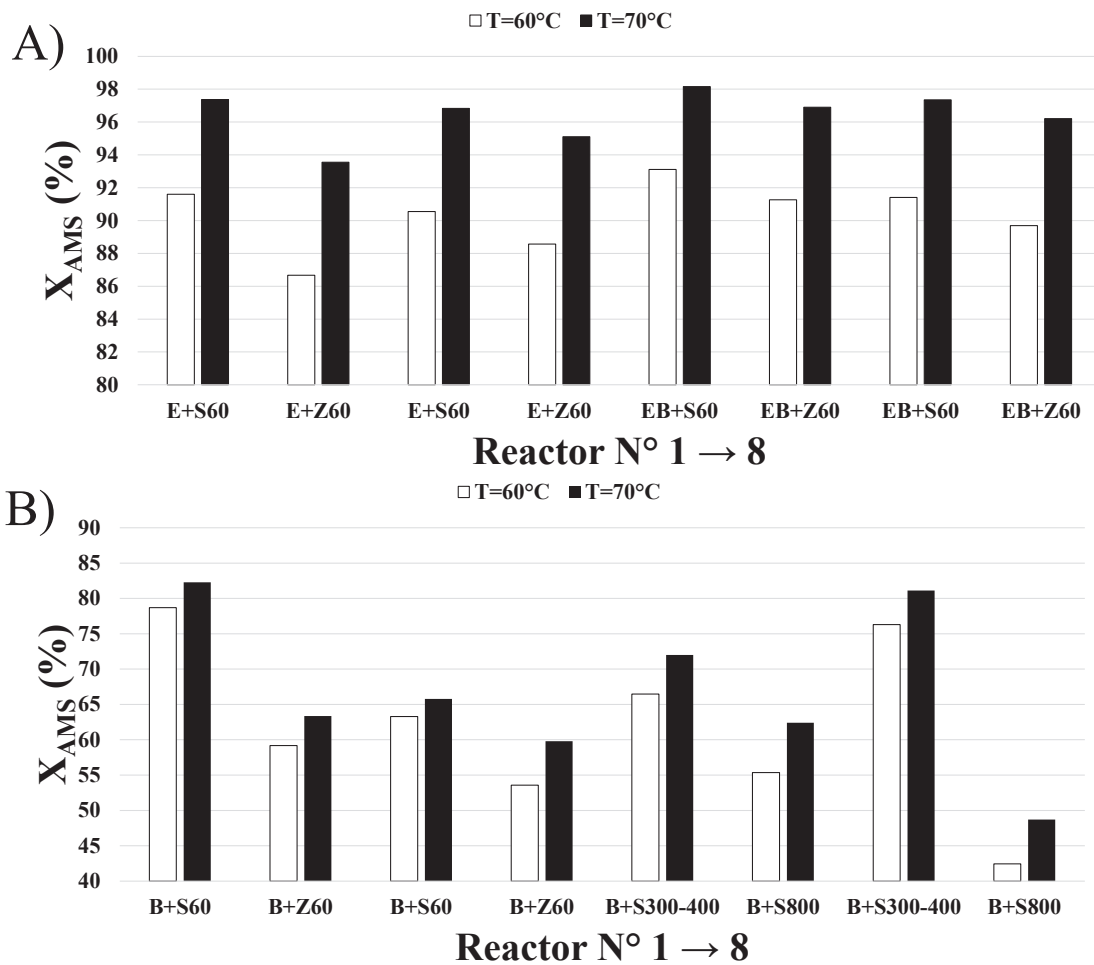


Figure 99. Effect of the temperature on the conversion. A) $D_r=2\text{ mm}$, $N_2/H_2=0.5$, $m_{cat}=50\text{ mg}$, $W_i=2.5\text{ g/h}$, catalyst quadrilobe extrudates + porosity fillers. B) $D_r=4\text{ mm}$, $N_2/H_2=0$, $m_{cat}=100\text{ mg}$, $W_i=2.5\text{ g/h}$, catalyst beads $2 < d_p < 2.8\text{ mm}$ + porosity fillers. B=Beads, E=Extrudate quadrilobes, EB=Extrudates elongated bed, S=SiC, Z=ZirBlast[®]. The numbers in the legend indicate the porosity filler size in μm

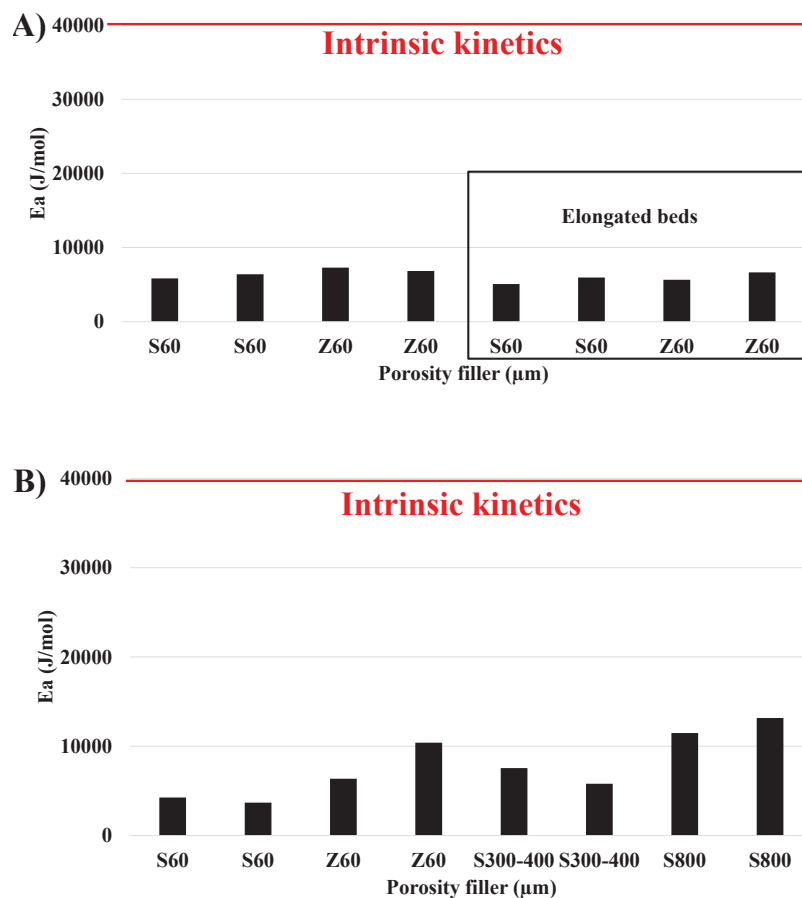


Figure 100. Apparent activation energy estimated values, for the different packings, according to the differences in conversion observed (Figure 99). A) $D_r=2$ mm, $N_2/H_2=0.5$, $m_{cat}=50$ mg, $W_i=2.5$ g/h, catalyst quadrilobe extrudates + porosity fillers. B) $D_r=4$ mm, $N_2/H_2=0$, $m_{cat}=100$ mg, $W_i=2.5$ g/h, catalyst beads $2 < d_p < 2.8$ mm + porosity fillers. S=SiC, Z=ZirBlast®

7.2.2.5 Hydrogen partial pressure effect

The hydrogen partial pressure has been varied during some of the experiments performed adding nitrogen in the gas feed and adjusting the N_2/H_2 ratio. As expected, the conversion increases with the increase of the hydrogen partial pressure and consequently of the reaction rate (Figure 101).

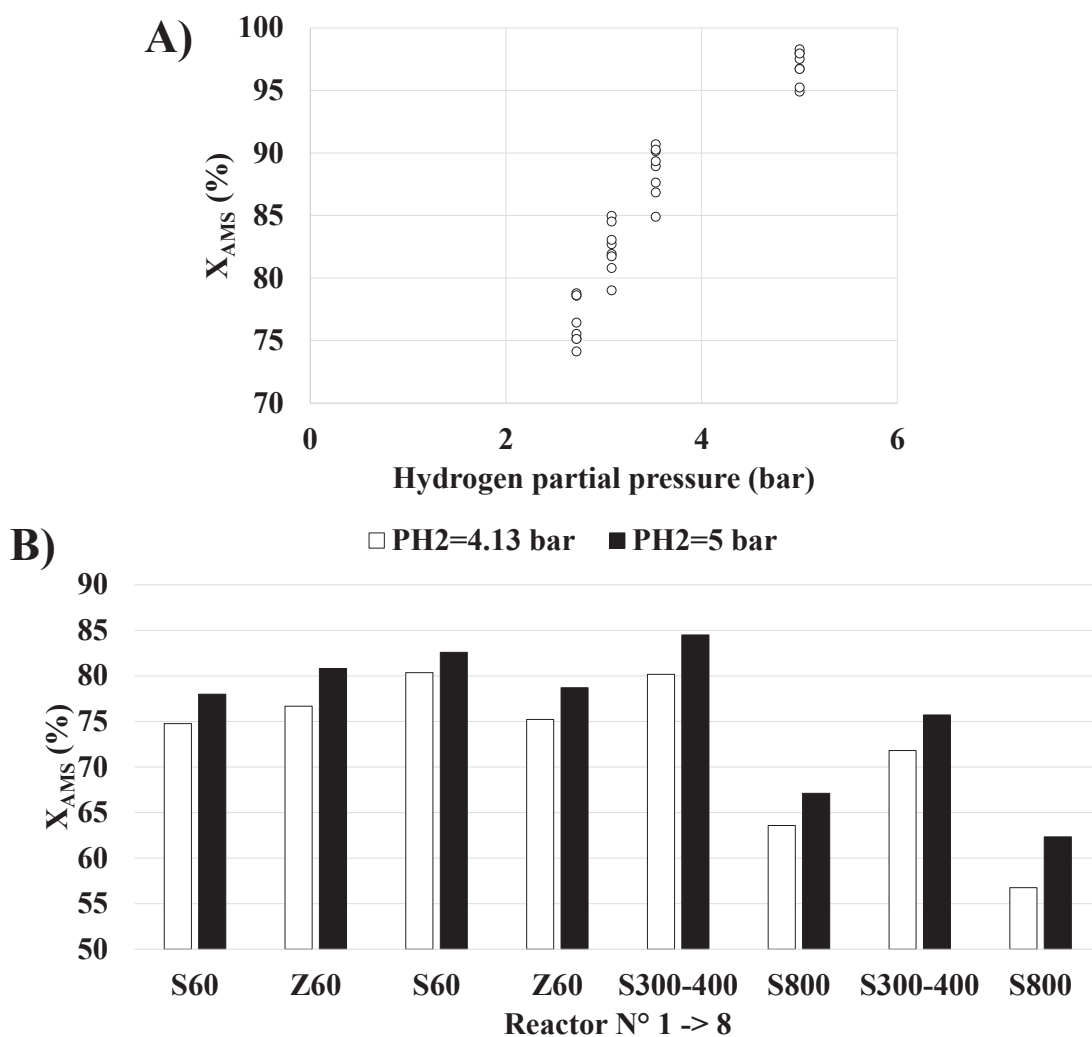


Figure 101. Effect of the hydrogen partial pressure on the conversion. A) $D_r=2$ mm, $T=60^\circ\text{C}$, $m_{cat}=50$ mg, $W_i=2.5$ g/h, catalyst quadrilobe extrudates + porosity fillers B) $D_r=4$ mm, $T=70^\circ\text{C}$, $m_{cat}=100$ mg, $W_i=2.5$ g/h, catalyst beads $2 < d_p < 2.8$ mm + porosity fillers. B=Beads, S=SiC, Z=ZirBlast[®]. The numbers in the legend indicate the porosity filler size in μm

7.2.2.6 Porosity filler effect

Extrudate quadrilobes: 2 mm internal diameter reactors

Three experiments are carried out in reactors of 2 mm internal diameter, packed with catalyst quadrilobes of 1.6 mm of diameter and ~3-4 mm of length, with and without porosity filler (photo of the packing without porosity filler in Figure 102). Their operating conditions are presented in Table 20.



Figure 102. Example of a $D_r=2$ mm reactor packed with catalyst quadrilobes

Table 20. Operating conditions for the tests performed in the 2 mm reactors packed with catalyst quadrilobes. The test name indicates the reactor diameter in mm (2), the catalyst particles used (E) and the test number

Test name	T (°C)	W ₁ (g/h)	Q ₁ (mL/h)	m _{cat} (mg)	N ₂ /H ₂ ratio	Effect explored
D2E/1	60	2.5	3.64	50	0	ZirBlast® 60 µm porosity filler
D2E/2	60	2.5	3.64	50	0	Porosity filler size and shape
D2E/3	[60; 70]	2.5	3.64	50	[0-1]	Porosity filler shape at 60 µm + bed elongation

For the conditions of the tests, the bed length is approximately 3.5 cm (7 cm for the elongated beds, see later). It is worthy to consider that, due to the very low amount of catalyst used, the number of catalyst particles packed in the reactors differs from test to test (less than 15) while the total catalyst mass is constant (50 mg). This number is very low and makes our result probably dependent on the catalyst batch homogeneity [68]. This may partially explain the difference observed sometimes for the reactors packed identically.

The results in of the test D2E/1, in which 4 reactors are packed without porosity filler and 4 with ZirBlast® 60 µm porosity filler, clearly indicate that the addition of ZirBlast® drastically increases the conversion (x2) (Figure 103). We can observe again the deactivation phenomenon along the test.

The Pe numbers measured in the hydrodynamic experiments closest to our conditions (reactor with D_r=2 mm, d_p=1.6x5 mm metal cylinders and L=9 cm) is around 3-4 for a length of 9 cm. Another measure on a single pellet string reactor (D_r=3 mm, d_p= 2x5 mm glass cylinders and L=9 cm) gave a Pe < 10. Considering a bed length of 3.5 cm the Pe number should be ~3 or less, so very low. With fine porosity fillers (<400 µm), the Pe should increase to values >20. The large differences in conversion observed cannot be explained by the Pe number difference between the reactors with

and without porosity filler. They should instead be caused by the better bed wetting and the higher liquid holdup.

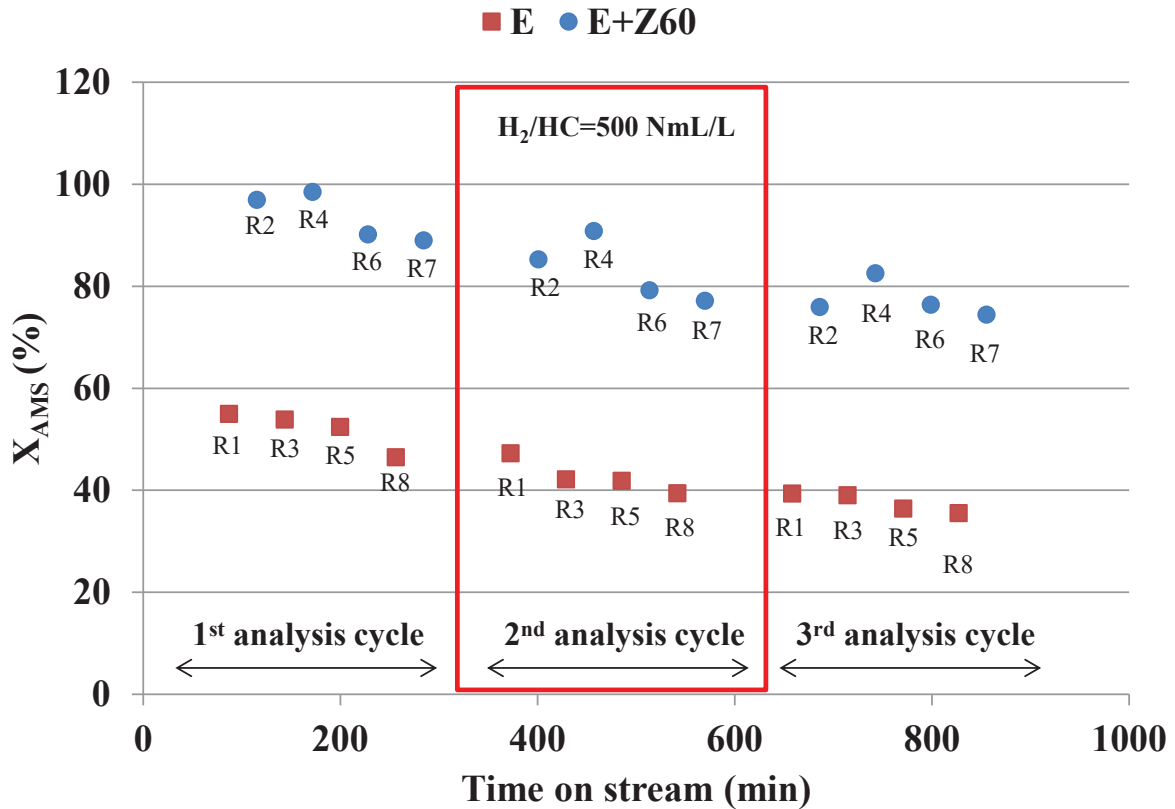


Figure 103. Conversion against time on stream for the Test D2E/1. Each analysis cycle includes the 8 reactors tested. Z= ZirBlast[®]. The number in the legend indicates the porosity filler size in μm . The labels on the data indicate the reactor number. $H_2/HC=250 \text{ NmL/L}$ if not indicated

The test D2E/2 and D2E/3 are aimed at investigating the effect of the porosity filler size and shape. All the packings are duplicated. In the test D2E/3 elongated beds are obtained alternating one catalyst particle and one inert alumina extrudate, so that the bed length is practically doubled.

Smaller and irregularly shaped porosity fillers (SiC) are more beneficial than spherical porosity fillers (ZirBlast[®]) (Figure 104).

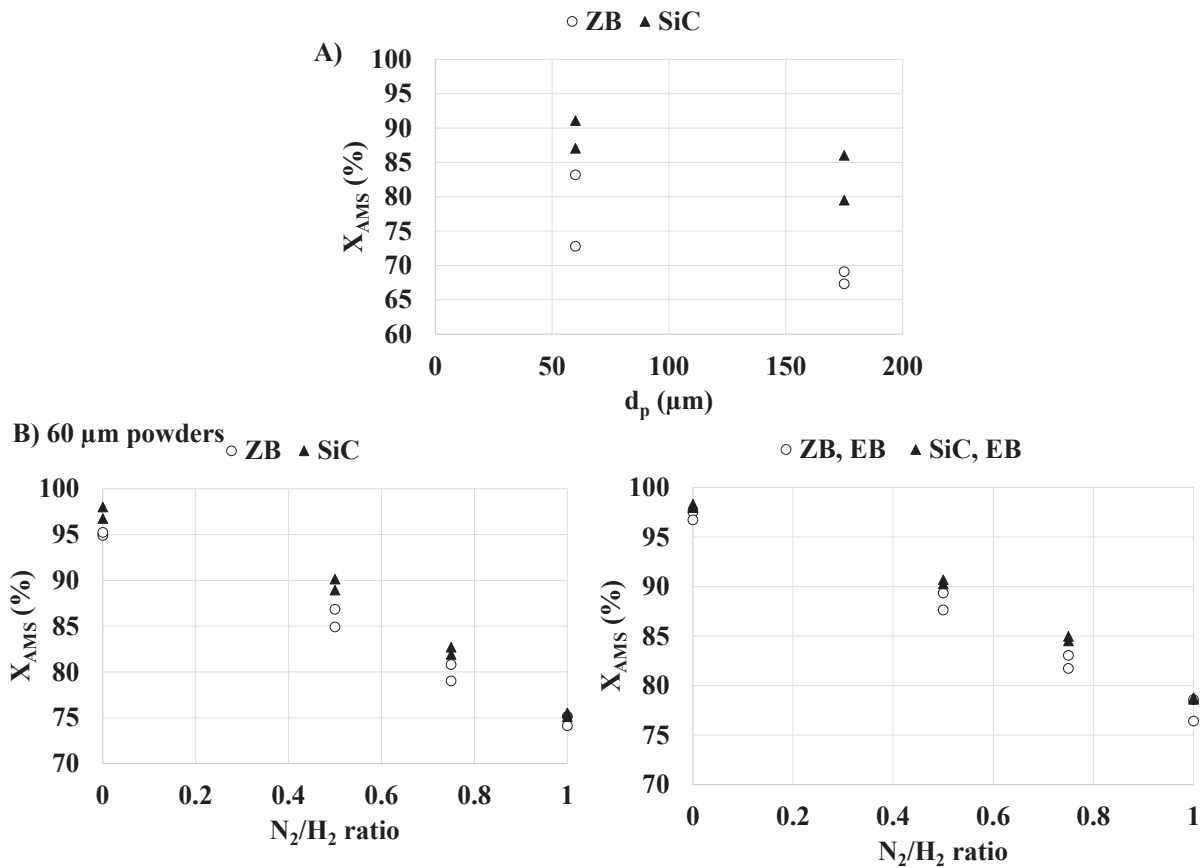


Figure 104. Conversion data for: A) Test D2E/2 as function of the porosity filler diameter (for sieved powders, the mean between the sieving extremes has been considered as particle diameter), B) Test D2E/3 as function of the N_2/H_2 ratio. EB=Elongated Bed, ZB= ZirBlast®.

The higher conversion observed in presence of SiC powder at both the grain sizes tested (60 μm and 150-200 μm) can probably be explained by an IFPEN observation of residual liquid holdup done using μ-tomography ([19], Figure 105). Spherical particles tend to pack in very dense clusters that form a barrier to gas flow and probably act as a dead zone regarding liquid circulation. In SiC filled catalyst beds, gas distribution is more uniform.

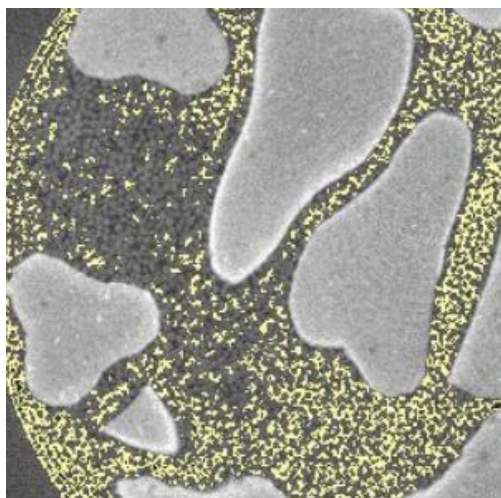


Figure 105. Examples of μ -tomography pictures showing zones without residual gas (unpublished results). Yellow: gas phase, dark grey: liquid, grey: spherical glass beads (or trilobitic catalyst)

Comparison of normal and elongated beds with the same porosity filler is quite interesting (Figure 106): whereas the hydrodynamics is probably the same, we observe higher performances with elongated beds. One reason could be the increase in bed length (higher Pe number) that, for a first order reaction and the conversion levels explored, would lead to differences of 3-4 conversion points that is what we find if considering the means of the conversion of identically packed reactors. Another reason that could explain the higher conversion of the elongated beds is a higher average dissolved H_2 content due to dissolution of H_2 in the inert “intermediate” beds.

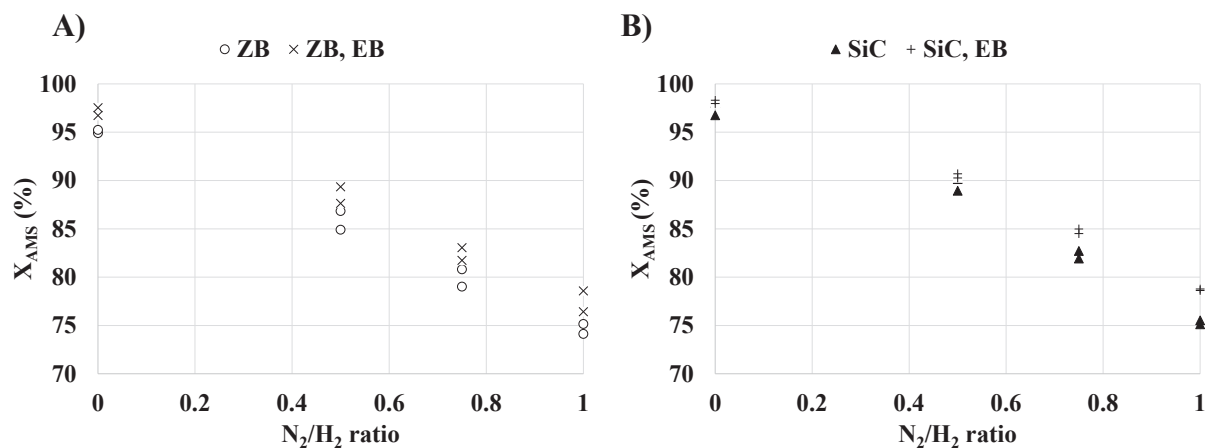


Figure 106. Comparison of elongated and normal beds for different N_2/H_2 ratios using $60\ \mu m$ porosity fillers (Test D2E/3). A) Porosity filler: ZirBlast[®], B) Porosity filler: SiC. EB=Elongated Bed, ZB= ZirBlast[®]. $T=60^\circ C$

Extrudate quadrilobes: 4 mm internal diameter reactors

Two experiments are carried out in reactors of 4 mm internal diameter packed with catalyst quadrilobes of 1.6 mm of diameter and $\sim 3-4$ mm of length, with and without porosity filler (photo of packings without porosity filler in Figure 107). Their operating conditions are presented in Table 21.



Figure 107. Left: Example of a $D_r=4$ mm reactor packed with catalyst quadrilobes. Right: Example of a $D_r=4$ mm reactor packing packed with catalyst quadrilobes in which the bed length has been elongated with inert alumina

Table 21. Operating conditions for the tests performed in the 4 mm reactors packed with catalyst quadrilobes. The test name indicates the reactor diameter in mm (4), the catalyst particles used (E) and the test number

Test name	T (°C)	W_1 (g/h)	Q_1 (mL/h)	m_{cat} (mg)	N_2/H_2 ratio	Effect explored
D4E/1	60	3	4.37	150	0.75	Bed elongation, ZirBlast® 60 μ m porosity filler
D4E/2	60	2.5	3.64	100	0.5	Porosity filler size and shape

For the conditions of the tests, the bed length is approximately 2.5-3 cm, depending on the catalyst mass. Considering that this is the shortest of the bed lengths tested, a first test includes the exploration of the bed elongation effect using inert alumina extrudates to lengthen the bed. The catalyst is separated in three sections with the same mass, spaced by two sections of inert alumina extrudates always with the same mass (Figure 107 right, the bed length is so increased of ~67%).

Pe number measurements have not been performed in a “randomly” packed bed millireactor with cylinders, because of the lack of non-porous cylinders with length < 4 mm. Anyway, considering that for all the reactors tested in $D_r=4$ mm (SPSRs and random packings with spheres) the Pe number is around 10-15 for a bed length of 9 cm, so that it is reasonable to consider a Pe number of ~3-4 for our conditions (5-7 in case of elongated beds). In case of addition of porosity fillers, the Pe number should increase to values $Pe>13$ (>20 for the elongated beds). The Pe numbers reported are the ones observed in the “worst” reactors of 4 mm tested.

Comparison of normal and elongated beds in the test D4E/1 (Figure 108) shows that, without porosity filler, higher performances are observed for the non-elongated beds. This is probably due to the fact that these reactors are non-isotherm so that in the beds elongated with inert alumina extrudates the flow cools down between one catalyst layer and another (see Figure 107, right) leading to lower conversions. On the contrary higher performances of the elongated beds are observed when using porosity fillers. Being the reactors more isotherm, the reason is probably the same as for the $D_r=2$ mm reactors: the increase in bed length (Pe number, 3-4 conversion points are expected for a first order reaction, so not all the difference observed) and a higher average dissolved H_2 content due to dissolution of H_2 in the inert intermediate beds.

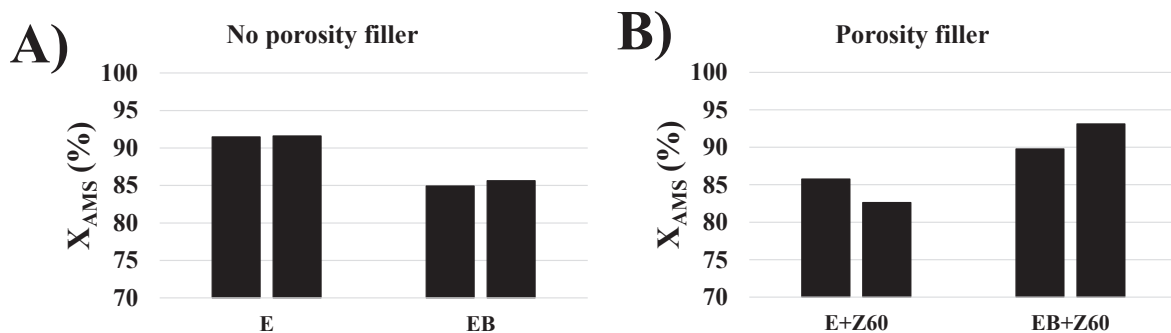


Figure 108. Comparison of normal and elongated beds (Test D4E/1): A) No porosity filler, B) Porosity filler: ZB. EB=Elongated Bed, Z and ZB=ZirBlast[®]. The numbers in the legend indicate the porosity filler size in μm (if present)

The porosity filler effect is explored in both tests. In the not elongated beds the addition of porosity filler does not yield a better conversion (Figure 109, A). The most likely explanation is that the not elongated beds without porosity filler are less isothermal (we did not test the isothermicity of the 4 mm reactors) and on average hotter. Adding powder improves the heat transfer and reduces the average temperature (through the solids thermal conductivity). Adding layers of inert material gives more time to cool down the bed. Indeed, elongated beds show less performance than normal beds (Figure 108, A) suggesting they are more isothermal.

In the elongated beds, the addition of porosity filler yields a better conversion (Figure 109, A). As the beds with porosity filler are more isothermal (cooler) and thus less “reactive”, this performance improvement is due to a positive effect of the porosity fillers on the flow regime, the Pe number (3-4 conversion points are expected for a first order reaction and our conversion levels) and/or catalyst wetting. SiC 60 μm increases even more the conversion than SiC 300-400 μm (Figure 109, B). Again, SiC seems to give better results than ZB for 300-400 μm particles, which confirms our previous result on 60 μm powders. A last comment is that the repeatability is better with SiC than ZB.

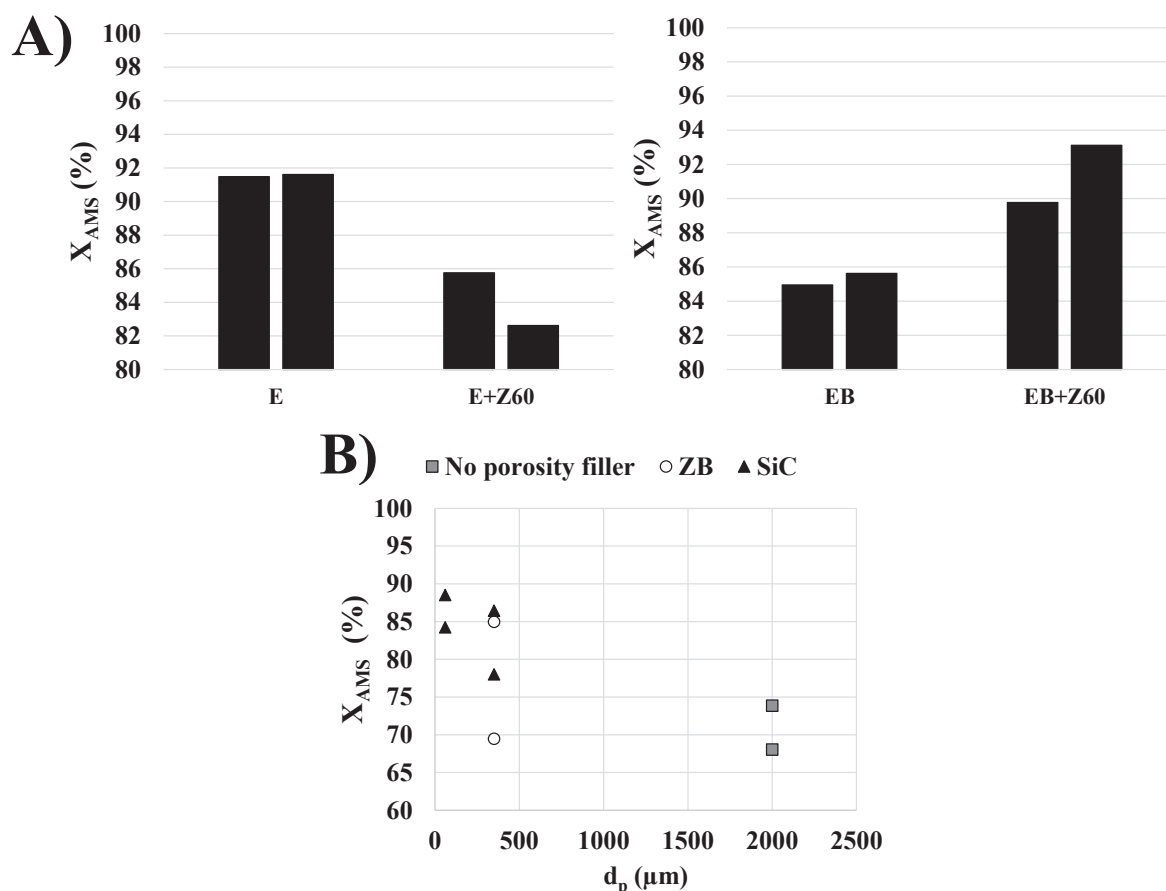


Figure 109. A) Porosity filler effect for normal beds and elongated beds (Test D4E/1), B) Packing particle diameter effect on elongated beds (Test D4E/2). For sieved powders, the mean between the sieving extremes has been considered as particle diameter. For the case without porosity filler an equivalent sphere diameter has been considered (~2 mm). EB=Elongated Bed, Z and ZB=ZirBlast®. The numbers in the legend indicate the porosity filler size in μm (if present).

2-2.8 mm beads: 4 mm internal diameter reactors

Three experiments are carried out in reactors of 4 mm internal diameter packed with catalyst beads with particle diameter between 2 and 2.8 mm, with and without porosity filler (see photos of the packings without porosity filler in Figure 110).



Figure 110. Examples of $D_r=4$ mm reactors packed with 2-2.8 mm sieved catalyst beads. On the left: mean particle size closer to 2.8 mm. On the right: mean particle size closer to 2 mm

As the bead sizes are not homogeneous, different bed geometries are possible when repeating the packings. It is possible to observe in Figure 110, left, a packing in which the beads touch alternately the wall following a zigzag path, leaving large spaces outside the beads plan sides. This packing occurs when the beads size is closer to 2.8 mm than 2 mm (δ near 1.5), and it is characterized by large passages on the sides where the liquid and the gas can flow without meeting the catalyst. In Figure 110, right, we can observe a packing that is more spiral-like, having smaller and shorter passages in correspondence of the walls. This packing occurs when the beads size is closer to 2 mm than 2.8 mm (δ near 2).

For the conditions of the tests, the bed length is approximately 3.5 cm. It corresponds to a number of beads around 15.

The operating conditions for each test are presented in Table 22.

Table 22. Operating conditions for the tests performed in the 4 mm reactors packed with 2-2.8 mm catalyst beads. The test name indicates the reactor diameter in mm (4), the catalyst particles used (B-) and the test number

Test name	T (°C)	W ₁ (g/h)	Q ₁ (mL/h)	m _{cat} (mg)	N ₂ /H ₂ ratio	Effect explored
D4B-/1	70	2.5	3.64	100	[0; 0.25]	Porosity filler effect + shape
D4B-/2	[60; 70]	2.5	3.64	100	[0; 0.25]	Porosity filler size and shape
D4B-/2bis	70	2.5	3.64	100	[0; 0.25]	Porosity filler size and shape

Pe number measurements have been performed packing a reactor of 4 mm with a mix of particles $d_p=2$ (glass), 2.3 (ZirBlast[®]) and 3 (glass) mm alternated, that we consider the reactor with the closest packing geometry (even if, as observed, in the reactive tests it is quite variable). Corrected to our bed length, a Pe number of 7 is expected without porosity filler, while a $Pe > 18$ with porosity filler.

The results of the Test D4B-/1, aiming at exploring the porosity filler effects and their shape, are shown in (Figure 111). The packings without porosity filler are not at all repeatable, with the lowest conversion achieved for the one arranged in a plane and with the smallest number of beads.

The high differences observed may be due to:

- Low amount of catalyst mass tested (heterogeneity of the catalyst batch) [68];
- Different particles disposition in the reactor (zigzag, spiral...);
- Different number of catalyst beads.

The batch inhomogeneity cannot fully explain the observed results, as the packings without porosity filler are the only ones with that poor conversion. It would be very unlikely that we would have sampled “bad grains” in only the same reactor type.

We will now explore the “number of beads” explanation using quick estimates. In these catalysts, the AMS hydrogenation is internally mass transfer limited and occurs only on a very thin layer [34]. The activity is thus related to the exposed area and can be estimated as follows:

$$S = \pi * d_p^2 * N_{beads} \quad \text{Equation 54}$$

As the number of beads can be expressed as $N_{beads} = \frac{V_{beads}}{\frac{\pi * d_p^3}{6}}$, we have that $S \sim 1/d_p \sim N_{beads}^{1/3}$. For

a first order reaction the conversion can be expressed as $X=1-e^{-k\tau}$ so that $X \sim N_{beads}^{1/3}$ if we develop e^{-x} with the Taylor series.

A difference between 14 and 15 beads would explain a difference of ~2.3% between the conversions. The beads number and the effect of catalyst surface area do not explain the results.

We think the main difference is due to the packing structure and that the liquid flows on the reactor walls without interacting with the catalyst. The presence of the porosity filler can drastically improve the situation increasing the wetting and homogenizing the distribution in the reactor.

We observe again that adding porosity fillers (300-400 μm) improve the reactor’s conversion and with a higher gain when using SiC rather than ZB. The gain in conversion is caused by the higher holdup, the better flow distribution (very important in this case because of the bed geometry), and higher Pe number (but only 3-4 conversion points are expected in this case for a first order reaction). Even if we have a limited number of repeated experiments, the reproducibility of the data improves when using powders, especially with SiC.

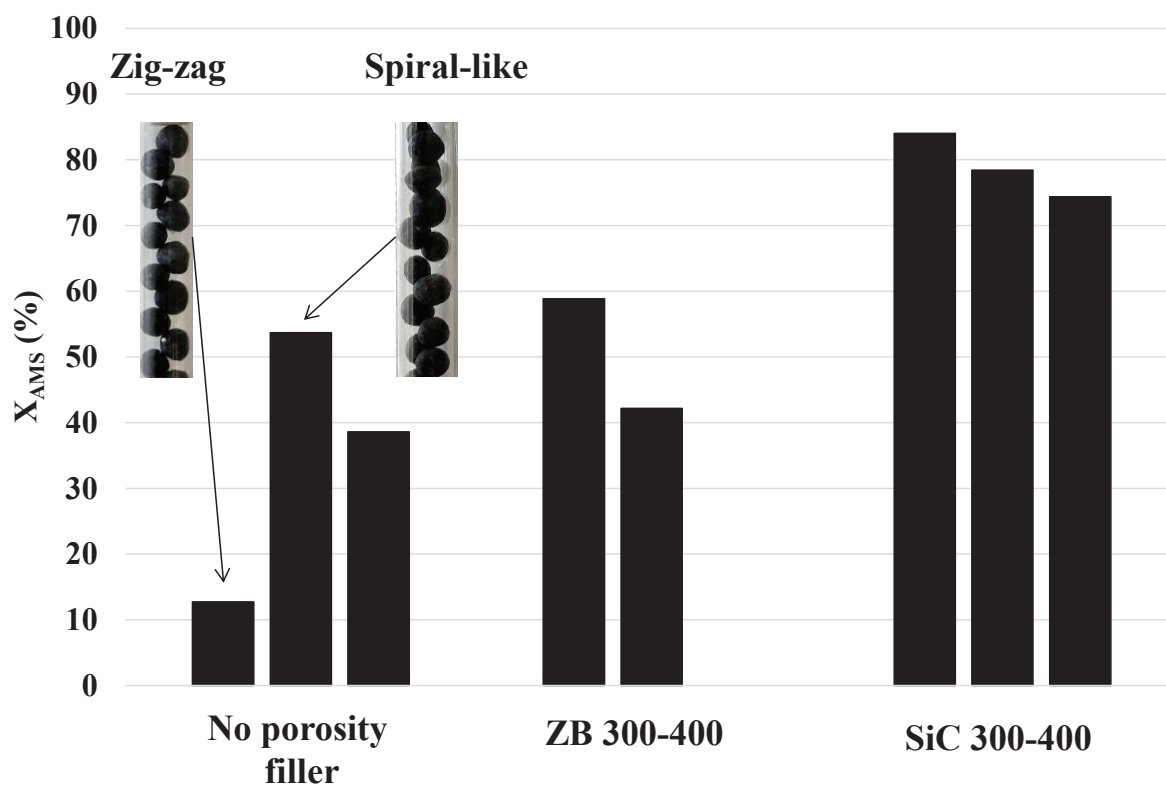


Figure 111. Conversion for the different packings of the Test D4B-/1. ZB=ZirBlast®. The numbers in the legend indicate the porosity filler size in μm (if present)

The tests D4B-/2 and 2bis, aimed at exploring the porosity filler shape and size, present a poor reproducibility of the duplicated reactors, up to almost 17 points of conversion (Figure 112), even if it is better if compared with the one without porosity fillers observed before. Reducing the porosity filler size from 800 μm to 300-400 μm is beneficial but reducing the powder size to 60 μm does not improve the situation (hidden in the uncertainty). It could be that with a powder size of 300-400 μm the catalyst wetting is already improved and the Pe number increased enough.

SiC powder proves again better than ZirBlast[®] powder for gas-liquid-solid applications for the Test D4B-/2 (Figure 112, left) while for the Test D4B-/2bis (Figure 112, right) both powders have the same performance.

In fact, the difference in conversion between the two tests for the reactors packed with ZirBlast[®] 60 µm is surprising. In general, we already observed more repeatable packings when using ZirBlast[®] instead of SiC.

We propose two explanations for the phenomenon:

- When using ZirBlast[®] 60 µm powder the probability of creating randomly high densely packed zones (in an uncontrolled manner) is the highest among all the porosity fillers. These zones have a negative effect on the reactive performances. The randomness with which these zones may be created can explain the differences observed;
- The variability may come from poor arrangements of the catalyst beads in of the reactors of test 4DB-2.

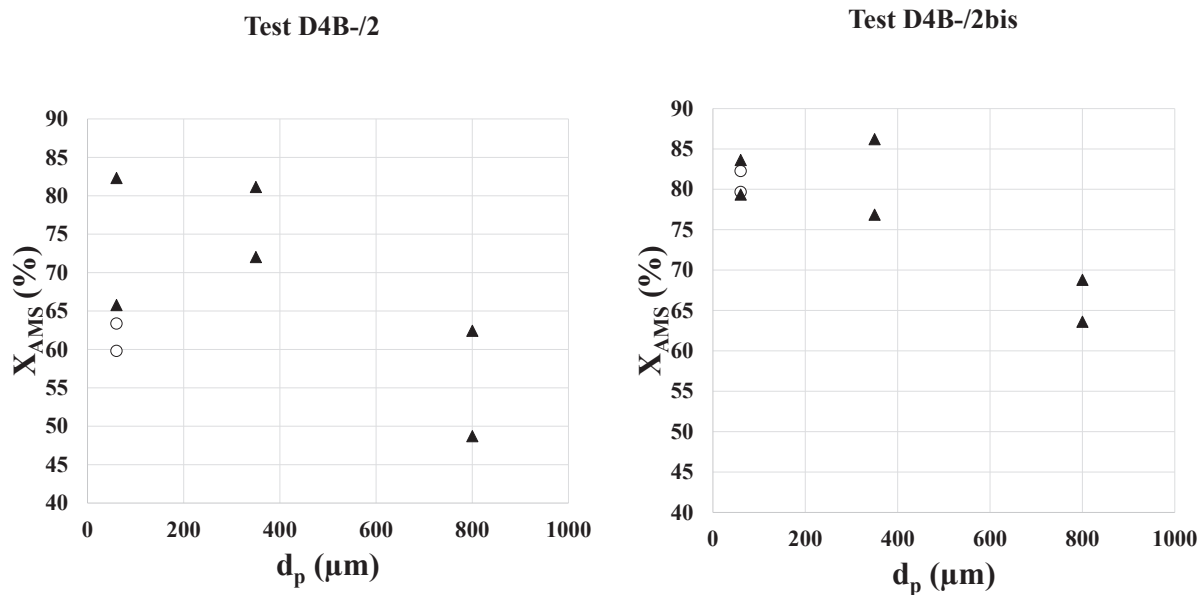


Figure 112. Porosity filler size and shape effect for the Test D4B-/2 and 2bis. Black triangles: SiC, white circles: ZirBlast[®]. $N_2/H_2=0$, $T=70^\circ\text{C}$

2.8-4 mm beads: 4 mm internal diameter reactors

One experiment is carried out in reactors of 4 mm internal diameter packed with catalyst beads with particle diameter between 2.8 and 4 mm, with and without porosity filler (photo of the packing without porosity filler in Figure 113).



Figure 113. Examples of $D_r=4$ mm reactors packed with 2.8-4 mm sieved catalyst beads

In this case, even if the beads size is not homogeneous, the packings obtained with these spheres are, with some minor differences (see again Figure 113), single pellet string reactors. The preferential passages on the walls are reduced compared to the case of beads with $2 < d_p < 2.8$.

For the conditions of the test, the bed length is approximately 3-3.5 cm. It corresponds to a number of beads $\sim < 10$.

Only one test is performed, and its operating conditions are presented in Table 23.

Table 23. Operating conditions for the test performed in the 4 mm reactors packed with 2.8-4 mm catalyst beads. The test name indicates the reactor diameter in mm (4), the catalyst particles used (B+) and the test number

Test name	T (°C)	W_1 (g/h)	Q_1 (mL/h)	m_{cat} (mg)	N_2/H_2 ratio	Effect explored
D4B+/1	70	2.5	3.64	125	0.25	Porosity filler effect + size and shape

Pe number measurements have been performed packing a reactor of 4 mm with 3 mm glass spheres, which is the reactor with the most similar packing structure. Adapted to our bed length, a Pe number of ~ 5 is expected without porosity filler, while a $Pe > 18$ with porosity filler.

The repeatability in the Test D4B+/1 is still very large in absence of porosity filler (Figure 114) and with 400 μm porosity filler, but compared with those observed the $2 < d_p < 2.8$ beads it is better. This is because of the more repeatable packing from the geometrical point of view. The repeatability is increased with 60 μm fillers.

In this case, as well, we confirm the beneficial effect of the porosity fillers. The 60 μm powder is better than 300-400 powder both in performance and repeatability (Figure 114). We think this can be explained by a geometrical effect: the 300-400 μm powder is too large to access all the void fraction of the catalytic bed. The smaller powder fills up the void fraction more uniformly. SiC 60 μm is in this case clearly better than ZB 60 μm .

An interesting result comes by observing the number of beads packed in each reactor. Each reactor has a duplicate and they have intentionally a different number of beads (8 and 9). With or without porosity filler, the reactors with 9 beads show higher conversion than the reactors with 8 beads (except for the reactor packed with SiC 60 μm that has good repeatability). The effect of particles number on the conversion is estimated at 4% of increase of the conversion (considering 8 and 9 beads). The increases in conversion observed are 27 and 20% respectively for the reactors packed without porosity filler and the one packed with SiC 300-400 μm . So, the difference in conversion is not only due to the surface of the catalyst but a consequence of the packing and flow distribution (the Pe number difference with/without powder cannot fully explain the differences).

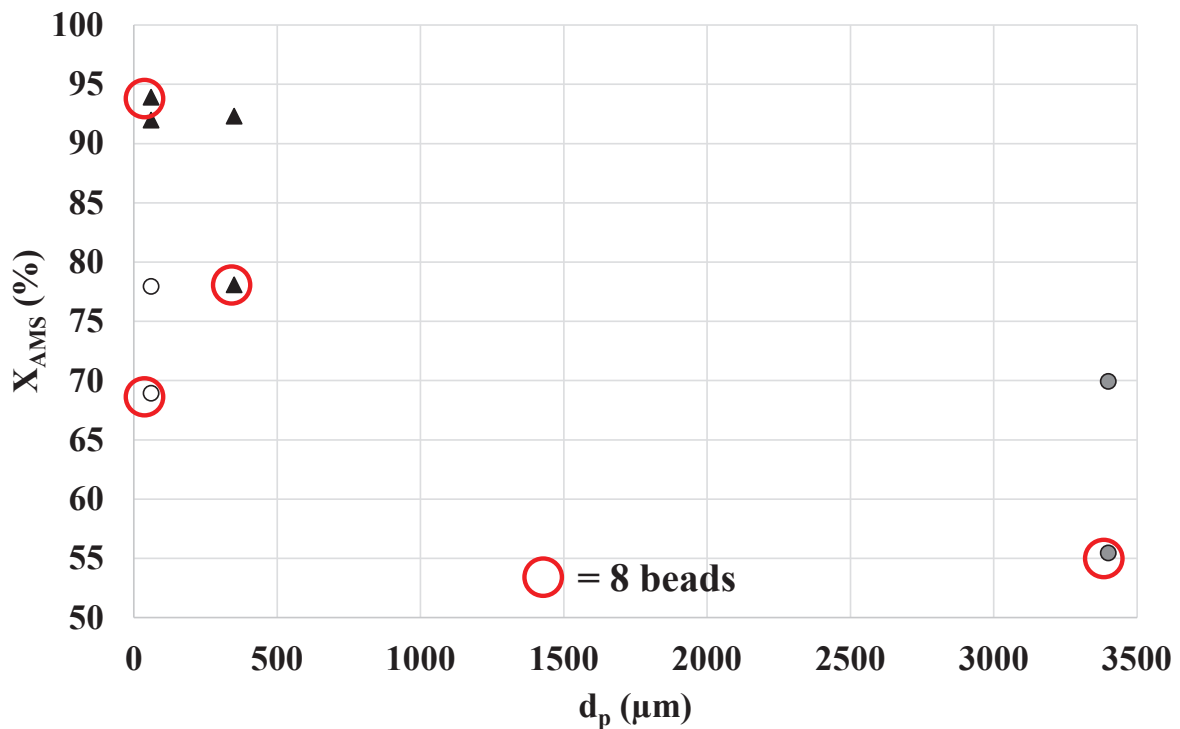


Figure 114. Effect of the packing particle diameter on the conversion. For sieved powders and particles, the mean between the sieving extremes has been considered as particle diameter (3.4 mm for the catalyst beads). Grey circles: no porosity filler, white circles: ZirBlast® porosity filler, black triangles: SiC porosity filler

Comparison of 3 and 4 mm internal diameter reactors with 2-2.8 mm catalyst beads

A test is performed to explore the effect of the choice of the reactor internal diameter using the same catalyst particles. Catalyst beads with $2 < d_p < 2.8$ mm have been used in reactors with internal diameter 3 and 4 mm. The packing geometry in case of the reactors of $D_r=4$ mm has already been presented (alternated/zigzag/spirals), while in the reactors of 3 mm the particles form a single string of aligned particles (a Single Pellet String Reactor). ZirBlast® 150-200 μm as porosity filler is added in some of the reactors. The operating conditions are presented in Table 24.

Table 24. Operating conditions for the tests performed in the 3 and 4 mm reactors packed with 2-2.8 mm catalyst beads

T (°C)	W ₁ (g/h)	Q ₁ (mL/h)	m ^{cat} (mg)	N ₂ /H ₂ ratio	Effect explored
70	[2.5]	[3.64]	120	[0-0.5]	Porosity filler + reactor diameter effects

The bed length is ~4 cm for the reactors with D_r=4 mm and ~5 cm for the reactors with D_r=3 mm. The Pe number are expected to be quite low in both cases (<10) but higher for the reactor of D_r=3 mm that is longer. The flow in absence of porosity fillers is expected to be pulsed for the reactor with D_r=4 mm (I=6.28x10⁻⁷) while in the transition area for the reactors with D_r=3 mm (I=1.12x10⁻⁶).

The results in absence of porosity filler, shown in Figure 115, clearly indicate that it is better to test the catalyst particles in the reactor of 3 mm for both the absolute performance and the repeatability. This can be explained by two effects:

- Smaller bypasses on the wall for the 3 mm case;
- Higher mass transfer for the 3 mm case due to higher liquid superficial velocities;

The higher Pe number for the 3 mm case, due to higher bed length may only explain a difference of 1-2 conversion points (for a first order reaction).

High difference in conversion is observed between the two duplicates for the reactors of D_r=4 mm confirming again that the bed structures created are not repeatable. In the reactors of D_r=3 mm the results are much closer and almost complete conversion is reached.

When adding porosity fillers (Figure 115) the conversions obtained with the two reactor diameters are closer but still in favor of the 3 mm reactor.

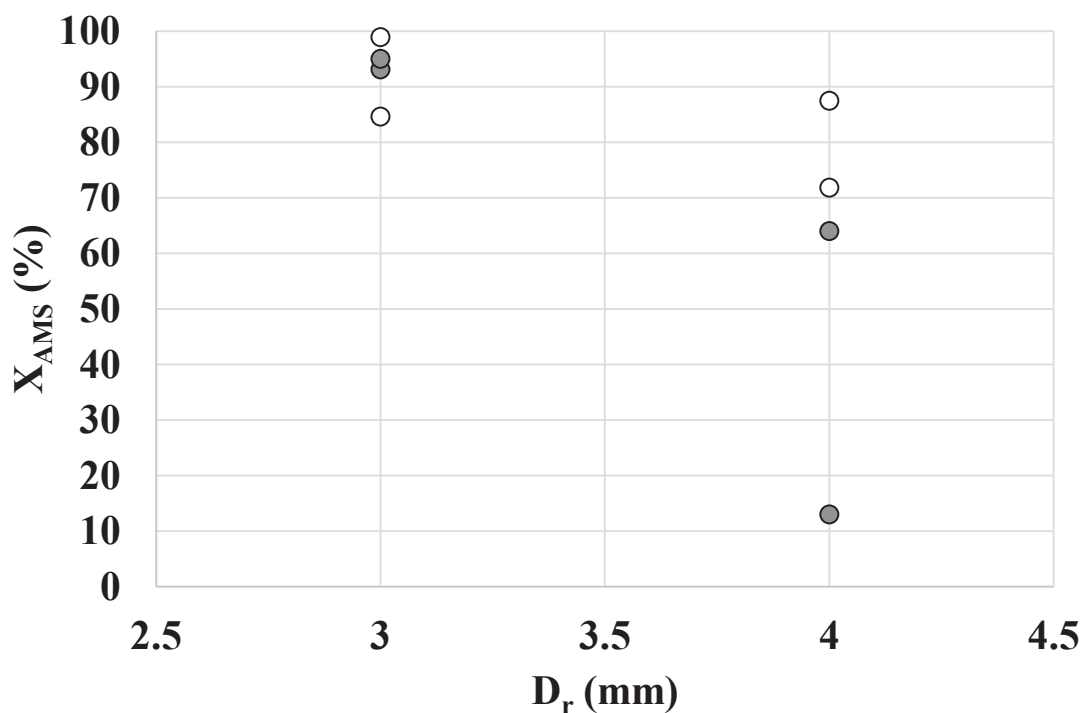


Figure 115. Comparison of the conversions obtained using catalyst beads $2 < d_p < 2.8$ mm in $D_r=3$ vs 4 mm reactors. $N_2/H_2=0.5$. Grey circles: no porosity filler, white circles: ZirBlast® 150-200 μ m porosity filler

7.2.3 Conclusions on the reactive tests

Reactive tests on the α -methylstyrene hydrogenation reaction have been carried out in a High Throughput Experimentation unit. Different types of reactors, catalyst particles and porosity fillers have been used. The tests have been performed with temperatures of 60-70°C and a flow rate of 20-24 g/h (for the 8 reactors). A low amount of catalyst has been used, having as consequences:

- Risk of sampling not representative of the catalyst batch;
- Small bed lengths (~3-4 cm);
- Low Pe numbers.

Catalyst deactivation has been observed, probably because of the water content present in the liquid feedstock and/or coke precursors formation. The deactivation rate has been found to be different for the reactors packed with or without porosity filler probably because of an easier removal of aromatic coke precursors by the liquid phase and/or a more homogeneous catalyst work due to the better fluid distribution on the reactor's section.

Experiments varying the temperature showed that the tests have been performed in presence of mass transfer limitations.

The geometrical disposition of the catalyst particles, affected by their size (and consequently by their number), has an important effect. Considering the short bed lengths, the packing defects are not smoothed. A lower packing repeatability has been observed when using a combination of reactor and particle size (that is not constant in a catalyst batch) in a way that multiple combinations are possible. Packings where the particles arrange with important spaces on the walls proved to be less performant. We recommend avoiding, if possible, these geometries, while Single Pellet String Reactors with δ close to 1 are instead recommended. Larger bed lengths are recommended as packing defects can be smoothed.

Porosity fillers are recommended in any case, with the use of the smallest grain size available. Irregular porosity fillers proved to be more beneficial for the conversion. We propose that this is because spherical porosity fillers create high densely packed zones in which the gas phase does not pass, with limitations on mass transfer. The gains in conversion and repeatability of the packings are explained by:

- Increase of the liquid Pe number and the liquid holdup. The increased liquid holdup increases the mass transfer;

- Porosity fillers homogenize and stabilize the flow preventing catalyst bypasses that in case of very fast reaction are particularly critical.

Table 25 resumes the porosity filler effect on the reaction.

Table 25. Porosity filler effect on the performance of the α -methylstyrene hydrogenation reaction

D_r (mm)	Catalyst	Porosity fillers effect			Comments
		Effect on conversion	Size effect	Shape effect	
2	E	Very positive	60 μm better	SiC (irregular) better	Higher activity of elongated beds
3	B-	N/A	N/A	N/A	Higher activity compared to $D_r=4$ mm
4	E	- Negative for normal beds - Positive for elongated beds	60 μm better	SiC (irregular) better	Probably non-isothermal beds if not elongated
4	B-	Very positive	60 μm better	SiC (irregular) better	Very bed packing reproducibility without porosity filler
4	B+	Positive	60 μm better	SiC (irregular) better	N/A

8 General conclusions and perspectives

8.1 Synthesis of the work

Packed bed millireactors, packed beds with millimeter-sized reactor diameters, are increasingly used for heterogeneous catalyst testing. The possibility to use these reactors for kinetic studies is quite attractive, but it requires a better knowledge of the flow characteristics.

The analysis of the extensive literature on packed bed reactors and the restricted one on packed bed millireactors does not clearly answer the following question: are these reactors suitable for a use in kinetic studies? Going more in detail, the questions are:

- How is the hydrodynamics of these reactors compared to the larger beds?
- What is the effect of using a catalyst particle size comparable to the reactor diameter (mm)?
- Can we use short beds/small amount of catalyst? What are the potential limitations? Can we define criteria?
- Do we need to use porosity fillers? Which ones?

The thesis work has been mainly divided in two areas: gas-solid (G/S) and gas-liquid-solid (G/L/S).

8.1.1 Gas-solid case

The hydrodynamics under G/S conditions has been explored experimentally with residence time distribution measurements and through CFD simulations.

The hydrodynamics (Pe/Bo number) of these reactors has been found similar to those of larger reactors, except for particular geometries in which the geometrical constraints lead to packing with large preferential flow passages. The hydrodynamics of these packings is poor, and they should be avoided. Except for these cases, acceptable values of Pe number in absence of porosity fillers have been found for short geometries (<10 cm), meaning that the dispersion effects can be neglected for

most reactions when performing kinetic studies. A correlation, based on a model already reported in literature for Single Pellet String Reactors only, is proposed to estimate the Pe/Bo number in packed bed millireactors.

Porosity fillers have been found beneficial in all the reactors tested, from both the hydrodynamic and the “reactive” point of view. Reactors with good hydrodynamics (high Pe number) have been found to benefit from the addition of porosity fillers, from 1 to 6/7 conversion points depending on the cases (an increase lower than 10%). We attributed this gain to an enhanced gas-solid mass transfer because of higher interstitial gas velocities. Repeated tests showed a higher beneficial (but very small) contribution of spherical porosity fillers (ZirBlast[®]) compared to irregularly shaped ones (SiC).

The use of small amounts of catalyst of the same reactor dimensions showed globally a repeatability of $\sim\pm 1$ point of conversion for identically packed reactors in gas-solid reactive applications for the explored range of conversions ($X=0.4-0.9$).

The CFD workflow that we developed proved to be efficient to accurately control the testing conditions (particles and reactor dimensions, fluid properties and velocity, etc.) and to access local information on the flow inside the packed bed millireactors. We recommend remaining careful about the CFD simulations for Single Pellet String Reactors with $\delta < 1.3$ because the Pe and Bo numbers are often overestimated, even if no evident reason was found to doubt the validity of the simulations.

8.1.2 Gas-liquid-solid case

The hydrodynamics under G/L/S conditions has been explored experimentally with a flow observation study and residence time distribution measurements.

Two main flow regimes were observed: a stable flow governed by capillary forces and an irregular flow governed by gravity. These flow patterns are not those observed in traditional packed bed reactors (trickle and pulsed flow). The transition between capillarity and gravity driven flows is well predicted using the Irrigation number and is determined by the liquid fluid velocity and the particle size. The flow in presence of millimetric particles is unstable. The use of porosity fillers stabilizes the flow inside the packed beds.

Low values of Pe (<10) number have been found for short geometries (<10 cm) in absence of porosity fillers so that dispersion effects cannot be neglected. The use of porosity fillers is highly recommended in this case.

Reactive tests showed a high sensitivity on the particle disposition inside the bed. When packing a reactor several times using the same particles, the final disposition is never the same. In our experimental results, we observed large differences in conversion between reactors packed with the same catalyst mass, but particles arranged differently. We explain this by the presence of bypasses such that the liquid fraction that flows along the reactor wall does not react. These bypasses are different when the particles are arranged differently. The use of small amounts of catalyst, in our case caused by the temperature and liquid flow rate constraints of the HTE unit, makes this aspect even more critical because eventual packing defects are not smoothed along the bed length. The effect is reduced, but still present, when using porosity fillers or when the packings are geometrically constrained and thus repeatable: this is the case of Single Pellet String Reactors with $\delta < \sim 1.5$ or when the beds are large compared to the particle size and thus more uniform.

Porosity fillers have been found beneficial in all the reactors tested, from both the hydrodynamic and the “reactive” point of view. Their use changes the flow regime from gravity driven to capillary forces driven, which ensures better catalyst wetting. Other reasons are a better hydrodynamics

(higher Pe number) and a more uniform distribution of the fluid phases on the reactor's section (a lower fraction of liquid passes along the bed walls without meeting the catalyst). Irregularly shaped porosity fillers proved to be more beneficial compared to the spherical ones. The reason is that spherically shaped porosity fillers can create locally high densely packed zones in which the liquid is likely to stagnate, and that are not accessible to the gas phase. Some catalyst grains can thus be shielded from liquid or gas.

8.1.3 Summary and recommendations when using packed bed millireactors

Table 26. Summary of the results found for the different operating conditions of packed bed millireactors. – and + indicate respectively a bad or good evaluation for the aspect in exam

	G/S without porosity filler	G/S with porosity filler	G/L/S without porosity filler	G/L/S with porosity filler
Flow regime	N/A	N/A	Gravity driven flow (unstable)	Capillary flow (stable)
Flow distribution	N/A	N/A	-	+
Liquid holdup values	N/A	N/A	<0.15	>0.2
Bo numbers	[0.5-7]	[0.1-0.5]	[0.1-0.5]	[0.05-0.2]
δ/particles disposition effect	Avoid large passages (i.e. $\delta=1.7, 2.6, 3.4$)	Good packing	Avoid large passages: (i.e. $\delta=1.7, 2.6, 3.4$)	Good packing
Mass transfer	+	++	-	+
Suggested minimum bed length (cm)	6-10, depending on the velocity	5	25	10-13, depending on the porosity filler size

In Table 26 we summarize the highlights of this work. Coming back to the questions we asked in paragraph §8.1, after the literature analysis, we can answer that:

- The hydrodynamics of packed bed millireactors in G/S conditions is similar to that of larger packed beds (similar Pe numbers) and close to plug-flow behavior in most cases. The hydrodynamics in G/L/S downflow conditions is instead not close to plug-flow behavior;

- The effect of using a spherical catalyst particle size comparable to the reactor diameter may create situations in which there are holes or large preferential passages in the structure ($\delta=1.5-1.7, 2.6, 3.4$). We recommend avoiding these configurations, in any case. In particular, for G/L/S applications the particles arrangement in the reactor proved to play a crucial role: homogeneous beds or beds with strong geometrical constraints (Single Pellet String Reactors with $\delta < 1.3$) are recommended;
- Using a small amount of catalyst has two consequences: a lower representativity of the catalyst batch (not all the catalyst particles are the same) and the lower catalyst bed lengths. The lower bed lengths do not allow packing defects to be smoothed. Packing defects proved to have a significant effect, particularly in G/L/S applications. In general, we recommend increasing the bed length as much as possible by increasing the catalyst mass or reducing the reactor diameter. Catalyst dilution is also an option but, as reported in literature, high dilution levels can be counterproductive so that attention is required in the packing methods;
- Porosity fillers are recommended in all cases. The best choice is to use small enough powders that can fill all the porosity. Then, for G/S applications we suggest spherical powders as they fill up better the porosity. For G/L/S applications we instead suggest irregularly shaped powders to avoid densely packed zones that can block the passage of the gas in specific zones of the reactor.

As a result of the work, we consider packed bed millireactors as more suitable to be used for kinetic studies in G/S conditions rather than in G/L/S conditions. Plug-flow behavior can be reached with shorter bed lengths (5-10 cm depending on the cases) while for G/L/S reactors 10 cm is often not enough even when using porosity fillers.

Mass transfer coefficient could not be deduced from the reactive experiments, so that they have been estimated only through CFD simulations. The results showed that, for single-phase flows, the literature correlations work better for the reactors without porosity filler. However, our G/L/S application (fast reaction) showed that in packed bed millireactors the particles dispositions may lead to important mass transfer limitations, probably due to a poor liquid distribution (liquid preferential passages).

8.2 Perspectives

8.2.1 Mass transfer coefficient calculations

As already discussed, we were not able to estimate mass transfer coefficients experimentally. Further work should focus on the estimation of mass transfer coefficients, particularly in presence of porosity fillers, to better understand the physics and compare it with larger packed beds. We propose to do it through both experiments (using fast reactions, comparing the results with a homogeneously packed reactor, and testing larger bed lengths) and CFD simulations (see §8.2.4).

8.2.2 The hydrodynamic descriptors

As observed in more than one occasion, the classic Bo number vs Pe_m number representation of the data on dispersion in packed beds is not sufficient to predict the dispersion values.

It is already known that the Sc number has an effect but our work shows that the bed geometry, for example the δ =reactor/particle diameter ratio, is also a key parameter especially for intermediate/high Pe_m number values where the governing dispersion mechanism switches from being diffusion controlled to convection controlled because of the higher fluid velocities.

The problem is not as easy as it may seem. The reactor hydrodynamics is affected by the presence and the size of the preferential passages. As observed in this work, there are some values of the

δ =reactor/particle diameter ratio in which preferential passages are more pronounced. There is no monotonous trend of these passages with the δ value so that a model taking into account this parameter (as done in this work) is for sure an improvement but it does not work in some cases (i.e. in the cases with large preferential passages in the reactor center).

A proposition is to introduce in the physical analysis other length scales that accounts for the fluid passage dimensions. In large reactors, the packing is random, and the fluid passages are isotropic, and the particle diameter is proportional and thus representative of the flow passage size in the bed. In small reactors, the reactor walls make the packing structure anisotropic and it is necessary to introduce transverse and axial length scales. We propose to get inspiration from the “hydraulic diameter” concept used in pressure drop models to derive a “dispersion diameter”.

8.2.3 G/L/S RTD tracer optimization

The G/L/S RTD experiments were performed using the *n*-heptane / iC16 system. To explain the shape and behavior of the curves obtained for the packed bed millireactors with fine porosity fillers, we proposed that the replacement of one liquid fluid by the other was “asymmetric”. The tracer exit was delayed because of the large difference in viscosity between the two liquids. We propose to check on this hypothesis by changing the tracer (iC16) for a less viscous tracer, for example aromatic species.

Aromatics (i.e. xylenes) have a viscosity comparable to that of *n*-heptane but still a different refractive index. This will allow keeping a good precision of the measurements. The only drawback is that aromatics are a little bit more difficult to handle and manipulate (more attention is required regarding safety and hazards).

8.2.4 CFD in presence of porosity fillers

The CFD simulations with porosity fillers require a lot of computing resources and we only explored short bed lengths (4 particles). We observed that inlet and outlet of the simulations impacted the dispersion results inside the packing up to two particles away. We recommend preparing a longer bed of at least eight particles which will probably require more than two months of DEM simulation. To avoid this, an idea could be to “repeat” the packing geometry obtained with the 4 spheres and translate it to obtain that the two packings are adjacent. Of course, there will be a “discontinuity” in the reactor packing in the point in which the packing is repeated.

Globally, in our experimental work, the smaller porosity fillers (60 μm) have been found the ones having the most “beneficial” effect. A study of different porosity fillers size will help to understand if there is a lower limit in porosity fillers size beyond which the size reduction becomes counterproductive, particularly for the mass transfer. CFD could then be used to study in which conditions the porosity filler can act as a “shield” by reducing transverse diffusion and preventing the molecules flowing near the reactor’s wall to interact with catalyst. A loss of performance was observed by IFPEN in some gas phase reactors filled with fine powder and a shielding effect was proposed. Our experimental work was too constrained to explore a wide enough range of conditions to study this phenomenon and we propose to perform a CFD study. We suspect in fact that this “lower limit” is strongly dependent from the geometry of the reactor defined by the packing of the millimetric particles. Screening effects are in fact more likely to occur in geometries with large preferential passages.

8.2.5 Polydisperse and « special » packings

In most cases, heterogeneous catalysts present a particle size distribution. Experimental or CFD simulation tests on polydisperse packings would be interesting to extend our study that was

performed on mono-sized particles. We did only one test in G/L/S conditions and it proved better. Due to the different particle size, polydisperse packings are expected to be more “uniform”, but this needs validation.

Another perspective would be to study packing geometries willingly built with special features like all the particles on the same side of the tube, perfect alignment of the particles in a plan etc., and compare the results with “standard” packings (a similar work has been done by Berger et al. on powder particles [106]). The goal would be to define criteria that ensure the reactor is not sensible to such overstressed defects.

Annex A: Vaporization problems in the HTE reactors

The flow distribution in the 8 reactors of the T1504 Avantium FLOWRENCE™ unit has been checked in all the experiments by performing a balance on the amount of carbon in moles measured by the GC and the one sent on the reactors:

$$\text{Carbon balance} = \frac{n_{C,out} - n_{C,in}}{n_{C,in}}$$

In which $n_{C,out}$ represents the moles of carbon detected by the GC analysis and $n_{C,in}$ represents the moles of the carbon sent by the pump.

For the reactors of 2 mm internal diameter no problem has been detected. The packing procedure provided only for a small layer of inert particles above the catalytic bed (~3 cm) leaving the rest of the reactor empty.

When passing to the reactors of $D_r=4$ mm and applying the same procedure, the GC analysis returns unacceptable carbon balance values ($>\pm 10\%$ of difference, Figure 116, A). The results in terms of conversion and selectivity are very fluctuating, indicating that the unit is not working properly. The problem is the liquid evaporation in the reactor, which is not done correctly. Falling liquid drops cause fluctuations feed of the hydrocarbons in the catalytic bed.

The problem has been solved filling the reactors until the top with inert powder (SiC or ZirBlast®) and glass socks. In this way the evaporation of the liquid droplets is promoted by the hot inert particles that also provide a correct flow distribution. In this way in fact, the GC analysis returns much more acceptable values of the carbon balance (Figure 116, B).

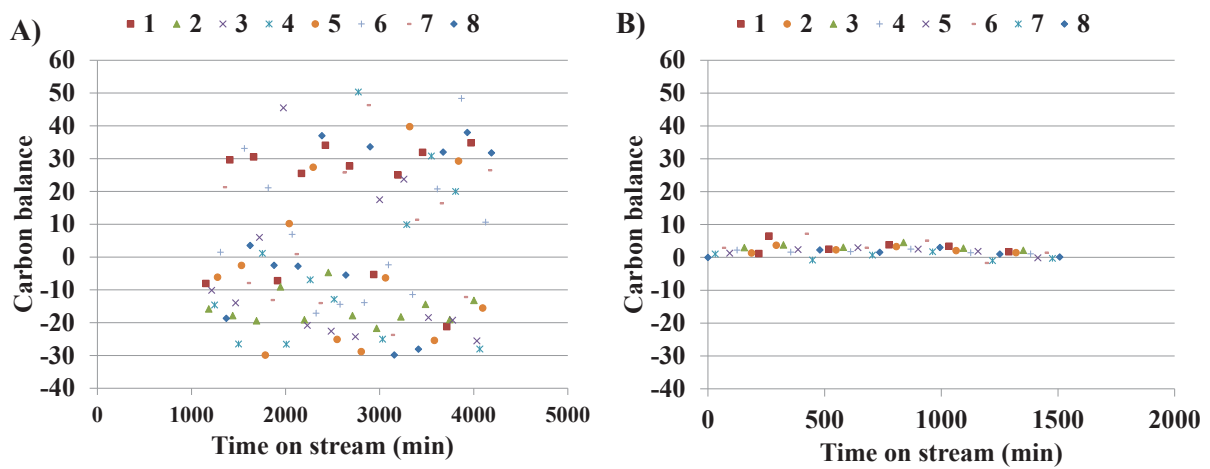


Figure 116. Carbon balance against the time on stream for two different reactor packing protocols. Reactors with $D_r=4$ mm. A) Only 3 cm filled with inert particles above the catalytic bed, B) The whole reactor above the catalytic bed is filled by inert powder and glass socks

Annex B: Deviations from the axial dispersion model in presence of porosity fillers

Small deviations from the axial dispersion model, mainly showing up differences in the “tail” of the RTD curves, are observed for almost all the experiments. However, when fine powder is added to the reactors, bigger deviations appear. One example is given in Figure 117.

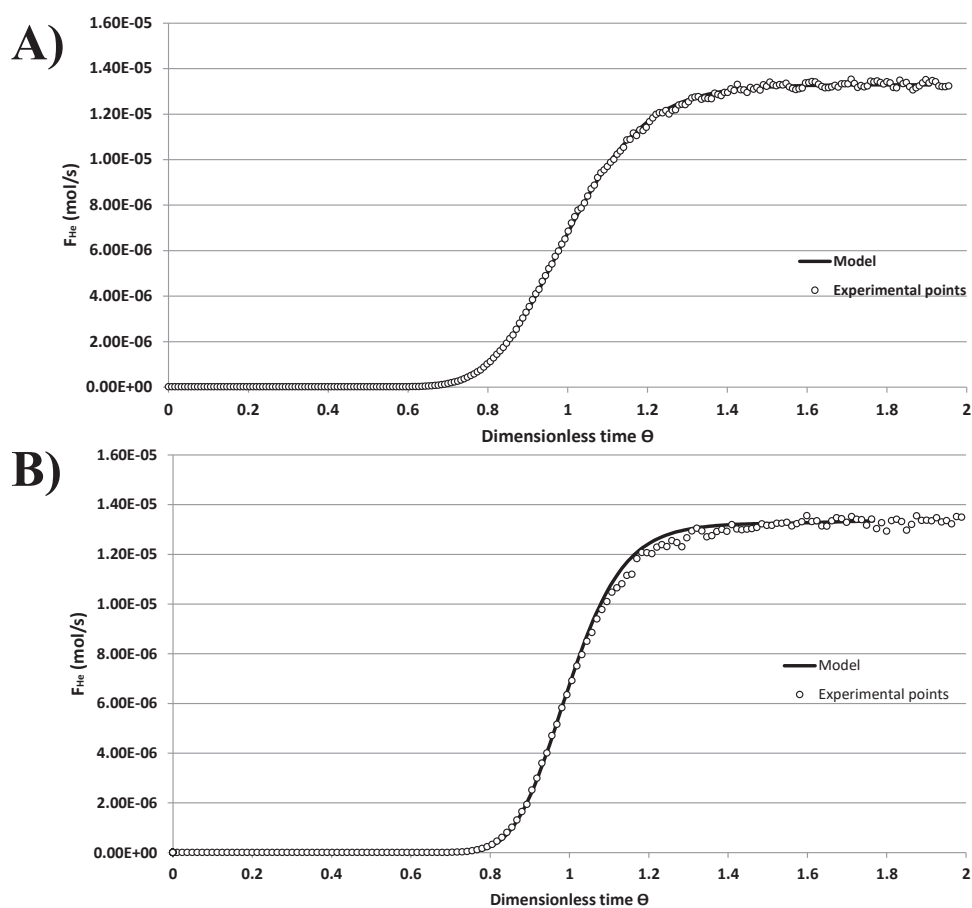


Figure 117. Example of deviation from the axial dispersion model in case of powder addition to the bed. Reactor with $D_r=7.75$ mm, $L=18.2$ cm, $d_p=5$ mm. A) No powder is used, B) Powder (SiC 0.2 mm) is used as porosity filler

The tail might indicate the presence of more dead volume zones when powder is added to the bed. This is rather unexpected as the fine powder improves the Pe number probably by preventing bypasses. This raises the question of the validity of the dispersion model to interpret these RTD curves. We propose that the fine powder prevents diffusion/dispersion from stagnant zones (near the contact points between the larger particles and with the walls) to the main flow.

The estimation of the “amount” of this deviation is difficult because of the noise of the tail of the signal.

Annex C: The Sc number effect (CFD simulations)

Keeping the reactor geometry fixed (δ), the variation of the fluid velocity (i.e. a doubling) and the variation of the molecular diffusion coefficient (i.e. a halving) are not equivalent. This means that the ratio u/D_m is not always an invariant parameter for the Bo and Pe numbers. Another dimensionless number starts to influence the physics: the Schmidt number (Sc), defined as:

$$Sc = \frac{\mu}{\rho * D_m}$$

In Figure 118 the results in a bed geometry with $\delta=1.55$ show that for lower values of Pe_m (<5) the Sc number has no impact on the Bo number while for higher values (>5) the Bo number values start to separate. So there is an influence of the Sc number, as also reported by Delgado [25].

The Sc number is varied between 0.2 and 16. When comparing the results at the same value of Pe_m , the green triangles have a Sc number that is 1.5 times the Sc number of the blue diamonds while the red squares have a Sc number 2 times the one of the blue diamonds. The higher the Sc number, the higher the Bo number and, consequently, the Pe number.

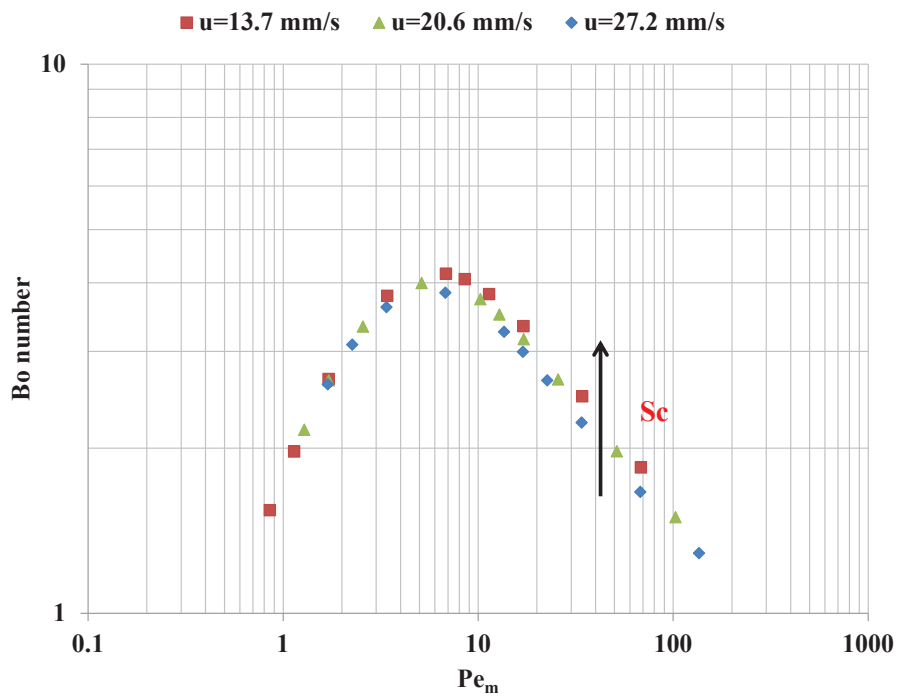


Figure 118. Evolution of the Bo number against Pe_m for three values of superficial velocities and various molecular diffusivities. $\delta=1.55$

Annex D: Second practical case of choosing the right combination of reactor and particle diameter (CFD simulations)

In paragraph §6.3.4.1 we presented a practical case in which we are designing a new catalyst testing unit and we want to decide the best reactor diameter. We will now present another case, less frequent, in which we already have a unit and a reactor whose dimensions are set, and we want to choose the best particle diameter.

To ensure the same catalyst mass in all the reactors, the length of the catalytic bed has to change according to the void fractions of the reactors:

$$L \sim \frac{1}{1 - \epsilon}$$

As we can see from a case in which the reactor diameter is 7.75 mm (Figure 119), there is a small effect of the particle diameter on the Pe number except near $\delta \sim 2.6$ (hole in the center) and for some conditions of very narrow reactors ($\delta < 1.2$).

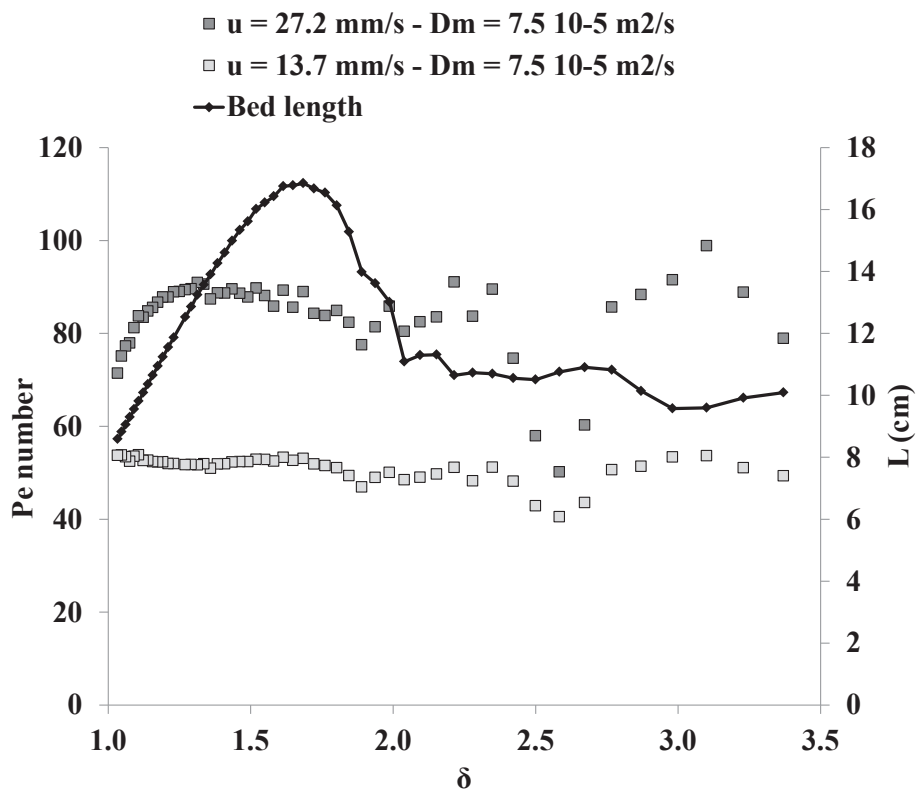


Figure 119. Evolution of Pe number and bed length against δ for a fixed reactor diameter $D_r=7.75 \text{ mm}$ and fixed flow rates ($1.28 \cdot 10^{-6} \text{ m}^3/\text{s}$ in dark grey and $6.4 \cdot 10^{-7} \text{ m}^3/\text{s}$ in light grey). The length is adjusted to have the same volume of beads in all the reactors ($\sim 2.53 \text{ mL}$)

The main recommendation is that all catalyst sizes are acceptable except near $\delta \sim 2.6$.

References

- 1 Moulíjn J.A., Pérez-Ramírez J., Berger R.J., Hamminga G., Mul G., Kapteijn F. (2003) High-throughput experimentation in catalyst testing and in kinetic studies for heterogeneous catalysis, *Catalysis Today*, Vol. 81 No. 3, Pag. 457–471. DOI: 10.1016/S0920-5861(03)00145-7.
- 2 Sie S.T. (1996) Miniaturization of hydroprocessing catalyst testing systems: Theory and practice, *AIChE Journal*, Vol. 42, No. 12, Pag. 3498–3507.
- 3 van Herk D., Castaño P., Makkee M., Moulíjn J.A., Kreutzer M.T. (2009) Catalyst testing in a multiple-parallel, gas–liquid, powder-packed bed microreactor, *Applied Catalysis A: General* 365, 2, 199–206. DOI: 10.1016/j.apcata.2009.06.010.
- 4 Templis C.C., Papayannakos N.G. (2017) Liquid-to-particle mass transfer in a structured-bed minireactor, *Chem. Eng. Technol.*, Vol. 40 No. 2, Pag. 385–394. DOI: 10.1002/ceat.201500733.
- 5 Zhang J., Teixeira A.R., Jensen K.F. (2017) Automated measurements of gas-liquid mass transfer in micropacked bed reactors, *AIChE Journal*, Vol. 64 No. 2, Pag. 564–570. DOI: 10.1002/aic.15941.
- 6 Moonen R., Alles J., Ras E.-j., Harvey C., Moulíjn J.A. (2017) Performance testing of hydrodesulfurization catalysts using a Single-Pellet-String Reactor, *Chem. Eng. Technol.*, Vol. 40 No. 11, Pag. 2025–2034. DOI: 10.1002/ceat.201700098.
- 7 Moulíjn J.A., Makkee M., Berger R.J. (2016) Catalyst testing in multiphase micro-packed-bed reactors; criterion for radial mass transport, *Catalysis Today* 259, 354–359. DOI: 10.1016/j.cattod.2015.05.025.
- 8 Bej S.K., Dabral R.P., Gupta P.C., Mittal K.K., Sen G.S., Kapoor V.K., Dalai A.K. (2000) Studies on the Performance of a Microscale Trickle Bed Reactor Using Different Sizes of Diluent, *Energy Fuels* 14, 3, 701–705. DOI: 10.1021/e990238c.
- 9 Chander A., Kundu A., Bej S.K., Dalai A.K., Vohra D.K. (2001) Hydrodynamic characteristics of cocurrent upflow and downflow of gas and liquid in a fixed bed reactor, *Fuel* 80, 8, 1043–1053. DOI: 10.1016/S0016-2361(00)00170-8.
- 10 Kallinikos L.E., Papayannakos N.G. (2007) Operation of a Miniscale String Bed Reactor in Spiral Form at Hydrotreatment Conditions, *Ind. Eng. Chem. Res.* 46, 17, 5531–5535. DOI: 10.1021/ie070309s.
- 11 Kallinikos L.E., Papayannakos N.G. (2010) Intensification of hydrodesulphurization process with a structured bed spiral mini-reactor, *Chemical Engineering and Processing: Process Intensification* 49, 10, 1025–1030. DOI: 10.1016/j.cep.2010.07.007.
- 12 Klyushina A., Pacultová K., Obalová L. (2015) Advantage of the single pellet string reactor for testing real-size industrial pellets of potassium-doped CoMnAl catalyst for the decomposition of N₂O, *Reac Kinet Mech Cat*, Vol. 115 No. 2, Pag. 651–662. DOI: 10.1007/s11144-015-0871-y.

- 13 Šolcova O., Schneider P. (2004) Axial dispersion in single pellet-string columns with non-porous packing, *Chemical Engineering Science*, Vol. 59 No. 6, Pag. 1301–1307. DOI: 10.1016/j.ces.2004.01.011.
- 14 Rob J. Berger, Javier Pérez-Ramirez, Freek Kapteijn, Jacob A. Moulijn (2002) Catalyst performance testing: bed dilution revisited.
- 15 Mueller G.E. (1992) Radial void fraction distributions in randomly packed fixed beds of uniformly sized spheres in cylindrical containers, *Powder Technology*, Vol. 72 No. 3, Pag. 269–275. DOI: 10.1016/0032-5910(92)80045-X.
- 16 Mueller G.E. (1991) Prediction of radial porosity distributions in randomly packed fixed beds of uniformly sized spheres in cylindrical containers, *Chemical Engineering Science*, Vol. 46 No. 2, Pag. 706–708. DOI: 10.1016/0009-2509(91)80032-T.
- 17 Leva, M. (1947) Pressure Drop through packed tubes, Part 3: Prediction of voids in packed tubes,” *Chem. Eng. Prog.*, 43(10), pp. 713–718.
- 18 De Klerk (2003) Voidage variation in packed beds at small column to particle diameter ratio, *AIChE Journal*, Vol. 49, No. 8.
- 19 Matthieu Rolland (2014) Thèse "Des limites à la réduction d'échelle en réacteur de test catalytique en lit fixe ?", Université Claude Bernard Lyon 1, Ecole Doctorale de Chimie.
- 20 Muthanna H. Al-Dahhan, Yuanxin Wu, and Milorad P. Dudukovic (1995) Reproducible Technique for Packing Laboratory-Scale Trickle-Bed Reactors with a Mixture of Catalyst and Fines.
- 21 van Herk D., Castaño P., Quaglia M., Kreutzer M.T., Makkee M., Moulijn J.A. (2009) Avoiding segregation during the loading of a catalyst–inert powder mixture in a packed micro-bed, *Applied Catalysis A: General* 365, 1, 110–121. DOI: 10.1016/j.apcata.2009.06.003.
- 22 Márquez N., Castaño P., Makkee M., Moulijn J.A., Kreutzer M.T. (2008) Dispersion and holdup in multiphase packed bed microreactors, *Chem. Eng. Technol.*, Vol. 31 No. 8, Pag. 1130–1139. DOI: 10.1002/ceat.200800198.
- 23 Zou R. and Yu A. (1995) The packing of spheres in a cylindrical container: the thickness effect, *Chemical Engineering Science*, Vol. 50, No. 9, pp. 151M-1507, 1995.
- 24 Charles Bonnin (2016) Thèse "Evaluation de l'expérimentation haut débit en milli lit fixe pour le screening de catalyseurs Fischer-Tropsch", Université des Sciences et Technologies de Lille 1, Ecole Doctorale Sciences de la Matière, du Rayonnement et de l'Environnement (EDSMRE).
- 25 Delgado J.M.P.Q. (2006) A critical review of dispersion in packed beds, *Heat Mass Transfer*, Vol. 42 No. 4, Pag. 279–310. DOI: 10.1007/s00231-005-0019-0.
- 26 Gierman H. (1988) Design of laboratory hydrotreating reactors. Scaling down of trickle-flow reactors, *Applied Catalysis*, Vol. 43 No. 2, Pag. 277–286. DOI: 10.1016/S0166-9834(00)82732-3.
- 27 Whitman W.G. (1923) The two-film theory of gas absorption, *Chem. Metall. Engng* 29, 146.

- 28 Ranz, W. E. and Marshall, W. R. (1952) Evaporation from drops. *Chemical Engineering Progress*, Vol. 48 No. 3 Pag. 141-146.
- 29 Kallinikos L.E., Papayannakos N.G. (2007) Fluid dynamic characteristics of a structured bed spiral mini-reactor, *Chemical Engineering Science* 62, 21, 5979–5988. DOI: 10.1016/j.ces.2007.06.006.
- 30 Reinecke N. and Mewes D. (1997) Investigation of the two-phase flow in trickle-bed reactors using capacitance tomography, *Chemical Engineering Science*, Vol. 52 No. 13, Pag. 2111-2127.
- 31 van Herk D., Kreutzer M.T., Makkee M., Moulijn J.A. (2005) Scaling down trickle bed reactors, *Catalysis Today* 106, 1-4, 227–232. DOI: 10.1016/j.cattod.2005.07.180.
- 32 Octave Levenspiel (1999) *Chemical Reaction Engineering*, third edition.
- 33 Faridkhou A., Hamidipour M., Larachi F. (2013) Hydrodynamics of gas–liquid micro-fixed beds – Measurement approaches and technical challenges, *Chemical Engineering Journal* 223, 425–435. DOI: 10.1016/j.cej.2013.03.014.
- 34 Ana Isabel Hipolito (2010) Thèse "Étude des phénomènes de transport dans un réacteur catalytique de type "filaire"", Université Claude Bernard Lyon 1, Ecole Doctorale de Chimie.
- 35 Johnson G.W., Kapner R.S. (1989) The dependence of axial dispersion on non-uniform flows in beds of uniform packing, *Chemical Engineering Science*, Vol. 45 No. 11, Pag. 3329-3339.
- 36 Hsiang, T.C.S. and Haynes Jr, H.W. (1977) Axial dispersion in small diameter beds of large, spherical particles, *Chemical Engineering Science*, Vol 32, Pag. 678-681.
- 37 Muthanna H. Al-Dahhan and Milorad P. Dudukovic (1994) Pressure drop and liquid holdup in high pressure trickle-bed reactors, *Chemical Engineering Science*, Vol. 49, No. 248, pp. 5681-5698.
- 38 Ranjit R. Kulkarni, Joseph Wood, and, John M. Winterbottom, and E. Hugh Stitt (2005) Effect of Fines and Porous Catalyst on Hydrodynamics of Trickle Bed Reactors.
- 39 Mills P.L., Dudukovic M.P. (1981) Evaluation of liquid-solid contacting in trickle-bed reactors by tracer methods, *AIChE J.* 27, 6, 893–904. DOI: 10.1002/aic.690270604.
- 40 McHenry K.W., Wilhelm R.H. (1957) Axial mixing of binary gas mixtures flowing in a random bed of spheres, *AIChE Journal*, Vol. 3 No. 1, Pag. 83–91. DOI: 10.1002/aic.690030115.
- 41 Edwards M.F., Richardson J.F. (1970) The correlation of axial dispersion data, *Can. J. Chem. Eng.*, Vol. 48 No. 4, Pag. 466–467. DOI: 10.1002/cjce.5450480421.
- 42 Scott D.S., Lee W. and Papa J. (1974) The measurement of transport coefficients in gas-solid heterogeneous reactions, *Chemical Engineering Science*, Vol. 29, Pag. 2155-2167.
- 43 de Carvalho, J. R. F. Guedes, Delgado, J. M. P. Q. (2003) Effect of fluid properties on dispersion in flow through packed beds, *AIChE J.* 49, 8, 1980–1985. DOI: 10.1002/aic.690490808.

- 44 Fernengel J., Bolton L., Hinrichsen O. (2019) Characterisation and design of single pellet string reactors using numerical simulation, *Chemical Engineering Journal* 373, 1397–1408. DOI: 10.1016/j.cej.2019.03.114.
- 45 Julcour-Lebigue C., Augier F., Maffre H., Wilhelm A.-M., Delmas H. (2009) Measurements and Modeling of Wetting Efficiency in Trickle-Bed Reactors: Liquid Viscosity and Bed Packing Effects, *Ind. Eng. Chem. Res.* 48, 14, 6811–6819. DOI: 10.1021/ie9002443.
- 46 Muthanna H. Al-Dahhan and Milorad P. Dudukovic (1995) Catalyst wetting efficiency in trickle-bed reactors at high pressure, *Chemical Engineering Science*, Vol. 50, No. 15, pp. 2377–2389,
- 47 Mordechay Herskowitz and Shelomo Mosseri (1983) Global rates of reaction in trickle-bed reactors: effects of gas and liquid flow rates, *Ind. Eng. Chem. Fundam.* 1983, 22, 4-6.
- 48 F. Pironti, D. Mizrahi, A. Acosta, D. González-Mendizabal (1999) Liquid-solid wetting factor in trickle-bed reactors: its determination by a physical method, *Chemical Engineering Science*, Vol. 54, pp. 3793-3800.
- 49 A. Kundu and K.D.P. Nigam (2003) Catalyst wetting characteristics in trickle-bed reactors, *AIChE Journal*, Vol. 49, No. 9.
- 50 Colombo A.J., Baldi G., Sicardi S. (1976) Solid-liquid contacting effectiveness in trickle bed reactors, *Chemical Engineering Science* 31, 12, 1101–1108. DOI: 10.1016/0009-2509(76)85019-1.
- 51 van Klinken, van Dongen (1980) Catalyst dilution for improved performance of laboratory trickle-flow reactors, *Chemical Engineering Science*, Vol 35, pp 59-66.
- 52 Muthanna H. Al-Dahhan and Milorad P. Dudukovic (1996) Catalyst bed dilution for improving wettig in laboratory trickle-bed reactors, *AIChE Journal*, Volume42, Issue9, Pages 2594-2606.
- 53 Bellos G.D., Gotsis K.P., Papayannakos N.G. (2007) The gas–liquid contacting effect on the operation of small scale upflow hydrotreaters, *Catalysis Today* 127, 1-4, 103–112. DOI: 10.1016/j.cattod.2007.05.004.
- 54 Pozzobon V., Colin J., Perré P. (2018) Hydrodynamics of a packed bed of non-spherical polydisperse particles: A fully virtual approach validated by experiments, *Chemical Engineering Journal* 354, 126–136. DOI: 10.1016/j.cej.2018.07.214.
- 55 Minhua Z., He D., Zhongfeng G. (2019) A particle-resolved CFD model coupling reaction-diffusion inside fixed-bed reactor, *Advanced Powder Technology* 30, 6, 1226–1238. DOI: 10.1016/j.apt.2019.03.019.
- 56 Bai H., Theuerkauf J., Gillis P.A., Witt P.M. (2009) A Coupled DEM and CFD Simulation of Flow Field and Pressure Drop in Fixed Bed Reactor with Randomly Packed Catalyst Particles, *Ind. Eng. Chem. Res.* 48, 8, 4060–4074. DOI: 10.1021/ie801548h.
- 57 Gilbert E. G., Johnson D. W., Keerthi S. S. (1988) A fast procedure for computing the distance between complex objects in three-dimensional space, *IEEE Journal of robotics and automation*, Vol. 4 No. 2, Pag. 193-203.

- 58 Rakotonirina A.D., Delenne J.-Y., Radjai F., Wachs A. (2019) Grains3D, a flexible DEM approach for particles of arbitrary convex shape—Part III: extension to non-convex particles modelled as glued convex particles, *Computational Particle Mechanics*, Vol. 6, Pag. 55-84.
- 59 Boccardo G., Augier F., Haroun Y., Ferré D., Marchisio D.L. (2015) Validation of a novel open-source work-flow for the simulation of packed-bed reactors, *Chemical Engineering Journal* 279, 809–820. DOI: 10.1016/j.cej.2015.05.032.
- 60 Liu M., Tilton J.N. (2010) Spatial distributions of mean age and higher moments in steady continuous flows, *AIChE J.* 56, 10, 2561–2572. DOI: 10.1002/aic.12151.
- 61 Liu M. (2011) A method for computing the degree of mixing in steady continuous flow systems, *Chemical Engineering Science*, Vol. 66 No. 13, Pag. 3045–3048. DOI: 10.1016/j.ces.2011.03.049.
- 62 Danckwerts P. V. (1958) The effect of incomplete mixing on homogeneous reactions, *Chemical Engineering Science*, Vol.8 No. 1-2, Pag. 93-102.
- 63 Zwietering Th. N. (1959) The degree of mixing in continuous flow systems, *Chemical Engineering Science*, Vol. 11 No. 1, Pag. 1-15.
- 64 Sandberg M. (1981) What is ventilation efficiency?, *Building and Environment*, Vol. 16 No. 2, Pag. 123-135.
- 65 Spalding D. B. (1958) A note on mean residence-times in steady flows of arbitrary complexity, *Chemical Engineering Science*, Vol. 9 No.1, Pag. 74-77.
- 66 Freund H., Zeiser T., Huber F., Klemm E., Brenner G., Durst F., Emig G. (2003) Numerical simulations of single phase reacting flows in randomly packed fixed-bed reactors and experimental validation, *Chemical Engineering Science* 58, 3-6, 903–910. DOI: 10.1016/S0009-2509(02)00622-X.
- 67 Partopour, B., & Dixon, A.G. (2018) n-butane partial oxidation in a fixed bed: A resolved particle computational fluid dynamics simulation, *The Canadian Journal of Chemical Engineering*, 96(9), 1946-1956.
- 68 Rolland M., Fonte C.P. (2015) Incertitude induced by testing a small number of catalytic pellets in fixed beds, *Chemical Engineering Science*, Vol. 138, Pag. 698–705. DOI: 10.1016/j.ces.2015.09.008.
- 69 Chu C. F., Ng K. M. (1989) Flow in packed tubes with a small tube to particle diameter ratio, *AIChE Journal*, Vol. 35, No. 1.
- 70 McGeary R.K. (1961) Mechanical packing of spherical particles, *Journal of the American Ceramic Society*, Vol. 44 No. 10, Pag. 513-522.
- 71 Saint Gobain ZirPro Website <https://www.zirpro.com/>.
- 72 Kariya N., Fukuoka A., Utagawa T., Sakuramoto M., Goto Y., Ichikawa M. (2003) Efficient hydrogen production using cyclohexane and decalin by pulse-spray mode reactor with Pt catalysts, *Applied Catalysis A: General*, Vol. 247 No. 2, Pag. 247–259. DOI: 10.1016/S0926-860X(03)00104-2.

- 73 Edwards M. F. and Richardson J. F. (1968) Gas dispersion in packed beds, *Chemical Engineering Science*, Vol. 23, Pag. 109-123.
- 74 Han N.W., Bhakta J., Carbonell R.G. (1985) Longitudinal and lateral dispersion in packed beds: Effect of column length and particle size distribution, *AIChE Journal*, Vol. 31 No. 2, Pag. 277-288.
- 75 Punčochář M., Drahoš J. (1993) The tortuosity concept in fixed and fluidized bed, *Chemical Engineering Science*, Vol. 48 No. 11, Pag. 2173–2175. DOI: 10.1016/0009-2509(93)80092-5.
- 76 Mears D.E. (1971) Diagnostic criteria for heat transport limitations in fixed bed reactors, *Journal of Catalysis*, Vol. 20, Pag. 127-131.
- 77 Mears D.E. (1976) On criteria for axial dispersion in nonisothermal packed-bed catalytic reactors, *Ind. Eng. Chem. Fundam.*, Vol. 15 No. 1, Pag. 20-23.
- 78 Yagi S. and Wakao N. (1959) Heat and mass transfer from wall to fluid in packed beds, *AIChE Journal*, Vol. 5 No. 1, Pag. 79-85.
- 79 Hanratty T.J. (1954) Nature of wall heat transfer coefficient in packed beds, *Chemical Engineering Science*, Vol. 5, Pag. 209-214.
- 80 De Wasch A. P. and Froment G. F. (1972) Heat transfer in packed beds, *Chemical Engineering Science*, Vol. 27, Pag. 567-576.
- 81 Li Chi-Hsiung and Finlayson B. A. (1977) Heat transfer in packed beds - A reevaluation, *Chemical Engineering Science*, Vol. 32, Pag. 1055-1066.
- 82 Specchia V. and Sicardi S. (1980) Heat transfer in packed bed reactors with one phase flow, *Chemical Engineering Communications*, Vol. 4 No. 1-3, Pag. 361-380.
- 83 Gunn D.J., Ahmad M.M. and Sabri M.N. (1987) Radial heat transfer to fixed beds of particles, *Chemical Engineering Science*, Vol. 42 No. 9, Pag. 2163-2171.
- 84 Bey O. and Eigenberger G. (2001) Gas flow and heat transfer through catalyst filled tubes, *Int. J. Therm. Sci.*, Vol. 40, Pag. 152–164.
- 85 Wakao N. and Funazkri T. (1978) Effect of fluid dispersion coefficients on particle-to-fluid mass transfer coefficients in packed beds, *Chemical Engineering Science*, Vol. 33, Pag. 1375-1384.
- 86 Hipolito A.I., Rolland M., Boyer C., Bellefon C. de (2010) Single Pellet String Reactor for Intensification of Catalyst Testing in Gas/Liquid/Solid Configuration, *Oil Gas Sci. Technol. – Rev. IFP Energies nouvelles* 65, 5, 689–701. DOI: 10.2516/ogst/2009079.
- 87 Petrazzuoli V., Rolland M., Mekki-Berrada A., Said-Aizpuru O., Schuurman Y. (Submitted in 2020) Choosing the right packing in packed bed millireactors under single phase gas flow, *Chemical Engineering Science*.
- 88 A. Müller, J. Petschick, R. Lange (2012) Model-Based Investigation of a Pellet String Reactor.
- 89 Augier F., Idoux F., Delenne J.-Y. (2010) Numerical simulations of transfer and transport properties inside packed beds of spherical particles, *Chemical Engineering Science* Vol. 65 No. 3, Pag. 1055-1064.

- 90 Michiel Nijemeisland, Anthony G. Dixon (2004) CFD Study of fluid flow and wall heat transfer in a fixed bed of spheres, *AICHE Journal*, Vol. 50, Pag. 906–921.
- 91 Partopour B., Dixon A.G. (2017) An integrated workflow for resolved-particle packed bed models with complex particle shapes, *Powder Technology*, Vol. 322, Pag. 258–272.
- 92 Cundall, Peter A. and Otto DL Strack (1979) A discrete numerical model for granular assemblies, *Geotechnique* Vol.29 N.1, Pag. 47-65.
- 93 Wachs A., Girolami L., Vinay G., Ferrer G. (2012) Grains3D, a flexible DEM approach for particles of arbitrary convex shape—Part I: Numerical model and validations, *Powder Technology*, Vol. 224, Pag. 374–389.
- 94 OpenFOAM Foundation OpenFOAM user guide - snappyHexMesh. Available at: <https://cfd.direct/openfoam/user-guide/v6-snappyhexmesh/>.
- 95 OpenFOAMWiki The openFOAM simpleFoam solver. Available at: <https://openfoamwiki.net/index.php/SimpleFoam>.
- 96 Rolland M., Rakotonirina A.D., Devouassoux A., Barrios G. J.L., Delenne J.-Y., Wachs A. (2019) Predicting average void fraction and void fraction uncertainty in fixed beds of poly lobed particles, *Ind. Eng. Chem. Res.*, Vol. 58, Pag. 3902–3911. DOI: 10.1021/acs.iecr.8b05557.
- 97 Dixon A.G. (1988) Correlations for wall and particle shape effects on fixed bed bulk voidage, *Can. J. Chem. Eng.* 66, 5, 705–708. DOI: 10.1002/cjce.5450660501.
- 98 R. F. Benenati and C. B. Brosilow (1962) Void fraction distribution in beds of spheres, *AICHE Journal*, Vol. 8 No. 3, Pag. 359-361.
- 99 Sie S.T. (1991) Scale effects in laboratory and pilot plant reactors for trickle-flow processes, *Revue Institut Français du Pétrole*, Vol. 46, Pag. 501-515.
- 100 Baussaron L., Julcour-Lebigue C., Wilhelm A.-M., Delmas H., Boyer C. (2007) Wetting topology in trickle bed reactors, *AICHE J.* 53, 7, 1850–1860. DOI: 10.1002/aic.11189.
- 101 van Houwelingen A.J., Sandrock C., Nicol W. (2006) Particle wetting distribution in trickle-bed reactors, *AICHE J.* 52, 10, 3532–3542. DOI: 10.1002/aic.10961.
- 102 Watson P. C. and Harold M. P. (1993) Dynamic effects of vaporization with exothermic reaction in a porous catalytic pellet, *AICHE Journal*, Vol. 39 No. 6, Pag. 989-1006.
- 103 Funk G. A., Harold M. P., Ng Ka M. (1991) Experimental study of reaction in a partially wetted catalytic pellet, *AICHE Journal*, Vol. 37 No. 2, Pag. 202-214.
- 104 Valérie Meille, Claude de Bellefon, and Daniel Schweich (2002) Kinetics of α -Methylstyrene Hydrogenation on Pd/Al₂O₃, *Ind. Eng. Chem. Res.*, Vol. 41, Pag. 1711-1715.
- 105 Valérie Meille, Claude de Bellefon (2004) Effect of Water on α -Methylstyrene Hydrogenation on Pd/Al₂O₃, *The Canadian Journal of Chemical Engineering*, Vol. 82, Pag. 190-193.
- 106 Berger R.J., Kapteijn F., Moulijn J.A. (2002) Catalyst performance testing Radial and axial dispersion related to dilution in fixed-bed laboratory reactors.